

# **SYNTHESIS, PROPERTIES, AND REACTIVITY OF SULFONAMIDE NEWTAML OXIDATION CATALYSTS**

Dissertation by

**Genoa R. Warner**

In Partial Fulfillment of the Requirements for the Degree of

**Doctor of Philosophy**

Thesis Advisor

**Terrence J. Collins**

Carnegie Mellon University

Pittsburgh, PA

Submitted May 29, 2017

## ABSTRACT

Worldwide, water is becoming increasingly contaminated with micropollutants, substances present at low concentrations that have undesired effects. Conventional wastewater treatments are ineffective against many of these hormones, pesticides, pharmaceuticals, personal care products, and other commonplace chemicals. TAML activators, small-molecule peroxide-activating oxidation catalysts, are one solution for removing organic pollutants during water purification. TAML activators have been iteratively improved over the past twenty years to be highly reactive, easy to prepare, and resistant to oxidation. However, modifications to the macrocyclic ligand such as the biuret tail have not significantly improved reactivity or lifetime. Further investigation into the structural source of the lifetime limitation of TAMLs has led to the design of “NewTAML” activators, a new family of catalysts featuring sulfonamides ( $\text{-NHSO}_2\text{-}$ ) instead of carbonamides ( $\text{-NHCO-}$ ) in the ligand. NewTAMLs are comprised of biochemically common elements, are cheaper to produce than our prior best-performing, fluorine-containing TAMLs, and are significantly more reactive—the concentrations employed in the presented model pollutant removal studies translate to one kilogram of catalyst treating 16,000–160,000 tonnes of municipal wastewater.

Seven NewTAML activators have been prepared and thoroughly characterized through various techniques including X-ray crystallography. NewTAML activators follow the accepted mechanism of catalysis established for previous “OldTAMLs.” In the bleaching of the model substrate Orange II, all NewTAMLs perform superiorly compared to their structural analogs at neutral pH. The electron-withdrawing sulfonamide groups in NewTAMLs increase the Lewis acidity of the metal resulting in decreased axial water

$pK_a$  by 1.2 units. The pH dependence of catalyst activity reveals that the decrease in  $pK_a$  has shifted maximum reactivity toward neutral pH. Additionally, NewTAMLs are ten times more resistant to specific acid demetalation at low pH and show no toxicity toward prepubertal mice. Lifetime studies of NewTAMLs reveal that these catalysts contain a significant pH-dependent inactivation pathway that limits the utility of NewTAMLs at pH 9 and above. This inactivation is presumably associated with deprotonation of the acidic methylene tail in the active state. However,  $CH_3$  for H substitution at the tail substantially reduces this inactivation pathway. Overall, NewTAMLs are highly reactive, easy to prepare oxidation catalysts with promise for water treatment applications.

## ACKNOWLEDGEMENTS

I applied to the PhD program in the Department of Chemistry at CMU five years ago with the specific intent of working for Professor Terry Collins at the Institute for Green Science (IGS). As an undergrad, I began my research career at the Center for Green Chemistry and Green Engineering at Yale, where I became hooked on sustainable environmental chemistry. I owe a huge thank you to my mentor, Dr. Katalin Barta, who trained me as a researcher and allowed me to design some of my own experiments. Thanks to Dr. Evan Beach for pointing me towards CMU for graduate school and to all of the green chemistry group members at Yale.

Terry has been the most supportive and encouraging advisor I could have hoped for. Even when I struggled for years in the synthetic lab trying to make new catalysts, Terry allowed me to work through problems at my own pace. Thank you, Terry, for giving me the freedom to both direct my own TAML projects and to pursue my sustainability interests outside of the lab. I have enjoyed and learned from arranging film screenings, talks, and outreach through the group without worrying about spending time away from the bench. I am especially grateful to Terry for helping to foster my interest in endocrine disruption by providing opportunities for reading, writing, and teaching.

The work in this thesis would not be possible without Dr. Aleksandr Ryabov, our kinetics guru. Sasha has worked tirelessly to train me in proper kinetic experimental design, analysis, and writing. Thank you, Sasha, for all of the editing that you have done for me over the years and for listening to so many painful first run-throughs of talks. Sasha also keeps our group running and provides a grounded foil to Terry's big picture outlook on TAMLs. I would not have had such a successful or enjoyable experience here without him.

During my first year at the IGS, Dr. Karla Arias was my mentor in the lab. Everything I know about synthetic chemistry I learned from Karla. I am greatly indebted to her for getting me started in the lab my first month here and helping me to prepare my first TAML (in Chapter 2) by the time she left to pursue patent law at the end of my first year. I continue to look up to Karla as an example of a great woman in science.



Our group would not be so successful without such a collaborative and supportive environment among the students. Thank you to all of my fellow students who I have worked with over the years here. Dr. Matthew Mills trained me on various instruments and answered so many questions. He prepared NewTAML **4** in Chapter 5 and contributed to Chapters 2 and 4. Dr. Liang Tang was the best office buddy. Dr. Matthew DeNardo helped with synthesis of NewTAMLs and understanding their lifetimes. Yogesh Somasundar and I have worked on many projects together over the past two years as I have transitioned out of the synthesis lab. Thank you Yogi for all of the instrumentation help and for being a great lab friend. Yogi performed all of the propranolol studies in Chapter 4. Thank you also to Dr. Longzhu Shen, with whom I share a passion for environmental outreach. Longzhu handed me the reins of the Environmental Group of the Pittsburgh Section of the American Chemical Society, which has provided support and funding for many of the environmental activities I have organized over the past five years. Thank you also to Dr. Soumen Kundu, Paul Kornbluh, Munmun Ghosh, and Clarissa Enslin.

I have been lucky to mentor three excellent undergraduate researchers during my graduate career. Kyle Jansen worked with me to prepare NewTAML activators, contributing significantly to the preparation of **2**, **6**, and **8**. Synthesis projects, especially involving untested procedures, are difficult to fit into an already busy schedule and can be emotionally draining when they fail, but Kyle was easygoing and flexible. Evan Kaaret started working with me in the lab during his freshman year and has grown into an inquisitive independent researcher. Evan studied the kinetics of NewTAML catalysis and was instrumental in continuing these projects after I stopped working actively in the lab. During manuscript writing, Evan was my go to guy to perform those random-seeming last few experiments to fill out each paper. His work can be found in chapters 4–7. Cindy Weng joined our group as an civil & environmental engineering student with an interest in water. Cindy was one of the quickest students in recent memory to start working independently in the lab. Cindy has worked on the degradation of the insecticide imidacloprid by NewTAMLs. Her work is not yet complete and not included in this thesis, but her results are exciting and should be published in 2018. Finally, David Zhang performed the NewTAML acid demetalation studies in Chapter 5 and 6.

Thank you to our collaborators around the world whose work appears in this thesis. Shantanu Pattanayak, Dr. Chakadola Panda, Dr. Tamas Kumar Panda, and Professor Sayam Sen Gupta at CSIR-National Chemical Laboratory in Pune, India contributed to Chapter 2 as well as Clarissa Enslin and Matt Mills. The mouse toxicity studies in Chapter 4 were performed by Professors Julia Taylor and Frederick vom Saal with experimental design help from Matt Mills. Wastewater treatment analysis was performed with help from Professor Rak Kanda at Brunel Univeristy. The crystal structure in Chapter 4 was determined by Gabrielle Pros and Professor Tomislav Pintauer at Duquesne University. EPR studies in Chapter 5 were performed by Saborni Biswas and Professor Michael Hendrich at CMU.

Many professors in the department have been influential mentors for me. Thank you to the members of my thesis committee, Professors Stefan Bernhard and Catalina Achim. Catalina has served as a mentor to me in both research and outreach and has constantly pushed me to be a better thinker and scientist. In particular, Catalina's encouragement to delegate tasks to my mentees and relinquish my perfectionism helped me learn how to become a mentor and has shaped my desire to pursue an academic research career. Thank you also to Professor Bruce Armitage, who welcomed me into his group as an honorary member as long as I continued to supply baked goods and has also provided invaluable academic guidance.

The collaborative atmosphere of our department made many of these experiments possible. Thank you to all of the groups, professors, and students from whom I have borrowed chemicals or instruments or turned to for guidance (or to commiserate) when my experiments failed, particularly the Armitage, Bruchez, Bernhard, and Noonan groups. Logan Plath, Professor Mark Bier, Dr. Gayathri Withers, and Professor Roberto Gil at the Center for Molecular Analysis have also been instrumental.

I owe huge thank you to all of the support people who keep this department running, including Dr. Rea Freeland, Valerie Bridge, Sara Wainer, Brenda Chambers, Tim Sager, and Patsey Haddock. You were the first people to welcome me into the department five years ago and I will always be grateful for your support during my time at CMU. Thank you also to Jack Thorpe in the mailroom, Paul Smith, Ray Butko, and

Melissa Powell in the stockroom, and Hannah Diorio-Toth and Donna Smith with DNAZone in CNASt.

I have made a number of great friends during my PhD including Alex, Lisa, Anna, Jon, Jonathan, Cheryl, Gayathri, Liang, Yogi, and many others who I started with in 2012. Thank you all for your love and support and for showing up to my evening environmental events.

Finally, thank you to my family and faraway friends, especially my siblings Brea and Cali and my parents Ruth and Steve, who have always encouraged me to follow my dreams and supported me every step of the way.

To my dear husband Taylor, I love you more than I can possibly express on this page. I could not have received a better gift from CMU than to meet you here. Experiencing science and life with you has deepened my knowledge, perspective, and creativity, and I can't wait for all of our future adventures together.

# TABLE OF CONTENTS

ABSTRACT .....	ii
ACKNOWLEDGEMENTS.....	iv
TABLE OF CONTENTS .....	viii
TABLE OF FIGURES .....	xii
TABLE OF TABLES.....	xvii
ABBREVIATIONS .....	xviii

## CHAPTER 1

<b>TAML Activators as a Sustainable Solution to Contamination of Water by Micropollutants</b> .....	1
1.1 Introduction.....	2
1.2 Sustainability Ethics.....	4
1.3 Micropollutants as a Global Water Treatment Challenge.....	7
1.4 The TAML Activator Solution .....	11
1.4.1 Iterative Design of TAML Activators.....	15
1.4.2 Orange II as a Tool for Kinetic Comparison of TAMLs.....	18
1.4.3 TAML Activators and Endocrine Disruption.....	20
1.5 Research Summary .....	24
1.6 References.....	26

## CHAPTER 2

<b>Kinetic Studies of Reactivity and Operational Stability of N-tailed TAMLs Through the Catalyzed Oxidation of Orange II by H<sub>2</sub>O<sub>2</sub></b> .....	30
2.1 Introduction.....	33
2.2 Results and Discussion .....	35
2.2.1 Synthesis and X-Ray Characterization of <b>7c</b> .....	35
2.2.2 Properties of <b>7a</b> in Aqueous Solution .....	36
2.2.3 Catalytic Activity of <b>7a</b> in Bleaching Orange II with H <sub>2</sub> O <sub>2</sub> .....	37
2.2.4 Properties and Catalytic Activity of <b>7b</b> in the Bleaching Orange II by H <sub>2</sub> O <sub>2</sub> .....	44
2.2.5 Catalytic Activity of <b>7c</b> in the Bleaching Orange II by H <sub>2</sub> O <sub>2</sub> .....	47
2.2.6 Operational Stability of TAML Activators <b>7</b> .....	48
2.2.7 Discussion .....	50
2.3 Conclusions.....	52
2.4 Experimental .....	53
2.4.1 Materials and Methods .....	53
2.4.2 Synthesis of <b>7a'</b> .....	53
2.4.3 Kinetics of TAML-catalyzed bleaching of Orange II by H <sub>2</sub> O <sub>2</sub> .....	54

2.4.4	Measurements of $pK_a$ .....	54
2.4.5	X-Ray structural investigation of <b>7c</b> .....	55
2.5	References.....	57

## CHAPTER 3

<b>Design and Synthesis of Sulfonamide-Containing NewTAMLs</b> .....	59
3.1 Introduction.....	60
3.2 Preparation of NewTAML Ligands.....	64
3.2.1 Preparation of TAML family <b>1</b> NewTAML analogs.....	65
3.2.2 Preparation of D* series NewTAMLs.....	72
3.2.3 Preparation of tetrasulfonamide <b>8</b> .....	74
3.3 Conclusions.....	75
3.4 References.....	76

## CHAPTER 4

Introducing “NewTAMLs” for Ultra-Dilute Catalytic Oxidation in Global Water Treatment		
Treatment	.....	78
4.1	Introduction.....	79
4.2	Results and Discussion .....	80
4.2.1	Catalytic Activity of NewTAMLs in the Degradation of Orange II with H <sub>2</sub> O <sub>2</sub> .....	81
4.2.2	Catalytic Activity of NewTAMLs in the Degradation of Propranolol with H <sub>2</sub> O <sub>2</sub> .....	86
4.2.3	Toxicity and Endocrine Disruption Assessment of <b>2</b> .....	88
4.3	Conclusions.....	94
4.4	Experimental.....	95
4.4.1	Materials and Methods .....	95
4.4.2	Instrumentation .....	95
4.4.3	General Preparation of <b>2</b> .....	96
4.4.4	X-ray Crystallography .....	99
4.4.5	Measurement of pK <sub>a</sub> .....	99
4.4.6	Kinetics of Catalyzed Bleaching of Orange II .....	99
4.4.7	Propranolol Degradation by Catalyst/H <sub>2</sub> O <sub>2</sub> .....	101
4.4.8	Animals .....	101
4.4.9	Mouse Drinking Water Treatment .....	102
4.4.10	Prepubertal Mouse Uterotropic Assay .....	103
4.4.11	Toxicity Screen.....	104
4.4.12	Mouse Data Analysis .....	104
4.5	References.....	105

## CHAPTER 5

<b>Understanding the Superior Catalytic Activity of NewTAMLs at Neutral pH</b>	107
5.1 Introduction	108
5.2 Results and Discussion	111
5.2.1 <i>Properties of Sulfonamide-tailed Activators</i>	111
5.2.2 <i>Hydrolytic Stability of NewTAML Activators</i>	115
5.2.3 <i>Catalytic Activity in Bleaching of Orange II with H<sub>2</sub>O<sub>2</sub></i>	117
5.2.4 <i>Comparison of Old- and NewTAMLs via Linear Free Energy Relationships</i>	122
5.3 Conclusions	125
5.4 Experimental	126
5.4.1 <i>Materials and Methods</i>	126
5.4.2 <i>Synthesis of 4</i>	126
5.4.3 <i>Acid Induced Demetalation</i>	127
5.4.4 <i>EPR Studies of 2a</i>	128
5.5 References	129

## CHAPTER 6

<b>Reactivity and Stability of a Second Generation Diphenyl NewTAML</b>	130
6.1 Introduction	131
6.2 Results and Discussion	133
6.2.1 <i>Preparation and Properties of 6</i>	133
6.2.2 <i>Catalytic Activity in the Bleaching of Orange II with H<sub>2</sub>O<sub>2</sub></i>	136
6.2.3 <i>Hydrolytic Stability of 6 in Acidic Solution</i>	140
6.3 Conclusions	142
6.4 Experimental	143
6.4.1 <i>Materials and Methods</i>	143
6.4.2 <i>Synthesis of 6</i>	143
6.4.3 <i>Acid Induced Demetalation</i>	145
6.5 References	146

## CHAPTER 7

<b>Lifetime Studies of NewTAML Activators</b>	148
7.1 Introduction	149
7.2 Results and Discussion	153
7.2.1 <i>Identification of the NewTAML Oxidative Inactivation Pathway</i>	153
7.2.2 <i>Nucleophilic Attack Inactivation Pathway in NewTAMLs</i>	157
7.2.3 <i>Kinetic Analysis of Catalyst Inactivation</i>	160
7.2.4 <i>Effect of oxidative inactivation on a tetrasulfonamide NewTAML</i>	167

7.3	Conclusions.....	169
7.4	Experimental.....	170
	7.4.1 <i>Materials and Methods</i> .....	170
	7.4.2 <i>Preparation of 8</i> .....	170
7.5	Appendix.....	173
7.6	References.....	174

## TABLE OF FIGURES

Figure 1.1 Comparison of percent removal of pollutants by TAML/H <sub>2</sub> O <sub>2</sub> from London wastewater.....	9
Figure 1.2 TAML activators discussed in this work .....	14
Figure 1.3 Mechanism of catalysis by TAML activators, including pathways of inactivation.....	15
Figure 1.4 One of the first <i>tetraamido macrocyclic ligands</i> (TAMLs), developed in 1989 .....	16
Figure 1.5 Iterative design process for TAML activators. ....	17
Figure 1.6 Speciation of Orange II in aqueous solution.....	19
Figure 1.7 Tiered Protocol for Endocrine Disruption (TiPED).....	21
 Figure 2.1 TAML activators mentioned in this chapter.....	 34
Figure 2.2 ORTEP representation of <b>7c</b> .....	35
Figure 2.3 Spectra of <b>7a</b> ( $6.3 \times 10^{-5}$ M) as a function of pH in 0.01 M phosphate buffer at 25 °C. ....	37
Figure 2.4 General stoichiometric mechanism of catalysis by TAML activators .....	39
Figure 2.5 The steady-state rate of <b>7a</b> -catalyzed Orange II bleaching by H <sub>2</sub> O <sub>2</sub> as a function of Orange II concentration.....	40
Figure 2.6 Rate constants $k_I$ (A) and $k_{II}$ (B) measured for <b>7a</b> -catalyzed bleaching of Orange II as a function of pH at 25 °C.....	41
Figure 2.7 Stoichiometric mechanism of catalysis by <b>7a</b> ( $k_I$ step).....	42
Figure 2.8 Spectra of <b>7b</b> ( $5.7 \times 10^{-6}$ M) at different pH at 25 °C and 0.01 M phosphate buffer.....	45
Figure 2.9 Spectra of <b>1a</b> ( $5.0 \times 10^{-5}$ M) at different pH at 25 °C and 0.0175 M wide range buffer.....	45
Figure 2.10 Spectra of <b>1b</b> ( $5.5 \times 10^{-5}$ M) at different pH at 25 °C and 0.0175 M wide range buffer. ....	46
Figure 2.11 Kinetic curves for incomplete bleaching of Orange II ( $5.4 \times 10^{-5}$ M) by H <sub>2</sub> O <sub>2</sub> (0.013 M) catalyzed by <b>7a</b> .....	49
Figure 2.12 Method of preparation of <b>7</b> .....	54



Figure 3.1 OldTAML structures that informed the design of NewTAMLs. ....	61
Figure 3.2 Linear free energy plot between $k_{II}$ and $k_I$ for OldTAMLs <b>1</b> , <b>3</b> , <b>5</b> , and <b>7</b> at 25 °C and pH 7.....	62
Figure 3.3 Proposed tetrasulfonamide ligand analogs of <b>1</b> and <b>7</b> .....	64
Figure 3.4 General preparation of TAML activators <b>1</b> .....	65
Figure 3.5 Investigated methods of preparation for 2-aminopropane-2-sulfonic acid via 2-propanimine .....	66
Figure 3.6 Failed preparation for sulfonamide NewTAML arms requiring bromination at step (a) that is not feasible due to steric constraints.....	67
Figure 3.7 A model synthetic procedure for the preparation of NewTAML head and arms with aniline as a model starting material. ....	68
Figure 3.8 Proposed procedure for preparation of an armless sulfonamide ligand intermediate that decomposed at step iv .....	69
Figure 3.9 Proposed methods of preparation of imido-bis(sulfuric acid) dichloride <b>M</b> and its methylated analog <b>N</b> .....	70
Figure 3.10 Proposed methods of preparation of sulfonic acid chloride analogs of compound <b>D</b> .....	71
Figure 3.11 Methods of preparation of NewTAMLs <b>2</b> and <b>4</b> following standard procedures for OldTAMLs .....	72
Figure 3.12 Typical preparation of TAMLs <b>5</b> .....	73
Figure 3.13 Preparation of NewTAML <b>6</b> following standard procedures for OldTAML <b>5</b> with pyridine as a base during cyclization.....	73
Figure 3.14 Preparation of NewTAML <b>8</b> following standard procedures for OldTAML <b>5</b> with pyridine as a base during cyclization.....	74
Figure 4.1 General mechanism of catalysis of OldTAMLs <b>1</b> and NewTAMLs <b>2</b> with substrates studied in this chapter.....	80
Figure 4.2 ORTEP diagram of <b>2a</b> .....	81
Figure 4.3 3D mesh plot of the initial rate of Orange II bleaching by $2.6 \times 10^{-8}$ M <b>2a</b> (a) and $2.3 \times 10^{-8}$ <b>2b</b> (b) with H <sub>2</sub> O <sub>2</sub> in pH 7 0.01 M phosphate at 25°C as functions of H <sub>2</sub> O <sub>2</sub> and Orange II concentrations. ....	82
Figure 4.4 Determination of pK <sub>a</sub> of <b>2b</b> ( $4.4 \times 10^{-5}$ M) with varying pH in 0.01 M phosphate 25°C.....	83

Figure 4.5 Comparison of the Technical Performance Parameters for NewTAMLs in the bleaching of Orange II with H <sub>2</sub> O <sub>2</sub> at 25°C .....	84
Figure 4.6 Comparison of $k_i$ for NewTAMLs in the bleaching of Orange II with H <sub>2</sub> O <sub>2</sub> at 25°C for pH 6–11.5.....	85
Figure 4.7 Degradation of propranolol by TAMLs ( $1.0 \times 10^{-7}$ M) with H <sub>2</sub> O <sub>2</sub> in HPLC-grade purified water over 75 minutes (a) and 1440 minutes (24 hours) (b) at pH 7.....	87
Figure 4.8 Degradation of propranolol by TAMLs ( $1.0 \times 10^{-7}$ M unless otherwise indicated) and H <sub>2</sub> O <sub>2</sub> in propranolol-spiked Allegheny River water at pH 7...	88
Figure 4.9 Body weight and liver and kidney weights in animals exposed to higher concentrations of <b>2a</b> without EE2.....	90
Figure 4.10 Uterine weight on postnatal day 22 after 3 days of EE2 treatment.....	91
Figure 4.11 Body weight and uterine weight at the time of tissue collection on postnatal day 22.....	92
Figure 4.12 Suppression of the uterotrophic response to EE2 by pretreatment of EE2 with 4 nM or 40 nM <b>2a</b> and 1 mM H <sub>2</sub> O <sub>2</sub> as a percentage of the full uterotrophic response to EE2.....	93
Figure 4.13 General method for preparation of <b>2</b> .....	97
Figure 5.1 Old- and NewTAML activators discussed in this chapter .....	108
Figure 5.2 Mechanism of catalysis of TAMLs discussed in this chapter.....	109
Figure 5.3 Comparison of degradation of propranolol (15 ppb, $\sim 5 \times 10^{-8}$ M) with TAMLs ( $1.0 \times 10^{-7}$ M) and H <sub>2</sub> O <sub>2</sub> ( $3.3 \times 10^{-4}$ M) in pH 7 HPLC-grade purified water at 25 °C .....	110
Figure 5.4 Spectra of <b>2a</b> (A) and <b>4</b> (B) at varying pH in 0.01 M phosphate buffer at 25 °C .....	113
Figure 5.5 EPR spectra of <b>2a</b> at pH 7.5 (top) and pH 10.5 (bottom) .....	114
Figure 5.6 Dependence of $k_{\text{obs}}$ on [HClO <sub>4</sub> ] for acid induced demetalation of <b>2a</b> and <b>2b</b> (A) and <b>3</b> and <b>4</b> (B) at 25 °C.....	117
Figure 5.7 The initial rates of Orange II bleaching with <b>2c</b> ( $1 \times 10^{-7}$ M) and H <sub>2</sub> O <sub>2</sub> ( $1.5 \times 10^{-3}$ M) as a function of Orange II concentration with 0.01 M pH 7 phosphate at 25 °C .....	119
Figure 5.8 Rate constant $k_i$ measured for <b>1b</b> , <b>2a</b> , and <b>2b</b> in the catalyzed bleaching of Orange II by H <sub>2</sub> O <sub>2</sub> at 25 °C in 0.01 M phosphate.....	120

Figure 5.9 Mechanism of reaction of TAMLs with H <sub>2</sub> O <sub>2</sub> described by $k_1$ .....	121
Figure 5.10 Linear free energy relationship between $k_1$ and $k_{II}$ for TAMLs of the <b>1–4</b> structural families measured at pH 7 and 25 °C .....	124
Figure 5.11 Linear free energy relationships between $k_1$ or $k_{II}$ and $pK_a$ for TAMLs of the <b>1–4</b> structural families measured at pH 7 and 25 °C .....	124
Figure 5.12 Preparation of <b>4</b> .....	127
Figure 6.1 Old- and NewTAML activators discussed in this chapter .....	132
Figure 6.2 Method of synthesis of <b>6</b> .....	133
Figure 6.3 pH titration of <b>6</b> at 25°C with 0.01 M phosphate.....	135
Figure 6.4 Initial rates of <b>6</b> -catalyzed bleaching of Orange II with H <sub>2</sub> O <sub>2</sub> as a function of [H <sub>2</sub> O <sub>2</sub> ] and [Orange II] with <b>6</b> ( $2.2 \times 10^{-7}$ M) at pH 7 and 25 °C with 0.01 M phosphate .....	137
Figure 6.5 Mechanism of catalysis of TAMLs.....	137
Figure 6.6 Mechanism of reaction of TAML with H <sub>2</sub> O <sub>2</sub> described by $k_1$ . ....	139
Figure 6.7 Rate constant $k_1$ measured for <b>6</b> in the catalyzed bleaching of Orange II by H <sub>2</sub> O <sub>2</sub> at 25 °C in 0.01 M phosphate .....	140
Figure 6.8 Dependence of $k_{obs}$ on [HClO <sub>4</sub> ] for acid induced demetalation of <b>6</b> at 25 °C. .....	141
Figure 7.1 Old- and NewTAML activators discussed in this chapter .....	150
Figure 7.2 Mechanism of catalysis of TAMLs discussed in this chapter.....	150
Figure 7.3 Comparison of $k_{II}$ and $k_i$ for <b>1c</b> (A) and <b>2b</b> (B) in the bleaching of Orange II with H <sub>2</sub> O <sub>2</sub> with 0.01 M phosphate at 25 °C.....	154
Figure 7.4 Linear free energy diagram of log $k_{II}$ vs log $k_i$ for <b>1c</b> and <b>2b</b> at various pH. ....	155
Figure 7.5 H/D exchange of methylene protons in D <sub>2</sub> O for ligand <b>A</b> .....	157
Figure 7.6 Linear free energy plot of $k_{II}$ vs. $k_i$ for TAMLs at pH 7 and 25°C .....	159
Figure 7.7 Dependence of $k_i$ on [H <sub>2</sub> O <sub>2</sub> ] in the incomplete bleaching of Orange II ( $5.0 \times$ $10^{-5}$ M) with <b>2b</b> ( $5 \times 10^{-8}$ M), <b>2d</b> ( $5 \times 10^{-8}$ M), and <b>6</b> ( $5 \times 10^{-9}$ M) at pH 7 and 25 °C with 0.01 M phosphate .....	160
Figure 7.8 Stoichiometric mechanism of the inactivation of the active catalyst <b>2b</b> and <b>2d</b> .....	162

Figure 7.9 Dependence of the values of $k_{i0}$ and $k_{iP}$ from Table 7.3 on $[\text{OH}^-]$ for <b>2b</b> fit to Equation 7.3 and Equation 7.4, respectively.....	165
Figure 7.10 3D mesh of the dependence of $k_i$ on $[\text{H}_2\text{O}_2]$ and $[\text{OH}^-]$ fit to Equation 7.5 for <b>2b</b> at pH 7.0–10.25 with 0.01 M phosphate or Carmody buffer at 25 °C ....	167
Figure 7.11 Tetrasulfonamide NewTAML <b>8</b> .....	168
Figure 7.12 Preparation of <b>8</b> .....	170
Figure 7.13 Dependence of $k_i$ on $[\text{H}_2\text{O}_2]$ in the incomplete bleaching of Orange II ( $5.0 \times 10^{-5}$ M) with <b>2b</b> ( $5 \times 10^{-8}$ M) at pH 7 and 25 °C with 0.01 M phosphate or Carmody buffer fit to Equation 7.2.....	173

## TABLE OF TABLES

Table 1.1 Endocrine disrupting micropollutants present in wastewater treatment effluent around the world.....	10
Table 1.2 Compounds oxidized by TAML activators in aqueous solutions .....	13
Table 1.3 Rate constants for TAMLs that predate this work in the degradation of Orange II with H <sub>2</sub> O <sub>2</sub> at pH 7 and 25 °C .....	19
Table 2.1 Values of pK <sub>a</sub> and rate constants $k_I$ and $k_{II}$ for the TAML-catalyzed oxidative bleaching of Orange II by H <sub>2</sub> O <sub>2</sub> in 0.01 M phosphate buffer at 25 °C .....	47
Table 4.1 Rate constants $k_I$ and $k_{II}$ for all catalysts discussed in this chapter at pH 7 in the bleaching of Orange II with H <sub>2</sub> O <sub>2</sub> at 25 °C .....	82
Table 5.1 Parameters for TAMLs at 25°C. Values of $k_I$ and $k_{II}$ are for Orange II bleaching in 0.01 M phosphate at pH 7 .....	120
Table 5.2 Rate constants (in M <sup>-1</sup> s <sup>-1</sup> ) for the interaction of TAML with H <sub>2</sub> O <sub>2</sub> at pH 7 with 0.01 M phosphate at 25°C .....	122
Table 6.1 Parameters for TAMLs at 25°C. Values of $k_I$ and $k_{II}$ are for Orange II bleaching with H <sub>2</sub> O <sub>2</sub> in 0.01 M phosphate at pH 7.....	138
Table 7.1 Rate constant $k_{II}$ and $k_I$ for TAMLs at pH 7 and 25 °C for the catalyzed bleaching of Orange II with H <sub>2</sub> O <sub>2</sub> .....	153
Table 7.2 Values of $k_{i0}$ , $K_P$ , and $k_{iP}$ for TAMLs at pH 7 and 25 °C generated from Equation 7.2.....	163
Table 7.3 Values of $k_{i0}$ , $K_P$ , and $k_{iP}$ for <b>2b</b> from pH 7.0–10.25 using Equation 7.2 .....	164

## ABBREVIATIONS

Ac	active catalyst
Boc	t-butyloxycarbonyl
BPA	bisphenol A
DABCO	1,4-diazabicyclo[2.2.2]octane
DABSO	1,4-diazabicyclo[2.2.2]octane bis(sulfur dioxide)
DDT	dichlorodiphenyltrichloroethane
DICL	diclofenac
ED	endocrine disruptor
EE2	ethinylestradiol
EPR	electron paramagnetic resonance
ERY	erythromycin
ESI-MS	electrospray ionization mass spectrometry
GD	gestation day
HPLC	high performance liquid chromatography
IGS	Institute for Green Science
LFER	linear free energy relationship
NMR	nuclear magnetic resonance
PD	postnatal day
PRO	propranolol
Rc	resting state catalyst
TAML	tetraamido macrocyclic ligand
TBHP	<i>t</i> -butyl hydroperoxide
TiPED	Tiered Protocol for Endocrine Disruption
TRI	triclosan
YES	Yeast Estrogen Screen

# **CHAPTER 1**

## **TAML Activators as a Sustainable Solution to Contamination of Water by Micropollutants**

## 1.1 Introduction

The first aniline dye mauveine was fortuitously discovered by William Henry Perkin, a nineteen-year-old student of chemistry, in 1856. Soon after, brilliant purple dye colored the clothing of Londoners and, presumably, the canal adjacent to the dyeworks.<sup>1</sup> Mass production of mauveine and other synthetic textile dyes helped spur the beginning of the modern chemical enterprise, giving rise to industry giants such as BASF (*Badische Anilin- und Soda-Fabrik*, for the aniline used in dye production).<sup>2</sup> Since the late 1800s, billions of tons of anthropogenic chemicals have been manufactured, mainly from petrochemicals, and marketed to consumers with the promise of “better living through chemistry.”<sup>3</sup> Pesticides, plastics, building materials, surfactants, flavorings, and cosmetics are just a few of the classes of synthetic chemicals that have made modern life easier, tastier, and more beautiful.

From the shipment of its first revenue-earning consignment in 1857, mauveine was a quick commercial success, but it wasn’t until the 1890s in Europe and early 1900s in America that the carcinogenicity of aniline dyes and the risk posed to workers was discovered.<sup>4</sup> Even after the causal link between employment in a dye production facility and a rare bladder cancer became clear, the industry suppressed or denied all scientific findings that would have compromised profits, a practice that has become the industry standard.<sup>4</sup> Since its inception, the chemical industry has prioritized profits by disregarding the health and environmental effects of its activities, deeming its products innocent until proven harmful and running interference when harm became apparent. This precedence of technical and economic performances of chemical technologies over



health and environmental effects has turned humans, wildlife, and entire ecosystems into unwitting guinea pigs.<sup>5</sup>

Public ignorance of the effects of chemical products on the environment was interrupted in the 1960s with the publishing of the landmark environmental exposition Silent Spring. Rachel Carson expounded on the effects of manmade chemicals, especially pesticides, on wildlife and human health, accusing government officials and consumers of accepting the poisonous offerings of the chemical industry without question in exchange for “better living.”<sup>6</sup> The revelations in Silent Spring on the risks of pesticides in the present and future helped lead to the formation of the US Environmental Protection Agency and spurred the environmental movement of the 1970s.

## 1.2 Sustainability Ethics

*“We stand now where two roads diverge. But unlike the roads in Robert Frost's familiar poem, they are not equally fair. The road we have long been traveling is deceptively easy, a smooth superhighway on which we progress with great speed, but at its end lies disaster. The other fork of the road — the one less traveled by — offers our last, our only chance to reach a destination that assures the preservation of the earth.”*

- Rachel Carson, Silent Spring

Rachel Carson recognized that the impacts of persistent pesticides such as dichlorodiphenyltrichloroethane (1,1'-(2,2,2-trichloroethane-1,1-diyl)bis(4-chlorobenzene, or DDT) would extend far into the future. Although DDT was phased out in the United States starting in 1972, DDT and its breakdown products are still regularly detected in the Great Lakes.<sup>7</sup> Other industrial, agricultural, and consumer chemical products, including the aniline dyes discussed above, lead paint, vinyl chloride, and perfluorooctanoic acid, have been found deep into their commercial lifetimes to pose serious health and environmental hazards.<sup>4,8-10</sup> In the quote above, the road less traveled is the one of precaution against these health and environmental risks that jeopardize the future of our world. Ironically, post-commercialization restriction and cleanup are infinitely more difficult than performing toxicological and ecological screenings during development, but the industrial chemical complex is focused only on short-term profits.<sup>11</sup> Unfortunately, the industry has not been sufficiently required to internalize the costs

associated with its destructive practices and will continue to operate in this manner until legislatively or economically forced to consider its negative, long-term effects.

Consequently, fifty years after the publication of Silent Spring, we are still barreling down the “easy” road that will ultimately lead to a more difficult future. Preserving environmental health and the future of our civilization requires the incorporation of sustainability into modern development sooner rather than later.<sup>5,12</sup> For chemists and the chemical enterprise, this requires a modification of priorities to incorporate safety and sustainability into modern products and processes. Truly sustainable chemistry requires interdisciplinary, trans-sectorial, and cross-cultural collaborations in design, stewardship, and regulation of the chemical enterprise to prioritize future health and environmental integrity over present profits.<sup>5</sup>

The field of green chemistry, established in the early 1990s, provides a solid foundation for orienting industrial synthetic chemistry toward sustainability. The “12 Principles of Green Chemistry” guide chemists toward reducing or avoiding the use or production of hazardous substances, minimizing waste, and considering the entire lifecycle of a chemical product.<sup>13</sup> Applying green chemistry practices to industrial chemical production is especially effective at reducing occupational hazards in the chemical industry. However, the narrow synthetic focus of these principles renders them inadequate for protecting future generations and vulnerable wildlife populations from the long-term effects of chemical technologies. Future-proof sustainable chemistry requires collaborations between green chemistry and the fields of environmental health sciences to incorporate protections against the destruction described in Silent Spring from chemical products like DDT. The TAML activators described in this work exemplify the

technological achievements possible through the practice of sustainable chemistry.

TAML catalysis is an example of modern sustainable chemical technology, designed for remediation and pollution prevention, that has been intentionally designed to incorporate protections against future harm without compromising remarkable technical and cost performance.

### 1.3 Micropollutants as a Global Water Treatment Challenge

One consequence of over one hundred years of predominating human disregard for the effects of modern society on the environment is worldwide water pollution. In particular, micropollutants, substances present in tiny concentrations (ng–µg/L) that have undesired effects, present a major risk in both developed and developing nations.<sup>14–17</sup> Common micropollutants include pesticides, pharmaceuticals, industrial chemicals, and personal care products; many are also endocrine disruptors (EDs), chemicals that can interfere with the action of hormones in biological systems.<sup>18</sup> The presence of micropollutants in water at small concentrations of ng–µg/L is especially concerning because hormones operate in the body at similar concentrations of low ng/L, posing an extraordinary risk during reproduction and development. The ability of measurable amounts of micropollutants to act as EDs defies the traditional toxicology axiom of “the dose makes the poison.”<sup>19</sup> In fact, these low doses can and often do elicit stronger biological responses than larger doses, a phenomenon called a non-monotonic dose response.<sup>19</sup> As a result of these properties, the endocrine disrupting micropollutants present in environmental waters, wastewater, and even finished waters can have adverse health effects in humans and wildlife.<sup>17,20</sup>

For example, male fish in rivers around the world have become feminized due to exposure to estrogen mimicking compounds including 17 $\alpha$ -ethinylestradiol (EE2), nonylphenol (4-(2,4-dimethylheptan-3-yl)phenol), and bisphenol A (BPA).<sup>21–23</sup> This effect is most noticeable downstream from wastewater treatment plants because of the ineffectiveness of conventional water treatment methods at removing these compounds.<sup>20,22</sup> Many of the micropollutants that are removed during water treatment are

absorbed into sludge and later reintroduced into the environment in the form of agricultural fertilizer.<sup>24–26</sup> Table 1.1 gives examples of common micropollutants that are ineffectively removed during wastewater treatment around the world.

For many of these pollutants, effective removal is only achieved through the use of advanced treatment, such as activated carbon and advanced oxidation processes.<sup>27</sup> Ozone is the most widely used advanced treatment in countries such as the Netherlands, Germany, and Switzerland that have taken explicit steps towards micropollutant removal.<sup>28</sup> However, ozone and other advanced treatment options are prohibitively expensive in all but the most affluent countries.<sup>29,30</sup> Furthermore, wastewater effluent in these more conscientious countries is already of high quality before micropollutant treatment upgrades; municipalities with dirtier effluent require even more expensive ozone treatment and are at risk for hazardous byproduct formation due to partial oxidation or reaction with chlorine or bromide.<sup>31</sup>

Effective treatment of micropollutants in waste streams worldwide will require a solution that is affordable in both capital and operating costs as well as safe for use on effluents of varying quality. The TAML activators presented here are one oxidative technology that promises to fulfill both requirements. In a pilot study of UK municipal wastewater, an older, lower performance TAML iteration than presented in this thesis was compared to ozone treatment in the removal of target micropollutants (Figure 1.1).<sup>32</sup> The ozone results were obtained from the only UK ozone pilot plant of the time at Hallam Fields in Ilkeston, Derbyshire while the TAML/peroxide results were obtained from an old low-performance plant in the London system. The results in Figure 1.1 show that TAML treatment of a dirty conventional waste stream is approximately equivalent to

the ozone pilot plant. Furthermore, as discussed later, wastewater treatment with TAML activators is expected to be significantly cheaper than ozone.

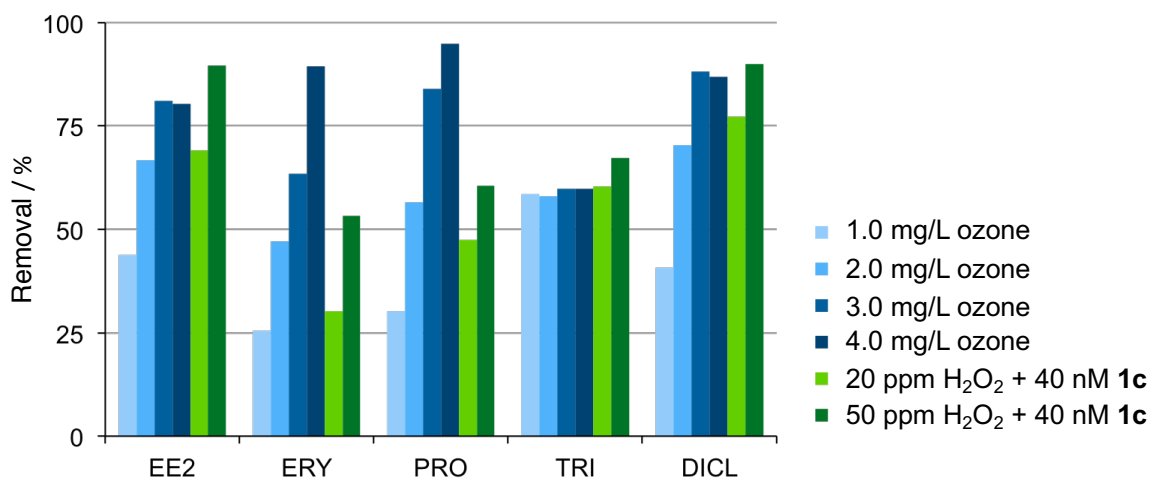


Figure 1.1 Comparison of percent removal of ethynylestradiol (EE2), erythromycin (ERY), propranolol (PRO), triclosan (TRI), and diclofenac (DICL) with ozone (blue) and TAML **1c** (see Section 1.4 and Figure 1.2 below) with H<sub>2</sub>O<sub>2</sub> (green) from London wastewater. At face value, 20 mg/l H<sub>2</sub>O<sub>2</sub> is approximately equivalent to 2.0 mg/l ozone, but it is important to note that the two waste streams were not of equivalent quality. Adapted from ref 32.

Table 1.1 Endocrine disrupting micropollutants present in wastewater treatment effluent around the world.

Class	Compound	Site	Effluent concentration (µg/L)	% removal	ED action	Endpoints affected	Ref.
Pharmaceutical	Ethinylestradiol (EE2)	China, France, Germany, Italy, Sweden, US	<0.001–0.002	43.8–100	Estrogenic	Male development (fish)	20,23
Pharmaceutical	Propranolol	US, UK, Germany	0.0044–1.90	0–94	unknown	Fish development	20,33–37
Personal care product	Triclosan	Spain, UK, US, Greece, Korea, France, EU	0.01–6.88	71.3–99.2	Antithyroid, androgenic, estrogenic	Increased uterine response to EE2	18–20
Industrial chemical	Nonylphenol	China, France, Germany, Greece, Italy, Spain, US, Balkans	<0.03–7.8	21.7–99	Binds estrogen receptor	Testosterone metabolism	19,20,38
Industrial chemical	Bisphenol A (BPA)	China, France, Greece, US, Balkans	<0.03–1.10	62.5–99.6	Binds nuclear and nonsteroid receptors, nongenomic pathways, ion channels	Prostate, mammary gland, brain development and behavior, reproduction, immune system, metabolism	18–20
Plasticizer	Di(2-ethylhexyl) phthalate (DEHP)	Austria, China, US	0.0001–54.0	25–97	Bind nuclear receptors	Male and female development, reproduction, metabolism	18,20
Pesticide	Atrazine	EU, France, Spain, Switzerland, Balkans	0.004–0.73	<0–25	Increases aromatase expression	Male sexual differentiation and development	18–20
Pesticide	Imidacloprid	US, China	0.045–0.106	0	unknown	Male and female reproduction and development (rats)	39–44



## 1.4 The TAML Activator Solution

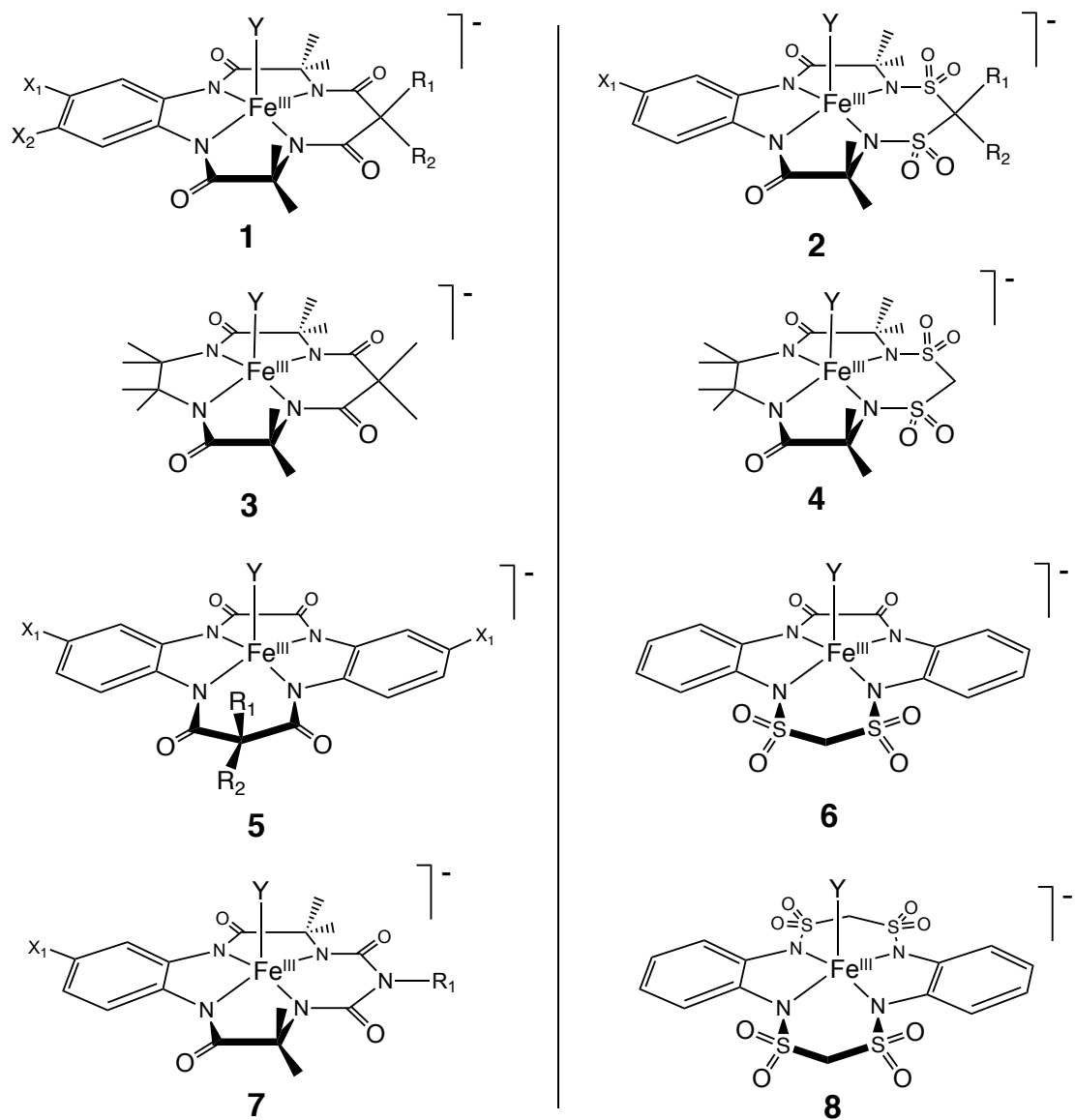
TAML activators (Figure 1.2), the first fully functional small molecule mimics of nature's oxidizing enzymes, are a promising accessible and affordable solution for removing micropollutants from waters around the world. TAML activators were designed over twenty years ago at the Institute for Green Science at Carnegie Mellon University to harness the major oxidants of nature, hydrogen peroxide and dioxygen, to perform safe and efficient oxidation chemistry.<sup>45</sup> To date, the catalytic activation of hydrogen peroxide to deliver efficient peroxide-like catalysis has been effectively mastered, while the enzyme mimicking activation of dioxygen is still in its infancy in TAML science. Unlike to chlorine-based oxidation processes, biochemical oxidations such as those performed by cytochrome P450 and peroxidase enzymes rarely produce persistent, bioaccumulative toxicants. Thus, enzyme-mimicking oxidation by TAML activators is less likely to generate hazardous byproducts.<sup>46</sup> This makes TAML processes well suited for remediation of aqueous micropollutants, provided that TAMLs and their degradation products are not themselves toxic. TAML activators have been shown to oxidize a wide range of substrates in water at low nanomolar concentrations, including estrogens, pesticides, pharmaceuticals, and bacterial spores (Table 1.2).

The remarkable oxidation chemistry performed by these catalysts is enabled by the structural design. TAML activators are composed of a highly oxidation resistant macrocyclic ligand featuring four negatively charged nitrogens complexed with an Fe<sup>III</sup> atom (Figure 1.2). This configuration resembles the porphyrin active center of peroxidases, but the rigidity of the TAML tetra-anion makes higher oxidation states more accessible. In general, the redox couple for iron-TAML systems fall at similar potentials

to porphyrins at one oxidation state lower, i.e. the  $\text{Fe}^{\text{IV/III}}$ -TAML formal reduction potentials are similar to those of the  $\text{Fe}^{\text{III/II}}$ -porphyrins. This enables the TAML iron center to easily access the higher oxidation states of V and IV to reproduce the key states in the catalytic cycle of peroxidase enzymes, namely Compounds I and II, respectively.<sup>47</sup> Despite the fact that the added donor capacity of the TAML systems should mute the comparative reactivity of high valent iron-TAML complexes, the reactivity remains extremely high, especially for the  $\text{Fe}^{\text{V}}$  state. This achievement is key to the remarkable catalytic efficiency of TAMLs.<sup>48</sup> No wasteful Fenton chemistry occurs, which involves the hydroxyl radical as a key oxidizing intermediate and proceeds with background disproportionation of  $\text{H}_2\text{O}_2$  to oxygen and water. Nor are large quantities of hydroxyl radicals formed.<sup>49</sup> After the active catalyst species oxidizes a substrate, the  $\text{Fe}^{\text{III}}$  resting catalyst is returned often with engagement of  $\text{Fe}^{\text{IV}}$  in its own oxidation processes as with Compound II. The two processes of catalyst activation and reaction with substrate are described by the rate constants  $k_{\text{I}}$  and  $k_{\text{II}}$ , respectively (Figure 1.3). Additionally, TAML activators eventually inactivate in solution. Inactivation from the resting state occurs via general acid (buffer induced) or specific acid (proton induced) demetalation, described by  $k_{\text{b}}$  and  $k_{\text{d}}$ , respectively (Figure 1.3). In the active state, the dominant inactivation pathway depends on the concentration of catalyst used. If the initial catalyst concentration exceeds ca.  $1 \times 10^{-6}$  M, the dominant pathway is intermolecular in catalyst and described by  $k_{2\text{i}}$ . If the initial catalyst concentration is less than ca.  $1 \times 10^{-6}$  M, the dominant pathway is unimolecular in catalyst and described by  $k_{\text{i}}$ .<sup>50,51</sup> Since most processes for TAML treatment of contaminated waters employ catalyst concentrations of less than  $1 \times 10^{-6}$  M, the latter  $k_{\text{i}}$  pathway typically determines the lifetime of functioning TAML catalysts.

Table 1.2 Compounds oxidized by TAML activators in aqueous solutions.

Class	Compound	Where found or used	References
Chlorophenols	Pentachlorophenol 2,4,6-Trichlorophenol	Pesticides, disinfectants, preservatives, personal care products	52
Dibenzothiophene derivatives	Dibenzothiophene 4-Methyl-dibenzothiophene 4,6-Dimethyl-dibenzothiophene	Diesel fuel	53
Bacterial spores	<i>Bacillus atrophaeus</i>	Anthrax surrogate	54
Organophosphorous pesticides	Fenitrothion Parathion Chlorpyrifos methyl Chlorpyrifos formulation (Pestban)	Insecticides	55,56
Azo and other dyes	Orange II Safranin O Pinacyanol chloride Tartrazine	Textile dyes	50,57–59
Steroid	Ethinylestradiol (EE2) Estradiol (E2) Estril Estrone	Pharmaceutical Natural hormones	60,61
Nitroaromatics	2,4,6-trinitrotoluene 1,3,5-trinitrobenzene	Explosives	62
Nitrophenols	Nitrophenols, dinitrophenols 2-Methyl-4-nitrophenol 3-Methyl- 4-nitrophenol 2,6-Dimethyl-4-nitrophenol 2-Methyl-4,6-dinitrophenol	High volume industrial chemicals	63
Alkaloids	Atropine Scopolamine Tropine Thebaine Oxycodone	Pharmaceuticals	64,65
Diphenyl ether	Triclosan	Personal care products, hospitals	66
Alkylphenol	Nonylphenol	Surfactant	66
Pharmaceuticals	Sertraline Propranolol	SSRI (Zoloft) $\beta$ -blocker (Inderal)	67 this work
Pesticide	Metaldehyde	Molluscicide	51,68
Bisphenol	Bisphenol A Tetrabromobisphenol A	Plasticizer, monomer, industrial chemicals, flame retardant	66,69
Neonicotinoid	Imidacloprid	Insecticide	



	1a	1b	1c	1d	2a	2b	2c	2d	5a	5b	5c	7a	7b	7c
X <sub>1</sub>	H	NO <sub>2</sub>	NO <sub>2</sub>	Cl	H	NO <sub>2</sub>	H	NO <sub>2</sub>	H	NO <sub>2</sub>	Cl	H	NO <sub>2</sub>	H
X <sub>2</sub>	H	H	H	Cl	—	—	—	—	—	—	—	—	—	—
R <sub>1</sub>	CH <sub>3</sub>	CH <sub>3</sub>	F	F	H	H	H	H	CH <sub>3</sub>	CH <sub>3</sub>	CH <sub>3</sub>	CH <sub>3</sub>	CH <sub>3</sub>	Ph
R <sub>2</sub>	CH <sub>3</sub>	CH <sub>3</sub>	F	F	H	H	CH <sub>3</sub>	CH <sub>3</sub>	CH <sub>3</sub>	CH <sub>3</sub>	CH <sub>3</sub>	—	—	—

Figure 1.2 TAML activators discussed in this work. Left: Original carbonamide-containing OldTAML; Right: Sulfonamide-containing NewTAMLs. Y is typically water.

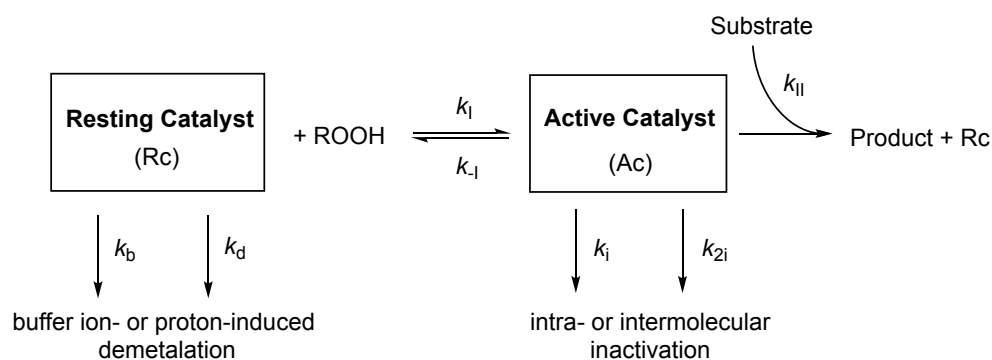


Figure 1.3 Mechanism of catalysis by TAML activators, including pathways of inactivation.

#### 1.4.1 Iterative Design of TAML Activators

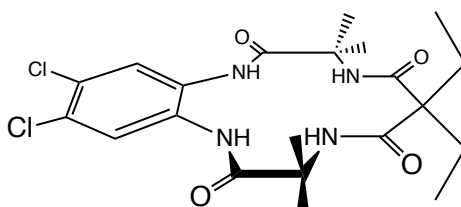
While enzymes contain larger tertiary structures to stabilize and protect the active site, the much smaller TAML catalysts are comprised of only four amino acid equivalent linked to form a macrocycle surrounding the metal center. As a result, the ligand must be extremely resistant to oxidation as well as capable of donating sufficient electron density to the metal center to allow it to support high oxidation states.<sup>70,71</sup> Over the past twenty years, the structure of TAML activators has been iteratively refined to yield more robust catalysts.<sup>70,72</sup> The original TAML ligand design was born from a set of guidelines for preparing suitable ligands for homogeneous metalloreredox-active oxidants developed by Terry Collins in the 1980s and 90s.<sup>70</sup> An iterative design process in which structural weaknesses were identified and fixed in each subsequent generation was instrumental in the development of the ligand protection rules listed below.

Rules for ligand design for oxidizing complexes:

1. No hydrogen atoms should be located on an atom  $\beta$  to the metal center if the bond order can be increased between the  $\alpha$  and  $\beta$  atoms.

2. No heteroatom should be attached to an atom  $\gamma$  to the metal center in a five-membered chelate ring if the heteroatom has a lone pair that could stabilize cleaving of the  $\beta$ - $\gamma$  bond.
3. No heteroatom should be an  $\alpha$  donor in a five-membered chelate ring if it has a lone pair that could stabilize cleaving of the  $\beta$ - $\gamma$  bond.
4. Amido-N chelate donors require stabilization against isomerization.

Following these four rules led TAML development to the structure H<sub>4</sub>[9] (Figure 1.4), a precursor to the prototype Fe-TAML **1**. Ligand H<sub>4</sub>[9] consists of a single macrocycle with strongly donating planar amides (rule 4) which contains strategically placed alkyl groups (rule 1) and does not incorporate heteroatoms in compromising positions (rules 2 and 3).



H<sub>4</sub>[9]

Figure 1.4 One of the first *tetraamido macrocyclic ligands* (TAMLs), developed in 1989.

Although Fe[9] is a successful oxidation catalyst capable of supporting a high oxidation state metal, the active catalysts still undergo slow inactivation that can limit the utility of the catalyst.<sup>48</sup> To inform the design of the next ligand, the iterative design process mentioned above was employed in which catalyst breakdown products were studied to reveal the site of weakness (Figure 1.5). Since Fe[9] was found catalyze the oxidation of nitrile solvents by presence of *t*-butyl hydroperoxide (TBHP), studies of the Fe[9] catalyst inactivation products were conducted in this system. A hydantoin ring-

containing catalyst inactivation product was eventually identified through a combination of infrared spectroscopy, mass spectrometry, and NMR.<sup>48</sup> A mechanism of active catalyst degradation consistent with the formation of the identified product was proposed that involved hydrogen abstraction from the methylene unit of the ethyl group at the malonamide “tail” of the ligand by the oxygen atom bound to the iron center of the active catalyst.<sup>48</sup> To block this weakness, the design of subsequent TAMLs, including the prototype **1a** (Figure 1.2), incorporated methyl R groups in place of the ethyl groups of Fe[**9**].

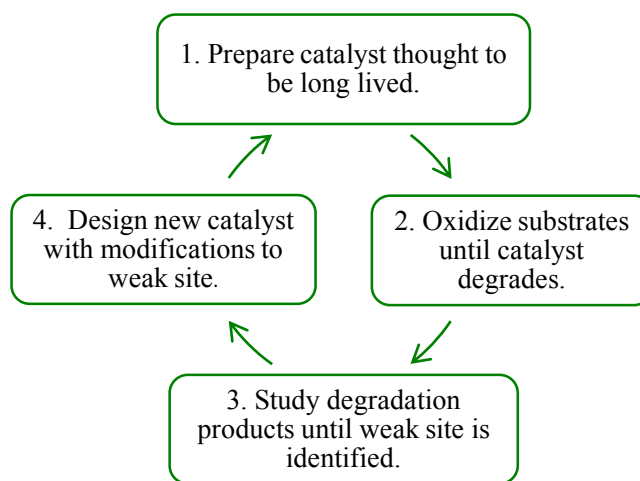


Figure 1.5 Iterative design process for TAML activators.

Although iterative design was successfully employed for the improvement of **9**, direct implementation of the design loop has become more difficult as TAMLs have become more reactive, requiring lower catalyst loadings. In processes developed for the removal of micropollutants, TAMLs are typically employed under ultradilute conditions (pM–low  $\mu$ M).<sup>51</sup> Consequently, isolation and identification of catalyst inactivation fragments is exceedingly difficult. Vulnerable catalyst sites can no longer be determined by direct analysis of inactive catalysts products. There is simply never enough material to

perform the structural analysis of the compounds in the catalyst degradation pathway as was done with **9**. Instead, mechanisms of inactivation must be identified indirectly through studies of the kinetics of the entire catalytic cycle (Figure 1.3) that focus on the relationship between the substrate oxidation and catalyst inaction rate constants  $k_{II}$  and  $k_i$ . NewTAMLs (Figure 1.2), the primary subject of this report, were developed by applying the findings of these studies to the iterative design cycle.

#### 1.4.2 *Orange II as a Tool for Kinetic Comparison of TAMLs*

Investigations of the kinetics of the oxidation of a model substrate by one oxidant catalyzed by a series of different TAMLs are useful for quantitatively comparing the performance of each TAML and deducing relationships between the structural features of the catalysts and reactivity. The azo dye Orange II, which exists predominantly as the keto tautomer in neutral aqueous solution (Figure 1.6), has proven to be a convenient substrate due.<sup>73</sup> The low redox potential of Orange II means that even the least reactive TAMLs can catalyze its oxidation, resulting in a visible reduction in solution color due to loss of the chromophore having an absorption maximum at 480 nm. This change allows the time progress of Orange II oxidation reactions to be easily followed by UV-vis spectrophotometry. From the initial rates of bleaching measured under any one set of conditions, the rate constants  $k_I$ ,  $k_{II}$ , and  $k_i$  in catalysis of the oxidation of Orange II by any TAML can be determined.<sup>57,74</sup> These rate constants have been determined for a broad set of TAMLs. Table 1.3 lists the rate constants for **1**-, **3**-, and **5**-catalyzed oxidation of Orange II by H<sub>2</sub>O<sub>2</sub> at pH 7 and 25 °C.<sup>74</sup>



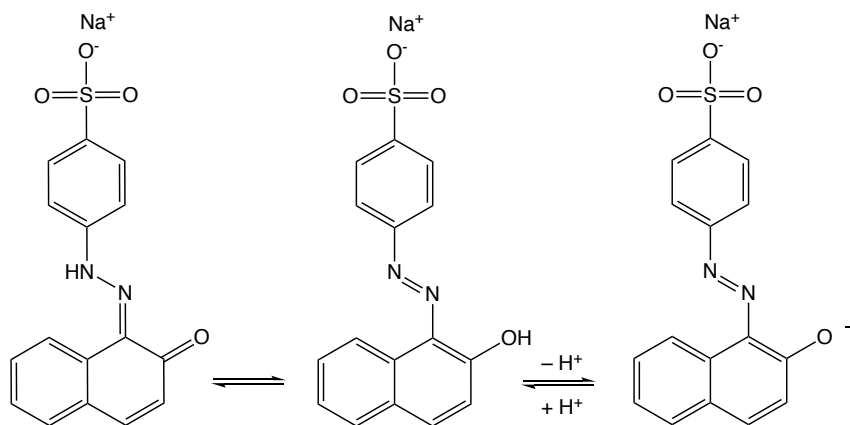


Figure 1.6 Speciation of Orange II in aqueous solution.

Table 1.3 Rate constants for TAMLs that predate this work in the degradation of Orange II with  $\text{H}_2\text{O}_2$  at pH 7 and 25 °C. Adapted from reference 74.

TAML	$\text{X}_1/\text{X}_2/\text{R}_1/\text{R}_2$	$k_1 / \text{M}^{-1} \text{s}^{-1}$	$10^{-4} \times k_{\text{II}} / \text{M}^{-1} \text{s}^{-1}$	$10^3 \times k_i / \text{s}^{-1}$
<b>1a</b>	H/H/Me/Me	$31.4 \pm 0.1$	$0.495 \pm 0.002$	$0.30 \pm 0.01$
<b>1b</b>	$\text{NO}_2/\text{H}/\text{Me}/\text{Me}$	$152 \pm 5$	$2.7 \pm 0.2$	$0.34 \pm 0.02$
<b>1c</b>	$\text{NO}_2/\text{H}/\text{F}/\text{F}$	$350 \pm 2$	$4.1 \pm 0.1$	$1.1 \pm 0.3$
<b>1d</b>	Cl/Cl/F/F	$361 \pm 1$	$12 \pm 1$	$2.50 \pm 0.03$
<b>1e</b>	H/H/Et/Et	$1.8 \pm 0.1$	$0.28 \pm 0.01$	$0.09 \pm 0.01$
<b>1f</b>	$\text{CO}_2\text{CH}_3/\text{H}/\text{Me}/\text{Me}$	$38 \pm 1$	$0.73 \pm 0.01$	$0.11 \pm 0.01$
<b>1g</b>	$\text{NH}_2/\text{H}/\text{Me}/\text{Me}$	$28 \pm 2$	$0.42 \pm 0.02$	$1.15 \pm 0.07$
<b>1h</b>	Me/Me/Me/Me	$49 \pm 3$	$0.90 \pm 0.05$	$0.42 \pm 0.01$
<b>3</b>	- / - /Me/Me	$0.63 \pm 0.02$	$(1.19 \pm 0.03) \times 10^{-4}$	$(4.1 \pm 0.1) \times 10^{-4}$
<b>5a</b>	H/ - /Me/Me	$250 \pm 60$	$0.084 \pm 0.003$	$\sim 6$
<b>5b</b>	$\text{NO}_2/- / \text{Me}/\text{Me}$	$1900 \pm 100$	$52 \pm 7$	$85 \pm 6$
<b>5c</b>	Cl/ - /Me/Me	$1490 \pm 20$	$4.0 \pm 0.2$	$11.0 \pm 0.4$
<b>5d</b>	CN/H/Me	$1850 \pm 90$	$26 \pm 1$	$20 \pm 1$

### 1.4.3 TAML Activators and Endocrine Disruption

The oxidative destruction of endocrine disrupting compounds in water is a major application of TAML activators. Ideally, the catalyzed oxidations will mineralize the ED, producing only non-hazardous H<sub>2</sub>O, CO, CO<sub>2</sub>, small acids, and other minerals such as nitrate or sulfate when heteroatoms are present.<sup>57</sup> The degradation pathways of many of the studied substrates listed in Table 1.2 have been characterized to assess the degree of mineralization and ensure no additional persistent endocrine disrupting compounds have been produced. In many cases, extensive mineralization has been found. Nevertheless, TAMLs and TAML processes have been thoroughly scrutinized to ensure that the catalysts, the catalyst inactivation products, the reaction mixtures, and the final products are free of endocrine disrupting effects.

During the development of TAMLs, a screening method created through collaborations between environmental health scientists and green chemists called the Tiered Protocol for Endocrine Disruption (TiPED) has been employed to ensure that TAMLs are not EDs.<sup>75</sup> The TiPED is a tool that allows chemists to check for endocrine disrupting properties during product development and consists of five levels of increasingly complex scrutiny, from computational assays to in vitro, in vivo, and finally whole animal assays (Figure 1.7) that cover all mechanisms and endpoints of endocrine disruption. If a compound in development fails any one test, these screens allow the designer to obtain the knowledge necessary to design away from the observed toxicity. By incorporating studies of toxicity into all stages of the design process, chemists can assess the balance of the technical, cost, health, and environmental performances of a technology before deployment to build a higher level of safety into the product. Giving

equal or greater weight to health and environmental performance during product design is necessary for ending the current destructive practice of determining utility and commercial viability before toxicity is even considered.

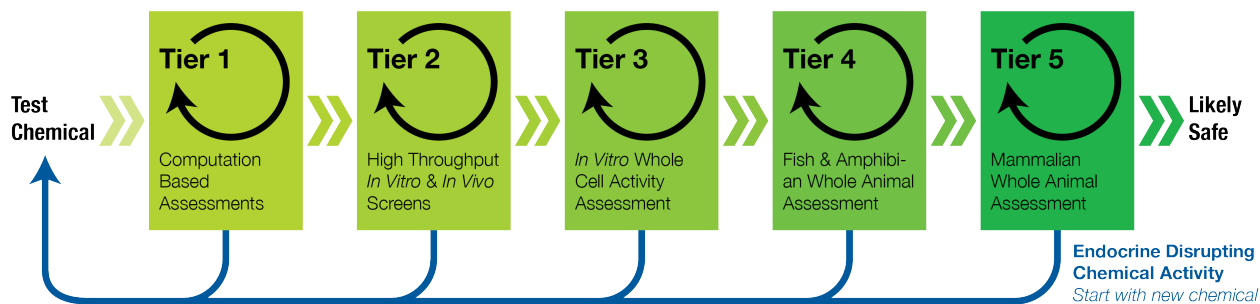


Figure 1.7 Tiered Protocol for Endocrine Disruption (TiPED). Image courtesy of Nicole Reading.

This is precisely how the TiPED has been deployed during TAML development. To ensure that TAMLs are not endocrine disruptors, the catalysts themselves have been subject to most levels of TiPED screening, most notably to fish and mammalian studies where the latter are described herein. In 2010, receptor binding assays for mammalian thyroid, androgen, and estrogen pathways were performed on **1a**, **1d**, and **5b**. None of the catalysts studied induced reporter gene activity.<sup>76</sup> However, a 2013 developmental zebrafish study did indicate that highly halogenated TAMLs with chlorine substituents in the X positions (**1d** and **5c**) significantly impacted fish development.<sup>77</sup> As a result, no further chlorine-containing TAMLs have been produced. Furthermore, in accordance with the precautionary principle, all halogens containing catalysts including the fluorine containing activators have been deemed unfit for scaled water treatment use despite superior, at the time, technical performances.<sup>46</sup>

In addition to testing the parent catalysts for toxicity, tests such as the Yeast Estrogen Screen (YES) have been performed on reaction and product mixtures to check for the formation of estrogenic intermediates and products. For example, long-lived estrogenic compounds such as EE2 may be readily transformed into additional endocrine disrupting molecules. As part of a study on the breakdown of EE2 by **1**/H<sub>2</sub>O<sub>2</sub>, estrogenicity of the reaction mixture as a function of time was tracked with periodic YES assays. Although short-lived estrogenic compounds were produced during the catalytic breakdown experiment, the final products showed no estrogenic activity.<sup>61</sup> Tests as illustrated in this study that identify the structures of the intermediates and/or the overall endocrine disrupting properties of the intermediate solutions are exceedingly important to ensure that TAML treatments do not create additional persistent endocrine disrupting products.

The toxicity of final TAML/H<sub>2</sub>O<sub>2</sub> treatment solutions have also been assessed for toxicity using flow through experiments similar to real world water treatment processes. In these experiments, the effects of ED-laced water on test animals are compared to ED-laced water that has been treated with TAML/H<sub>2</sub>O<sub>2</sub> before the water is administered to the animals. At this point, all TAML has been inactivated; the animals are exposed to substrate and TAML degradation products as well as any remaining peroxide in solution. These tests have been performed on **1c**/H<sub>2</sub>O<sub>2</sub> treated EE2-laced waters to determine if TAML treatment protects against the feminization of male fish by EE2 such as that occurring in environmental waters due to waste water treatment plant effluent discharge.<sup>61</sup> While male fish subject to EE2-laced water showed increased egg protein levels, a biomarker for exposure to estrogenic compounds, TAML treatment protected

against this effect with no negative side effects. In a later chapter, the results of a similar study of exposure of mammals to untreated and NewTAML/H<sub>2</sub>O<sub>2</sub> treated solutions will be discussed.

Performing the various toxicity experiments discussed here on a wide range of living systems are vital for ensuring that TAML activator treatments do not produce any harmful products. Should any questionable results from TiPED or similar tests be obtained, the designers of TAML are adept at return to the drawing board to circumvent the toxicity before commercialization is considered.

## 1.5 Research Summary

In this work, a new class of TAML activators called NewTAMLs is described and investigated. The design of NewTAML activators was informed through use of the iterative design loop (Figure 1.5) following many years of mechanistic studies to determine the vulnerable sites of the ligand and the nature of the lifetime-determining catalyst inactivation in ultra-dilute aqueous conditions. The design elements incorporated into the NewTAML ligand structure to block these inactivation processes also sufficiently enhance the reactivity to render the incorporation of halogens unnecessary.

First, the preparation, properties, and performance of OldTAMLs **7** is presented in Chapter 2. These TAMLs, which feature a substituted biuret tail, conform to the same trend of increased reactivity correlating with decreased lifetime in studies of Orange II oxidation as do the **1** catalysts. This reinforced the prior conclusion that the malonamide position  $\alpha$  to the two carbonyl carbons at the tail ( $-\text{CR}_1\text{R}_2$ ) is not the location of the primary catalyst inactivation processes.

Chapter 3 describes the ligand design and preparation methods for NewTAML activators, including the many failed pathways attempted during their production. Negative results are included where possible to ensure that future synthetic group members are aware of unstable intermediates and to explain the selection of the R groups used in NewTAMLs.

Chapter 4 introduces NewTAML activators and provides an overview of their properties with a focus on water treatment applications. Studies of NewTAML catalysis of the model substrate Orange II and the persistent pollutant propranolol performed in collaboration with graduate student Yogesh Somasundar highlight the technical

performance and commercial potential of NewTAMLs. Mammalian toxicity studies of the prototype NewTAML are also presented.

Chapters 5 and 6 are comparative evaluations of the different families of NewTAMLs in which the kinetics of the NewTAMLs are quantified by the rate constants  $k_I$  and  $k_{II}$ . The properties of NewTAMLs and mechanism of NewTAML catalysis are examined in depth and compared to those of previous TAMLs. Chapter 7 focuses on the lifetime of NewTAMLs, described by the rate constant  $k_i$ . In this chapter, an inactivation pathway unique to NewTAMLs is investigated and the success of NewTAMLs at mitigating the primary inactivation pathway of OldTAMLs is discussed.

## 1.6 References

1. Travis, A. S. *Technol. Cult.* **1990**, 31 (1), 51–82.
2. 1865-1901: The Birth of the Chemical Industry and the Era of Dyes  
<https://www.basf.com/en/company/about-us/history/1865-1901.html> (accessed Apr 25, 2017).
3. Shanken, A. M. *Enterp. Soc.* **2006**, 7 (3), 485–519.
4. Fagin, D. *Toms River: A Story of Science and Salvation*; Bantam: New York, 2013.
5. Warner, G. R.; Collins, T. J. In *Integrative Environmental Medicine*; Cohen, A., Vom Saal, F. S., Eds.; Oxford University Press, 2017; pp 305–337.
6. Carson, R. *Silent Spring*; Houghton Mifflin Company, 1962.
7. Khairy, M.; Muir, D.; Teixeira, C.; Lohmann, R. *Env. Sci Technol* **2014**, 48 (16), 9315–9324.
8. Markovitz, G.; Rosner, D. *Deceit and Denial: The Deadly Politics of Industrial Pollution*; University of California Press and the Milbank Memorial Fund: Berkley and New York, 2002.
9. Barry, V. Winquist, A. Steenland, K. *Environ. Health Perspect.* **2013**, 121 (11–12), 1313–1318.
10. Steenland, K.; Fletcher, T.; Savitz, D. A. *Environ. Health Perspect.* **2010**, 118 (8), 1100–1108.
11. Frisbee, S. J.; Brooks, A. P.; Maher, A.; Flensburg, P.; Arnold, S.; Fletcher, T.; Steenland, K.; Shankar, A.; Knox, S. S.; Pollard, C.; Halverson, J. A.; Vieira, V. M.; Jin, C.; Leyden, K. M.; Ducatman, A. M. *Environ. Health Perspect.* **2009**, 117 (12), 1873–1882.
12. Jonas, H. *The Imperative of Responsibility: In Search of an Ethics for the Technological Age*; University of Chicago Press, 1984.
13. Anastas, P. T.; Warner, J. C. *Green Chemistry: Theory and Practice*; Oxford University Press: New York, 1998.
14. Daughton, C. G.; Ternes, T. A. *Environ. Toxicol.* **2009**, 28 (12), 2663–2670.
15. Schwarzenbach, R. P.; Escher, B. I.; Fenner, K.; Hofstetter, T. B.; Johnson, C. A.; von Gunten, U.; Wehrli, B. *Science*. **2006**, 313 (5790), 1072–1077.
16. Colborn, T.; vom Saal, F. S.; Soto, A. M. *Environ. Health Perspect.* **1993**, 101 (5), 378–384.
17. Benotti, M. J.; Trenholm, R. a; Vanderford, B. J.; Holady, J. C.; Stanford, B. D.; Snyder, S. a. *Environ. Sci. Technol.* **2009**, 43 (3), 597–603.
18. Gore, A. C.; Chappell, V. A.; Fenton, S. E.; Flaws, J. A.; Nadal, A.; Prins, G. S.; Toppari, J.; Zoeller, R. T. *Endocr. Rev.* **2015**, 36 (February), E1–E150.
19. Vandenberg, L. N.; Colborn, T.; Hayes, T. B.; Heindel, J. J.; Jacobs, D. R.; Lee, D.-H.; Shioda, T.; Soto, A. M.; Vom Saal, F. S.; Welshons, W. V.; Zoeller, R. T.; Myers, J. P. *Endocr. Rev.* **2012**, 33 (June), 1–78.
20. Luo, Y.; Guo, W.; Ngo, H. H.; Nghiem, L. D.; Hai, F. I.; Zhang, J.; Liang, S.; Wang, X. C. *Sci. Total Environ.* **2014**, 473–474, 619–641.
21. Sumpter, J. P.; Jobling, S. *Environ. Toxicol. Chem.* **2013**, 32 (2), 249–251.
22. Jobling, S.; Nolan, M.; Tyler, C. R.; Brighty, G.; Sumpter, J. P. *Environ. Sci. Technol.* **1998**, 32 (17), 2498–2506.
23. Gross-Sorokin, M. Y.; Roast, S. D.; Brighty, G. C. *Environ. Health Perspect.*



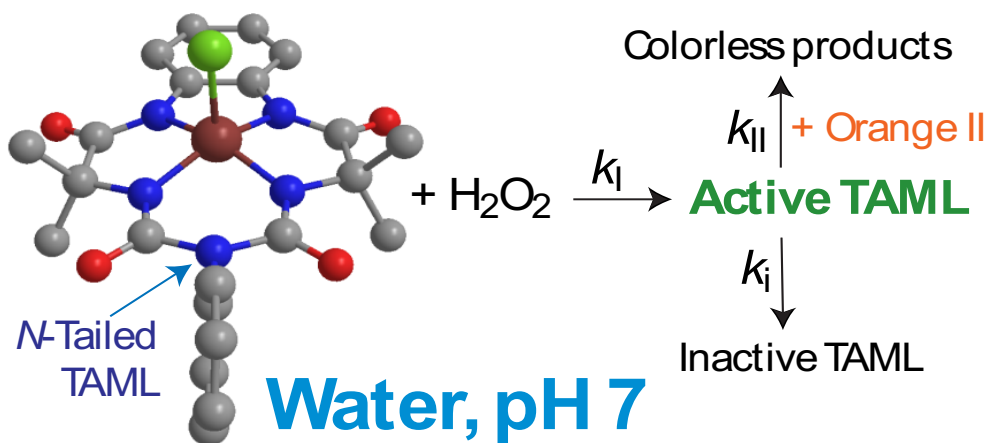
- 2005**, 114 (S-1), 147–151.
24. Wu, X.; Dodgen, L. K.; Conkle, J. L.; Gan, J. *Sci. Total Environ.* **2015**, 536, 655–666.
  25. Citulski, J. A.; Farahbakhsh, K. *Environ. Sci. Technol.* **2010**, 44 (22), 8367–8376.
  26. Kinney, C. A.; Furlong, E. T.; Zaugg, S. D.; Burkhardt, M. R.; Werner, S. L.; Cahill, J. D.; Jorgensen, G. R. *Environ. Sci. Technol.* **2006**, 40 (23), 7207–7215.
  27. Margot, J.; Kienle, C.; Magnet, A.; Weil, M.; Rossi, L.; de Alencastro, L. F.; Abegglen, C.; Thonney, D.; Chèvre, N.; Schärer, M.; Barry, D. A. *Sci. Total Environ.* **2013**, 461–462, 480–498.
  28. Mulder, M.; Antakyali, D.; Ante, S. Costs of Removal of Micropollutants from Effluents of Municipal Wastewater Treatment Plants <http://www.tapes-interreg.eu/uploads/Stowa TAPES Final report.pdf>.
  29. Schröder, P.; Helmreich, B.; Škrbić, B.; Carballa, M.; Papa, M.; Pastore, C.; Emre, Z.; Oehmen, A.; Langenhoff, A.; Molinos, M.; Dvarioniene, J.; Huber, C.; Tsagarakis, K. P.; Martinez-Lopez, E.; Pagano, S. M.; Vogelsang, C.; Mascolo, G. *Environ. Sci. Pollut. Res.* **2016**, 23 (13), 12835–12866.
  30. Owen, R.; Jobling, S. *Nature* **2012**, 485 (7399), 441–441.
  31. Von Gunten, U. *Water Res.* **2003**, 37, 1469–1487.
  32. Churchley, J.; Collins, T.; Jobling, S. *Catalytic Oxidation of Pharmaceutical Compounds in Wastewater Effluents. UKWIR Report 13/WW/17/14*; London, 2013.
  33. Huggett, D. B.; Khan, I. A.; Foran, C. M.; Schlenk, D. *Environ. Pollut.* **2003**, 121 (2), 199–205.
  34. Kostich, M. S.; Batt, A. L.; Lazorchak, J. M. *Environ. Pollut.* **2014**, 184, 354–359.
  35. Roberts, P. H.; Thomas, K. V. **2005**.
  36. Wick, A.; Fink, G.; Joss, A.; Siegrist, H.; Ternes, T. A. *Water Res.* **2009**, 43 (4), 1060–1074.
  37. Finn, J.; Hui, M.; Li, V.; Lorenzi, V.; de la Paz, N.; Cheng, S. H.; Lai-Chan, L.; Schlenk, D. *Aquat. Toxicol.* **2012**, 122–123, 214–221.
  38. Vandenberg, L. N.; Colborn, T.; Hayes, T. B.; Heindel, J. J.; Jacobs, D. R.; Lee, D.-H.; Myers, J. P.; Shioda, T.; Soto, A. M.; vom Saal, F. S.; Welshons, W. V.; Zoeller, R. T. *Reprod. Toxicol.* **2013**, 38, 1–15.
  39. Sadaria, A. M.; Supowit, S. D.; Halden, R. U. *Environ. Sci. Technol.* **2016**, 50, 6199–6206.
  40. Qi, W.; Singer, H.; Berg, M.; Müller, B.; Pernet-Coudrier, B.; Liu, H.; Qu, J. *Chemosphere* **2015**, 119, 1054–1061.
  41. Kapoor, U.; Srivastava, M. K.; Srivastava, L. P. *Food Chem. Toxicol.* **2011**, 49 (12), 3086–3089.
  42. Najafi, G.; Razi, M.; Hoshyar, A.; Shahmohammadloo, S.; Feyzi, S. *Int. J. Fertil. Steril.* **2010**, 4 (1), 9–16.
  43. Bal, R.; Naziroğlu, M.; Türk, G.; Yilmaz, Ö.; Kuloğlu, T.; Etem, E.; Baydas, G. *Cell Biochem. Funct.* **2012**, 30 (6), 492–499.
  44. Gu, Y.; Li, Y.; Huang, X.; Zheng, J.; Yang, J.; Diao, H.; Yuan, Y.; Xu, Y.; Liu, M.; Shi, H.; Xu, W. *PLoS One* **2013**, 8 (7), e70112.
  45. Collins, T. J. *Acc. Chem. Res.* **2002**, 35 (9), 782–790.
  46. Collins, T. *Science*. **2001**, 291, 48–49.

47. Veitch, N. C. *Phytochemistry* **2004**, 65 (3), 249–259.
48. Bartos, M.; Gordon-Wylie, S. *Coord. Chem. Rev.* **1998**, 174, 361–390.
49. Ghosh, A.; de Oliveira, F. T. *J. Am. Chem. Soc.* **2005**, No. Iv, 2505–2513.
50. Chanda, A.; Ryabov, A. D.; Mondal, S.; Alexandrova, L.; Ghosh, A.; Hangun-Balkir, Y.; Horwitz, C. P.; Collins, T. J. *Chem. - A Eur. J.* **2006**, 12 (36), 9336–9345.
51. Tang, L. L.; DeNardo, M. A.; Schuler, C. J.; Mills, M. R.; Gayathri, C.; Gil, R. R.; Kanda, R.; Collins, T. J. *J. Am. Chem. Soc.* **2017**, 139 (2), 879–887.
52. Gupta, S. Sen; Stadler, M.; Noser, C.; Ghosh, A.; Steinhoff, B.; Lenoir, D.; Horwitz, C. P.; Schramm, K.-W.; Collins, T. J. *Science* **2002**, 296 (5566), 326–328.
53. Mondal, S.; Hangun-Balkir, Y.; Alexandrova, L.; Link, D.; Howard, B.; Zandhuis, P.; Cugini, A.; Horwitz, C. P.; Collins, T. J. *Catal. Today* **2006**, 116 (4), 554–561.
54. Banerjee, D.; Markley, A. L.; Yano, T.; Ghosh, A.; Berget, P. B.; Minkley, E. G.; Khetan, S. K.; Collins, T. J. *Angew. Chemie Int. Ed.* **2006**, 45 (24), 3974–3977.
55. Chanda, A.; Khetan, S. K.; Banerjee, D.; Ghosh, A.; Collins, T. J. *J. Am. Chem. Soc.* **2006**, 128 (37), 12058–12059.
56. Kundu, S.; Chanda, A.; Espinosa-Marvan, L.; Khetan, S. K.; Collins, T. J. *Catal. Sci. Technol.* **2012**, 2 (6), 1165–1172.
57. Chahbane, N.; Popescu, D.-L.; Mitchell, D. A.; Chanda, A.; Lenoir, D.; Ryabov, A. D.; Schramm, K.-W.; Collins, T. J. *Green Chem.* **2007**, 9 (1), 49–57.
58. Mitchell, D. A.; Ryabov, A. D.; Kundu, S.; Chanda, A.; Collins, T. J. *J. Coord. Chem.* **2010**, 63 (14–16), 2605–2618.
59. Beach, E. S.; Malecky, R. T.; Gil, R. R.; Horwitz, C. P.; Collins, T. J. *Catal. Sci. Technol.* **2011**, 1 (3), 437–443.
60. Shappell, N. W.; Vrabel, M. a; Madsen, P. J.; Harrington, G.; Billey, L. O.; Hakk, H.; Larsen, G. L.; Beach, E. S.; Horwitz, C. P.; Ro, K.; Hunt, P. G.; Collins, T. J. *Environ. Sci. Technol.* **2008**, 42 (4), 1296–1300.
61. Mills, M. R.; Arias-Salazar, K.; Baynes, A.; Shen, L. Q.; Churchley, J.; Beresford, N.; Gayathri, C.; Gil, R. R.; Kanda, R.; Jobling, S.; Collins, T. J. *Sci. Rep.* **2015**, 5, 10511.
62. Kundu, S.; Chanda, A.; Khetan, S. K.; Ryabov, A. D.; Collins, T. J. *Environ. Sci. Technol.* **2013**, 47 (10), 5319–5326.
63. Kundu, S.; Chanda, A.; Thompson, J. V. K.; Diabes, G.; Khetan, S. K.; Ryabov, A. D.; Collins, T. J. *Catal. Sci. Technol.* **2014**, 5, 1775–1782.
64. Do Pham, D. D.; Kelso, G. F.; Yang, Y.; Hearn, M. T. W. *Green Chem.* **2014**, 16 (3), 1399.
65. Do Pham, D. D.; Kelso, G. F.; Yang, Y.; Hearn, M. T. W. *Green Chem.* **2012**, 14 (4), 1189–1195.
66. Onundi, Y. B. Oxidation of Bisphenol A , Triclosan and 4- Nonylphenol by Fe-B \* activated peroxide, The University of Aukland, 2015.
67. Shen, L. Q.; Beach, E. S.; Xiang, Y.; Tshudy, D. J.; Khanina, N.; Horwitz, C. P.; Bier, M. E.; Collins, T. J. *Environ. Sci. Technol.* **2011**, 45 (18), 7882–7887.
68. Tang, L. L.; DeNardo, M. A.; Gayathri, C.; Gil, R. R.; Kanda, R.; Collins, T. J. *Environ. Sci. Technol.* **2016**, 50, 5261–5268.
69. Onundi, Y.; Drake, B. A.; Malecky, R. T.; DeNardo, M. A.; Mills, M. R.; Kundu,

- S.; Ryabov, A. D.; Beach, E. S.; Horwitz, C. P.; Simonich, M. T.; Truong, L.; Tanguay, R. L.; Wright, L. J.; Singhal, N.; Collins, T. J. **2017**, submitted.
70. Collins, T. *Acc. Chem. Res.* **1994**, 27 (12), 279–285.
  71. Collins, T. J.; Powell, R. D.; Slebodnick, C.; Uffelman, E. S. *J. Am. Chem. Soc.* **1991**, 113 (22), 8419–8425.
  72. Horwitz, C.; Fooksman, D. *J. Am. Chem. Soc.* **1998**, 1 (17), 4867–4868.
  73. Ibáñez, G. A.; Olivieri, A. C.; Escandar, G. M. *J. Chem. Soc. - Faraday Trans.* **1997**, 93 (4), 545–551.
  74. DeNardo, M. A.; Mills, M. R.; Ryabov, A. D.; Collins, T. J. *J. Am. Chem. Soc.* **2016**, 138 (9), 2933–2936.
  75. Schug, T. T.; Abagyan, R.; Blumberg, B.; Collins, T. J.; Crews, D.; DeFur, P. L.; Dickerson, S. M.; Edwards, T. M.; Gore, a. C.; Guillette, L. J.; Hayes, T.; Heindel, J. J.; Moores, A.; Patisaul, H. B.; Tal, T. L.; Thayer, K. a.; Vandenberg, L. N.; Warner, J. C.; Watson, C. S.; vom Saal, F. S.; Zoeller, R. T.; O'Brien, K. P.; Myers, J. P. *Green Chem.* **2013**, 15 (1), 181–198.
  76. Ellis, W. C.; Tran, C. T.; Roy, R.; Rusten, M.; Fischer, A.; Ryabov, A. D.; Blumberg, B.; Collins, T. J. *J. Am. Chem. Soc.* **2010**, 132 (28), 9774–9781.
  77. Truong, L.; DeNardo, M. A.; Kundu, S.; Collins, T. J.; Tanguay, R. L. *Green Chem.* **2013**, 15, 2339–2343.

## CHAPTER 2

### Kinetic Studies of Reactivity and Operational Stability of *N*-tailed TAMLs Through of the Catalyzed Oxidation of Orange II by $\text{H}_2\text{O}_2$



# CHEMISTRY

## A European Journal

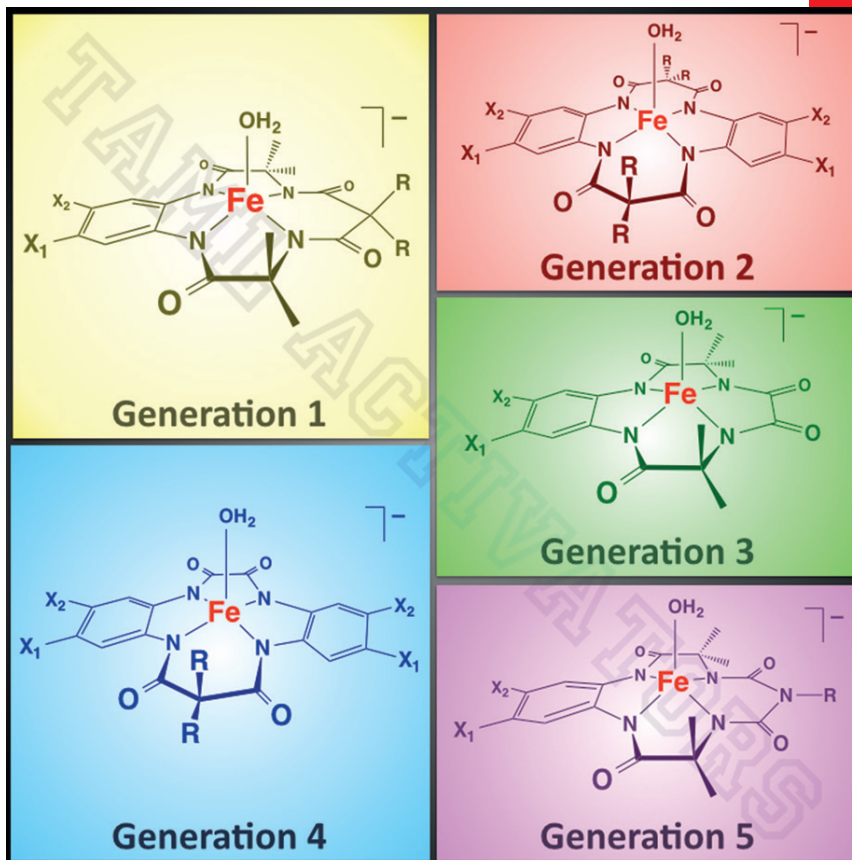
www.chemeurj.org

A Journal of



ChemPubSoc  
Europe

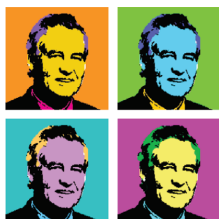
2015-21/16



Supported by  
**ACES**

WILEY-VCH

# Reactivity and Operational Stability of *N*-Tailed TAMLs through Kinetic Studies of the Catalyzed Oxidation of Orange II by H<sub>2</sub>O<sub>2</sub>: Synthesis and X-ray Structure of an *N*-Phenyl TAML



Invited for the cover of this issue are Terrence J. Collins and co-workers at Carnegie Mellon University (USA) and the National Chemical Laboratory (India). The image depicts five generations of tetraamido macrocyclic ligand (TAML) activators, which are small molecule, full-functional mimics of oxidizing enzymes that arguably outperform the peroxidase enzymes they mimic. Read the full text of the article at 10.1002/chem.201406061.

## *In one word, how would you describe your research?*

Thrilling!

## *What was the inspiration for this cover design?*

The Collins team works in Pittsburgh, Pennsylvania, the childhood home to Andy Warhol, the superstar of mid-twentieth century pop art. His paintings, like *Oxidations* were sometimes created using impious chemistry (urinating into canvas covered with metallic paint causing oxidation). TAML chemistry is graciously disruptive—the first catalytically spectacular, small molecule mimics of oxidizing enzymes. The cover design draws its inspiration from Warhol's now-famous image of Marilyn Monroe, a perfect template for delivering the beauty of transformative scientific ideas—the replica with Terry Collins (top left) created by his students may recall the famous Marilyn original.

## *Who contributed to the idea behind the cover?*

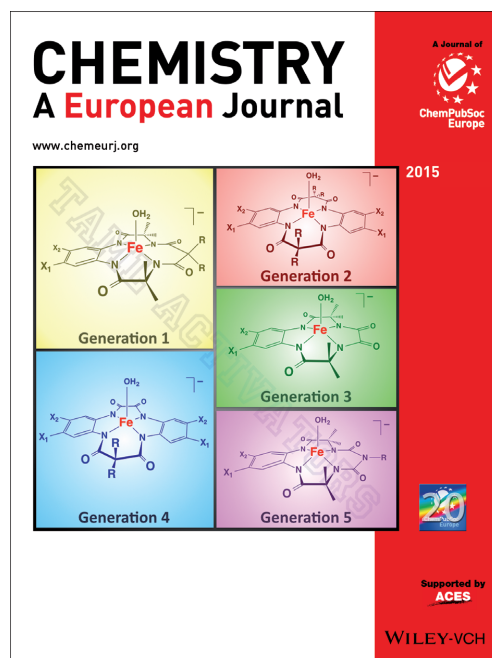
The cover art idea and design was a group effort at Carnegie Mellon including Taylor Canady, a close friend of the lead author Genoa Warner and a graduate student in another chemistry group who made the Warhol suggestion. Dr. Collins produced the cover art with help from the team. He has for many years worked with computer graphics programs for the satisfaction these deliver in facilitating powerful artistic presentations of ideas.

## *Did this work pose any ethical questions?*

TAML activators resulted from a catalyst design program started in 1980 with the goal of enabling water disinfection with hydrogen peroxide to avoid toxic chlorinated disinfection byproducts. Today, TAML activators underpin new approaches for removing endocrine disruptors from municipal wastewater offering a possible partial resolution to one of the great sustainability ethics challenges confronting the chemical enterprise. It is hoped that TAML activators will be used in technologies that mitigate the impact of endocrine disruptors on the aquatic environment.

## *How would you describe to the layperson the most significant result of this study?*

There are now over 20 TAML activators. Significant insight for deciding which ones will be the most advantageous in commercial applications can be gained by studying the relative catalytic performances. This study shows that one of the new fifth-generation TAML activators, with a biuret functional group in the macrocycle, is among those with attractive performance parameters under the most common conditions of acidity (pH 7) for water treatment.



## 2.1 Introduction

The long-term, strategic iterative design of TAML activators of peroxides<sup>1,2</sup> has resulted in the creation of functional, small replicas of peroxidase enzymes; the most common early generation catalysts **1** and **5** are shown in Figure 2.1.<sup>3,4</sup> Activators **1** and **5** catalyze a variety of oxidations by H<sub>2</sub>O<sub>2</sub>,<sup>5</sup> making them useful for applied processes. Recently, a new (fifth) generation of TAML activators (**7**) has been introduced<sup>6</sup> and examined in several applications.<sup>6-9</sup> Catalysts **7** feature an N-R for CR<sub>2</sub> substitution in the “tail” part of the prototypical activators **1**. This substitution introduces a pair of  $\pi$  electrons into the tail six-membered ring and reduces steric bulk around the iron active site associated with the boat conformation of the six-membered ring of **1**.<sup>10</sup> Additionally, the biuret nitrogen  $\pi$  lone pair of **7** could stabilize planarity in the six-membered ring to hinder the known intramolecular suicidal degradation of the ligand system of **1**.<sup>10</sup>

These potential advantages of **7** made it important to compare the kinetic details of their reactivity with previous TAML activators in the catalysis of H<sub>2</sub>O<sub>2</sub> activations in aqueous medium.<sup>11,12</sup> In this chapter, the properties of **7** and their reactivity toward the azo dye Orange II (Figure 1.6) by H<sub>2</sub>O<sub>2</sub> at various pHs is compared to previously obtained results for **1** and **5** (Figure 2.1). Compounds **7b** and **7c** were prepared Shantanu Pattanayak, Chakadola Panda, and Tamas Kumar Panda from the group of Sayam Sen Gupta at CSIR-National Chemical Laboratory in Pune, India. Kinetic studies were performed in collaboration with Matthew Mills, Clarissa Enslin, and Aleksandr Ryabov at the IGS.

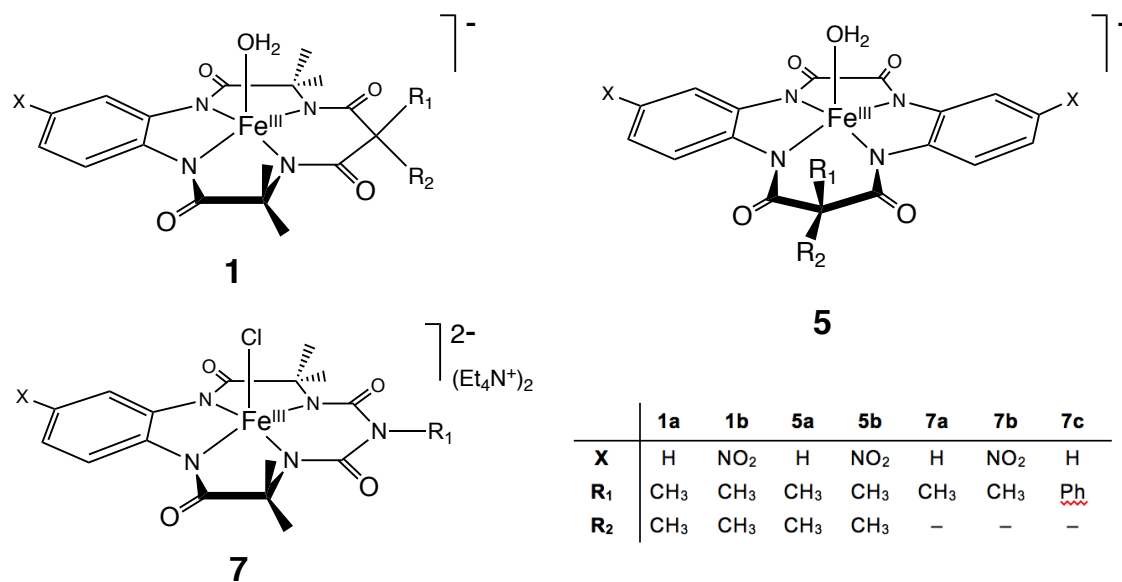


Figure 2.1 TAML activators mentioned in this chapter. Complex **7a'**, which is a structural analogue of **7a** with an axial MeOH ligand instead of Cl<sup>–</sup> and Li<sup>+</sup> instead of (Et<sub>4</sub>N<sup>+</sup>)<sub>2</sub> was also synthesized and explored in this chapter.



## 2.2 Results and Discussion

### 2.2.1 Synthesis and X-Ray Characterization of **7c**

Activator **7c** was prepared using the same procedure as previously described for **7a** and **7b**.<sup>6</sup> The identity of **7c** was proven by various techniques including X-ray crystallography, which revealed the square pyramidal structure with an axial chloride that is typical of ferric TAML complexes in the solid state (Figure 2.2)—the axial chloride ligand arises from treatment of **7c** with an anion-exchange resin in the chloride salt form. As typically found for ferric TAMLs, the iron-chloride bond is elongated<sup>3</sup> (Fe–Cl = 2.391(2) Å) by the strong equatorial  $\sigma$ -donor capacity of the TAML macrocycle, predicting ready hydrolysis in water to form the corresponding aqua complexes.

Complex **7a'**, containing an axial MeOH ligand instead of Cl<sup>−</sup> (Figure 2.1), was also prepared and used in this work. As it will be shown below, the spectral and catalytic properties of **7a** and **7a'** are essentially the same in water due to the hydrolysis of axial chloride and methanol in **7a** and **7a'**, respectively, to afford the corresponding aqua species.

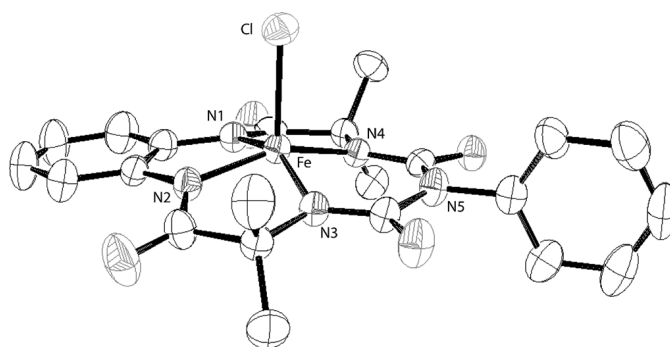
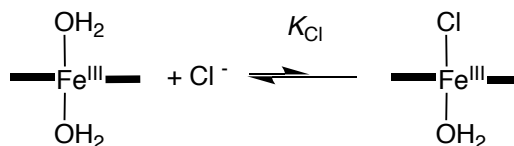


Figure 2.2 ORTEP representation of **7c** (H atoms and two counter ions PPh<sub>4</sub><sup>+</sup> are not shown for clarity, thermal ellipsoids are at 50% probability level). Selected bond distances (in Å): Fe–Cl 2.391(2), Fe–N<sub>1-4</sub> 1.885(4), 1.868(4), 1.884(4) and 1.882(4), respectively. Iron sits 0.44 Å above the plane of four amide nitrogens. The plane of the N-tail phenyl ring is almost perpendicular to the average plane of the four amide nitrogens coordinated with iron.

### 2.2.2 Properties of **7a** in Aqueous Solution

Square pyramidal compounds **7a-c** were all isolated as solids with chloride as an axial ligand.<sup>6</sup> Two of these (**7a** and **7c**) have been characterized by X-ray crystallography. The previously investigated TAML activators **1** and **5** were crystallized with axial water, chloride, or methanol ligands.<sup>3,4</sup> Irrespective of the monodentate axial ligand, iron(III) TAMLs all exist as six-coordinated diaqua species  $[\text{FeL}(\text{H}_2\text{O})_2]^+$  in water at neutral pH.<sup>13,14</sup> Complexes **7** behave similarly, i.e. they undergo hydrolysis in water and Equation 2.1 is strongly shifted to the left. Correspondingly, the UV-vis spectra of aqueous solutions of **7a** and **7a'** are identical and remain unchanged in the presence of 0.008-0.240 M KCl at pH 7.2. Unless otherwise stated, when working in water it is understood that the principal species is a diaqua complex regardless of whether **7a** or **7a'** is chosen as a source material.



Equation 2.1

There is no evidence for aggregation of **7a** in water, since Beer's law holds across the concentration range studied  $(0.38\text{--}4.7) \times 10^{-4}$  M both in pure water and water buffered by 0.01 M phosphate at pH 7 ( $\epsilon_{353} = 2200 \text{ M}^{-1} \text{ cm}^{-1}$  in both cases).

As has been established previously for **1**,<sup>13</sup> the UV-vis spectrum of **7a** is also strongly affected by pH. The band at 353 nm disappears reversibly as pH increases from 7 to 12 with an isosbestic point at 332 nm (Figure 2.3). The absorbance at 353 nm depends on pH as shown in Inset A to Figure 2.3 whereas Inset B demonstrates the data linearization according to Equation 2.2 ( $A$  is the observed absorbance at any pH;  $A_{\text{H}}$  and

$A_{\text{OH}}$  are the absorbances at the acidic and basic plateau regions, respectively), which allows one to calculate from the intercept the  $\text{p}K_{\text{a}}$  value for **7a** of  $10.32 \pm 0.03$ .

$$\log \frac{A_{\text{H}} - A}{A - A_{\text{OH}}} = \text{pH} - \text{p}K_{\text{a}}$$

Equation 2.2

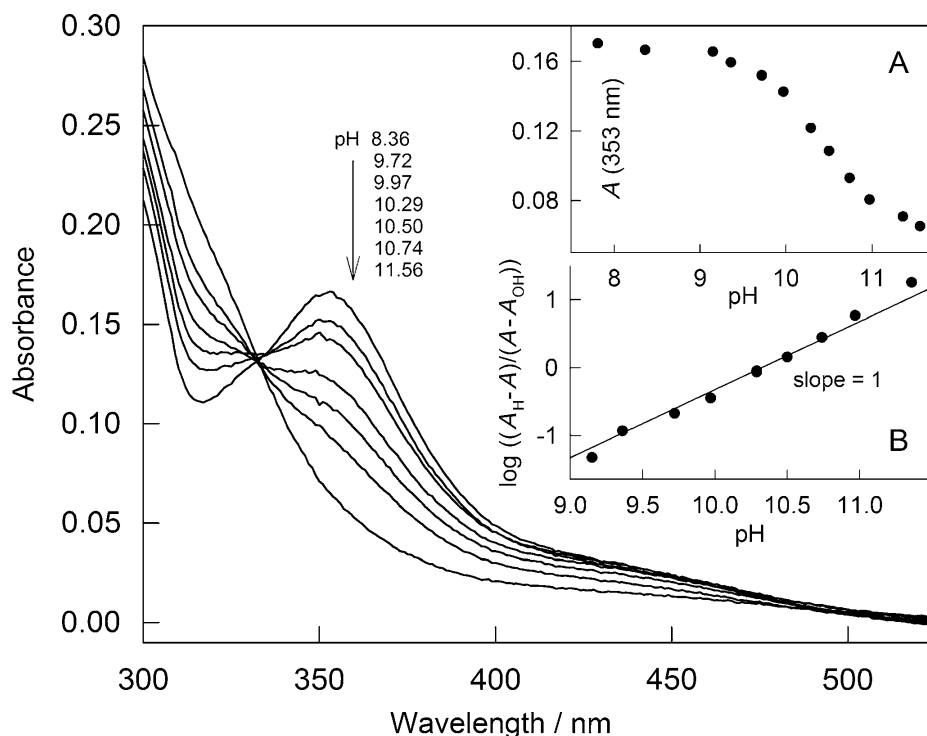


Figure 2.3 Spectra of **7a** ( $6.3 \times 10^{-5}$  M) as a function of pH in 0.01 M phosphate buffer at 25 °C. Inset A shows absorbance at 353 nm versus pH. Inset B is a linearization of the data in Inset A in terms of Equation 2.2 used for determining  $\text{p}K_{\text{a}}$ .

### 2.2.3 Catalytic Activity of **7a** in Bleaching Orange II with $\text{H}_2\text{O}_2$

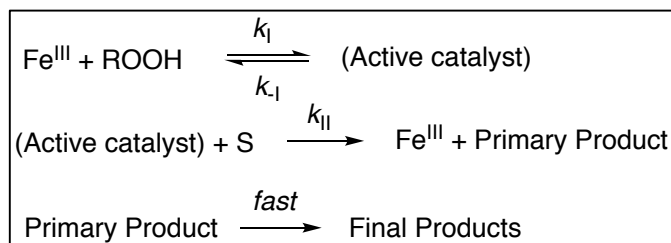
The dye Orange II has proven to be a convenient substrate for assaying the catalytic activity of metal complexes in oxidations by  $\text{H}_2\text{O}_2$  and other oxidants.<sup>12,14–18</sup>

Therefore, the kinetics of bleaching of Orange II by  $\text{H}_2\text{O}_2$  in the presence of **7a** has been investigated. Measurements emphasize pH 7 because of our long-term goal of using

TAMLs for the purification of municipal waters. The steady-state rate of fading of the Orange II band at 484 nm is a linear function of [7a] over the broad range from  $8.9 \times 10^{-8}$  to  $1.3 \times 10^{-5}$  M at pH 7 with  $[\text{H}_2\text{O}_2] = 4.2 \times 10^{-4}$  M and  $[\text{Orange II}] = 2.75 \times 10^{-5}$  M (data not shown). The rate first increases with increasing [Orange II], then it levels off, and finally decreases (phases 1–3 in Figure 2.5, respectively). These observations are not unusual for catalysis by TAMLs. Phases 1 and 2 agree both with the general mechanism of catalysis by TAMLs (Figure 2.4) and the rate expression Equation 2.3.<sup>3</sup> At  $[\text{Orange II}] > 2.75 \times 10^{-5}$  M, the rate is virtually independent of the dye concentration. Therefore, if Equation 2.3 holds, the rate should be a linear function of  $[\text{H}_2\text{O}_2]$  because under such conditions Equation 2.3 reduces to  $-d[\text{S}]/dt = k_1[\text{H}_2\text{O}_2][\text{Fe}_t]$ . The data in the inset to Figure 2.5 are consistent with this prediction. At  $[\text{H}_2\text{O}_2] = (0.21\text{--}2.9) \times 10^{-3}$  M, the reaction rate is strictly proportional to  $[\text{H}_2\text{O}_2]$ , but starts to level off at higher concentrations as predicted by Equation 2.3. The value of  $k_1$  of  $104 \pm 2 \text{ M}^{-1} \text{ s}^{-1}$  was calculated from the linear portion of the plot.

The data in Figure 2.5 have been used for estimating the rate constants  $k_1$  and  $k_{II}$  by their fitting to Equation 2.3. Provided the data point obtained at the highest Orange II concentration is neglected (see below), the values of  $k_1$  and  $k_{II}$  equal  $140 \pm 20$  and  $(3 \pm 2) \times 10^4 \text{ M}^{-1} \text{ s}^{-1}$ , respectively. Note that  $k_1$  calculated from the data in Figure 2.5 and in the inset agree satisfactorily. The rate constant  $k_{II}$  of  $(2.3 \pm 0.2) \times 10^4 \text{ M}^{-1} \text{ s}^{-1}$  was more accurately determined from the slope of the linear double inverse plot of  $v^{-1}$  vs.  $[\text{S}]^{-1}$ . Absolute values of  $k_1$  and  $k_{II}$  (Table 2.1) indicate that the rate-limiting step of 7a-catalyzed Orange II bleaching by  $\text{H}_2\text{O}_2$  is the interaction between the catalyst and peroxide ( $k_1$ ) under the chosen experimental conditions. Therefore, performance is limited

by  $k_1$  which becomes the appropriate measure of relative reactivity of **7a** and **1a**. For **1a**, the rate constant  $k_1$  is  $52 \text{ M}^{-1} \text{ s}^{-1}$  at pH 7.<sup>19</sup> Thus, there is a three-fold reactivity advantage of **7a** as compared to the prototype TAML activator **1a**.



*steady state approximation:*  $\frac{d[\text{Ac}]}{dt} = \frac{d[\text{Fe}^{\text{III}}]}{dt} - \frac{d[\text{P}]}{dt}$

$$\frac{d[\text{Ac}]}{dt} = 0 = k_1[\text{ROOH}][\text{Fe}^{\text{III}}] - k_{-1}[\text{Ac}] - k_{11}[\text{Ac}][\text{S}]$$

$$k_1[\text{ROOH}][\text{Fe}^{\text{III}}] = [\text{Ac}](k_{-1} + k_{11}[\text{S}])$$

*mass balance:*  $\text{Fe}_t = [\text{Fe}^{\text{III}}] + [\text{Ac}]$

$$k_1[\text{ROOH}](\text{Fe}_t - [\text{Ac}]) = [\text{Ac}](k_{-1} + k_{11}[\text{S}])$$

$$k_1[\text{ROOH}]\text{Fe}_t = [\text{Ac}](k_{-1} + k_{11}[\text{S}] + k_1[\text{ROOH}])$$

$$[\text{Ac}] = \frac{k_1[\text{ROOH}]\text{Fe}_t}{k_{-1} + k_1[\text{ROOH}] + k_{11}[\text{S}]}$$

*rate expression:*  $-\frac{d[\text{S}]}{dt} = k_{11}[\text{Ac}][\text{S}] = \frac{k_1 k_{11}[\text{ROOH}][\text{S}]\text{Fe}_t}{k_{-1} + k_1[\text{ROOH}] + k_{11}[\text{S}]}$

Figure 2.4 General stoichiometric mechanism of catalysis by TAML activators and derivation of Equation 2.3 using the steady state approximation for the Active catalyst (Ac) species.

$$-\frac{d[\text{S}]}{dt} = \frac{k_1 k_{11}[\text{ROOH}][\text{S}]\text{Fe}_t}{k_{-1} + k_1[\text{ROOH}] + k_{11}[\text{S}]}$$

Equation 2.3

The phase 3 behavior has also been discovered previously and analyzed in detail in the **1**-catalyzed bleaching of the blue pinacyanol chloride dye by  $\text{H}_2\text{O}_2$ .<sup>20</sup> The

retardation is accountable by a fast and reversible binding of the dye to the resting state of the catalyst ( $\text{Fe}^{\text{III}}$ ) that slows down the key interaction with  $\text{H}_2\text{O}_2$ . Here the retardation manifests at higher dye concentrations; it is negligible and can be ignored at lower dye loadings. Thus, if the data point obtained at  $5.8 \times 10^{-5}$  M Orange II is neglected, the rate as a function of [Orange II] is satisfactorily approximated by the hyperbolic Equation 2.3.

Next,  $k_{\text{I}}$  and  $k_{\text{II}}$  were determined in the pH range of 6.0–12.0. The  $k_{\text{I}}$  values could be obtained either by fitting the experimental data to Equation 2.3 as described above for the data in Figure 2.5, or by using the expression  $-d[\text{S}]/dt = k_{\text{I}}[\text{ROOH}][\text{Fe}^{\text{III}}]$  as in the inset to Figure 2.5. At low pH the latter approach is more appropriate. The rate constants  $k_{\text{I}}$  are summarized in Figure 2.6A where they are plotted against pH.

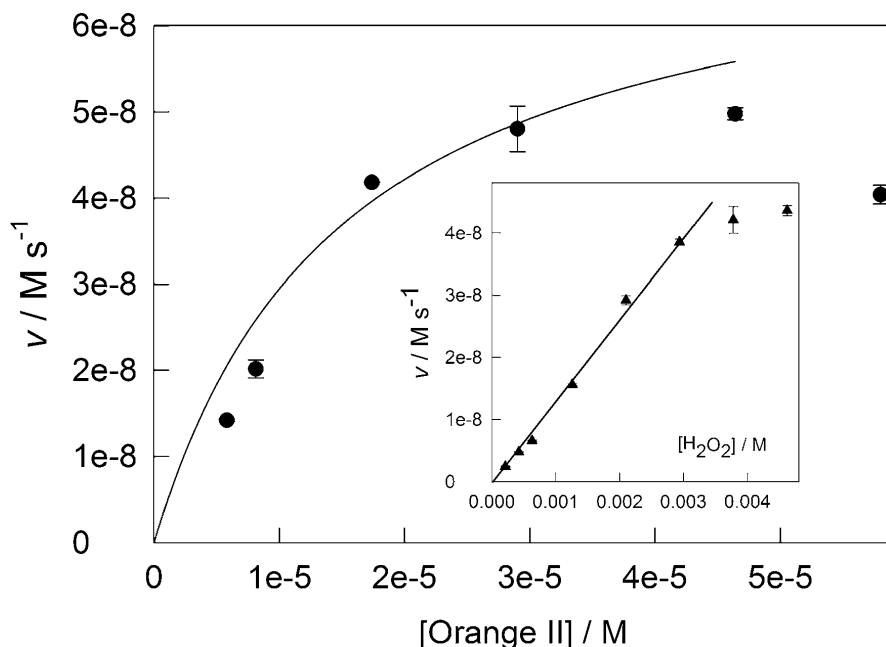


Figure 2.5 The steady-state rate of **7a**-catalyzed Orange II bleaching by  $\text{H}_2\text{O}_2$  as a function of Orange II concentration at  $[\text{H}_2\text{O}_2] = 4.2 \times 10^{-3}$  M. Inset shows rate vs.  $[\text{H}_2\text{O}_2]$  plot at  $[\text{Orange II}] = 2.75 \times 10^{-5}$  M. Other conditions:  $[\text{7a}] = 1.27 \times 10^{-7}$  M, pH 7 (0.01 M phosphate), 25 °C.

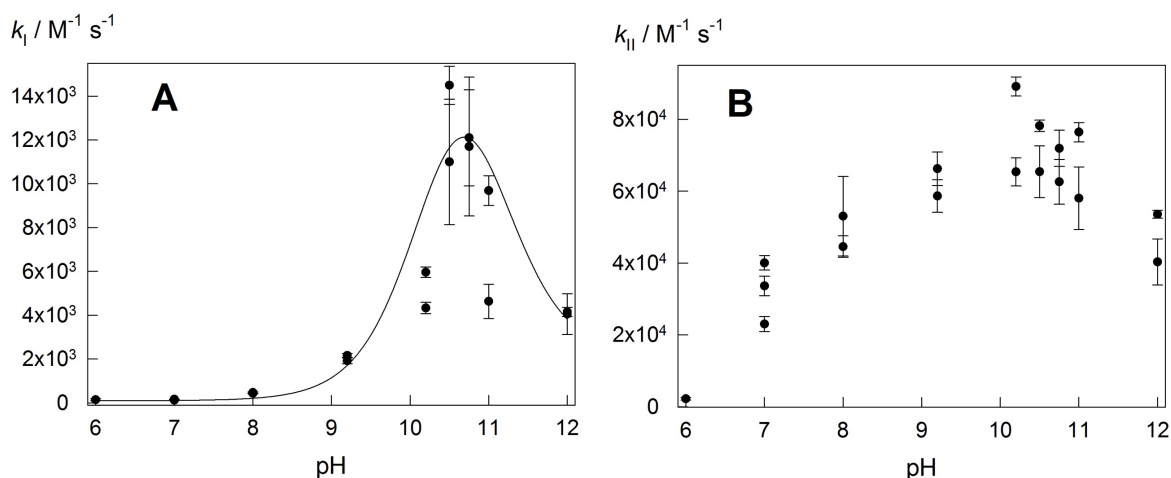
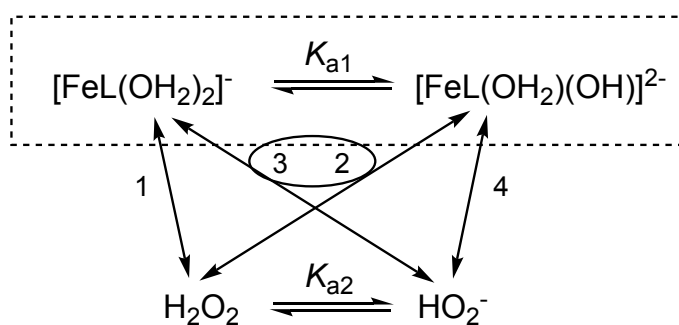


Figure 2.6 Rate constants  $k_I$  (A) and  $k_{II}$  (B) measured for **7a**-catalyzed bleaching of Orange II as a function of pH at 25 °C. The solid line in A is the calculated dependence using Equation 2.4 and its parameters given in the text.

The bell-shaped profile in Figure 2.6A is similar to those previously reported for **1**, **5**, and their derivatives.<sup>15,19,21</sup> It is consistent with the mechanism shown in Figure 2.7 according to which two forms of **7a**, related by an acid-base equilibrium, react pairwise with  $\text{H}_2\text{O}_2$  and its conjugate base  $\text{HO}_2^-$  to give the oxidized TAML species. The corresponding expression for  $k_I$ , derived in Figure 2.7, is given by Equation 2.4.



$$\begin{aligned}
&\text{equilibrium expressions:} \quad K_{a1} = \frac{[\text{FeL}(\text{OH}_2)(\text{OH})]^{2-}[\text{H}^+]}{[\text{FeL}(\text{OH}_2)_2]^-} \quad K_{a2} = \frac{[\text{HO}_2^-][\text{H}^+]}{[\text{H}_2\text{O}_2]} \\
&\text{mass balance:} \quad \text{Fe}_t = [\text{FeL}(\text{OH}_2)(\text{OH})]^{2-} + [\text{FeL}(\text{OH}_2)_2]^- \\
&\quad \quad \quad \text{P}_t = [\text{H}_2\text{O}_2] + [\text{OH}_2^-] \\
&\text{substitution into mass balance:} \quad \text{Fe}_t = [\text{FeL}(\text{OH}_2)_2]^- + \frac{[\text{FeL}(\text{OH}_2)_2]^- K_{a1}}{[\text{H}^+]} \\
&\quad \quad \quad [\text{FeL}(\text{OH}_2)_2]^- = \frac{\text{Fe}_t[\text{H}^+]}{[\text{H}^+] + K_{a1}} \quad [\text{FeL}(\text{OH}_2)(\text{OH})]^{2-} = \frac{\text{Fe}_t K_{a1}}{[\text{H}^+] + K_{a1}} \\
&\quad \quad \quad [\text{HO}_2^-] = \frac{\text{P}_t K_{a2}}{[\text{H}^+] + K_{a2}} \quad [\text{H}_2\text{O}_2] = \frac{\text{P}_t[\text{H}^+]}{[\text{H}^+] + K_{a2}} \\
&\text{rate expression:} \quad \frac{d[\text{Ac}]}{dt} = k_1[\text{FeL}(\text{OH}_2)_2]^-[\text{H}_2\text{O}_2] + k_2[\text{FeL}(\text{OH}_2)(\text{OH})]^{2-}[\text{H}_2\text{O}_2] \\
&\quad \quad \quad + k_3[\text{FeL}(\text{OH}_2)_2]^-[\text{OH}_2^-] + k_4[\text{FeL}(\text{OH}_2)(\text{OH})]^{2-}[\text{HO}_2^-] \\
&\text{substitution into rate expression:} \quad \frac{d[\text{Ac}]}{dt} = \frac{k_1 \text{Fe}_t \text{P}_t [\text{H}^+]^2}{([\text{H}^+] + K_{a1})([\text{H}^+] + K_{a2})} + \frac{k_2 \text{Fe}_t \text{P}_t K_{a1} [\text{H}^+]}{([\text{H}^+] + K_{a1})([\text{H}^+] + K_{a2})} \\
&\quad \quad \quad + \frac{k_3 \text{Fe}_t \text{P}_t K_{a2} [\text{H}^+]}{([\text{H}^+] + K_{a1})([\text{H}^+] + K_{a2})} + \frac{k_4 \text{Fe}_t \text{P}_t K_{a1} K_{a2}}{([\text{H}^+] + K_{a1})([\text{H}^+] + K_{a2})} \\
&\quad \quad \quad = \frac{k_1 [\text{H}^+]^2 + (k_2 K_{a1} + k_3 K_{a2}) [\text{H}^+] + k_4 K_{a1} K_{a2}}{[\text{H}^+]^2 + (K_{a1} + K_{a2}) [\text{H}^+] + K_{a1} K_{a2}} (\text{Fe}_t \text{P}_t) \\
&\text{\textit{k}_1 expression (Figure 2.4):} \quad \frac{d[\text{Ac}]}{dt} = k_1 \text{Fe}_t \text{P}_t \\
&\quad \quad \quad k_1 = \frac{k_1 [\text{H}^+]^2 + (k_2 K_{a1} + k_3 K_{a2}) [\text{H}^+] + k_4 K_{a1} K_{a2}}{[\text{H}^+]^2 + (K_{a1} + K_{a2}) [\text{H}^+] + K_{a1} K_{a2}}
\end{aligned}$$

Equation 2.4

Figure 2.7 Stoichiometric mechanism of catalysis by **7a** ( $k_1$  step) which is consistent with the data in Figure 2.6A and derivation of Equation 2.4. Numerals at the two-sided arrows 1–4 correspond to the rate constants  $k_1$ – $k_4$ , respectively. Pathways 2 and 3 are kinetically indistinguishable (see text for details).



The data in Figure 2.6A were fitted to Equation 2.4 for estimating relative reactivities of the TAML species involved. The  $K_{a1}$  value of  $10^{-10.3}$  M found in the UV-vis titration experiment was used in the fitting procedure similar to treatments we have developed previously.<sup>19</sup> Here, the data in Figure 2.6A were fitted to Equation 2.4 to achieve the best visual match between the calculated and experimental the  $k_1$  versus pH data. Since  $k_2$  and  $k_3$  pathways are kinetically indistinguishable, the  $k_3$  pathway was ignored to calculate the upper limit for  $k_2$ . Then  $k_2$  was assumed to be negligible for calculating the upper limit for  $k_3$ . The rate constants  $k_1$ – $k_4$ , which were estimated at  $\pm 50\%$ , were used to calculate the profile in Figure 2.6A, equal 100,  $2.3 \times 10^4$ ,  $12 \times 10^4$  and  $0.2 \times 10^4 \text{ M}^{-1} \text{ s}^{-1}$ , respectively.

The rate constant  $k_{II}$  as a function of pH is shown in Figure 2.6B. The values of  $k_{II}$  exceed those of  $k_I$ , a relationship that has been commonly found for small molecule synthetic activators of peroxides.<sup>4</sup> A very broad maximum of activity in the bleaching of Orange II is found for  $k_{II}$  and this drops significantly in mildly acidic media on going from pH 7 to pH 6. In general, the dependence agrees with the existence of multiple high-valent oxidizing iron species across the studied pH range. This is consistent with the recent detailed studies of the speciation of oxidized TAMLs where fast reacting  $\text{Fe}^V$  and slower reacting  $\text{Fe}^{IV}$  species are produced from both **1a** and its fluorinated ( $R = F$ ), ring-dichloro counterpart using  $[\text{Fe}(\text{CN})_6]^{4-}$  as an electron donor.<sup>22</sup> However, the asymmetric bell-shaped  $k_{II}$  vs. pH profiles with  $[\text{Fe}(\text{CN})_6]^{4-}$  were much sharper and there was a significant rate decline on going from pH 10 to 12. Figure 2.6B indicates more pronounced reactivity at pH 12 which we attribute to the deprotonation of Orange II ( $pK_a = 11.3$ )<sup>23</sup> leading to a more oxidatively susceptible phenolate form of the dye as

compared to its protonated neutral form. No attempt was made to quantify the results in Figure 2.6B as performed for the data in Figure 2.6A because of the complex speciation of both reagents in the system. In fact, in addition to the at least four oxidized  $\text{Fe}^{\text{IV}}$  species,<sup>22</sup> Orange II equilibrates between the corresponding keto, enol, and deprotonated species (Figure 1.6).<sup>23</sup>

#### 2.2.4 *Properties and Catalytic Activity of 7b in the Bleaching Orange II by $\text{H}_2\text{O}_2$*

The acid-base properties of **7b** were spectrophotometrically studied in the pH range of 6–12. The data in Figure 2.8 indicate major variations of absorbance with pH around 350 nm as found for **7a** (Figure 2.3). There are however two isosbestic points at 332 and 407 nm as opposed to just one for **7a** at 322 nm. The absorbance vs. pH curve was expectedly shifted by ca. 0.3 pH units to the acidic region compared to **7a** (inset A to Figure 2.8) and the  $\text{p}K_{\text{a1}}$  value of  $10.03 \pm 0.03$  has been calculated for **7b** using Equation 2.2 as shown in Inset B to Figure 2.8 (cf. with  $\text{p}K_{\text{a1}} = 10.32 \pm 0.03$  measured for **7a**). The  $\text{p}K_{\text{a}}$  value for **7b** is 0.3 lower than that of **7a**. To make sure that the shift induced by the ring nitro-group is typical of TAMLs, we remeasured the  $\text{p}K_{\text{a}}$  of **1a** for better accuracy<sup>13</sup> and also obtained the  $\text{p}K_{\text{a}}$  of **1b** (Figure 2.9 and Figure 2.10). The  $\text{p}K_{\text{a}}$  values of  $10.3 \pm 0.1$  and  $10.00 \pm 0.05$  were found for **1a** and **1b**, respectively, revealing that (i) these are identical to those of **7a** and **7b**, respectively, and (ii) they differ by 0.3. Thus, a nitro group at the aromatic ring of either **1** or **7** produces similar changes in  $\text{p}K_{\text{a}}$  of the axial water. The saddle point of Figure 2.10, observed previously for nitro-substituted TAMLs with low  $\text{p}K_{\text{a}}$  values, suggests that the **1b** complex is beginning to undergo deprotonation of the second axial ligand.<sup>14</sup>

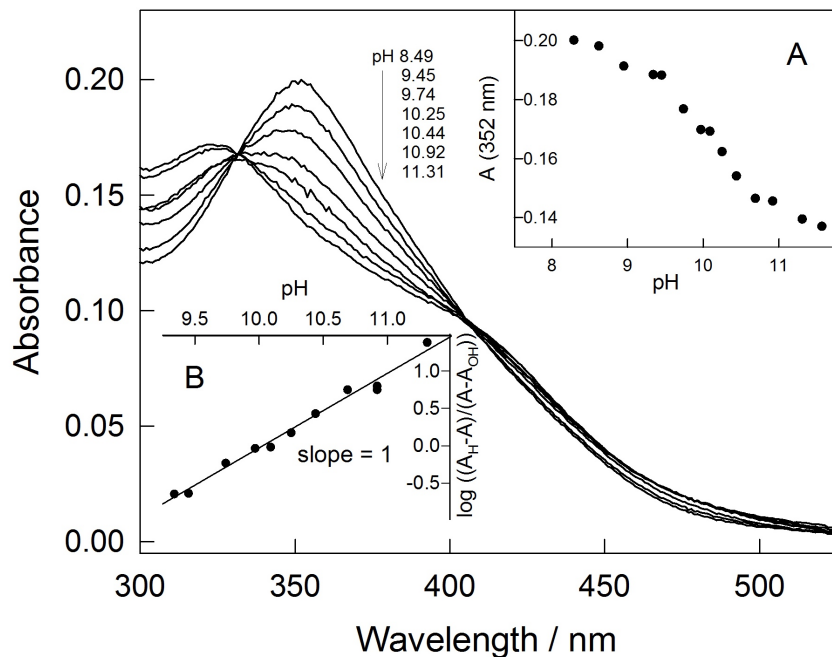


Figure 2.8 Spectra of **7b** ( $5.7 \times 10^{-6}$  M) at different pH at 25 °C and 0.01 M phosphate buffer. Inset A shows absorbance at 353 nm versus pH. Inset B is a linearization of the data in Inset A in terms of Equation 2.2.

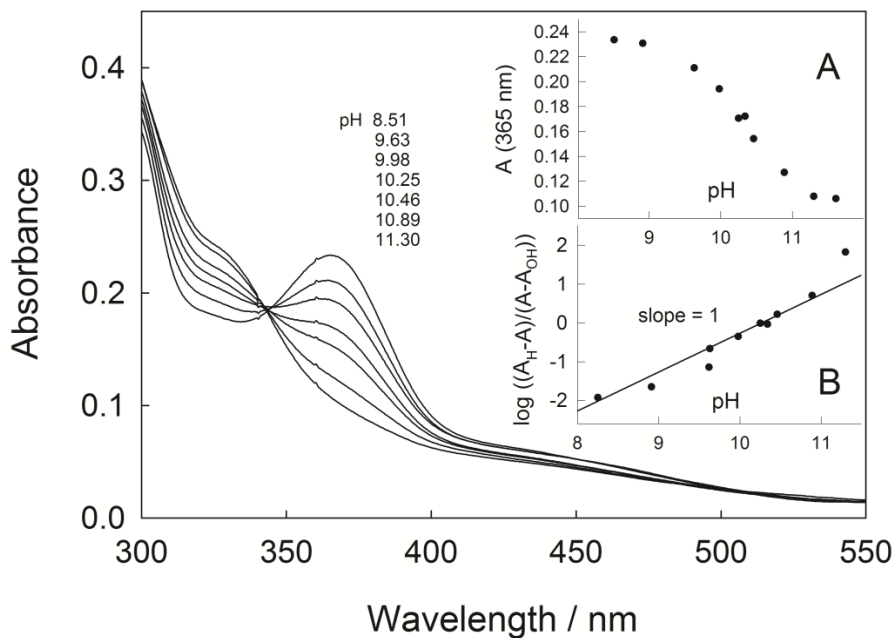


Figure 2.9 Spectra of **1a** ( $5.0 \times 10^{-5}$  M) at different pH at 25 °C and 0.0175 M wide range buffer. Inset A shows absorbance at 365 nm versus pH. Inset B is a linearization of the data in Inset A in terms of Equation 2.2.

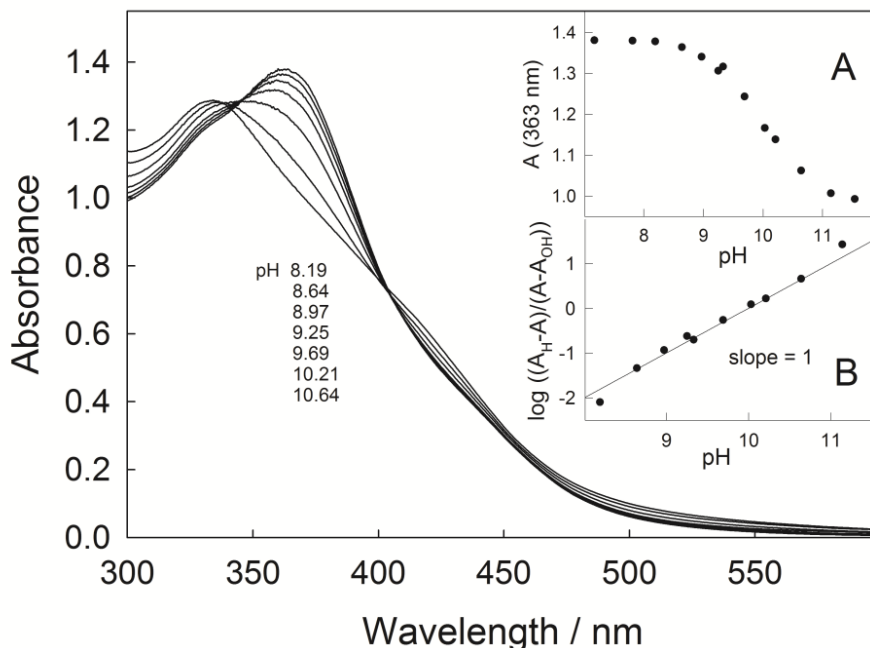


Figure 2.10 Spectra of **1b** ( $5.5 \times 10^{-5}$  M) at different pH at 25 °C and 0.0175 M wide range buffer. Inset A shows absorbance at 363 nm versus pH. Inset B is a linearization of the data in Inset A in terms of Equation 2.2.

Kinetic experiments with **7b** indicated the expected enhanced catalytic activity around pH 7 when compared with **7a**. The bleaching proceeded at higher rates at neutral and mildly basic conditions. It was verified that the steady-state rate of Orange II bleaching depended linearly on [**7b**] in the range of  $(0.26\text{--}2.6) \times 10^{-7}$  M at pH 7 and 25 °C. As it was previously measured for **5b**,<sup>15</sup> kinetic data for **7b** were collected at three critical pH values, viz. 7, 9 and 11. The rate constants  $k_I$  and  $k_{II}$  obtained as described above for **7a** (Table 2.1) show that at pH 7, in terms of  $k_I$ , **7b** is more than three times more reactive than **7a**, while in terms of  $k_{II}$ , **7b** exceeds **7a** by only 21%. The latter difference is however less important than the former, because  $k_I \ll k_{II}$  and in most instances the activation of  $\text{H}_2\text{O}_2$  ( $k_I$ ) is the rate-limiting step.

Table 2.1 Values of  $pK_a$  and rate constants  $k_I$  and  $k_{II}$  for the TAML-catalyzed oxidative bleaching of Orange II by  $H_2O_2$  in 0.01 M phosphate buffer at 25 °C.

TAML	pH	$k_I / M^{-1} s^{-1}$	$10^{-4} \times k_{II} / M^{-1} s^{-1}$	$10^3 \times k_I / s^{-1}$	$pK_a$
<b>7a</b>	7	$140 \pm 20$	$2.3 \pm 0.2$	$3.0 \pm 0.4$	$10.32 \pm 0.03$
<b>7b</b>	7	$470 \pm 30$	$2.9 \pm 0.2$	$0.66 \pm 0.03$	$10.03 \pm 0.03$
<b>7c</b>	7	$85 \pm 3$	$0.19 \pm 0.01$	$0.23 \pm 0.05$	
<b>7b</b>	9	$1370 \pm 90$	$4.6 \pm 0.2$	$1.2 \pm 0.1$	
<b>7b</b>	11	$3200 \pm 700$	$3.3 \pm 0.2$	$0.5 \pm 0.3$	
<b>5b</b>	7	$1900 \pm 100^a$	$52 \pm 2^a$		

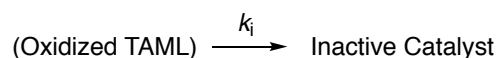
<sup>a</sup> From ref. 15

#### 2.2.5 Catalytic Activity of **7c** in the Bleaching Orange II by $H_2O_2$

The catalytic activity of **7c**, which differs from **7a** in having a phenyl instead of a methyl group at the tail nitrogen, has been investigated at pH 7 and 25 °C. The effective rate constants  $k_I$  and  $k_{II}$  for **7c**, evaluated as described above for **7a** and summarized in Table 2.1, indicate that the phenyl for methyl substitution is disadvantageous for the catalysis in terms of both  $k_I$  and  $k_{II}$ . The less than two-fold decrease in  $k_I$  and more than tenfold decrease in  $k_{II}$  signals a greater retardation of the bimolecular substrate oxidation than the bimolecular  $H_2O_2$  activation. This small sensitivity of  $k_I$  to ligand modifications is by now well established for TAMLs.<sup>19</sup> In a comparison of  $k_{II}$  for **7a** and **7c** it is possible that steric effects play a role in the interaction of the oxidized TAML species with Orange II. However, since the phenyl ring is well removed from the vicinity of the iron (see Figure 2.2), the steric effect may be weak and possible electron-donating properties the phenyl group may retard the reactivity. Since **7c** showed weaker reactivity compared with **7a**, no attempts were made to evaluate the values of  $k_I$  and  $k_{II}$  at different pHs.

### 2.2.6 Operational Stability of TAML Activators 7.

Although the rate constants  $k_I$  and  $k_{II}$  describe adequately the catalytic activity of oxidation catalysts, they are often insufficient to fully portray reactivity due to the well-established fact that synthetic oxidation catalysts undergo structure-dependent suicidal inactivation described by the rate constant  $k_i$ . Note that catalyst degradation is an advantage for environmental applications and has come to constitute a key component of the real world value of TAML activator processes. Thus, the degradation feature of functional catalysis (Equation 2.5) should be added to Figure 2.4



Equation 2.5

The rate constants  $k_i$  characterize the operational stability of TAMLs. The feedback given by  $k_i$  is essential in the design of TAML catalysts for practical applications and, since one should avoid introducing persistent compounds into the environment, especially for water purification processes.

The objectives and procedure for calculating  $k_i$  were first addressed a decade ago.<sup>24</sup> In that work, it was demonstrated that when the mechanism in Figure 2.4 is operative and the condition  $k_I[\text{ROOH}] \gg k_{II}[\text{S}]$  holds, i.e. the first step is significantly faster, a simple relation between  $k_{II}$ ,  $k_i$ , and the total concentration of added catalyst  $[\text{Fe}^{\text{III}}]$  holds:

$$\ln \left( \frac{S_0}{S_\infty} \right) = \left( \frac{k_{II}}{k_i} \right) [\text{Fe}^{\text{III}}]$$

Equation 2.6

Here  $S_0$  and  $S_\infty$  are substrate concentrations at time zero and infinity, respectively. The application of Equation 2.6 requires that the conversion of S should be incomplete under the experimental conditions. The regime of incomplete conversion such as in Figure 2.11, realized by the example of **7a**, is achieved trivially by using a low loading of the catalyst. Very recently, a collaboration between mathematical and chemical research teams allowed us to reach the important conclusion that Equation 2.6 actually holds under all conditions, regardless of the contributions from the  $k_I[\text{ROOH}]$  and  $k_{II}[\text{S}]$  terms.<sup>25</sup> This allowed us to experimentally evaluate and compare the rate constants  $k_i$  for the new family of TAMs **7** at pH 7 when  $k_I[\text{ROOH}] < k_{II}[\text{S}]$ .

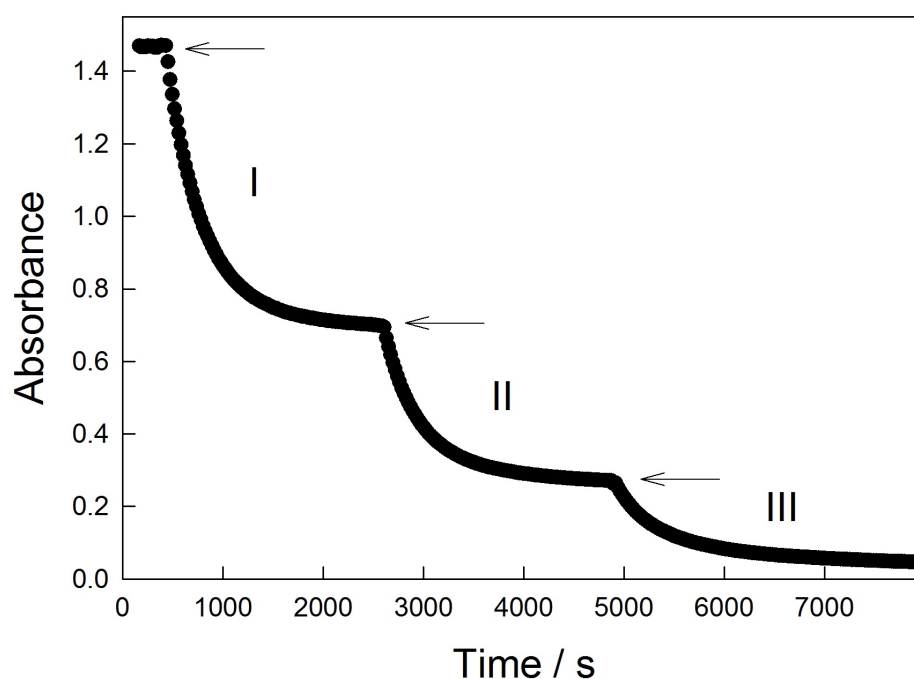


Figure 2.11 Kinetic curves for incomplete bleaching of Orange II ( $5.4 \times 10^{-5}$  M) by  $\text{H}_2\text{O}_2$  (0.013 M) catalyzed by **7a** measured at 480 nm. Arrows indicate when an aliquot of catalyst was added to return the catalyst concentration to  $1.3 \times 10^{-7}$  M at pH 7 and 25 °C.

Incomplete bleaching of Orange II in Figure 2.11 is observed with  $[7a] = 1.3 \times 10^{-7}$  M,  $[H_2O_2] = 0.013$  M and  $[S] = 5.4 \times 10^{-5}$  M. The oxidation is restored upon adding a second aliquot of **7a** showing that the stalled reactivity is indeed due to catalyst degradation. The data of Figure 2.11 make it possible to calculate  $k_i$  from the portions **I** and **II** of the curve when the values of  $S_0$  and  $S_\infty$  (which can be replaced with the corresponding absorbances) could be reliably estimated. Portion **III** is less appropriate for evaluating  $k_i$ , because “incomplete conversion” does not hold strictly resulting in ambiguous estimation of  $S_\infty$ . The average value of  $k_i$  calculated using Equation 2.6 from portions **I** and **II** of Figure 2.8 together with calculated similarly  $k_i$  for **7b** and **7c** are shown in Table 2.1.

#### 2.2.7 Discussion

The kinetic and equilibrium studies reported herein indicate that the properties of the fifth generation **7** TAMLs are close to those of the first generation **1** TAMLs. Similarities include (i) ready hydrolysis of the chloro ligand, (ii) acidity ( $pK_a$ 's) of the axially coordinated water, and (iii) a common reaction mechanism of oxidation of Orange II by  $H_2O_2$  summarized in Figure 2.4 and Equation 2.5. TAMLs **7** (as well as **1**) and **5** differ in the lack of evidence for the deprotonation of the second axial water at pH up to 12 for the former two. A closer look at the  $pK_a$  values reveals an interesting feature. The  $pK_a$  values for **7** and **1** are similar, indicative of an equal Lewis acidity of the central iron. All previous evidence<sup>3,4</sup> suggests that **7** should be as aggressive ratewise as **1**. The values of  $k_I$  and  $k_{II}$  in Table 2.1 indicate, however, that this is not the case at pH 7. The reactivity of **7a** exceeds that of **1a** by the factor of ca. 3 in terms of  $k_I$  ( $k_I = 52 \text{ M}^{-1} \text{ s}^{-1}$  for **1a** at pH 7),<sup>19</sup> i.e. in the activation of  $H_2O_2$  by  $Fe^{III}$ . An input into the catalytic activity of **7** is likely



due to some other perturbation which we speculate is a steric factor associated with the changes in the six-membered ring of TAMLs. The hypothesis finds support in the markedly lower reactivity of **7c** compared to **7a** in which a phenyl group is attached to the  $sp^2$  nitrogen. The corresponding values of  $k_I$  and  $k_{II}$  drop by a factor of ca. 2 and 10, respectively, between **3a** and **3c**. The rate decrease is more pronounced for the  $k_{II}$  step and is consistent with the degree of steric control because the larger Orange II molecule should experience increased steric retardation compared to the smaller  $H_2O_2$ . At this time, this discussion does not preclude contributions from electronic effects (see above) including those arising from angular changes and from delocalization of the biuret nitrogen lone pair into the six-membered ring of **7**.

The reactivity of **7b** in terms of  $k_I$  and  $k_{II}$  is lower than that of **5b** at pH 7, i.e. TAMLs **5** remain the most catalytically active so far (Table 2.1). Activator **5b** is almost an order of magnitude more aggressive in terms of  $k_{II}$ . Thus, the overall reactivity of TAMLs discussed in this chapter decreases in the series: **5** > **7** > **1** (Table 1.3).

The highest operational stability (the lowest  $k_i$ ) belongs to the least reactive catalyst **7c**. As in the study performed at pH 11 with **1**,<sup>24</sup> the nitro group attached to head aryl group of **7b** protects the catalyst from suicidal degradation and the protecting effect, manifested by a factor of 4.5 in  $k_i$ , is significant. This suggests again that introduction of the nitro substituent is beneficial for increasing the operational stability of TAMLs in oxidations by  $H_2O_2$ .

### 2.3 Conclusions

In conclusion, the mechanism of action of the *N*-tailed TAML activators **7** in bleaching of Orange II by  $\text{H}_2\text{O}_2$  is identical to that established for the first generation TAMLs **1**. The same rate law Equation 2.3 holds though the rate constants  $k_{\text{I}}$  and  $k_{\text{II}}$  are several times greater than those for related complexes **1**. Complexes **7** are more advantageous than **1** for oxidizing purposes at neutral pH though they are still less aggressive compared to the fourth generation TAMLs **5**.

## 2.4 Experimental

### 2.4.1 Materials and Methods

Complex **7a** was synthesized according to published method.<sup>6</sup> The synthesis of variant of **7a**, complex **7a'** with the axial MeOH ligand and Li<sup>+</sup> as a counterion, is described below. Synthesis of **7b** is described elsewhere.<sup>26</sup> Compound **7c** was prepared by students of Prof. Sayam Sen Gupta.<sup>27</sup> *N,N*-Bis(chloroformyl)methylamine was purchased from ChemCollect. H<sub>2</sub>O<sub>2</sub> (30%) was obtained from Fischer and its concentration was verified daily by UV-vis spectroscopy using  $\epsilon$  72.8 M<sup>-1</sup> cm<sup>-1</sup> at 230 nm.<sup>28</sup> Orange II was purchased from Acros and recrystallized from aqueous ethanol. All other reagents and solvents (at least ACS reagent grade) were purchased from commercial sources and used as received, or, if necessary, purified using standard procedures.<sup>29</sup>

### 2.4.2 Synthesis of **7a'**

Steps of preparation of **7a'** are shown in Figure 2.12. Compounds **A**, **B**, and **C** were synthesized are described elsewhere.<sup>6,30</sup> Ligand **C** was metallated as follows: Dry THF (5 mL) and **C** (25 mg) were combined in a 3-neck round bottom flask under Ar. *n*-BuLi (0.2 mL, 1.6 M in hexane) was added at 0 °C followed by anhydrous FeCl<sub>3</sub> (25 mg). The mixture was stirred at 22 ± 2 °C overnight. The precipitate formed was filtered through a glass frit and purified by column chromatography using basic alumina (Et<sub>3</sub>N:MeOH:CH<sub>2</sub>Cl<sub>2</sub> = 1:5:94 v/v). The solvent was removed and **7a'** was recrystallized by vapor diffusion of ether into MeCN. Yield 9 mg (29%). Anal: Found: C, 50.01; H, 7.00; N, 13.45. Calculated for C<sub>17</sub>H<sub>19</sub>FeN<sub>5</sub>O<sub>4</sub>Li·CH<sub>3</sub>OH·C<sub>4</sub>H<sub>10</sub>O: C, 50.21; H, 6.32; N,

13.31%. UV-vis:  $\lambda_{\text{max}}(\text{H}_2\text{O})$  353 nm ( $\epsilon$  2200  $\text{M}^{-1} \text{cm}^{-1}$ ). ESI-MS (negative mode):  $m/z$  413.3 (M, 100%; calculated for  $\text{C}_{17}\text{H}_{19}\text{FeN}_5\text{O}_4$ : 413.1).

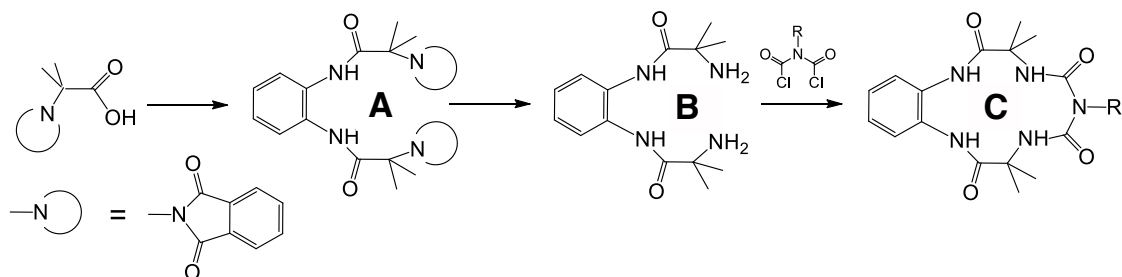


Figure 2.12 Method of preparation of **7**; R = Me for **7a** and **7a'**.

#### 2.4.3 Kinetics of TAML-catalyzed bleaching of Orange II by $\text{H}_2\text{O}_2$ .

Reaction progress was followed by monitoring a decrease in absorbance of Orange II at 484 nm using an Agilent 8453 spectrophotometer as described in detail elsewhere.<sup>12</sup> Stock solutions of TAMLs (ca.  $1.3 \times 10^{-3}$  M) and Orange II ( $1.2 \times 10^{-3}$  M) were prepared in HPCL grade water. Orange II and a TAML catalyst were combined in 1.0 mL of 0.01 M phosphate buffer in polystyrene cuvettes. A solution of  $\text{H}_2\text{O}_2$  was then added to initiate the reaction. All kinetic measurements were performed at 25 °C. Initial rates of Orange II bleaching were calculated from the linear absorbance vs. time plots using the extinction coefficient for Orange II of 20,200 and 20,600  $\text{M}^{-1} \text{cm}^{-1}$  at pH 6–8 and 9–12, respectively. All initial rates reported are the mean values of at least three determinations. Calculations were performed using a SigmaPlot 12.5 package.

#### 2.4.4 Measurements of $pK_a$ .

Spectrophotometric titrations of **7a** and **7b** were performed using a double beam Cary 300 Bio UV-vis instrument at 25 °C. Aliquots of TAMLs were added to a quartz

cuvette with 0.01 M phosphate buffer and HPLC grade water. Solution pH was adjusted with concentrated KOH and H<sub>3</sub>PO<sub>4</sub> from pH 7 to 12 and back to 7 to confirm reversibility. The pK<sub>a</sub> values were calculated using Equation 2.2.

Spectrophotometric titrations of **1a** and **1b** were performed using a double beam Shimadzu UV-1800 instrument at 25 °C. Aliquots of TAMLs were added to a quartz cuvette with 0.0175 M the wide range buffer<sup>31</sup> (0.01 M borate, 0.005 phosphate, 0.0025 M citrate) and HPLC grade water. Solution pH was adjusted with concentrated KOH and H<sub>3</sub>PO<sub>4</sub> from pH 7 to 12 and back to 7 to confirm reversibility. The pK<sub>a</sub> values were calculated using Equation 2.2.

#### 2.4.5 *X-Ray structural investigation of 7c.*

The PPh<sub>4</sub><sup>+</sup> salt of **7c** was made by slow vapor diffusion of diethyl ether over the solution the ingredients in CH<sub>2</sub>Cl<sub>2</sub>. The X-ray data were collected at 100 K on a Super Nova Dual source X-ray Diffractometer system (Agilent Technologies) equipped with a CCD area detector and operated at 250 W (50 kV, 0.8 mA) to generate MoK $\alpha$  radiation ( $\lambda = 0.71073$  Å). The crystal was mounted on Nylon CryoLoops with Paratone-N (Hampton Research). Initial scans were performed to obtain preliminary unit cell parameters and to assess the mosaicity (breadth of spots between frames) of the crystal for selecting the required frame width for data collection. CrysAlis<sup>Pro</sup> software was used to carry out overlapping  $\phi$  and  $\omega$  scans at detector ( $2\theta$ ) settings ( $2\theta = 28^\circ$ ). Following data collection, reflections were sampled from all regions of the Ewald sphere to redetermine unit cell parameters. In no data collection was evidence for crystal decay. The data were integrated using CrysAlis<sup>Pro</sup> software with a narrow frame algorithm and

corrected for absorption using SCALE3 ABSPACK scaling algorithm. The structure was solved directly and refined using SHELXTL-97. The final model was refined anisotropically until full convergence was achieved. Hydrogen atoms were placed in calculated positions ( $C-H = 0.93 \text{ \AA}$ ) and included as riding atoms with isotropic displacement parameters 1.2–1.5 times  $U_{eq}$  of the attached C atoms. The structure was examined using the Addsym subroutine of PLATON to assure that no additional symmetry could be applied to the model. Crystallographic data have been deposited in CCDC as deposition No. CCDC 1006325. Copies of the data can be obtained, free of charge, on application to the CCDC, 12 Union Road, Cambridge CB2 1EZ, U.K. [fax: þ 44 (1223) 336 033; e-mail: [deposit@ccdc.cam.ac.uk](mailto:deposit@ccdc.cam.ac.uk)].

## 2.5 References

1. Collins, T. *Acc. Chem. Res.* **1994**, 27 (12), 279–285.
2. Collins, T. J. *Acc. Chem. Res.* **2002**, 35 (9), 782–790.
3. Ryabov, A.; Collins, T. *Adv. Inorg. Chem.* **2009**, 61, 471–521.
4. Ryabov, A. D. *Adv. Inorg. Chem.* **2013**, 65, 118–163.
5. Collins, T. J.; Khetan, S. K.; Ryabov, A. D. In *Handbook of Green Chemistry*; Anastas, P. T., Crabtree, R. H., Eds.; Wiley-VCH Verlag GmbH & Co. KGaA, 2010; p 39.
6. Panda, C.; Ghosh, M.; Panda, T.; Banerjee, R.; Sen Gupta, S. *Chem. Commun.* **2011**, 47, 8016–8018.
7. Malvi, B.; Panda, C.; Dhar, B. B.; Sen Gupta, S. *Chem. Commun.* **2012**, 48 (43), 5289–5291.
8. Panda, C.; Dhar, B. B.; Malvi, B.; Bhattacharjee, Y.; Sen Gupta, S. *Chem. Commun.* **2013**, 49 (22), 2216–2218.
9. Ghosh, M.; Singh, K. K.; Panda, C.; Weitz, A.; Hendrich, M. P.; Collins, T. J.; Dhar, B. B.; Gupta, S. *J. Am. Chem. Soc.* **2014**, 136 (27), 9524.
10. Bartos, M.; Gordon-Wylie, S. *Coord. Chem. Rev.* **1998**, 174, 361–390.
11. Horwitz, C.; Fooksman, D. *J. Am. Chem. Soc.* **1998**, 120 (17), 4867–4868.
12. Chahbane, N.; Popescu, D.-L.; Mitchell, D. A.; Chanda, A.; Lenoir, D.; Ryabov, A. D.; Schramm, K.-W.; Collins, T. J. *Green Chem.* **2007**, 9 (1), 49–57.
13. Ghosh, A.; Ryabov, A. D.; Mayer, S. M.; Horner, D. C.; Prasuhn, D. E.; Sen Gupta, S.; Vuocolo, L.; Culver, C.; Hendrich, M. P.; Rickard, C. E. F.; Norman, R. E.; Horwitz, C. P.; Collins, T. J. *J. Am. Chem. Soc.* **2003**, 125 (41), 12378–12379.
14. Ellis, W. C.; Tran, C. T.; Roy, R.; Rusten, M.; Fischer, A.; Ryabov, A. D.; Blumberg, B.; Collins, T. J. *J. Am. Chem. Soc.* **2010**, 132 (28), 9774–9781.
15. Ellis, W. C.; Tran, C. T.; Denardo, M. A.; Fischer, A.; Ryabov, A. D.; Collins, T. J. *J. Am. Chem. Soc.* **2009**, 131 (50), 18052–18053.
16. Theodoridis, A.; Maigut, J.; Puchta, R.; Kudrik, E. V.; Eldik, R. van. *Inorg Chem* **2008**, 47 (8), 2994–3013.
17. Ember, E.; Rothbart, S.; Puchta, R.; van Eldik, R. *New J. Chem.* **2009**, 33 (1), 34.
18. Rothbart, S.; Ember, E. E.; van Eldik, R. *New J. Chem.* **2012**, 36 (3), 732–748.
19. Ghosh, A.; Mitchell, D. a; Chanda, A.; Ryabov, A. D.; Popescu, D. L.; Upham, E. C.; Collins, G. J.; Collins, T. J. *J. Am. Chem. Soc.* **2008**, 130 (45), 15116–15126.
20. Mitchell, D. A.; Ryabov, A. D.; Kundu, S.; Chanda, A.; Collins, T. J. *J. Coord. Chem.* **2010**, 63 (14–16), 2605–2618.
21. Popescu, D.-L.; Vrabel, M.; Brausam, A.; Madsen, P.; Lente, G.; Fabian, I.; Ryabov, A. D.; van Eldik, R.; Collins, T. J. *Inorg. Chem.* **2010**, 49 (24), 11439–11448.
22. Kundu, S.; Annavajhala, M.; Kurnikov, I. V.; Ryabov, A. D.; Collins, T. J. *Chem. - A Eur. J.* **2012**, 18 (33), 10244–10249.
23. Ibáñez, G. A.; Olivieri, A. C.; Escandar, G. M. *J. Chem. Soc. - Faraday Trans.* **1997**, 93 (4), 545–551.
24. Chanda, A.; Ryabov, A. D.; Mondal, S.; Alexandrova, L.; Ghosh, A.; Hangun-Balkir, Y.; Horwitz, C. P.; Collins, T. J. *Chem. - A Eur. J.* **2006**, 12 (36), 9336–9345.

25. Emelianenko, M.; Torrejon, D.; DeNardo, M. A.; Socolofsky, A. K.; Ryabov, A. D.; Collins, T. J. *J. Math. Chem.* **2014**, *52* (5), 1460–1476.
26. Panda, C.; Debgupta, J.; Díaz Díaz, D.; Singh, K. K.; Sen Gupta, S.; Dhar, B. B. *J. Am. Chem. Soc.* **2014**.
27. Warner, G. R.; Mills, M. R.; Enslin, C.; Pattanayak, S.; Panda, C.; Panda, T. K.; Gupta, S. Sen; Ryabov, A. D.; Collins, T. J. *Chem. - A Eur. J.* **2015**, *21* (16), 6226–6233.
28. George, P. *Biochem. J.* **1953**, *54*, 267–276.
29. Chai, C.; Armarego, W. L. F. *Purification of Laboratory Chemicals*, Fifth Ed.; Butterworth-Heinemann, 2003.
30. Ghosh, A.; Ramidi, P.; Pulla, S.; Sullivan, S. Z.; Collom, S. L.; Gartia, Y.; Munshi, P.; Biris, A. S.; Noll, B. C.; Berry, B. C. *Catal. Letters* **2010**, *137* (1–2), 1–7.
31. Carmody, W. R. *J. Chem. Educ.* **1961**, *38* (11), 559.



## **CHAPTER 3**

### **Design and Synthesis of Sulfonamide-Containing NewTAMLs**

### 3.1 Introduction

The preparation of TAML activators has evolved over the years to become safer and higher yielding, increasing the potential for commercial use. The original azide-based synthetic route has been replaced, allowing commercial production of the prototype TAML **1a** (Figure 3.1).<sup>1</sup> Although **1a** proved to be a successful catalyst capable of performing many commercially relevant oxidation processes, wide-scale adoption has been unsuccessful due in large part to the cost of TAML compared to its productivity before inactivation.<sup>2–5</sup> Methods of increasing reactivity, increasing lifetime, and decreasing cost of synthesis have all been investigated to improve the commercial appeal of TAML activators for scaled use.<sup>5–8</sup>

Early augmentation of the reactivity of **1a** was achieved through substitution of various groups at the X and R positions. The most successful substituent at the X position at the “head” of the catalyst was a nitro (NO<sub>2</sub>) group (TAML **1b**). The strongly electron withdrawing properties of the NO<sub>2</sub> group increased the Lewis acidity of the metal center, favorably increasing reactivity at neutral pH and providing a small increase in stability.<sup>6,7</sup> At the tail, introducing fluorines as the R groups further increased activity and decreased susceptibility of the resting state catalyst to hydrolysis ( $k_b$ , Figure 1.3).<sup>9,10</sup> Although TAML **1c**, with both NO<sub>2</sub> and F substituents, was a highly reactive catalyst, the complexity and cost of preparation increased compared to **1a**. Furthermore, even though fluorine-containing TAMLs have so far passed all toxicity tests (see Chapter 1),<sup>11</sup> the use of halogen atoms in materials designed to be released into the environment is undesirable to avoid potential persistence and toxicity.<sup>12</sup> The ideal TAML catalyst for commercial

development will have an easy-to-prepare, robust ligand that contains only biochemically common elements.

Further study of TAMLs **1** revealed an additional design problem. Although TAML **1c** was highly active, when the lifetime of the catalyst was quantified in comparison to the rate of reaction with a substrate, the lifetime was discovered to have decreased in proportion to the reactivity increase. In other words, the productivity gains of **1c** due to fast reactivity were negated by quick inactivation. This trend was found to hold for all TAML activators with varying substituents and of various structure types. Figure 3.2 shows a linear free energy relationship of the rate of substrate oxidation ( $k_{II}$ , Figure 1.3) compared to the rate of inactivation ( $k_i$ ) for all OldTAML activators. The relationships between activity and stability for **3** and **7** are discussed below.<sup>13</sup>

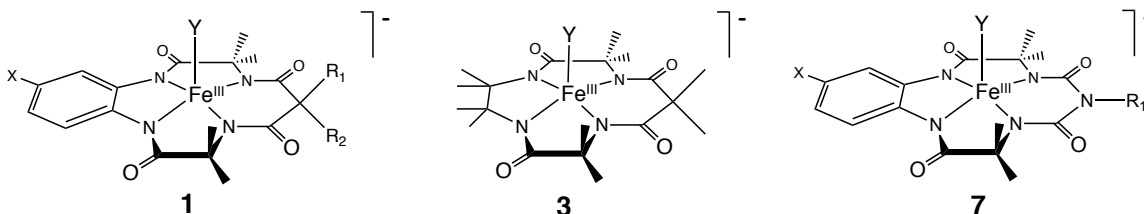


Figure 3.1 OldTAML structures that informed the design of NewTAMLs.

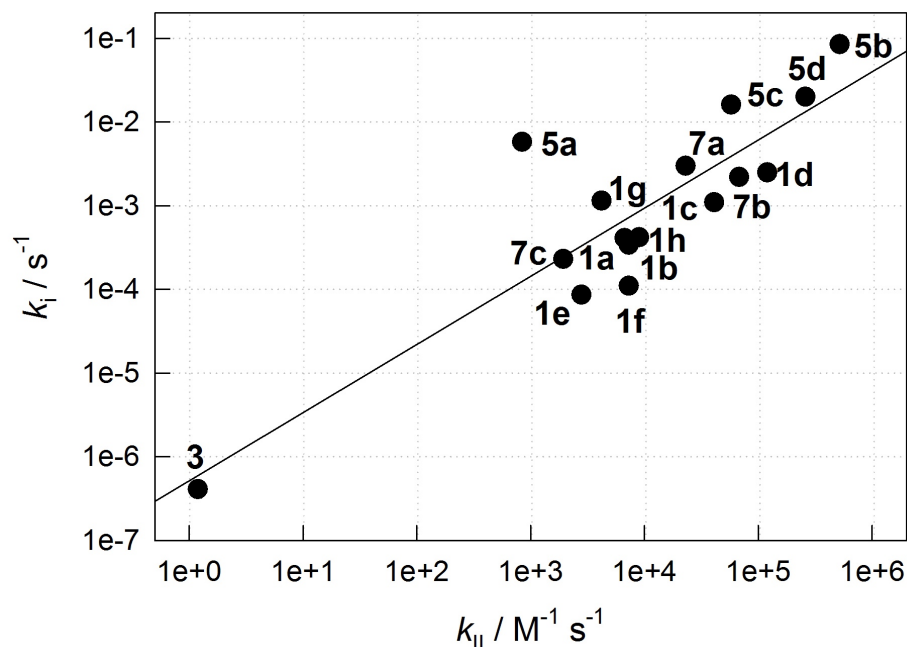


Figure 3.2 Linear free energy plot between  $k_{II}$  and  $k_i$  for OldTAMLs **1**, **3**, **5**, and **7** at 25 °C and pH 7. Values of  $k_{II}$  are for the bleaching of Orange II. Adapted from ref 13.

Resistance to intramolecular oxidative inactivation was one of the key design features of TAML activators, but the “live fast, die young” properties of **1c** proved that another turn of the iterative design loop (Chapter 1, Figure 1.5) was necessary to produce robust catalysts. Unfortunately, the ultra-dilute conditions in which modern TAMLs are used make collection and identification of catalyst degradation products nearly impossible for identifying the weak site. The more indirect routes of designing ligands with modifications to key structural features and further mechanistic studies to reveal the source of the trend in Figure 3.2 were pursued. Beheaded TAML **3** and biuret TAMLs **7**, the latter discussed in Chapter 2, revealed that neither the phenyl head group nor the  $CR_2$  tail group were responsible for the inactivation relationship in Figure 3.2. Both catalyst types fall precisely on the trend line, with **3** extending the proportionality to cover six orders of magnitude in  $k_{II}$ .<sup>13</sup>

This left only the iron center or the amides as the source of TAML inactivation. Recently, mathematical insight into the data in Figure 3.2 has led to the proposal of a mechanism to explain the activity/lifetime relationship that is not oxidative in nature. Unexpectedly, the source inactivation appears to be nucleophilic attack at the amide carbonyl carbons by peroxide and hydroxide.<sup>14</sup> Blocking this inactivation pathway to create a longer lived TAML activator requires elimination of the amide carbonyl groups. Removal of the carbonyls, in addition to avoiding fluorine and substituting electron-withdrawing substituents such as NO<sub>2</sub>, formed the basis of NewTAML design.

### 3.2 Preparation of NewTAML Ligands

NewTAMLs activators are a new class of TAML catalyst containing blocking functionalities such as sulfonamides or phosphonamides in place of some or all of the carbonamides in the ligand.<sup>15</sup> To date, seven NewTAML activators have been produced with various structures (Figure 1.2). However, preparing NewTAMLs is much more complex than simply switching from carbonyl- to sulfonyl-substituted building blocks as synthetic sulfur chemistry is significantly more limited. As a result, many pathways for the synthesis of NewTAMLs were investigated before any were successfully prepared. NewTAMLs were originally conceived with the goal of producing tetrasulfonamide analogs of **1** or **7** (Figure 3.3), but the method of synthesis and availability of building blocks has limited the structures of the NewTAMLs prepared so far.

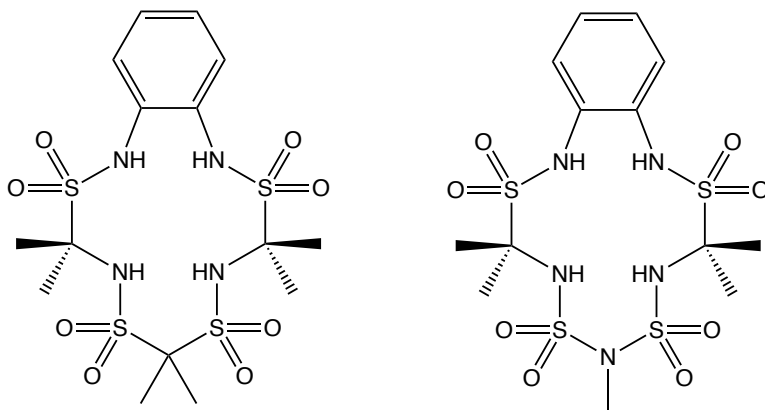


Figure 3.3 Proposed tetrasulfonamide ligand analogs of **1** and **7**.

This chapter details the pathways investigated for the preparation of NewTAML activators, including many failed attempts. Negative results are included for the benefit of future synthetic group members and to show how the limited successful syntheses informed the structures of **2**, **4**, **6**, and **8**. Experimental details are not included for any of the negative results in this chapter. Methods for the successful procedures can be found in

the experimental sections of the following chapters in which the structures and properties of the catalysts are discussed in detail.

### 3.2.1 Preparation of TAML family **1** NewTAML analogs

TAMLs **1**, also known as the B\* series,<sup>16</sup> are typically prepared following the multistep procedure shown in Figure 3.4. First,  $\beta$ -amino acids, referred to as the “arms,” are protected. Two protected arms are then attached to the phenylenediamine “head.” After deprotection, the acid chloride “tail” is added to close the ring, and finally the macrocyclic ligand is metallated. Of the three necessary building blocks, highlighted with dashed boxes in Figure 3.4, the amino acid and malonic acid (or biuret, for **7**) derivatives contain carbonyl groups that can be replaced with more oxidation resistant functionalities.

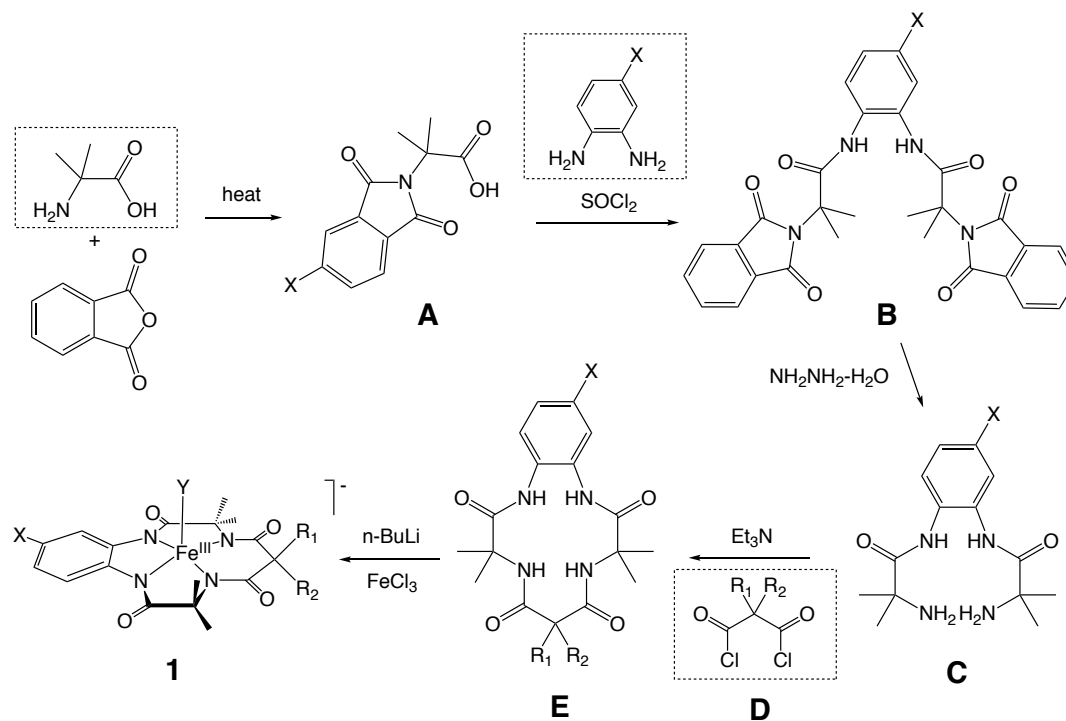


Figure 3.4 General preparation of TAML activators **1**. Building blocks are in dashed boxes.

First, preparation of sulfonate-containing amino acids was investigated. The desired product, 2-aminopropane-2-sulfonic acid, was pursued through three potential pathways involving an imine intermediate (Figure 3.5). However, 2-aminopropane-2-sulfonic acid proved elusive, suggesting that it is an unstable product.

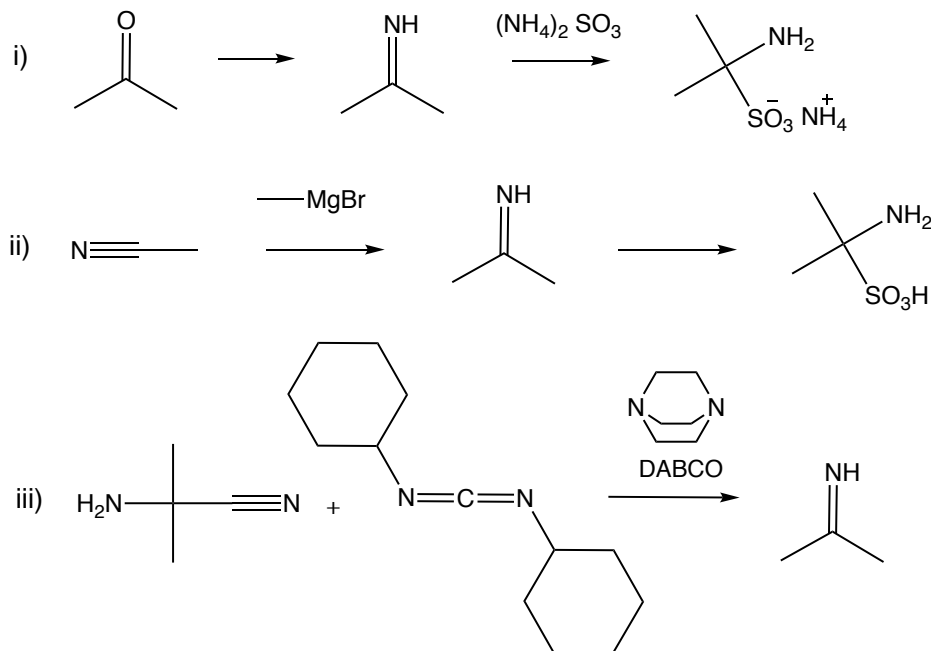


Figure 3.5 Investigated methods of preparation for 2-aminopropane-2-sulfonic acid via 2-propanimine.<sup>17–19</sup>

As preparation of an amino sulfonic acid building block was unsuccessful, the direct preparation of the sulfonyl chloride analog of **A**, structure **H** in Figure 3.6, was investigated next. DABSO, or 1,4-diazabicyclo[2.2.2]octane bis(sulfur dioxide), the sulfur dioxide adduct of nucleophilic amine DABCO (1,4-diazabicyclo[2.2.2]octane, Figure 3.5), is a convenient source of sulfur dioxide that has been used for one-pot preparation of sulfonamides.<sup>20</sup> However, the proposed procedure in Figure 3.6 failed at step (a), which required a brominating agent such as N-bromosuccinimide,  $\text{CBr}_4$ ,  $\text{HBr}$ , or



Br<sub>2</sub>.<sup>21–23</sup> Although  $\beta$ -bromoethylphthalimide is easily prepared, the two methyl groups of **F** created too much steric hindrance for bromination to proceed.<sup>24</sup>

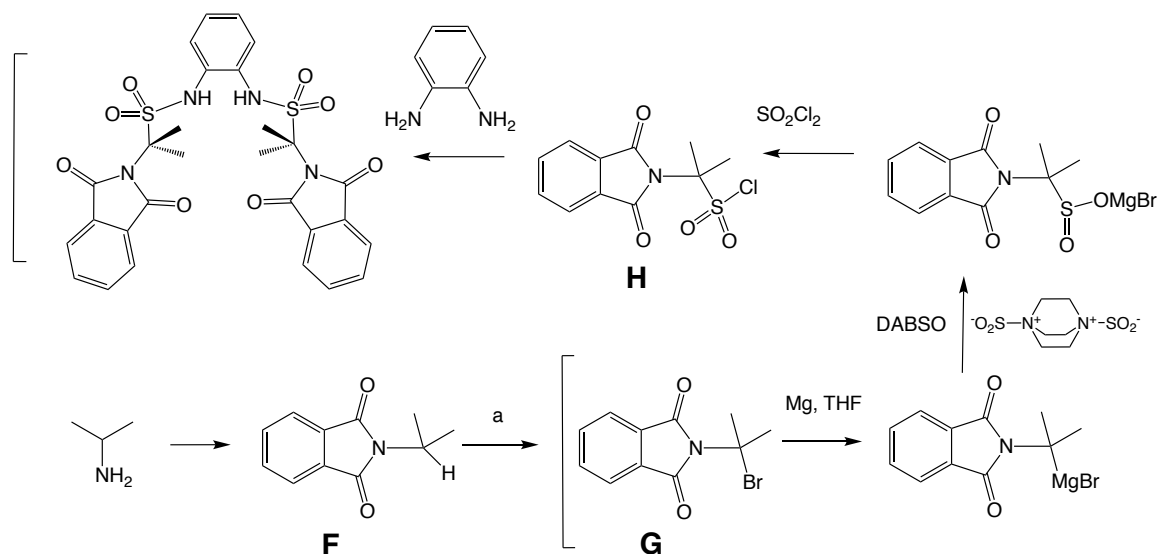


Figure 3.6 Failed preparation for sulfonamide NewTAML arms requiring bromination at step (a) that is not feasible due to steric constraints.

Following the difficulty of preserving the general procedure in Figure 3.4 for preparation of NewTAMLs, a direct “top down” method was investigated in which the arms would be assembled directly on the phenylenediamine. Figure 3.7 shows a proposed example of a top down procedure using aniline as a model reagent. Substituted benzyl ethers were considered as protecting groups. However, the reaction of isopropyl sulfonyl chloride with *o*-phenylenediamine yielded mostly single rather than double addition products, and protecting with benzyl ethers resulted in additional side products. In addition, the last step of Figure 3.7 would likely require an dangerous azide intermediate to produce the final amine product, so this method was not pursued after difficulties in the first and second steps were encountered.

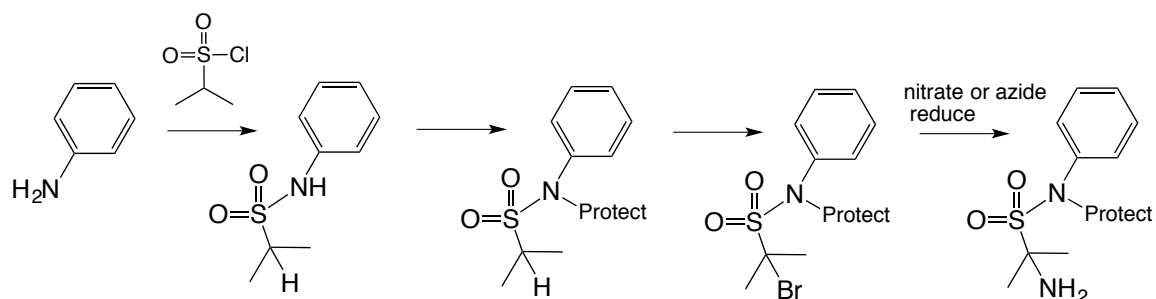


Figure 3.7 A model synthetic procedure for the preparation of NewTAML head and arms with aniline as a model starting material. Executing this procedure with phenylenediamine instead of aniline proved difficult.

Although preparation of 2-aminopropane-2-sulfonic was not successful, aminomethanesulfonic acid is commercially available and was pursued as a model arm group to find out if the general synthetic method for **1** in Figure 3.4 would otherwise work. The “armless” intermediate **L** (Figure 3.8) would most likely not form a useful catalyst after cyclization because without the methyl groups, the structure breaks Rule 1 for design of oxidizing catalysis (Chapter 1). However, a catalyst with this structure was never prepared because of difficulties with deprotection in step iv. Compound **K** was successfully prepared, but deprotection attempted using various reagents including hydrazine and methylamine resulted in decomposition of the product.<sup>25</sup> Further literature research corroborated this result;  $\alpha$ -amino sulfonamide compounds have limited stability and cannot withstand removal of the phthaloyl group.<sup>26–29</sup> It is not likely that deprotection would be successful should this procedure be attempted with substituted  $\alpha$ -amino sulfonic acid starting materials. However,  $\beta$ -amino sulfonic acids such as 2-aminoethanesulfonic acid (taurine) are more stable and may be useful in the preparation of NewTAMLs with larger chelate rings.<sup>26</sup>

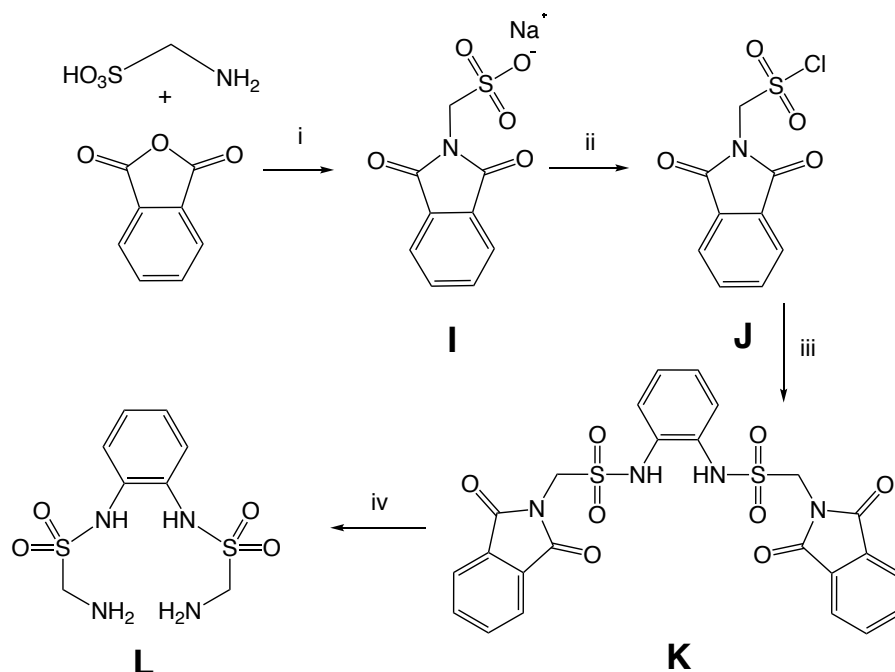


Figure 3.8 Proposed procedure for preparation of an armless sulfonamide ligand intermediate that decomposed at step iv. Reaction conditions: i) 1 eq NaOAc, acetic acid, reflux, recrystallized from water; ii) 1 eq SOCl<sub>2</sub>, catalytic DMF; iii) 0.5 eq o-phenylenediamine, 4 eq Et<sub>3</sub>N, THF, 0 °C; iv) H<sub>4</sub>N<sub>2</sub>, EtOH, reflux.<sup>30,31</sup>

Sulfonamide substitution at the tail was more successful. Preparation of sulfonamide analogs of the malonamide **1** tail (compound **D**, Figure 3.4) and the biuret **7** tail (Chapter 2) were explored. Although imido-bis(sulfuric acid) dichloride **M** (Figure 3.9) was successfully prepared following literature methods and confirmed via IR,<sup>32,33</sup> neither methylation with methyl iodide, dimethyl sulfate, or silver oxide nor repeating the reaction with methylsulfamic acid was successful.<sup>34–37</sup> Preparation of **N** has been reported through methylation of **M** with diazomethane, but this was not attempted due to safety reasons.<sup>35</sup> The highly reactive compound **M** did not combine with **C** to form a viable ligand.

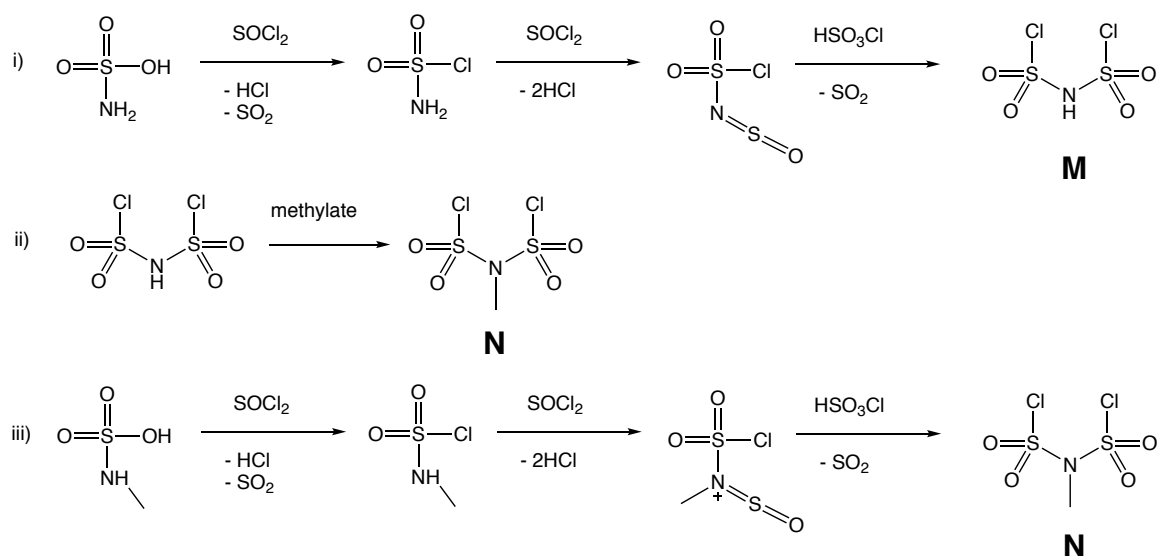


Figure 3.9 Proposed methods of preparation of imido-bis(sulfuric acid) dichloride **M** and its methylated analog **N**. Compound **M** was successfully prepared; compound **N** was not.

Methanedisulfonyl dichloride (**O**, Figure 3.10) is commercially available and readily prepared in the laboratory. When incorporated into a TAML macrocycle, the R = H groups at the tail do not break any of the rules for oxidizing complexes described in Chapter 1. Following literature methods, disulfonyl dichloride compounds **O** and **P** have been prepared and incorporated into NewTAMLs (Figure 3.10).<sup>38–40</sup> However, modification of the synthetic method using isobutyric acid as a starting material to produce **Q**, while claimed under a Japanese patent, has not proven successful.<sup>40</sup>

OldTAMLs **1** with R = H have not been successfully prepared for direct comparison to **2a**. Attempted formation of the ligand **E** (Figure 3.4) with R<sub>1</sub> = R<sub>2</sub> = H using **O** instead of **D** at the tail was unsuccessful.

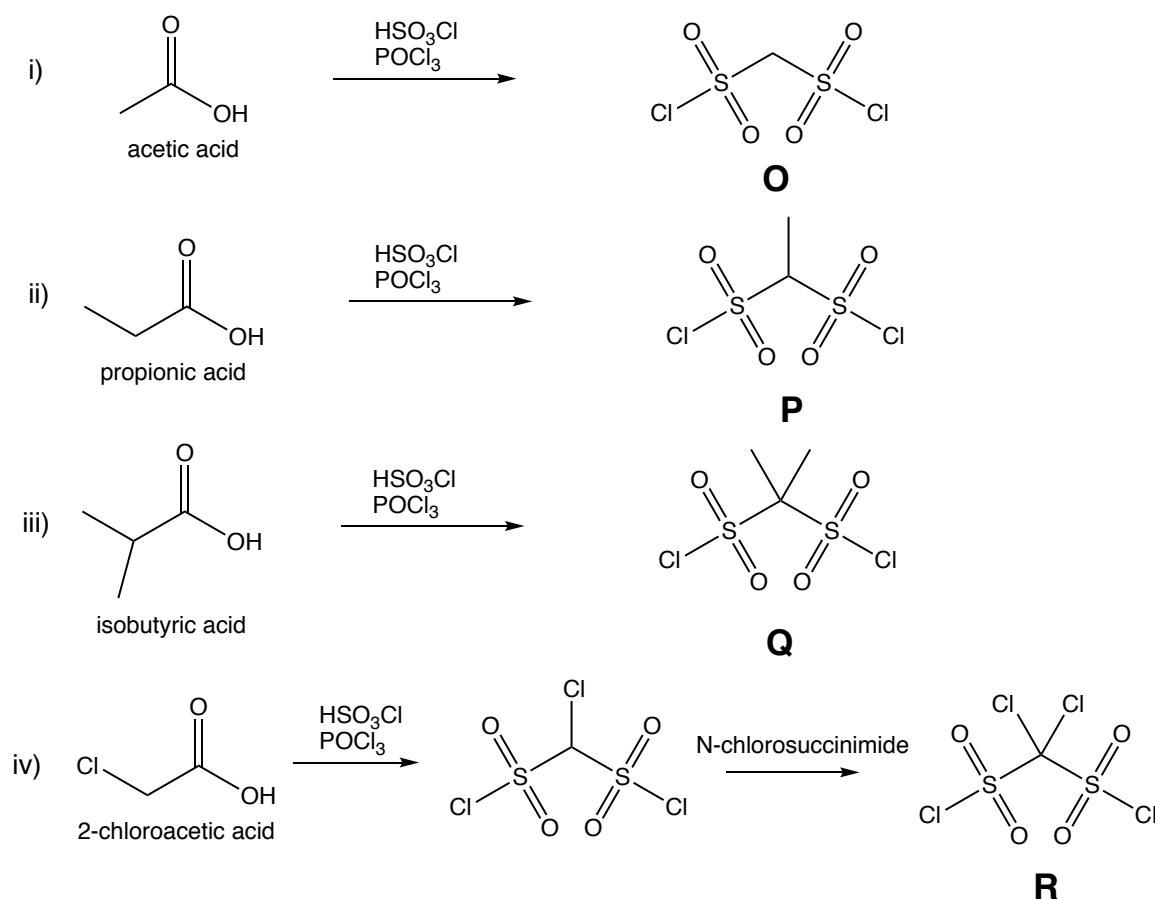


Figure 3.10 Proposed methods of preparation for sulfonic acid chloride analogs of compound **D**. Compounds **O** and **P** were successfully prepared and incorporated into NewTAML activators. Compound **Q** has not been prepared. Preparation of compound **R** is reported in the literature.<sup>38</sup>

As only preparation of sulfonamide-substituted tail building blocks was successful, all NewTAML activators (with the exception of **8**, discussed below) are hybrid activators with two carbonamide and two sulfonamide groups. Cyclization and metalation of the ligands for NewTAMLs **2** and **4** were performed following standard procedures for TAML activators using amide-containing head/arm intermediates and **O** or **P** for the tail (Figure 3.11). Complete methods for the preparation of **2** and **4** can be found in Chapters 4 and 5, respectively.

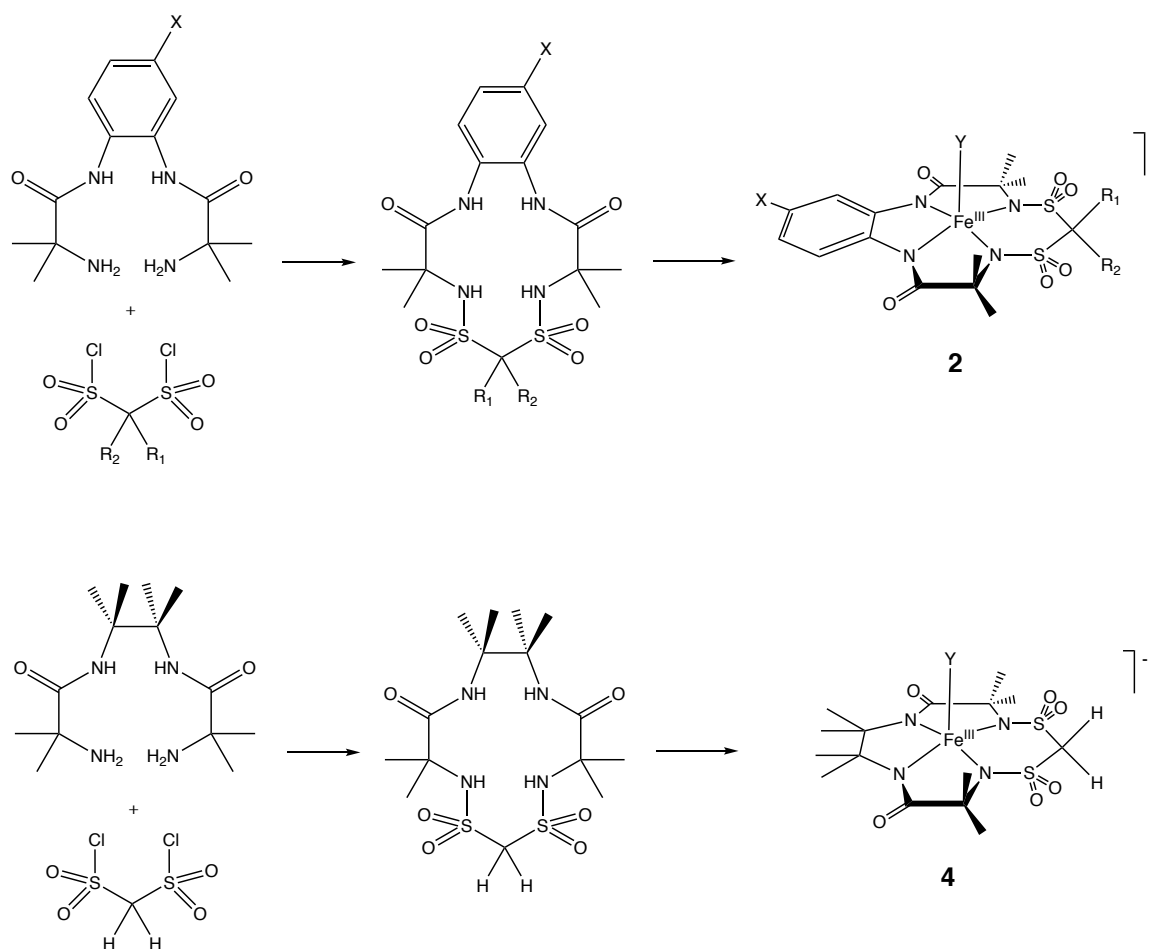


Figure 3.11 Methods of preparation of NewTAMLS **2** and **4** following standard procedures for OldTAMLS.

### 3.2.2 Preparation of *D*\* series NewTAMLS

The ligands of TAMLS **5** feature two phenyl rings between an oxamide and a malonamide (Figure 3.12). In the typical method of preparation (Figure 3.12), two *t*-butyloxycarbonyl (Boc) protected phenylenediamine molecules are joined with a substituted malonyl dichloride before deprotection with trifluoroacetic acid. The ligand is cyclized with oxalyl chloride and a base before metalation with *n*-butyllithium and iron(III) chloride.<sup>41</sup> After methylenedisulfonyl dichloride **O** was identified as a viable sulfonamide building block, NewTAML **6** was prepared with **O** instead of a substituted

malonyl dichloride in Figure 3.12. Other than substitution of pyridine for triethylamine in the cyclization step, no other modifications to the standard protocol were necessary for preparation of **6** (Figure 3.13). A complete method for the preparation of **6** can be found in Chapter 6.

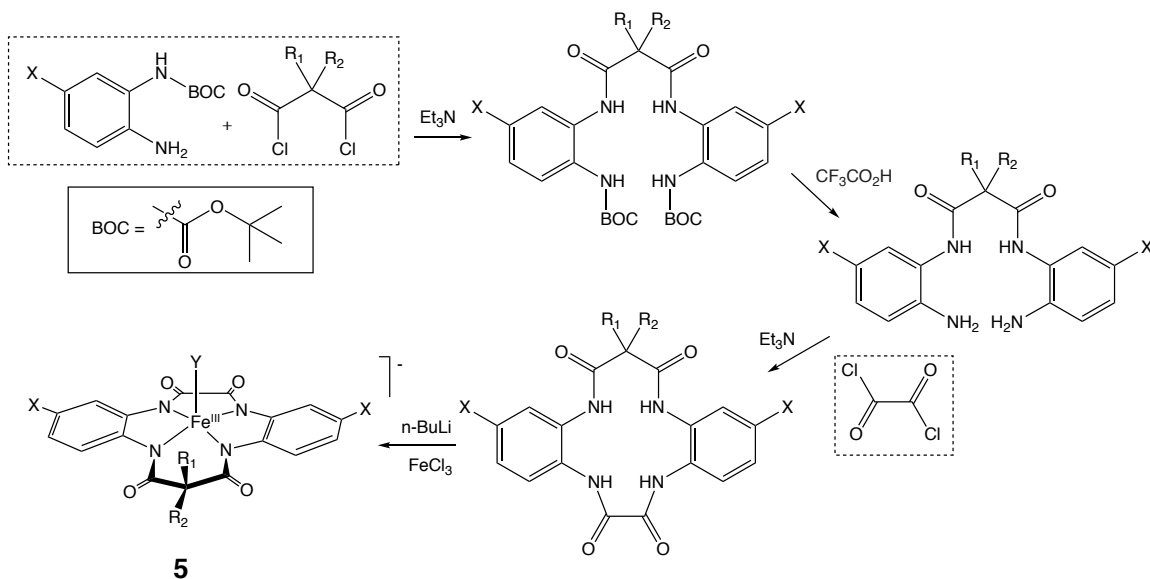


Figure 3.12 Typical preparation of TAMLs **5**. Building blocks are in dashed boxes.

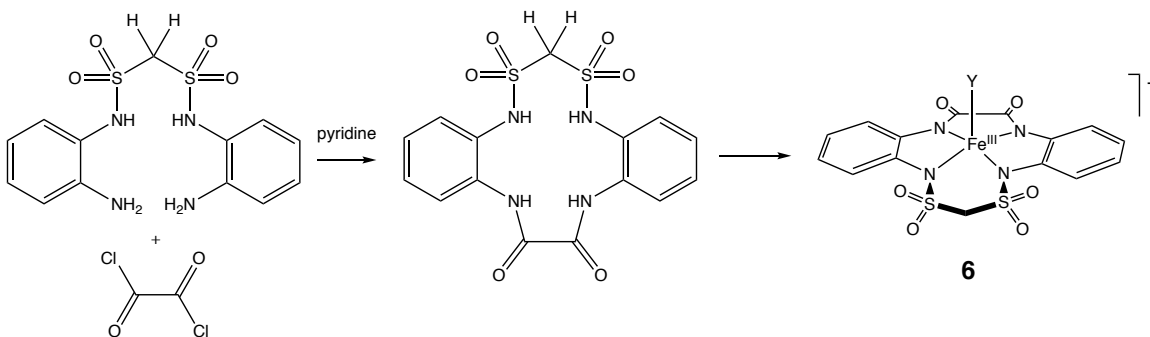


Figure 3.13 Preparation of NewTAML **6** following standard procedures for OldTAML **5** with pyridine as a base during cyclization.

### 3.2.3 Preparation of tetrasulfonamide **8**

NewTAML **8** was also prepared following the general method in Figure 3.12 with a second **O** instead of oxalyl chloride during cyclization (Figure 3.14). The resulting ligand has a larger cavity for the iron due to the chelate ring containing one additional atom. With the iron complexed to the nitrogens, **8** has two six membered rings within the ligand (a 5-6-5-6 ligand) compared to only one for **5** and **6** (5-5-5-6 ligands). A previously prepared TAML activator with a 5-6-5-6 tetraamido ligand was found to be unstable in water due to iron ejection,<sup>9</sup> but sulfonamide S-N bonds are shorter than carbonamide C-N bonds so we were hopeful that **8** would be more stable as a metallated complex in aqueous solution.<sup>42,43</sup> Complex **8** is a purple solid while all other NewTAMLs are red. To date, NewTAML **8** is the only tetrasulfonamide NewTAML. A complete method for the preparation of **8** can be found in Chapter 7.

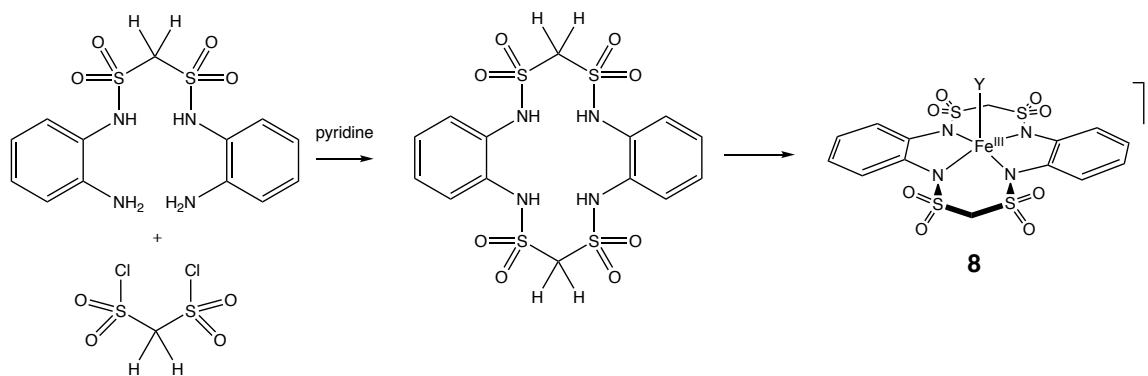


Figure 3.14 Preparation of NewTAML **8** following standard procedures for OldTAML **5** with pyridine as a base during cyclization.



### 3.3 Conclusions

The preparation of sulfonamide-containing NewTAML activators proved more challenging than expected due to the difficulty of finding or preparing sulfonyl building blocks. Ultimately, only methanedisulfonyl dichloride and ethane-1,1-disulfonyl dichloride were prepared and incorporated into ligands. No sulfonamide-substituted amino acids groups were successfully prepared. In the following chapters, the details of the structures, properties, and reactivity of NewTAMLs **2**, **4**, **6**, and **8** are described.

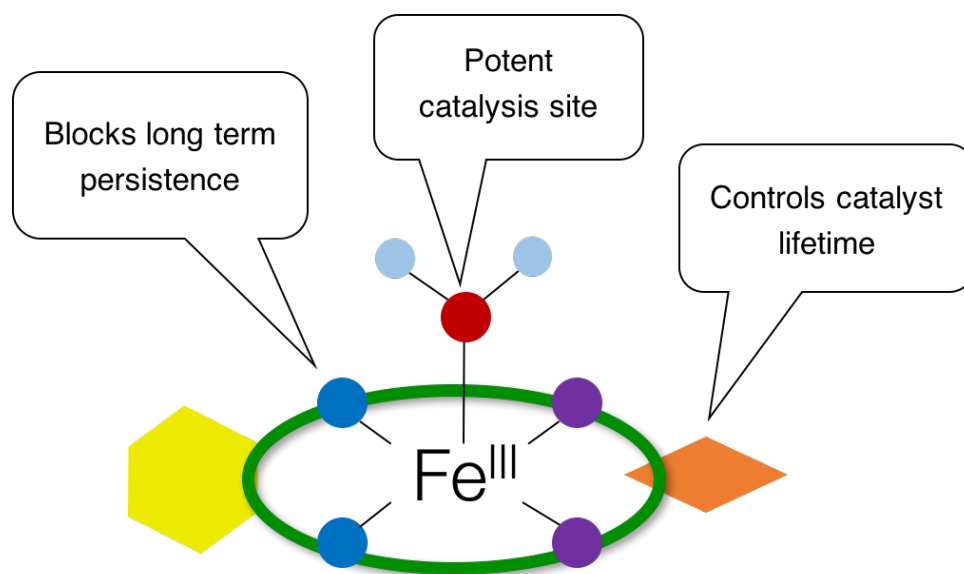
### 3.4 References

1. Uffelman, E. S. Macrocyclic Tetraamido-N Ligands that Stabilize High Valent Complexes of Chromium, Manganese, Iron, Cobalt, Nickel, and Copper, California University of Technology, 1992.
2. Beach, E. S.; Duran, J. L.; Horwitz, C. P.; Collins, T. J. *Ind. Eng. Chem. Res.* **2009**, *48* (15), 7072–7076.
3. Beach, E. S.; Malecky, R. T.; Gil, R. R.; Horwitz, C. P.; Collins, T. J. *Catal. Sci. Technol.* **2011**, *1* (3), 437–443.
4. Horwitz, C. P.; Collins, T. J.; Spatz, J.; Smith, H. J.; Wright, L. J.; Stuthridge, T. R.; Wingate, K. G.; McGrouther, K. *ACS Symp. Ser.* **2006**, *921*, 156–169.
5. Collins, T. J. *Acc. Chem. Res.* **2002**, *35* (9), 782–790.
6. Chanda, A.; Ryabov, A. D.; Mondal, S.; Alexandrova, L.; Ghosh, A.; Hangun-Balkir, Y.; Horwitz, C. P.; Collins, T. J. *Chem. - A Eur. J.* **2006**, *12* (36), 9336–9345.
7. Popescu, D. L.; Chanda, A.; Stadler, M. J.; Mondal, S.; Tehranchi, J.; Ryabov, A. D.; Collins, T. J. *J. Am. Chem. Soc.* **2008**, *130* (37), 12260–12261.
8. Tang, L. L.; DeNardo, M. A.; Gayathri, C.; Gil, R. R.; Kanda, R.; Collins, T. J. *Environ. Sci. Technol.* **2016**, *50*, 5261–5268.
9. Ghosh, A.; Ryabov, A. D.; Mayer, S. M.; Horner, D. C.; Prasuhn, D. E.; Sen Gupta, S.; Vuocolo, L.; Culver, C.; Hendrich, M. P.; Rickard, C. E. F.; Norman, R. E.; Horwitz, C. P.; Collins, T. J. *J. Am. Chem. Soc.* **2003**, *125* (41), 12378–12379.
10. Polshin, V.; Popescu, D. J. *J. Am. Chem. Soc.* **2008**, *130* (13), 4497–4506.
11. Truong, L.; DeNardo, M. A.; Kundu, S.; Collins, T. J.; Tanguay, R. L. *Green Chem.* **2013**, *15*, 2339–2343.
12. Collins, T. *Science.* **2001**, *291*, 48–49.
13. DeNardo, M. A.; Mills, M. R.; Ryabov, A. D.; Collins, T. J. *J. Am. Chem. Soc.* **2016**, *138* (9), 2933–2936.
14. DeNardo, M. A.; Tang, L. L.; Ryabov, A. D.; Collins, T. J. **2017**, in preparation.
15. Collins, T. J.; DeNardo, M. A.; Warner, G. R.; Gordon-Wylie, S. W.; Ellis, W. C. Superior Oxidation Catalysts Based on Macrocyclic Compounds. PCT International Patent Application No. PCT/US2016/053105.
16. Chanda, A.; de Oliveira, F. T.; Collins, T. J.; Münck, E.; Bominaar, E. L. *Inorg. Chem.* **2008**, *47* (20), 9372–9379.
17. Meza-León, R.-L.; Dávila-García, A.; Sartillo-Piscil, F.; Quintero, L.; Rivadeneyra, M. S.; Cruz-Gregorio, S. *Tetrahedron Lett.* **2013**, *54* (50), 6852–6854.
18. Feigl, D.; Mosher, H. *J. Org. Chem.* **1968**, *37* (32), 4242–4245.
19. Findeisen, K.; Heitzer, H.; Dehnicke, K. *Synthesis (Stuttg.)* **1981**, *9*, 702–704.
20. Woolven, H.; González-Rodríguez, C.; Marco, I.; Thompson, A. L.; Willis, M. C. *Org. Lett.* **2011**, *13* (18), 4876–4878.
21. Nishina, Y.; Ohtani, B.; Kikushima, K. *Beilstein J. Org. Chem.* **2013**, *9*, 1663–1667.
22. Li, Y.; Ju, J.; Jia, J.; Sheng, W.; Han, L.; Goa, J. *Chinese J. Chem.* **2010**, No. 20876148, 2428–2432.
23. Schreiner, P.; Lauenstein, O.; Kolomitsyn, I.; Nadi, S.; Fokin, A. A. *Agnew. Chem.*

- Int. Ed.* **1998**, No. 13, 1895–1897.
24. Benedict, H. C. *Org. Synth.* **1941**, *1*, 119.
  25. Sen, S. E.; Roach, S. L. *Synthesis (Stuttg)*. **1995**, 756–758.
  26. Moree, W. J.; Van Gent, L. C.; Van der Marel, G. A.; Liskamp, R. M. J. *Tetrahedron* **1993**, *49* (5), 1133–1150.
  27. Moree, W. J.; Van Der Marel, G. A.; Van Boom, J. H.; Liskamp, R. M. J. *Tetrahedron* **1993**, *49* (47), 11055–11064.
  28. Moe, G. R.; Sayre, L. M.; Portoghese, P. S. *Tetrahedron Lett.* **1981**, *22* (6), 537–540.
  29. Merricks, D.; Sammes, P. G.; Walker, E. R. H.; Henrick, K.; McPartlin, M. M. *J. Chem. Soc. Perkin Trans. 1* **1991**, 2169–2176.
  30. Karimi Zarchi, M. A.; Tayefi, M.; Tirgir, F.; Sabzalian, M. R. *J. Appl. Polym. Sci.* **2011**, *121* (5), 2573–2583.
  31. Bosshard, H. H.; Mory, R.; Schmid, M.; Zollinger, H. *Helv. Chim. Acta* **1959**, *42* (175), 1653–1658.
  32. Beran, M.; Prihoda, J. *Zeitschrift fur Anorg. und Allg. Chemie* **2005**, *631* (1), 55–59.
  33. Paul, R. C.; Kapoor, P.; Kapoor, R.; Verma, R. D. *J. Inorg. Nucl. Chem.* **1978**, *40*, 2005–2008.
  34. Paul, R.; Kapoor, P. *Indian J. Chem.* **1975**, *13*, 619–620.
  35. Sapper, E.; Blaschette, A. *Zeitschrift fuer Naturforschung, Tl. B Anorg. Chemie, Org. Chemie, Biochem. Biophys. Biol.* **1970**, *25* (12), 1490–1491.
  36. Ruff, K. *Inorg. Chem.* **1965**, *4* (10), 1446–1449.
  37. Paul, R. C.; Kapoor, P.; Kapoor, R.; Dev Verma, R. *J. Inorg. Nucl. Chem.* **1977**, *39* (3), 441–442.
  38. Fild, V. M.; Rieck, H.-P. *Chemiker-Zeitung* **1976**, *100* (9), 391–392.
  39. Castro, A.; Erickson, S. K.; Shechter, I.; Spencer, T. *Bioorg. Chem.* **1996**, *24*, 242–250.
  40. Murakami, S.; Onozuka, T.; Fujita, K. Preparation of methylenedisulfonic acid compounds and cyclic methylenedisulfonate compounds. JP 2014062076, A, 2014.
  41. Sullivan, S. Z.; Ghosh, A.; Biris, A. S.; Pulla, S.; Brezden, A. M.; Collom, S. L.; Woods, R. M.; Munshi, P.; Schnackenberg, L.; Pierce, B. S.; Kannarpady, G. K. *Chem. Phys. Lett.* **2010**, *498* (4–6), 359–365.
  42. Cotton, F. A.; Stokely, P. F. *J. Am. Chem. Soc.* **1970**, *705* (3), 294–302.
  43. Oae, S. *Organic Chemistry of Sulfur*; Springer Science & Business Media, 2012.

## CHAPTER 4

### Introducing “NewTAMLs” for Ultra-Dilute Catalytic Oxidation in Global Water Treatment



## 4.1 Introduction

TAML activators are high performance, mechanistically faithful, miniaturized (<1% in size) peroxidase enzyme replicas. For decades, we have optimized TAML design for cheap, safe, and effective peroxide-based water treatment for micropollutant removal<sup>1–10</sup> and rapid disinfection of pathogenic microbes.<sup>11</sup> In 2013, studies on London municipal wastewater indicated that TAML/peroxide promises micropollutant remediation rivaling ozone,<sup>12</sup> but we remained concerned about biological safety. Despite passing low-dose adult and embryonic developmental fish toxicity studies,<sup>5,13</sup> the most technically effective TAMLs contained fluorine, posing an environmental concern for large-scale use.<sup>14</sup> In 2015, we discovered that lifetimes in the expanding TAML family had switched from being limited by oxidative to nucleophilic decay.<sup>15</sup> Resulting iterative redesign has delivered vastly superior catalysts called “NewTAMLs,” rendering all prior TAMLs, now “OldTAMLs,” effectively obsolete for water treatment.

Here we introduce “NewTAMLs” as the strongest performers from our 35-year iterative catalyst design program and highlight their potential to transform water purification. NewTAMLs are comprised of biochemically common elements, are cheaper to produce than our prior best-performing, fluorine-containing TAMLs, and deliver optimum water treatment at near neutral pH. Lower catalyst costs and higher efficiencies promise large savings for treatment of municipal waters with expected micropollutant reductions of >90% at ca. 10–20% the operating cost of ozone.

Included in this chapter are propranolol studies by Yogesh Somasundar, crystallography by Gabrielle Pros and Tomislav Pintauer of Duquesne University, and mouse toxicity studies by Julia A. Taylor and Frederick S. vom Saal of the University of

Missouri. Cost estimations were performed with help from Rakesh Kanda of Brunel University London.

## 4.2 Results and Discussion

NewTAMLs of structure **2** contain two sulfonamide groups in place of the carbon amides of **1** at the malonamide “tail” (Figure 4.1). X-ray crystallography confirmed that **2a** is five coordinate in the solid state with an axial water molecule, consistent with OldTAMLs (Figure 4.2). In macrocycle design, structural modifications that decrease electron donation of the amides to the metal center improve peroxide catalysis.<sup>16</sup> This reduces the water ligand  $pK_a$ , favoring a hydroxo-ligated resting catalyst that reacts faster with peroxide near neutral pH to form the active catalyst (in what is typically the rate-determining step) and also makes the active intermediate more oxidizing.<sup>17</sup> The rate constants  $k_I$ ,  $k_{II}$ , and  $k_i$  for **2** catalysts, which conform to the typical TAML/ $H_2O_2$  mechanism (Figure 4.1), represent Technical Performance Parameters<sup>15,16</sup> that define catalytic utility, reveal pH-dependent relationships, and guide iterative design.

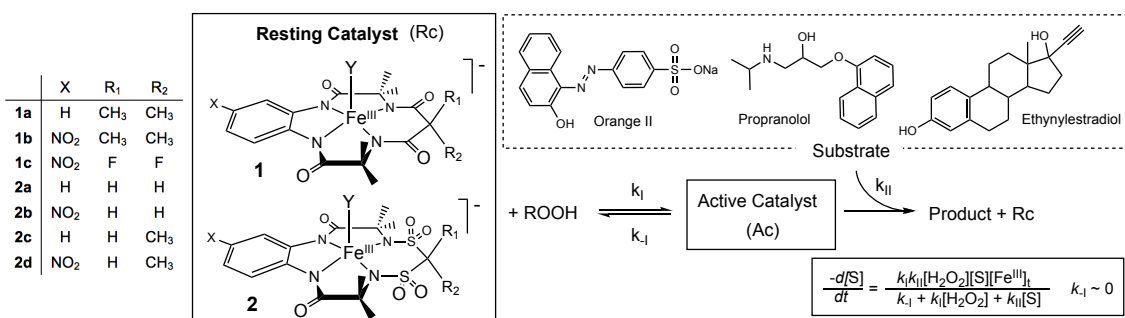


Figure 4.1 General mechanism of catalysis of OldTAMLs **1** and NewTAMLs **2** with substrates studied in this chapter. Y is typically water and ROOH is typically  $H_2O_2$ .

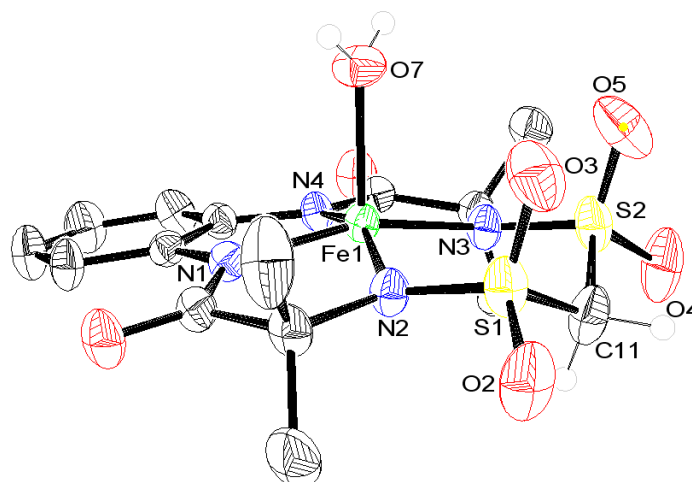


Figure 4.2 ORTEP diagram of **2a**. The H atoms at all positions except O<sub>7</sub> and C<sub>11</sub> and the NMe<sub>4</sub><sup>+</sup> counterion were omitted for clarity. Select bond distances (in Å): Fe-N<sub>1-4</sub> 1.885, 1.876, 1.918, 1.942, Fe-O 2.116. The Fe atom lies above the plane of the four nitrogen atoms by 0.387 Å.

#### 4.2.1 Catalytic Activity of NewTAMLs in the Degradation of Orange II with H<sub>2</sub>O<sub>2</sub>

The Technical Performance Parameters for the prototype NewTAML **2a** and its NO<sub>2</sub>-substituted analog **2b** were measured by studying the oxidation with H<sub>2</sub>O<sub>2</sub> of the standard TAML model substrate Orange II<sup>18</sup> (Figure 4.1). For **2a** and **2b**, rate constants  $k_I$  and  $k_{II}$  at pH 7 were determined using a 3D plot of the dependences of the initial rate of bleaching on [Orange II] and [H<sub>2</sub>O<sub>2</sub>] fit to the rate equation in Figure 4.1 (Figure 4.3). The pH 7 rate constants in Table 1.3 reveal an over tenfold increase in reactivity for **2a** compared to its structural analog, the prototype TAML **1a**. Substitution with NO<sub>2</sub> in **2b** affords a further doubling of the  $k_I$  rate.

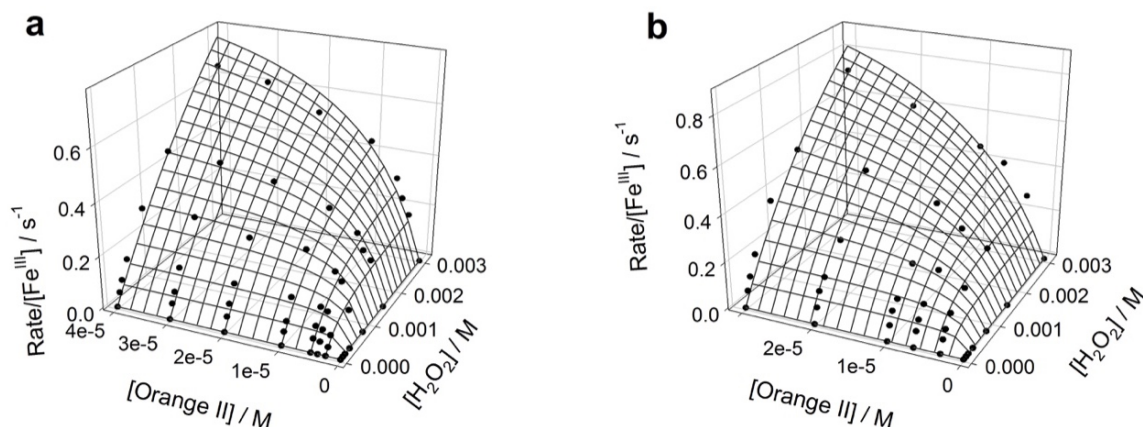


Figure 4.3 3D mesh plot of the initial rate of Orange II bleaching by  $2.6 \times 10^{-8}$  M **2a** (a) and  $2.3 \times 10^{-8}$  M **2b** (b) with  $\text{H}_2\text{O}_2$  in pH 7 0.01 M phosphate at  $25^\circ\text{C}$  as functions of  $\text{H}_2\text{O}_2$  and Orange II concentrations.

Table 4.1 Rate constants  $k_I$  and  $k_{II}$  for all catalysts discussed in this chapter at pH 7 in the bleaching of Orange II with  $\text{H}_2\text{O}_2$  at  $25^\circ\text{C}$ .

TAML	X/R <sub>I</sub> /R <sub>2</sub>	$k_I / \text{M}^{-1} \text{s}^{-1}$	$10^{-4} \times k_{II} / \text{M}^{-1} \text{s}^{-1}$
<b>1a</b> <sup>a</sup>	H/Me/Me	$31.4 \pm 0.1$	$0.495 \pm 0.002$
<b>1b</b> <sup>a</sup>	NO <sub>2</sub> /Me/Me	$152 \pm 5$	$2.7 \pm 0.2$
<b>1c</b> <sup>a</sup>	NO <sub>2</sub> /F/F	$350 \pm 2$	$4.1 \pm 0.1$
<b>2a</b>	H/H/H	$330 \pm 20$	$8.5 \pm 1.8$
<b>2b</b>	NO <sub>2</sub> /H/H	$630 \pm 50$	$10 \pm 2$
<b>2c</b>	H/H/Me	$390 \pm 4$	$4.2 \pm 0.1$
<b>2d</b>	NO <sub>2</sub> /H/Me	$690 \pm 20$	$8.9 \pm 0.2$

<sup>a</sup> Values from reference 16

Excellent performance around neutral pH is critical for the application of NewTAML activators in water treatment settings. Superior nitro-substituted OldTAMLs **1b** and **1c** reach maximum activity at pH 10 and 11, respectively (Figure 4.5), a significant drawback for municipal wastewater treatment where the pH is near neutral. Strongly electron-withdrawing nitro groups increase Lewis acidity at iron center, manifesting in lower  $pK_a$  values for the deprotonation of the axial water ligand in



aqueous solutions and increased performance at neutral pH. For NewTAML **2b**, the combined electron-withdrawing effects of the nitro and sulfonamide groups in **2b** lower the  $pK_a$  to  $8.8 \pm 0.3$  (Figure 4.4) compared to  $10.0 \pm 0.1$  for structurally analogous **1b** (Figure 2.10).

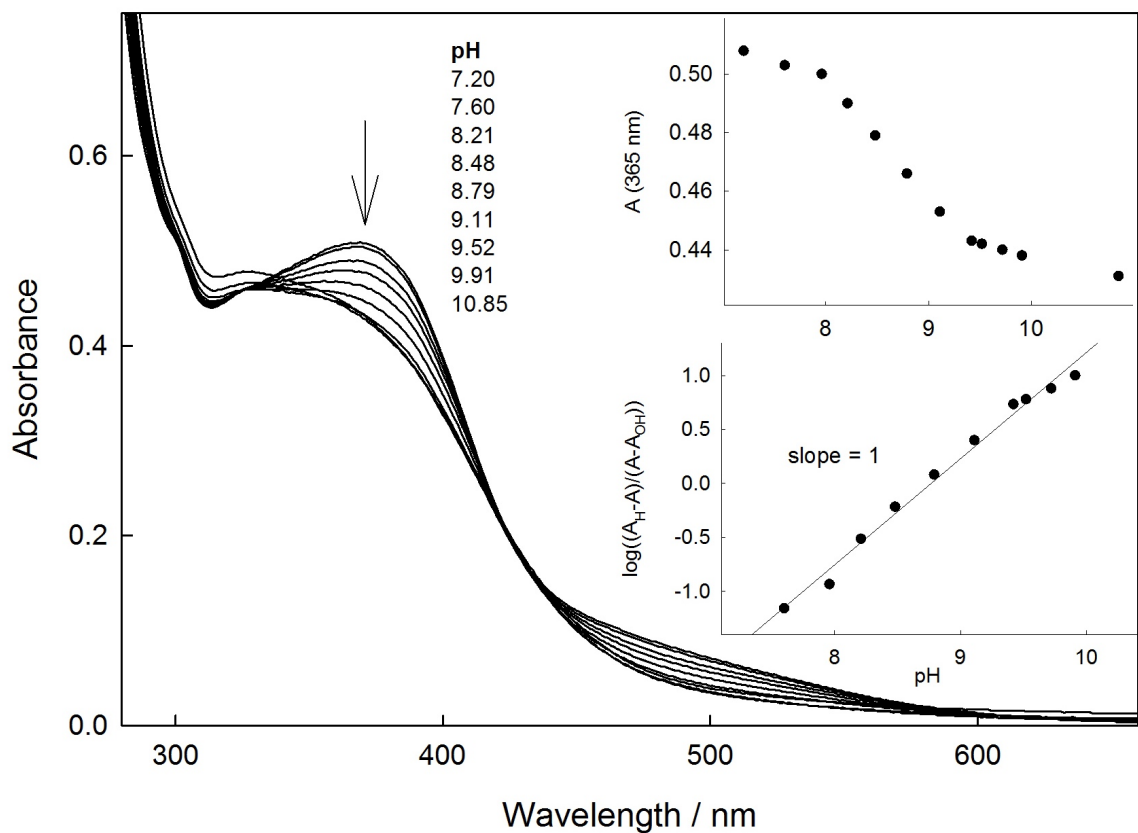


Figure 4.4 Determination of  $pK_a$  of **2b** ( $4.4 \times 10^{-5}$  M) with varying pH in 0.01 M phosphate 25°C. Insets: (upper) Absorbance as a function of pH at 365 nm. (lower) linearization of the data using the equation  $\log((A_H - A)/(A - A_{OH})) = pH - pK_a$  wherein  $A_H$ ,  $A_{OH}$ , and  $A$  are absorbances at the most acidic, most basic, and intermediate pHs, respectively. The resulting straight line with a slope of one results in a y-intercept equal to  $-pK_a$ .

The pH dependence of  $k_I$  and  $k_{II}$  for **2a** and **2b** in the bleaching of Orange II with  $H_2O_2$  is compared to that of **1b** and **1c** in Figure 4.5. As predicted by  $pK_a$ , NewTAMLs reach maximum activity at more neutral pH. In the highlighted neutral pH region, the  $NO_2$ -substituted NewTAMLs **2b** and **2d** are up to twofold more reactive than **1c** and outperform non-fluorinated **1b** up to eightfold (Figure 4.5). Orange II is a fast-reacting substrate where the comparative rate behaviors for very fast-acting TAML catalysts are difficult to distinguish—slow-reacting propranolol (see below) reveals multiple comparative subtleties between the different catalysts that are relevant to water purification.

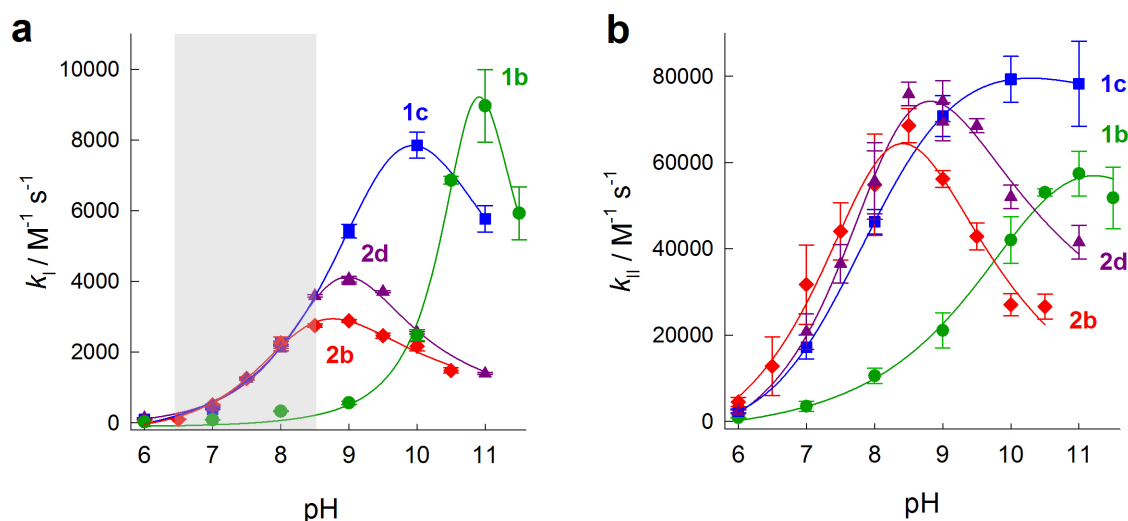


Figure 4.5 Comparison of the Technical Performance Parameters for NewTAMLs in the bleaching of Orange II with  $H_2O_2$  at 25°C. Relative  $k_I$  (a) and  $k_{II}$  (b) values at pH 6–11.5 were measured using a plate reader. Lines are for emphasis only.

The operational stability of dilute TAMLs ( $< 1 \mu M$ ) is captured by the unimolecular degradation rate constant  $k_i$  (see Figure 4.1).<sup>16</sup> In OldTAMLs,  $k_i$  is relatively pH-insensitive in the 6–11 region (Figure 4.6). However, for **2a** and **2b**,  $k_i$  increases sharply with pH above 8 leading to irreversible inactivation in minutes at  $pH \geq$

9, signaling the presence of a novel pH-sensitive degradation process. This loss of activity led to the hypothesis that the site of inactivation is the carbon acid of the  $-\text{SO}_2\text{CH}_2\text{SO}_2-$  unit. As discussed in Chapter 3,  $\text{R} = \text{H}$  groups at the ligand tail are unique to NewTAML activators. Deprotonation of one of the  $\text{C}-\text{H}$  bonds at the tail of the active catalysts in the iron(V)oxo reactive intermediate stage,<sup>19</sup> where the Lewis acidity of the iron and the Brønsted acidity of the  $-\text{CH}_2-$  would be greatest, could lead to rapid carbanion oxidation and catalyst death. We hypothesized that substituting  $\text{R}_2 = \text{H}$  (**2a** and **2b**) with  $\text{R}_2 = \text{CH}_3$  (**2c** and **2d**) to reduce the acidity of the remaining  $\text{C}-\text{H}$  group would yield longer-lived catalysts. This is precisely what was found; Figure 4.6 shows the resulting reduction in  $k_i$  of **2d** after R group substitution compared to unsubstituted **2b** at high pH. This observation is further substantiated in Figure 4.7 and Figure 4.8 below and will be discussed in depth in Chapter 7.

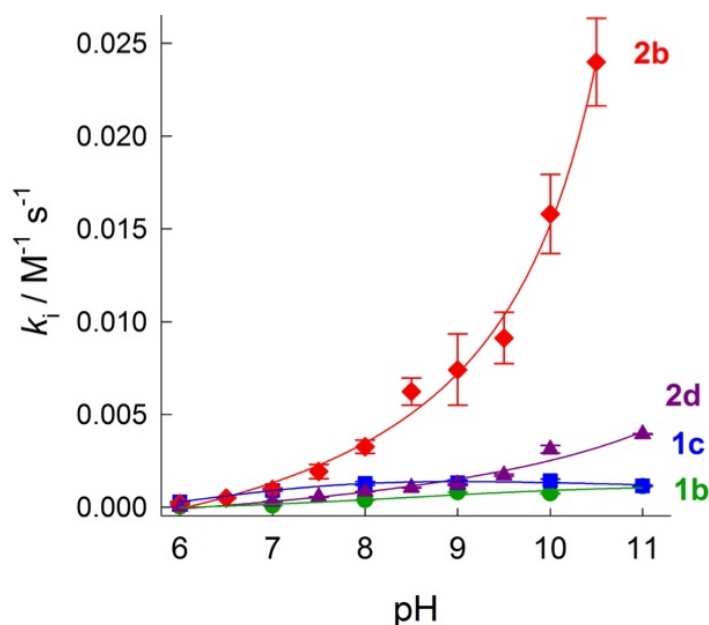


Figure 4.6 Comparison of  $k_i$  for NewTAMLs in the bleaching of Orange II with  $\text{H}_2\text{O}_2$  at  $25^\circ\text{C}$  for pH 6–11.5. Note: when  $\text{R}_2$  is changed from H (**2b**) to  $\text{CH}_3$  (**2d**), the pH dependent inactivation pathway is significantly slowed, but not completely suppressed. Lines are for emphasis only.

#### 4.2.2 Catalytic Activity of NewTAMLs in the Degradation of Propranolol with $H_2O_2$

Study of propranolol degradation, which is much more resistant to oxidation than Orange II, shows that **2b** and **2d** significantly outperform fluorinated **1c** and illustrates the reactivity gain in **2d** over **2b** with more recalcitrant substrates. Propranolol is the active pharmaceutical ingredient in the  $\beta$ -blocker blood pressure medication Inderal and is found at up to ppb concentrations in US municipal effluents.<sup>20</sup> It is difficult to remove from London municipal wastewater with either ozone or **1c**/ $H_2O_2$  treatment, which perform comparably (Figure 1.1).

In pH 7 HPLC-grade purified water with 100 nM catalyst loading and fish-safe 0.33 mM (11.2 ppm)  $H_2O_2$ ,<sup>12</sup> ~50 nM (12-16 ppb) propranolol is 35% degraded by **1b** in 75 minutes, while **1c** accomplishes 100% removal in 35 minutes. In contrast, NewTAMLs **2a** and **2c** remove 55% and 88%, respectively, in 75 minutes (Figure 4.7a). Over a longer timescale, the concentration of propranolol remaining after **2c** treatment falls below the limit of detection in ~200 minutes (Figure 4.7b). Remarkably, **2b** and **2d** remove propranolol to below the limit of detection in less than 5 minutes, a significant increase in performance over 75 minute **1b** and **1c** treatment, respectively. (Figure 4.7a).

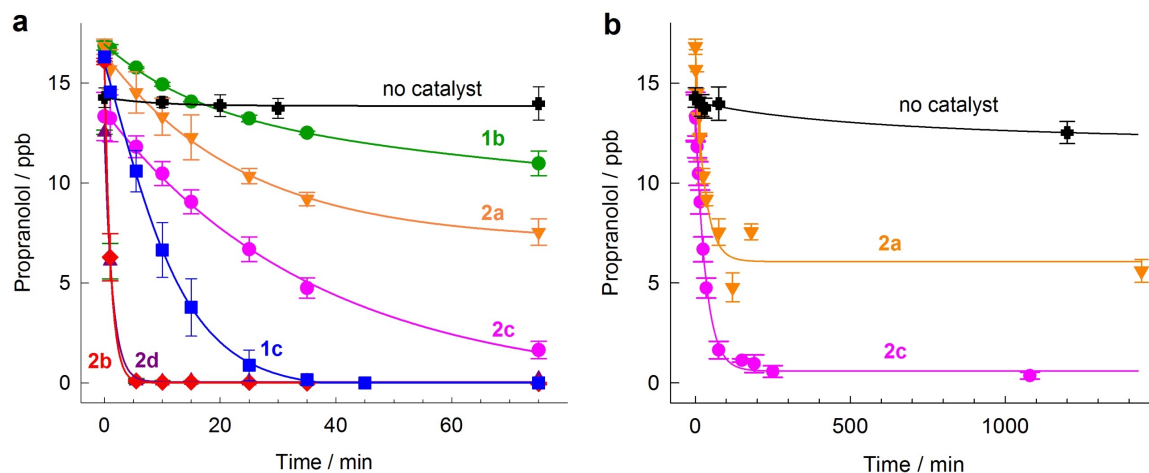


Figure 4.7 Degradation of propranolol by TAMs ( $1.0 \times 10^{-7}$  M) with  $\text{H}_2\text{O}_2$  in HPLC-grade purified water over 75 minutes (a) and 1440 minutes (24 hours) (b) at pH 7. Lines are for emphasis only.

To model the multiple-contaminant nature of wastewater and natural waters, analogous experiments were performed using raw Allegheny River water. Here, propranolol removal was slower, as expected from competition with natural organic matter, and the lifetime advantages of **2c** and **2d** ( $\text{R}_2 = \text{CH}_3$ ) over **2a** and **2b** ( $\text{R}_2 = \text{H}$ ) are even more apparent. In unbuffered river water spiked with propranolol ( $\sim 15$  ppb), **2b** deactivated after 77% removal in 25 minutes, while **2d** removed propranolol to below the limit of detection in 25 minutes (Figure 4.8a). Even at 10 nM **2d** in unbuffered river water, a concentration equivalent to treating ca. 160,000 tonnes of wastewater with one kilogram of catalyst, 77% removal of propranolol was achieved before deactivation after ca. 6 hours (Figure 4.8b). In these difficult oxidation conditions, **2d** at  $1.0 \times 10^{-8}$  M performed comparably to **2b** at  $1.0 \times 10^{-7}$  M.

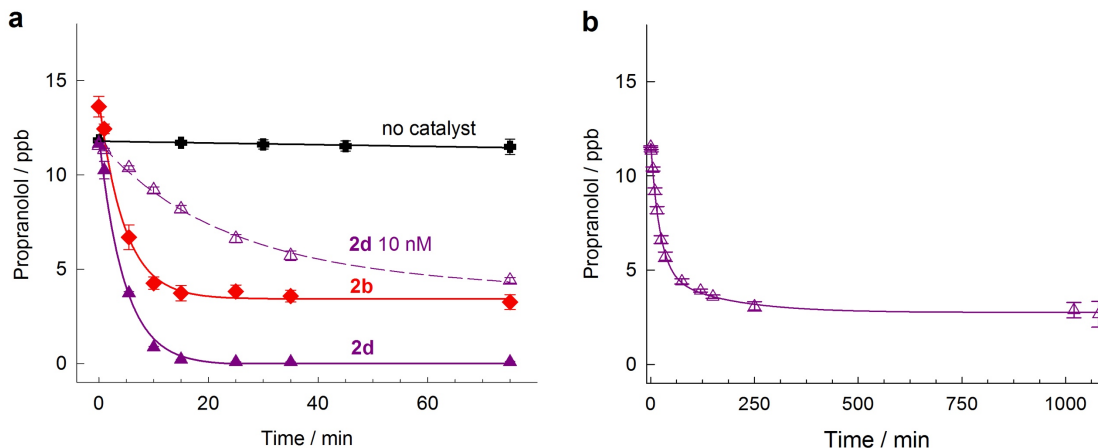


Figure 4.8 Degradation of propranolol by TAMLs ( $1.0 \times 10^{-7}$  M unless otherwise indicated) and  $\text{H}_2\text{O}_2$  in propranolol-spiked Allegheny River water at pH 7. (b) In river water, **2d** ( $1.0 \times 10^{-8}$  M) removed 77% of propranolol before deactivation. Lines are for emphasis only.

Extending the lifetime of **2d** compared to **2b** via  $\text{R}_2 = \text{CH}_3$  substitution illustrates the tunable nature of the NewTAML inactivation pathway. This will allow NewTAML functional lifetimes to be optimized to suit the prescribed task more precisely and to avoid releases of NewTAMLs to the environment. Thus, NewTAMLs **2** are best viewed as trifunctional platforms, containing (i) a tunable fast-acting and potently oxidizing peroxide catalysis site, (ii) a tunable inactivation pathway for controlling releases in homogeneous processes, and (iii) two slowly hydrolyzed amide sites that act as blockers of long-term catalyst persistence.<sup>21</sup>

#### 4.2.3 Toxicity and Endocrine Disruption Assessment of **2**

To detect and avoid toxicity, especially endocrine disruption, in scaled applications, TAMLs have been subjected to various cellular and whole organism assays of the Tiered Protocol for Endocrine Disruption (TiPED).<sup>5,13,22,23</sup> In the present study, a

TiPED Tier 5 mammalian assay was added by subjecting **2a** to prepubertal mouse uterotrophic assays. A toxicity screen with **2a**-laced drinking water administered from postnatal days 19–22 showed no adverse effects on body weight, behavior, or overall health. No effects of catalyst exposure at the doses tested were observed on liver, kidney, or spleen weights (Figure 4.9). Examination of liver histopathology revealed no effects of any treatment/dose on hematopoiesis, perivascular/portal inflammatory infiltrates, or the incidence of mitotic figures and microgranulomas (data not shown). Consumption of ethinylestradiol (EE2) spiked drinking water stimulated an approximately 6.2-fold increase in uterine wet weight in the prepubertal mice (Figure 4.10), and pretreatment of the EE2-laced drinking water with **2a**/H<sub>2</sub>O<sub>2</sub> resulted in a dose-dependent reduction in the uterotrophic response. No effect of **2a** alone was seen on body weight or uterus weight compared to animals receiving water alone (Figure 4.11a-b). Pretreatment with 4 nM **2a**/1 mM H<sub>2</sub>O<sub>2</sub> and 40 nM **2a**/1 mM H<sub>2</sub>O<sub>2</sub> reduced the uterotrophic response to ~40% and ~3%, respectively, of that found for animals given untreated EE2 drinking water (Figure 4.12) and the latter did not differ significantly from either the control or **2a**/H<sub>2</sub>O<sub>2</sub>-only responses (Figure 4.11c).

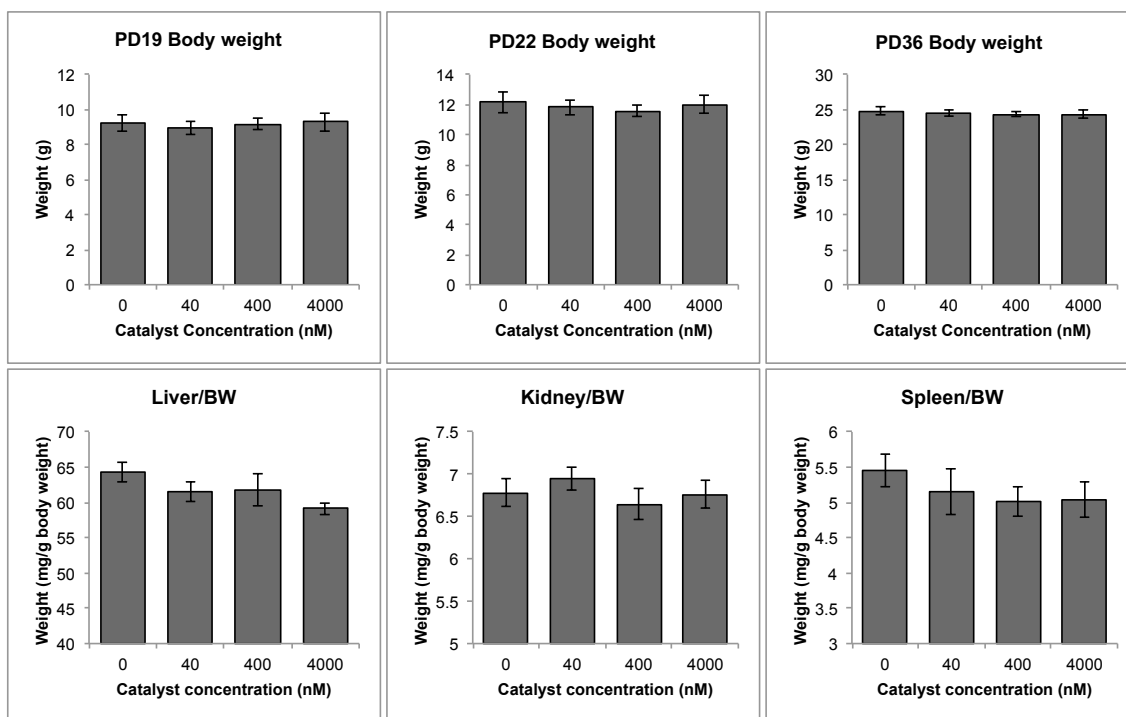


Figure 4.9 Body weight and liver and kidney weights in animals exposed to higher concentrations of **2a** without EE2. The sample sizes for the 0, 40, 400, and 4000 nM treatments were 10, 10, 11, and 12, respectively. Body weights (upper row) are shown for postnatal day (PD) 19, prior to the start of catalyst exposure, PD 22, at the end of the treatment period, and PD36, two weeks after the end of the treatment period. Organ weights are presented as a relative to body weight (lower row).



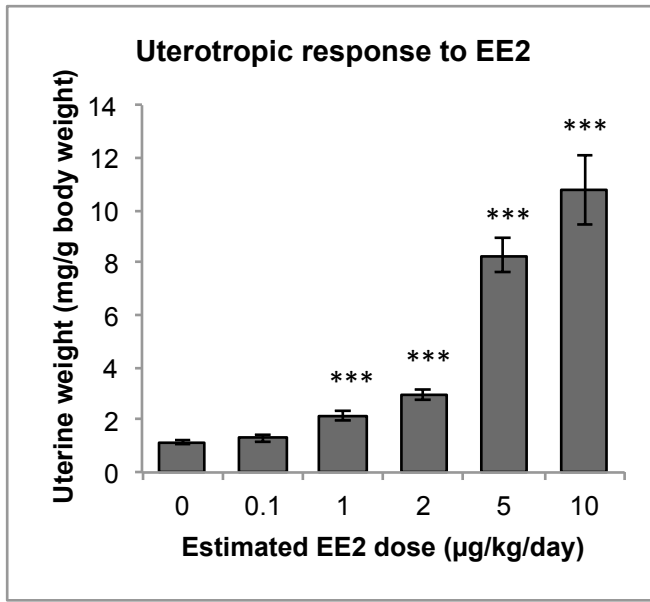


Figure 4.10 Uterine weight on postnatal day 22 after 3 days of EE2 treatment. The uterotrophic response to EE2 administered in drinking water for three days. The sample sizes are 6, 4, 7, 3, 4, and 3 animals for 0, 0.1, 1, 2, 5, and 10 µg/kg/day doses, respectively. \*\*\*P<0.0001 vs. control (0 µg/kg/day dose).

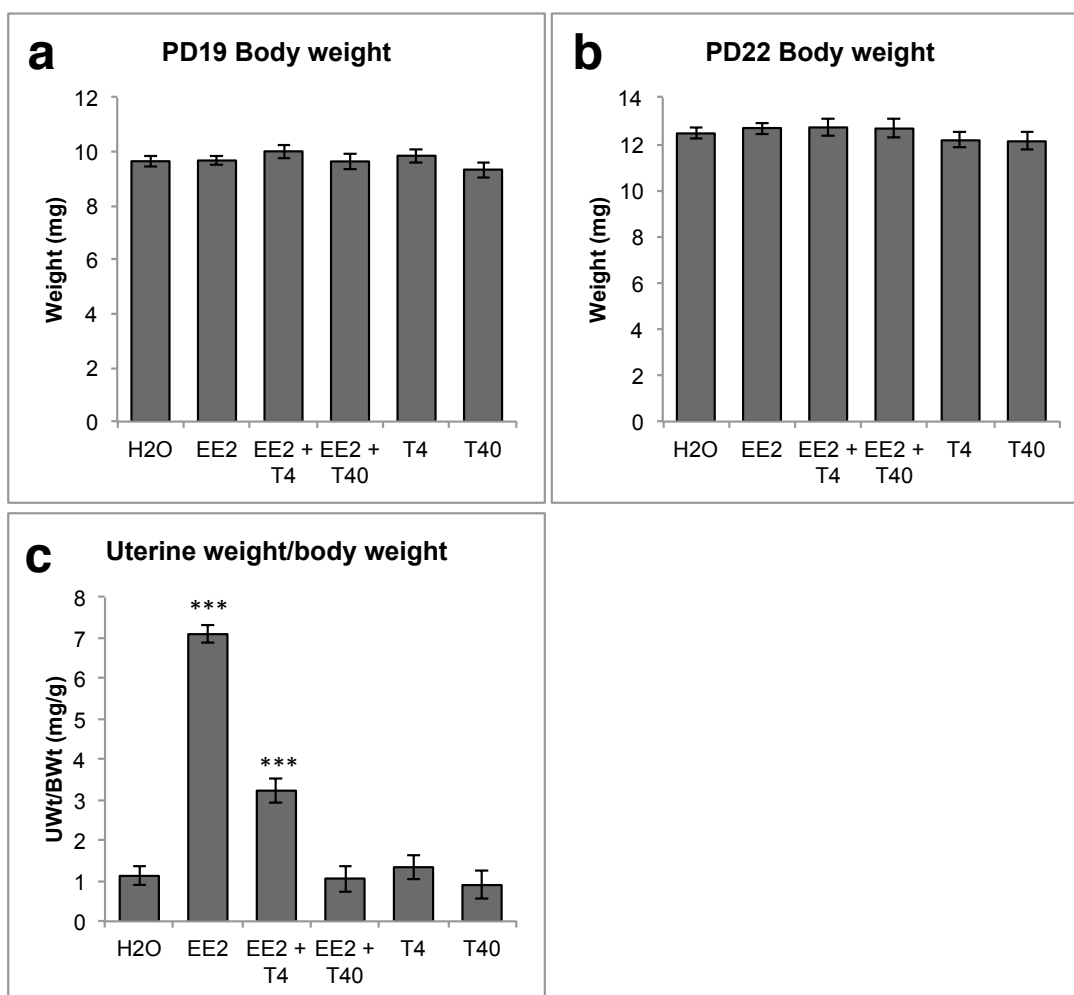


Figure 4.11 Body weight and uterine weight at the time of tissue collection on postnatal day 22. (a) Body weights on PD19, before exposure to the indicated solution and (b) on PD22, after exposure to the indicated solution for three days and (c) uterine weight corrected for body weight on PD22. The compositions of the exposure solutions were as follows; H<sub>2</sub>O: water control; EE2: 84 EE2; EE2+T4: 84 EE2 treated with 4 nM **2a** and 1 mM H<sub>2</sub>O<sub>2</sub> for 1 hour and quenched with 0.5 ppm catalase; EE2 +T40: 84 EE2 treated with 40 nM **2a** and 1 mM H<sub>2</sub>O<sub>2</sub> for 3 hours and quenched with 0.5 ppm catalase; T4: 4 nM **2a**; and T40: 40 nM **2a**. The sample sizes for the H<sub>2</sub>O, EE2, EE2+T4, EE2+T40, T4 and T40 treatments were 20, 20, 11, 12, 10 and 9 animals, respectively. \*\*\* P<0.0001 against the H<sub>2</sub>O data.

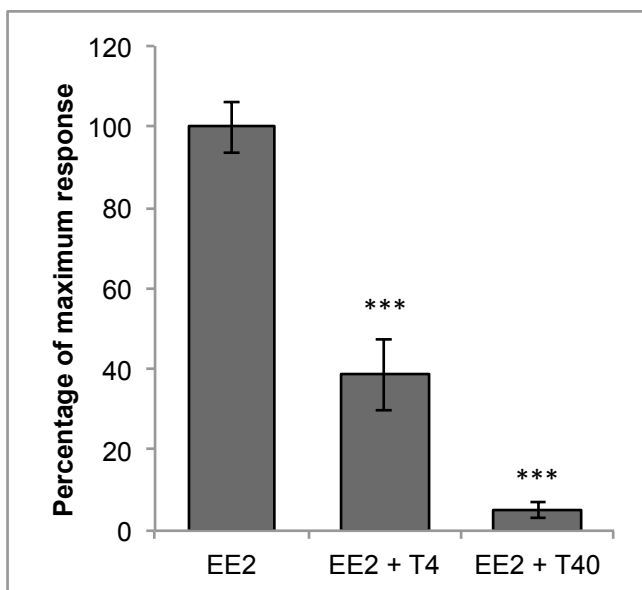


Figure 4.12 Suppression of the uterotrophic response to EE2 by pretreatment of EE2 with 4 nM or 40 nM **2a** and 1 mM H<sub>2</sub>O<sub>2</sub> as a percentage of the full uterotrophic response to EE2. Treatment group N = 20, 11, and 10 for EE2, EE2 pretreated with 4 nM **2a** (EE2 + T4) and EE2 pretreated with 40 nM catalyst (EE2 + T40) respectively. \*\*\*P<0.0001 vs EE2 alone.

### 4.3 Conclusions

Sulfonamide NewTAMLs **2** are a new class of oxidation catalysts with potential for commercial treatment of micropollutants in wastewater. NewTAMLs outperform our best previous fluorine-containing TAMLs in the breakdown of the model micropollutants Orange II and propranolol and are cheaper to produce. However, further studies on the degradation of micropollutants in real world wastewater effluent comparing NewTAMLs with ozone treatment are necessary to further the case for scaled production of NewTAML activators. The data in this chapter provides evidence that NewTAMLs follow the same general mechanism of catalysis as OldTAMLs, but contain an additional unique but controllable inactivation pathway. The next three chapters will explore the properties of NewTAMLs and kinetic details of NewTAML catalysis, including investigation of the inactivation processes.

## 4.4 Experimental

### 4.4.1 Materials and Methods

Fe<sup>III</sup>-TAML<sup>®</sup> complexes **1a** and **1b** were prepared according to published methods<sup>24</sup> or obtained from GreenOx Catalysts, Inc. Methods for preparation of Fe<sup>III</sup>-NewTAML complexes are given below. Methane disulfonyl dichloride was purchased from TCI or prepared as described elsewhere.<sup>25</sup> H<sub>2</sub>O<sub>2</sub> (30% w/w) was obtained from Fischer and its concentration was verified by UV/Vis spectroscopy using  $\epsilon = 72.8 \text{ M}^{-1} \text{ cm}^{-1}$  at 230 nm.<sup>26</sup> Orange II was purchased from Acros and recrystallized in aqueous ethanol. Catalase solutions (from *Aspergillus niger*, 2350 U/mg) were prepared daily. Allegheny River water was collected on August 23, 2016, stored in a glass bottle at 4 °C, and filtered before use in August–October 2016. All other reagents and solvents (at least ACS reagent grade) were obtained from commercial sources and used as received or purified according to standard procedures.<sup>27</sup>

### 4.4.2 Instrumentation

<sup>1</sup>H and <sup>13</sup>C NMR data were collected on Bruker Avance III 300 and 500 MHz instruments. Elemental analyses were performed by Midwest Microlabs, LLC. Mass spectrometry measurements were made on a Thermo-Fisher LCQ ESI/APCI Ion Trap. Solution pH was measured with a Corning 220 pH meter. Spectrophotometric titration of **2b** was performed using a double beam Shimadzu UV-1800 UV/Vis instrument with a CPS-240A 6-cell thermostated controller at 25 °C. UV-vis measurements were performed at 25 °C on an Agilent 8453 spectrophotometer equipped with an automatic thermostated 8-cell positioner using capped acrylic cuvettes or on a TECAN Infinite M1000 Plate

Spectrometer in 96-well polystyrene plates. High Performance Liquid Chromatography (HPLC) studies were performed with a Shimadzu LC system equipped with LC 20AB pump, SIL 20A autosampler, CTO 20A column oven, a RF 20A XS fluorescence detector, and a Kinetex (Phenomenex) EVO C18 100cA column ( $4.6 \times 50$  mm,  $5 \mu\text{M}$ ).

#### 4.4.3 *General Preparation of 2*

Compounds **A–C** (Figure 4.13) were prepared as described elsewhere.<sup>24,28</sup> Under Ar, a solution of **C** (1.5 mmol) and  $\text{Et}_3\text{N}$  (0.21 mL) in dry THF (40 mL) and a solution of **D** (1.5 mmol) in dry THF (40 mL) were added dropwise with a syringe pump to THF (250 mL) at  $0^\circ\text{C}$ . The solution was allowed to warm overnight, then filtered. The solvent was partially removed and the residue purified by column chromatography (silica gel, eluent 3:1:1 EtOAc/heptane/ $\text{CH}_2\text{Cl}_2$ ) to yield ligand **E**. A solution of  $n\text{BuLi}$  (0.567 mmol of 1.6 M in hexane, 4.1 eq) was added at  $0^\circ\text{C}$  to a solution of **E** (0.138 mmol) in 10 mL dry THF under Ar. The mixture stirred for 30 min before addition of solid anhydrous  $\text{FeCl}_3$  (0.166 mmol). The mixture was stirred at room temperature overnight. The solvent was removed and the solids suspended in a minimum amount of 9:1 (v/v) water/methanol and filtered through a fine glass frit. The filtrate was partially reduced in vacuo and purified by flash chromatography on a C-18 silica gel column with 9:1 (v/v) water/methanol as the eluent. The lithium cation was replaced by tetramethylammonium using cationic exchange column (Amberlite IR-120) presaturated with  $[\text{NMe}_4]^+$ . The red product was eluted in methanol and further purified by flash chromatography (C-18 silica gel,  $\text{CH}_3\text{OH}/\text{H}_2\text{O}$ , gradient elution).

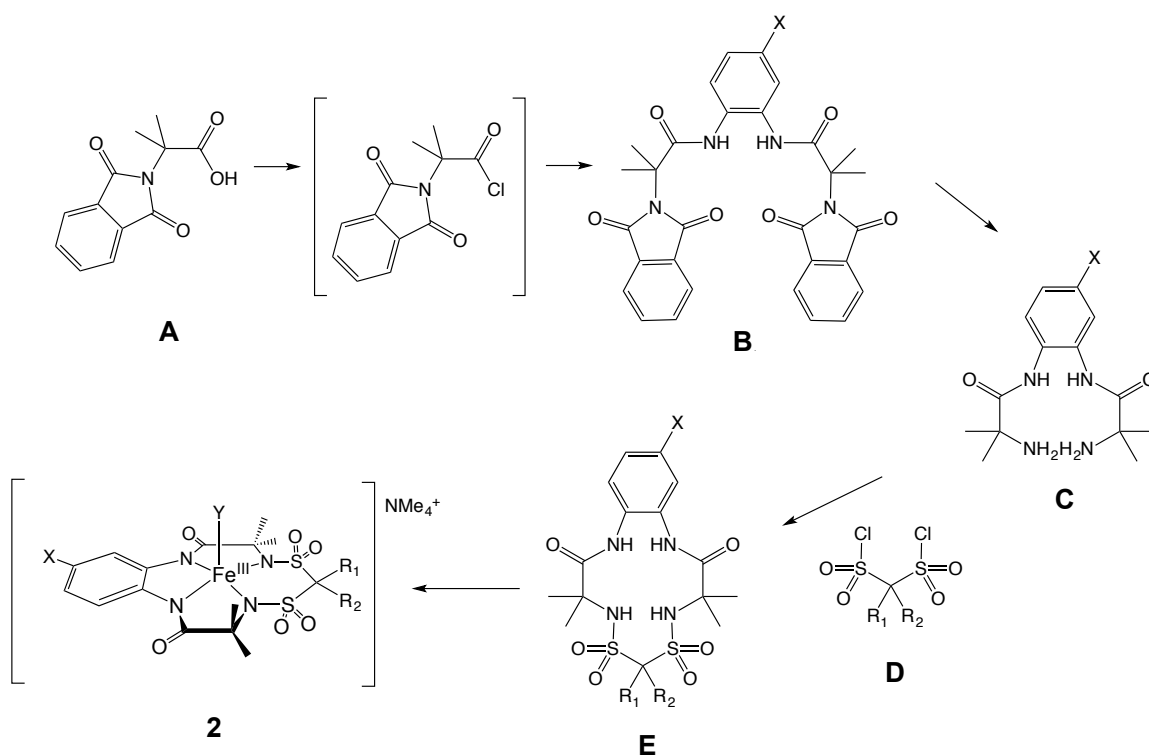


Figure 4.13 General method for preparation of **2**. Y is typically  $\text{H}_2\text{O}$ .

**Preparation of 2a** The general procedure for **2** with **C** ( $\text{X} = \text{H}$ ) and **D** ( $\text{R}_1 = \text{R}_2 = \text{H}$ ) gave **E** ( $\text{X} = \text{H}$ ,  $\text{R}_1 = \text{R}_2 = \text{H}$ ) in 25% yield.  $^1\text{H}$  NMR (300 MHz,  $\text{DMSO}-d_6$ )  $\delta$  9.07 (s, 2H), 8.16 (s, 2H), 7.60 (dd,  $J = 6.0, 3.6$  Hz, 2H), 7.20 (dd,  $J = 6.1, 3.5$  Hz, 2H), 5.15 (s, 2H), 1.56 (s, 12H).  $^{13}\text{C}$  NMR (500 MHz,  $\text{DMSO}-d_6$ )  $\delta$  172.86, 130.61, 125.81, 125.59, 71.35, 61.00, 27.57. ESI-MS (neg mode):  $m/z$  417.2 ( $\text{M}-\text{H}^+$ , 100%). Metalation of **E** gave **2a** at 23% yield. UV/Vis in  $\text{H}_2\text{O}$ :  $\lambda_{\text{max}} = 385$  nm ( $\epsilon = 4710$   $\text{cm}^{-1} \text{M}^{-1}$ ); ESI-MS (neg mode):  $m/z$  calcd: 470.0; found: 470.1 ( $\text{M}^-$ , 100%); anal. calcd (%) for  $\text{C}_{19}\text{H}_{32}\text{FeN}_5\text{O}_7\text{S}_2 \cdot \frac{1}{3}\text{Et}_2\text{O}$ : C 41.59, H 6.07, N 11.93; found: C 41.52, H 6.48, N 11.86.

**Preparation of 2b** The general procedure for **2** with **C** ( $X = \text{NO}_2$ ) and **D** ( $R_1 = R_2 = \text{H}$ ) gave **E** ( $X = \text{NO}_2$ ,  $R_1 = R_2 = \text{H}$ ) in 24% yield.  $^1\text{H}$  NMR (300 MHz,  $\text{DMSO-}d_6$ )  $\delta$  9.42 (s, 1H), 9.31 (s, 1H), 8.45 (d,  $J = 2.6$  Hz, 1H), 8.28 (d,  $J = 11.8$  Hz, 2H), 8.14 (dd,  $J = 9.1$ , 2.7 Hz, 1H), 8.05 (d,  $J = 9.1$  Hz, 1H), 5.19 (s, 2H), 1.59 (s, 12H). ESI-MS (neg mode):  $m/z$  462 ( $\text{M-H}^+$ , 100%). Metalation of **E** gave **2b** in 27% yield. UV/Vis in  $\text{H}_2\text{O}$ :  $\lambda_{\text{max}} = 365$  nm ( $\epsilon = 11300 \text{ cm}^{-1} \text{ M}^{-1}$ ); ESI-MS (neg mode):  $m/z$  calcd: 514.99; found: 514.1 ( $\text{M}^-$ , 100%); anal. calcd (%) for  $\text{C}_{19}\text{H}_{31}\text{FeN}_6\text{O}_9\text{S}_2$ : C 37.57, H 5.14, N 13.84; found: C 37.95, H 5.15, N 12.70.

**Preparation of 2c** Ethane-1,1-disulfonyl chloride was prepared as previously described.<sup>29</sup> The general procedure for **2** with **C** ( $X = \text{H}$ ) and **D** ( $R_1 = \text{H}$ ,  $R_2 = \text{CH}_3$ ) gave **E** ( $X = \text{H}$ ,  $R_1 = \text{H}$ ,  $R_2 = \text{CH}_3$ ) in 39% yield.  $^1\text{H}$  NMR (300 MHz,  $\text{DMSO-}d_6$ )  $\delta$  9.20 (s, 2H), 8.08 (s, 2H), 7.69 (s, 2H), 7.22 (s, 2H), 5.10 (q, 1H), 1.68 (d, 3H), 1.55 (d, 12H). ESI-MS (neg mode):  $m/z$  431.2 ( $\text{M-H}^+$ , 100%). Metalation of **E** gave **2c** in 79% yield. UV/Vis in  $\text{H}_2\text{O}$ :  $\lambda_{\text{max}} = 385$  nm ( $\epsilon = 4180 \text{ cm}^{-1} \text{ M}^{-1}$ ); ESI-MS (neg mode):  $m/z$  calcd: 484.02; found: 484.2 ( $\text{M}^-$ , 100%); elemental anal. calcd (%) for  $\text{C}_{20}\text{H}_{34}\text{FeN}_5\text{O}_7\text{S}_2$ : C 41.67, H 5.94, N 12.15; found: C 40.12, H 6.04, N 11.34.

**Preparation of 2d** The general procedure for **2** with **C** ( $X = \text{NO}_2$ ) and **D** ( $R_1 = \text{H}$ ,  $R_2 = \text{CH}_3$ ) gave **E** ( $X = \text{NO}_2$ ,  $R_1 = \text{H}$ ,  $R_2 = \text{CH}_3$ ) in 48% yield.  $^1\text{H}$  NMR (300 MHz,  $\text{DMSO-}d_6$ )  $\delta$  9.62 (s, 1H), 9.41 (s, 1H), 8.50 (s, 1H), 8.18 (m, 4H), 5.13 (q, 1H), 1.67 (d, 6H), 1.58 (d, 6H), 1.54 (d, 3H). ESI-MS (neg mode):  $m/z$  476.2 ( $\text{M-H}^+$ , 100%). Metalation of **E** gave **2d** in 44% yield. UV/Vis in  $\text{H}_2\text{O}$ :  $\lambda_{\text{max}} = 360$  nm ( $\epsilon = 9660 \text{ cm}^{-1} \text{ M}^{-1}$ ); ESI-MS (neg



mode): m/z calcd: 529.00; found: 529.2 ( $M^+$ , 100%); elemental analysis calcd (%) for  $C_{20}H_{33}FeN_6O_9S_2$ : C 38.65, H 5.35, N 13.52; found: C 38.23, H 5.66, N 12.15.

#### 4.4.4 X-ray Crystallography

X-ray quality crystals of **2a** formed upon slow diffusion of diethyl ether into a solution of the  $NMe_4^+$  salt of **2a** in acetonitrile. Crystallographic data for compound **2a** were collected at 296(2) K using graphite-monochromated Mo  $K\alpha$  radiation (0.71073 Å) on a Bruker Smart Apex II CCD diffractometer. Data reduction included absorption corrections by the multiscan method using SADABS and refinement by full-matrix least squares using the SHELXTL 6.1 bundled software package. The H atoms were positioned geometrically (aromatic C–H 0.93, methylene C–H 0.97, and methyl C–H 0.96) and treated as riding atoms during subsequent refinement, with  $U_{iso}(H) = 1.2[U_{eq}(C)]$  or  $1.5[U_{eq}(\text{methyl } C)]$ . The methyl groups were allowed to rotate about their local 3-fold axes.

#### 4.4.5 Measurement of $pK_a$

The  $pK_a$  of **2b** was performed as described in detail previously.<sup>30</sup>

#### 4.4.6 Kinetics of Catalyzed Bleaching of Orange II

The initial rates of consumption of Orange II in the presence of TAML and  $H_2O_2$  were measured as described in detail elsewhere<sup>18,30</sup> using a UV-Vis spectrometer or a plate reader. All reported values are the mean of at least three determinations. All calculations were made using Sigma Plot (versions 12.0 and 12.5).

**UV-Vis Method** Stock solutions of catalyst (ca.  $1 \times 10^{-6}$  M), Orange II ( $5 \times 10^{-4}$  M), and  $\text{H}_2\text{O}_2$  ( $4 \times 10^{-2}$  M) were prepared in HPLC-grade water. Catalyst and Orange II were added to 1 cm acrylic cuvettes containing 0.01 M phosphate buffer or Carmody buffer<sup>31</sup> and the reactions were initiated by addition of peroxide. Values for  $k_{\text{I}}$  and  $k_{\text{II}}$  at pH 7 given in Table 1.3 were determined from initial rates as functions of  $\text{H}_2\text{O}_2$  and Orange II concentrations. For **2a** ( $2.6 \times 10^{-8}$  M) and **2b** ( $2.3 \times 10^{-8}$  M), the data in 3D mesh plots were fit to the rate equation in Figure 4.1, assuming  $k_{\text{I}}$  to be negligible<sup>18</sup> (Figure 4.3). For **2c** ( $9.8 \times 10^{-8}$  M) and **2d** ( $1.0 \times 10^{-7}$  M),  $k_{\text{I}}$  and  $k_{\text{II}}$  were determined from linear plots of  $v^{-1}$  vs.  $[\text{H}_2\text{O}_2]^{-1}$  with  $2.6 \times 10^{-5}$  M Orange II or  $v^{-1}$  vs.  $[\text{Orange II}]^{-1}$  with  $1.6 \times 10^{-3}$  M  $\text{H}_2\text{O}_2$ , respectively (data not shown).

**Plate Reader Method** Initial rates as a function of  $[\text{H}_2\text{O}_2]$  over pH 6–11.5 were measured using a plate reader. Hydrogen peroxide ( $0.07\text{--}3.0 \times 10^{-3}$  M) and Orange II ( $2 \times 10^{-5}$  M) were combined in 96-well plates with Carmody buffer and the reactions were initiated with catalyst. Values for  $k_{\text{I}}$  and  $k_{\text{II}}$  given in Fig. 2b–c for **1b**, **1c**, **2b**, and **2d** ( $0.5\text{--}2 \times 10^{-7}$  M) were determined as above from linear plots of  $v^{-1}$  vs.  $[\text{H}_2\text{O}_2]^{-1}$ .

**Incomplete Bleaching** Measurements to determine  $k_{\text{I}}$  were performed on the UV-Vis as described in detail previously<sup>16</sup> with minimal catalyst concentrations ( $0.1\text{--}1 \times 10^{-7}$  M) and Orange II ( $4.5 \times 10^{-5}$  M),  $\text{H}_2\text{O}_2$  ( $1.6 \times 10^{-3}$  M), and phosphate (0.01 M) or Carmody buffer.

#### 4.4.7 *Propranolol Degradation by Catalyst/H<sub>2</sub>O<sub>2</sub>*

Stock solutions of catalyst ( $1 \times 10^{-5}$  M), propranolol ( $4 \times 10^{-6}$  M), and H<sub>2</sub>O<sub>2</sub> (1 M) were prepared in HPLC grade water. Appropriate volumes of phosphate buffer (0.01 M), propranolol, and catalyst stock solutions were combined and equilibrated to  $25 \pm 2^\circ\text{C}$  in a water bath. For the river water reactions, Allegheny River water was used in place of buffer. Upon addition of propranolol stock solution to the river water, the pH of the reaction mixture was  $\sim 8.5$ . This was adjusted to  $\sim 7.2$  using dilute HCl and the degradation experiments were performed at pH 7.2. The reaction was initiated by the addition of an appropriate volume of the peroxide stock solution to give a final volume of 10 mL with  $1.0 \times 10^{-7}$  M catalyst,  $3.3 \times 10^{-4}$  M H<sub>2</sub>O<sub>2</sub>, and  $5.8 \times 10^{-8}$  M propranolol. At pre-determined time intervals, aliquots were withdrawn and the concentration of propranolol was determined using HPLC. The LC method consisted of 1 mL/min flow rate, 35% methanol/65% pH 3 0.01 M phosphate buffer, 40 °C column temperature, and fluorescence detection by excitation at 230 nm and monitoring of the 340 nm emission wavelength. For the measurement of parts per billion concentrations of propranolol, the sensitivity was set to medium with 4X gain for the signal and the sample injection volume for the analysis was 100  $\mu\text{L}$ . All propranolol peaks were integrated automatically and the data was analyzed using Lab solutions software. All reported values are the mean of three determinations.

#### 4.4.8 *Animals*

Animal care conformed to the NIH Guide, and The Animal Care and Use Committee at the University of Missouri approved all procedures prior to conducting the

study. Ten week-old male and female CD-1 mice were purchased from Charles River Laboratories (Raleigh, NC) and were housed in polypropylene cages with corncob bedding in a temperature- and humidity-controlled facility on a 12L:12D cycle. Water was purified by ion exchange followed by a series of carbon filters and supplied in glass bottles, and both water and rodent chow (Purina 5001) were available ad libitum. After a one-week acclimatization period, females were time-mated to male mice. Mating was confirmed by the presence of a vaginal plug, and the day of mating was set as gestation day (GD) 0. Pregnant females were singly housed on GD 17 and allowed to deliver naturally on GD19 [postnatal day (PD) 1]. The number and sex of pups in the litters was determined on PD 12. Litters were not disturbed again until PD 19, when female offspring were weaned and housed 2 – 4 females per cage.

#### 4.4.9 *Mouse Drinking Water Treatment*

The drinking water used for this study was purified by anion exchange and carbon filtration (pH ~7.0). All drinking solutions used in these studies were prepared fresh daily, and contained either EE2, NewTAML **2a**, **2a**/H<sub>2</sub>O<sub>2</sub>-treated EE2, or water alone. A pilot study was conducted to determine the optimum concentration of EE2 for the uterotrophic assay studies. Based on the results from the pilot study (Figure S5), the optimal EE2 concentration in drinking water was 84 nM (25 ng/mL). The estimated EE2 intake was 5-9 µg/kg/day, based on volume consumed, body weight and concentration administered. The concentrations of catalyst administered in drinking water ranged from 4-4000 nM.

For drinking solutions containing **2a**/H<sub>2</sub>O<sub>2</sub>-treated EE2, EE2 (84 nM) was added to 4 nM or 40 nM solutions of catalyst in drinking water, and 1 mM hydrogen peroxide was added to initiate the degradation reaction. The reaction was allowed to progress for one hour (40 nM catalyst) or 3 hours (4 nM catalyst) and was terminated by the addition of 0.5 ppm catalase dissolved in water. The **2a**/H<sub>2</sub>O<sub>2</sub>-only water treatment (4, 40, 400 or 4000 nM) was identical to the catalyst+EE2 treatment except that EE2 was omitted. Catalyst-only treatments were conducted for one hour (40, 400 and 4000 nM treatments) or three hours (4 nM treatment) prior to providing the solution to the test animals.

The control (water only) and EE2 treatments were tested both with and without added hydrogen peroxide and catalase. No significant effects of peroxide/catalase on body weight or uterine response were observed, and these groups were combined in the final analysis.

#### *4.4.10 Prepubertal Mouse Uterotropic Assay*

On PD 19, female offspring were rehoused at 2 - 4 animals per cage and transferred from Purine 5008 breeder chow to the Purina 5001 maintenance diet. Drinking water was administered in 50 ml polypropylene centrifuge tubes equipped with a stopper and sipper tube, and contained either EE2, EE2 pretreated with 4 or 40 nM **2a**, the 4 or 40 nM **2a** treatment only, or water alone. On PD 22, after three days' exposure to the test solutions, the animals were sacrificed, and the uteri were collected and weighed (fresh solutions were prepared each day).

#### *4.4.11 Toxicity Screen*

Female mice were weaned on PD 19 and re-housed as described above. Animals were treated with 0, 40, 400 or 4000 nM **2a** in drinking water as described. After three days' exposure to the catalyst-treated water, the animals were given regular drinking water in glass bottles for the remainder of the study. In accordance with FDA guidelines for Acute Toxicity Testing for Pharmaceuticals, the animals were observed daily for 14 days for signs of morbidity. At 14 days post-exposure the animals were weighed, euthanized and liver, kidney and spleen were weighed and fixed for further evaluation. Uterine weights were not measured, since by this time the animals should have been cycling.

#### *4.4.12 Mouse Data Analysis*

Data were analyzed using the General Linear Means (GLM) model in SAS. Data were examined for effects of litter size and body weight on dependent variables. For uterotrophic assays litter size was strongly correlated with outcomes, and ANCOVA-derived adjusted means with litter size as the covariate are given in the results. Organ weights were strongly correlated with body weight and these are shown as organ weight/body weight to correct for this variable.

## 4.5 References

1. Gupta, S. Sen; Stadler, M.; Noser, C.; Ghosh, A.; Steinhoff, B.; Lenoir, D.; Horwitz, C. P.; Schramm, K.-W.; Collins, T. J. *Science* **2002**, 296 (5566), 326–328.
2. Chanda, A.; Khetan, S. K.; Banerjee, D.; Ghosh, A.; Collins, T. J. *J. Am. Chem. Soc.* **2006**, 128 (37), 12058–12059.
3. Shen, L. Q.; Beach, E. S.; Xiang, Y.; Tshudy, D. J.; Khanina, N.; Horwitz, C. P.; Bier, M. E.; Collins, T. J. *Environ. Sci. Technol.* **2011**, 45 (18), 7882–7887.
4. Kundu, S.; Chanda, A.; Espinosa-Marvan, L.; Khetan, S. K.; Collins, T. J. *Catal. Sci. Technol.* **2012**, 2 (6), 1165–1172.
5. Mills, M. R.; Arias-Salazar, K.; Baynes, A.; Shen, L. Q.; Churchley, J.; Beresford, N.; Gayathri, C.; Gil, R. R.; Kanda, R.; Jobling, S.; Collins, T. J. *Sci. Rep.* **2015**, 5, 10511.
6. Tang, L. L.; DeNardo, M. A.; Gayathri, C.; Gil, R. R.; Kanda, R.; Collins, T. J. *Environ. Sci. Technol.* **2016**, 50, 5261–5268.
7. Shappell, N. W.; Vrabel, M. a; Madsen, P. J.; Harrington, G.; Billey, L. O.; Hakk, H.; Larsen, G. L.; Beach, E. S.; Horwitz, C. P.; Ro, K.; Hunt, P. G.; Collins, T. J. *Environ. Sci. Technol.* **2008**, 42 (4), 1296–1300.
8. Kundu, S.; Chanda, A.; Khetan, S. K.; Ryabov, A. D.; Collins, T. J. *Environ. Sci. Technol.* **2013**, 47 (10), 5319–5326.
9. Kundu, S.; Chanda, A.; Thompson, J. V. K.; Diabes, G.; Khetan, S. K.; Ryabov, A. D.; Collins, T. J. *Catal. Sci. Technol.* **2014**, 5, 1775–1782.
10. Beach, E. S.; Malecky, R. T.; Gil, R. R.; Horwitz, C. P.; Collins, T. J. *Catal. Sci. Technol.* **2011**, 1 (3), 437–443.
11. Banerjee, D.; Markley, A. L.; Yano, T.; Ghosh, A.; Berget, P. B.; Minkley, E. G.; Khetan, S. K.; Collins, T. J. *Angew. Chemie Int. Ed.* **2006**, 45 (24), 3974–3977.
12. Churchley, J.; Collins, T.; Jobling, S. *Catalytic Oxidation of Pharmaceutical Compounds in Wastewater Effluents. UKWIR Report 13/WW/17/14*; London, 2013.
13. Truong, L.; DeNardo, M. A.; Kundu, S.; Collins, T. J.; Tanguay, R. L. *Green Chem.* **2013**, 15, 2339–2343.
14. Collins, T. *Science*. **2001**, 291, 48–49.
15. Collins, T. J.; DeNardo, M. A.; Warner, G. R.; Gordon-Wylie, S. W.; Ellis, W. C. Superior Oxidation Catalysts Based on Macrocyclic Compounds. PCT International Patent Application No. PCT/US2016/053105.
16. DeNardo, M. A.; Mills, M. R.; Ryabov, A. D.; Collins, T. J. *J. Am. Chem. Soc.* **2016**, 138 (9), 2933–2936.
17. Ghosh, A.; Mitchell, D. a; Chanda, A.; Ryabov, A. D.; Popescu, D. L.; Upham, E. C.; Collins, G. J.; Collins, T. J. *J. Am. Chem. Soc.* **2008**, 130 (45), 15116–15126.
18. Chahbane, N.; Popescu, D.-L.; Mitchell, D. A.; Chanda, A.; Lenoir, D.; Ryabov, A. D.; Schramm, K.-W.; Collins, T. J. *Green Chem.* **2007**, 9 (1), 49–57.
19. Tiago de Oliveira, F.; Chanda, A.; Banerjee, D.; Shan, X.; Mondal, S.; Que, L.; Bominaar, E. L.; Münck, E.; Collins, T. J. *Science* **2007**, 315 (5813), 835–838.
20. Huggett, D. B.; Khan, I. A.; Foran, C. M.; Schlenk, D. *Environ. Pollut.* **2003**, 121 (2), 199–205.

21. Polshin, V.; Popescu, D. *J. Am. Chem. Soc.* **2008**, *130* (13), 4497–4506.
22. Ellis, W. C.; Tran, C. T.; Roy, R.; Rusten, M.; Fischer, A.; Ryabov, A. D.; Blumberg, B.; Collins, T. J. *J. Am. Chem. Soc.* **2010**, *132* (28), 9774–9781.
23. Schug, T. T.; Abagyan, R.; Blumberg, B.; Collins, T. J.; Crews, D.; DeFur, P. L.; Dickerson, S. M.; Edwards, T. M.; Gore, A. C.; Guillet, L. J.; Hayes, T.; Heindel, J. J.; Moores, A.; Patisaul, H. B.; Tal, T. L.; Thayer, K. a.; Vandenberg, L. N.; Warner, J. C.; Watson, C. S.; vom Saal, F. S.; Zoeller, R. T.; O'Brien, K. P.; Myers, J. P. *Green Chem.* **2013**, *15* (1), 181–198.
24. Collins Group Patents  
[http://igs.chem.cmu.edu/index.php?option=com\\_content&view=article&id=347&Itemid=505](http://igs.chem.cmu.edu/index.php?option=com_content&view=article&id=347&Itemid=505).
25. Fild, V. M.; Rieck, H.-P. *Chemiker-Zeitung* **1976**, *100* (9), 391–392.
26. George, P. *Biochem. J.* **1953**, *54*, 267–276.
27. Chai, C.; Armarego, W. L. F. *Purification of Laboratory Chemicals*, Fifth Ed.; Butterworth-Heinemann, 2003.
28. Ghosh, A.; Ramidi, P.; Pulla, S.; Sullivan, S. Z.; Collom, S. L.; Gartia, Y.; Munshi, P.; Biris, A. S.; Noll, B. C.; Berry, B. C. *Catal. Letters* **2010**, *137* (1–2), 1–7.
29. Murakami, S.; Onozuka, T.; Fujita, K. Preparation of methylenedisulfonic acid compounds and cyclic methylenedisulfonate compounds. JP 2014062076, A, 2014.
30. Warner, G. R.; Mills, M. R.; Enslin, C.; Pattanayak, S.; Panda, C.; Panda, T. K.; Gupta, S. Sen; Ryabov, A. D.; Collins, T. J. *Chem. - A Eur. J.* **2015**, *21* (16), 6226–6233.
31. Carmody, W. R. *J. Chem. Educ.* **1961**, *38* (11), 559.



## **CHAPTER 5**

### **Understanding the Superior Catalytic Activity of NewTAMLs at Neutral pH**

## 5.1 Introduction

The iterative design of TAML activators (Figure 5.1) described in Chapter 1 has produced a family of fully functional mimics of peroxidase enzymes. Strengthening features of the catalysts such as the rate of activation of peroxide, the pH of maximum activity, and the hydrolytic and operational stabilities has guided the iterative design process to optimize TAMLs for degrading micropollutants in aqueous solution.<sup>1</sup> However, investigation into the lifetime control of TAML activators has revealed an activity-stability wall of structural origin that prevents an increase in activity without a corresponding decrease in lifetime.<sup>2</sup> Recent mechanistic insight into the nature of this activity-stability relationship, summarized in Chapter 3, has shown that the structural weakness derives from nucleophilic attack at the carbonyl groups of the *N*-amides.<sup>3</sup>

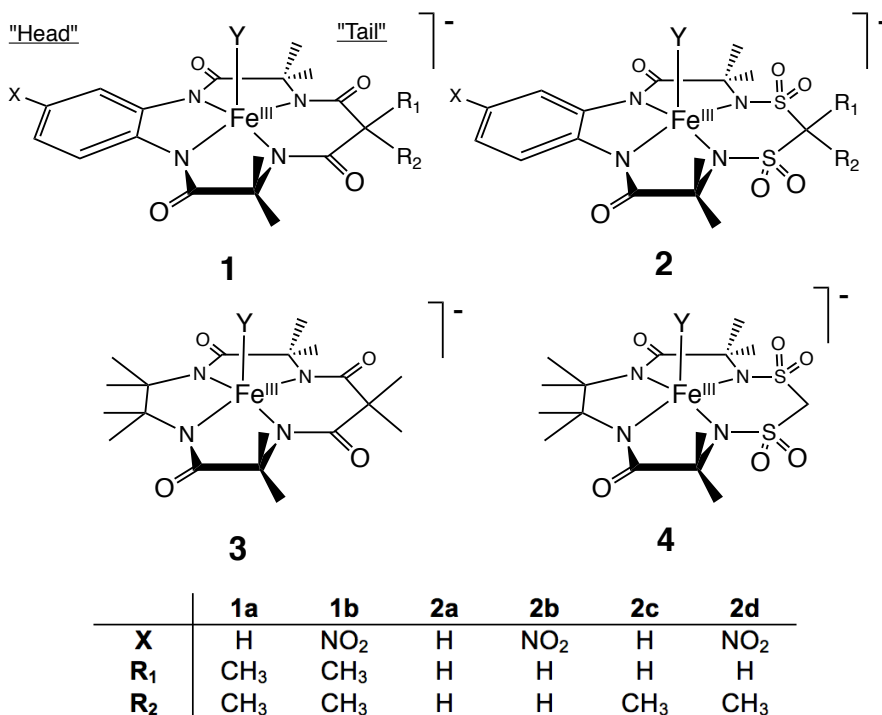


Figure 5.1 Old- and NewTAML activators discussed in this chapter; Y is typically water.

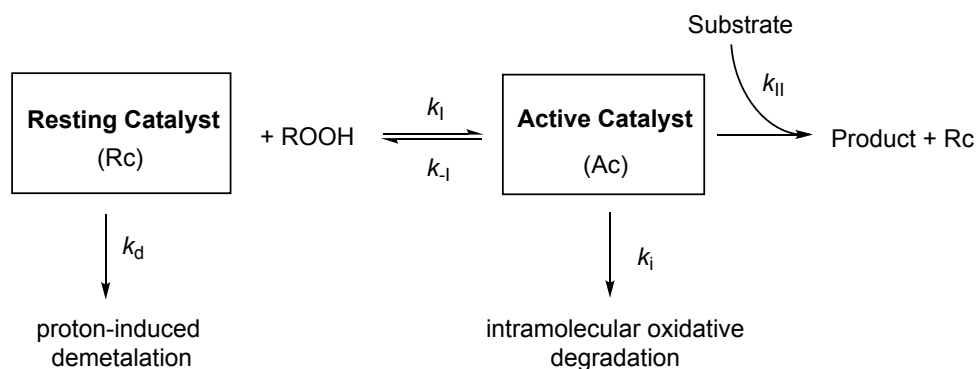


Figure 5.2 Mechanism of catalysis of TAMLs discussed in this chapter, including deactivation processes.

This revelation has necessitated a redesign of the TAML ligand to remove *N*-amides in favor of more resilient functional groups. Chapter 4 introduced a new family of TAML activators containing sulfonamide groups in the “tail” of the macrocyclic ligand (Figure 5.1; **2** and **4**). The nucleophile-resistant sulfonamide groups have the additional benefit of strong electron withdrawing properties. Electron withdrawing groups in the tail have been previously demonstrated to increase hydrolytic stability of the resting state of the catalysts at acidic pH.<sup>4,5</sup> The structural changes in **2** and **4** result in increased Lewis acidity at the metal center, stabilizing the high valent iron active species that form upon activation of peroxide (Figure 5.2) and significantly increasing catalyst activity close to neutral pH.

Prototype “NewTAMLs” are superior in reactivity compared to structurally analogous “OldTAMLs” and have been examined for use in scaled water treatment applications. In the degradation of the persistent drug propranolol presented in Chapter 4, NewTAML **2b** with H<sub>2</sub>O<sub>2</sub> was shown to remove propranolol to below the limit of detection in under five minutes, compared to only 35% removal in 75 minutes by structurally analogous **1b** (Figure 5.3). This advance represents a remarkable increase in

performance in the removal of a common wastewater pollutant and the largest improvement in TAML activity from a single structural modification.

In this chapter, the mechanistic features of the family of NewTAMLs containing disulfonamide tails are described. NewTAML rate constants for degradation of the model substrate Orange II, pH of maximum activity, and hydrolytic stabilities are compared with existing analogous OldTAMLs. EPR studies were performed by Saborni Biswas and Michael P. Hendrich. Hydrolytic stability measurements were performed in collaboration with Zheng (David) Zhang.

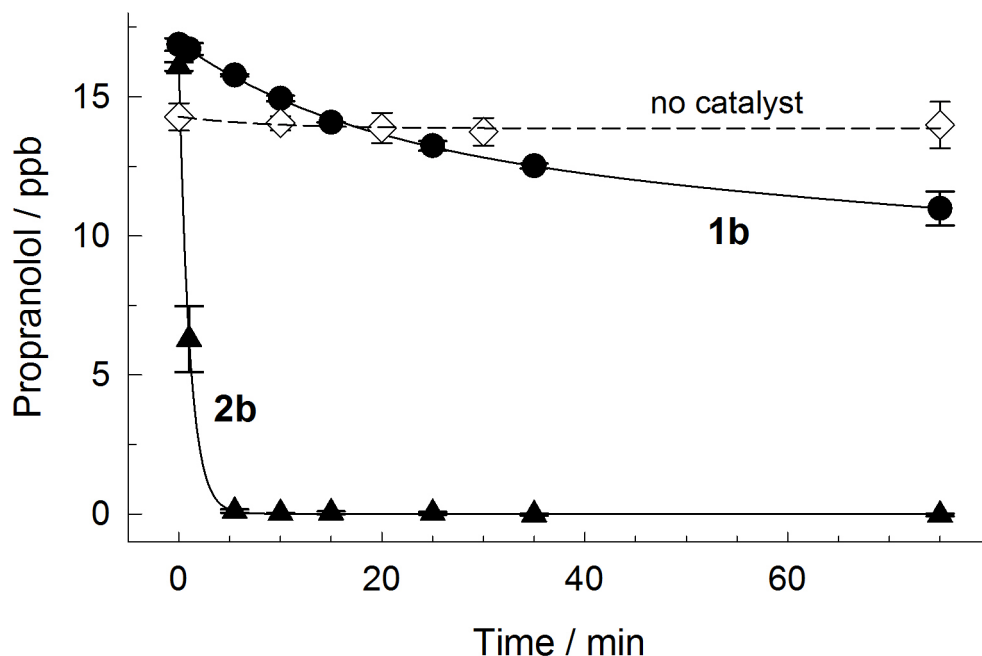


Figure 5.3 Comparison of degradation of propranolol (15 ppb,  $\sim 5 \times 10^{-8}$  M) with TAMLs ( $1.0 \times 10^{-7}$  M) and  $\text{H}_2\text{O}_2$  ( $3.3 \times 10^{-4}$  M) in pH 7 HPLC-grade purified water at 25 °C. Adapted from Figure 4.7. Lines are for emphasis only.

## 5.2 Results and Discussion

### 5.2.1 Properties of Sulfonamide-tailed Activators

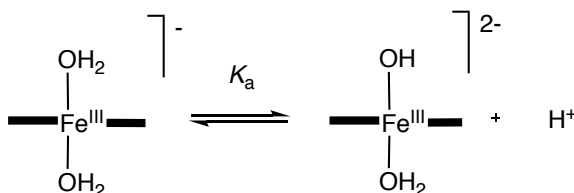
NewTAMLs **2** and **4** are structural analogs of OldTAMLs **1** and **3**, respectively, with disulfonamide groups ( $-\text{NSO}_2\text{CR}_1\text{R}_2\text{SO}_2\text{N}-$ ) substituted for dimethyl malonyl ( $-\text{NCOCMe}_2\text{CON}-$ ) in the tail (Figure 5.1). While all OldTAMLs in this study have methyl groups at  $\text{R}_1$  and  $\text{R}_2$  in the tail, NewTAMLs **2a** and **2c** have  $\text{R}_1 = \text{R}_2 = \text{H}$  and **2b** and **2d** have  $\text{R}_1 = \text{H}$  and  $\text{R}_2 = \text{CH}_3$ . The R groups at the tail of **2** and **4** have so far yielded very few property differences between methylated and unmethylated catalysts (**2a/2c** and **2b/2d**) aside from the pH-dependent inactivation pathway introduced in Chapter 4. All NewTAML catalysts were prepared as tetramethylammonium salts and crystallized with an axial water molecule. The crystal structure of **2a** was presented in Chapter 4 (Figure 4.2). Of note, the six-membered ring of the tail sits in a chair conformation with the methylene group below the plane of the ligand.

In aqueous solution at neutral pH, most TAML activators form diaqua species  $[\text{Fe}^{\text{III}}\text{L}(\text{H}_2\text{O})_2]^-$ .<sup>4</sup> The unchanging UV/Vis spectra of NewTAMLs **2b** in the presence of 0.005–0.25 M KCl at pH 7 supports the same diaqua speciation for NewTAMLs in aqueous solutions (Equation 2.1). There is no evidence of aggregation in buffered and unbuffered aqueous solution, with Beer's law holding across  $(0.02\text{--}2.3) \times 10^{-3}$  M for NewTAMLs.

The UV/Vis and EPR spectra of NewTAMLs are strongly affected by pH, as shown previously for OldTAMLs.<sup>4,6,7</sup> As solution pH increases, one axial ligand is reversibly deprotonated (Equation 5.1), resulting in absorbance changes and clear isosbestic points in the range of 300–400 nm (Figure 5.4). Linearization of absorbance

changes at  $\lambda_{\max}$  using Equation 5.2, where  $A_H$ ,  $A_{OH}$ , and  $A$  are absorbances at the most acidic, most basic, and intermediate pHs, respectively, results in a straight line with a slope of one and a y-intercept equal to  $-pK_a$ .

EPR studies of **2a** at pH 7.5 and 10.5 reveal the difference in speciation between the protonated and deprotonated forms (Figure 5.5). At pH 7.5, the spectrum of **2a** is characteristic of an  $S = 3/2$  complex, typical for TAMLs with two axial water molecules.<sup>4,7</sup> Interestingly, the spectrum of the deprotonated **2a** species reveals high spin ( $S = 5/2$ ).



Equation 5.1

$$\log \frac{A_H - A}{A - A_{OH}} = \text{pH} - pK_a$$

Equation 5.2

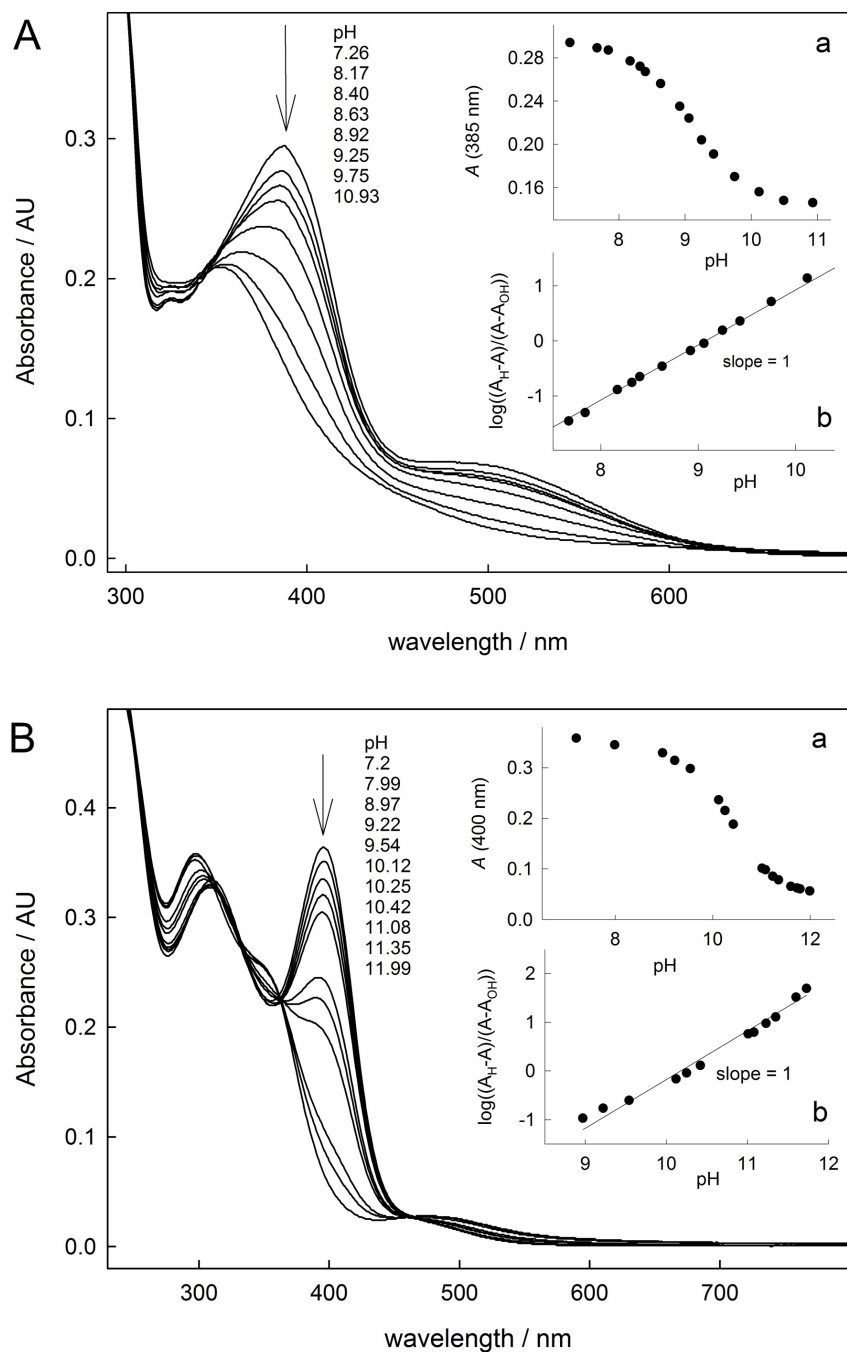


Figure 5.4 Spectra of **2a** (A) and **4** (B) at varying pH in 0.01 M phosphate buffer at 25 °C. Insets (a) show absorbance at 385 and 400 nm versus pH for **2a** and **4**, respectively. Insets (b) are linearizations of the data in insets (a) in terms of Equation 5.2.

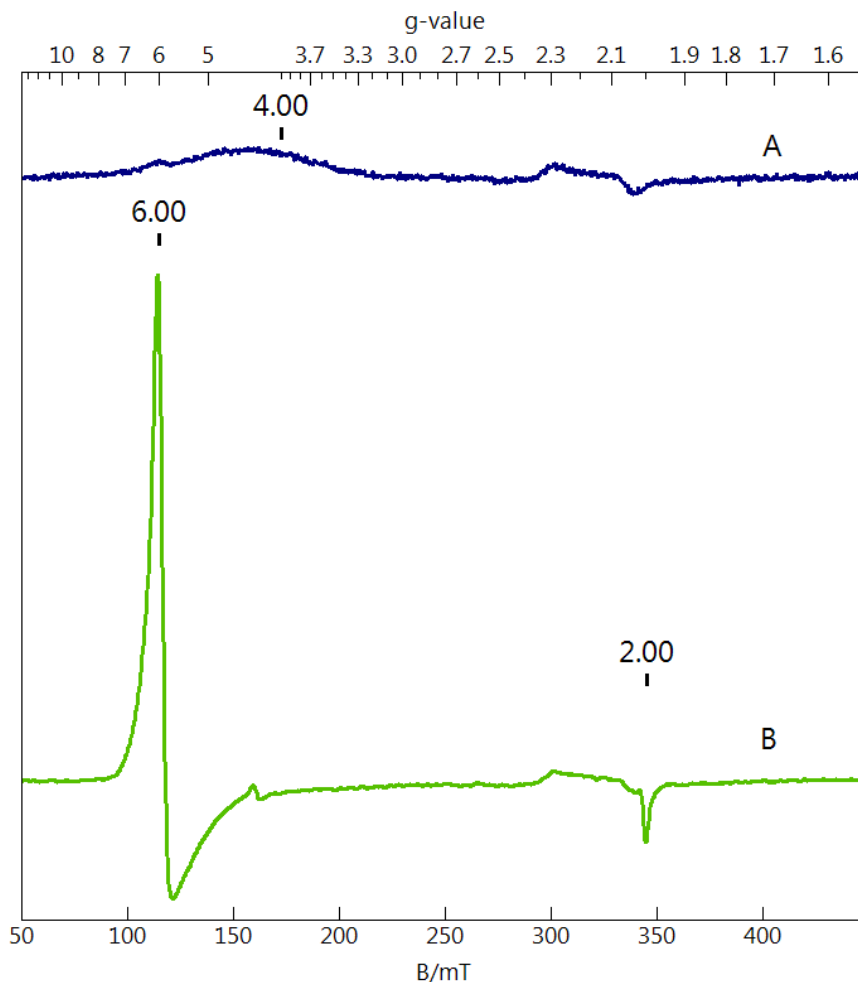


Figure 5.5 EPR spectra of 0.1 mM **2a** in phosphate buffer, 15% glycerol at (A) pH 7.5 and (B) pH 11.5. Experimental conditions: temperature, 12.6 K; microwaves, 0.2 mW at 9.645 GHz, modulation 1 mT at 100 KHz. The signal with  $g = 2.3, 2.05$  is a baseline impurity.

The values of  $pK_a$  determined for all disulfonamide NewTAMLs are listed in Table 5.1. Of note, the introduction of the disulfonamide tail decreases the  $pK_a$  by approximately 1.2 units between otherwise structurally analogous catalysts (**1/2** and **3/4**). Substitution of electron withdrawing fluorine into the tail ( $-\text{CMe}_2-$  to  $-\text{CF}_2-$ ) only provides a 0.6 pH unit decrease.<sup>8</sup> This is a major advance in TAML design because the  $pK_a$  of the axial water molecule influences the pH of maximum activity of the catalyst,



discussed in detail below. Fluorine substitution was previously the most effective tail modification for decreasing  $pK_a$ , but it is highly undesirable due the toxicity and persistence risk posed by halogen substituents.<sup>9</sup> The introduction of a nitro group in **2b** further decreased the  $pK_a$  by the expected 0.3 units compared to **1b**, as previously demonstrated for **1a/1b** (Chapter 2).<sup>6</sup> The  $pK_a$  of 8.8 for **2b** and **2d** the lowest reported yet for any TAML activator of the **1–4** structural family.

### 5.2.2 Hydrolytic Stability of NewTAML Activators

In the presence of acids, all TAML activators are known to undergo demetalation (Figure 5.2).<sup>8</sup> The pseudo-first-order rate constant  $k_{obs}$  for TAMLs **1** is dependent on  $[H^+]$ , indicating specific acid catalysis. The acceleration of  $k_{obs}$  is described by Equation 5.3, with the linear term dominant in mildly acidic conditions and the third order term dominant in strongly acidic conditions.<sup>4</sup> The third order pathway requires peripheral pre-equilibrium protonation of the macrocycle, which has been suggested to occur at the tail amide O-atoms.<sup>8</sup>

$$k_{obs} = k_1*[H^+] + k_3*[H^+]^3$$

Equation 5.3

The relationship between  $k_{obs}$  and  $[H^+]$  for NewTAMLs **2a** and **2b** was determined in the presence of 0.002–0.25 M  $HClO_4$ . The linear plots in Figure 5.6A show only the first order pathways and are consistent with  $k_{obs} = k_1*[H^+]$  when  $k_3* \approx 0$ . The value of  $k_1*$  decreases for **2a** and **2b** by 1 and 2 orders of magnitude, respectively, compared to **1a** (Table 5.1). The introduction of the  $NO_2$  group in **2b** increases stability 15-fold compared to **2a**.

Macrocycle protonation required for the third order pathway can be minimized by substitution of electron withdrawing groups such as fluorine atoms in the tail.<sup>4</sup> Up to 0.25 M HClO<sub>4</sub>,  $k_{\text{obs}}$  describing the demetalation of **2a** and **2b** shows no contribution from a third order term, providing further evidence for the amides as the site of protonation. As a result of the stability provided by sulfonamide substitution, complexes **2a** and **2b** may be functional catalysts under acidic conditions.

The electron-rich “beheaded” OldTAML **3** has an exceptionally low value of  $k_1^*$  and displays an unusual leveling off of  $k_{\text{obs}}$  consistent with Equation 5.4 at 0.002–2.5 M HClO<sub>4</sub> (Figure 5.6B).<sup>10</sup>

$$k_{\text{obs}} = \frac{k_1[\text{H}^+]}{K + [\text{H}^+]}$$

Equation 5.4

Analogously beheaded NewTAML **4** does not display the same levelling off of  $k_{\text{obs}}$  with increasing  $[\text{H}^+]$ , and in fact conforms to Equation 5.3. The value of  $k_1^*$  for **4** is 10 times lower than  $k_1/K$  for **3** (Table 5.1), and the value of  $k_3^*$  of  $(1.1 \pm 0.03) \times 10^{-5} \text{ M}^{-3} \text{ s}^{-1}$  is the lowest ever measured for any TAML catalyst. The acid stability of **3** has proven useful for applications other than water treatment; recently, iron(V)oxo species of **3** were generated in pure water from pH 2–10.6.<sup>11</sup> As the most stable TAML under even very acidic conditions, **4** may prove useful for similar studies.

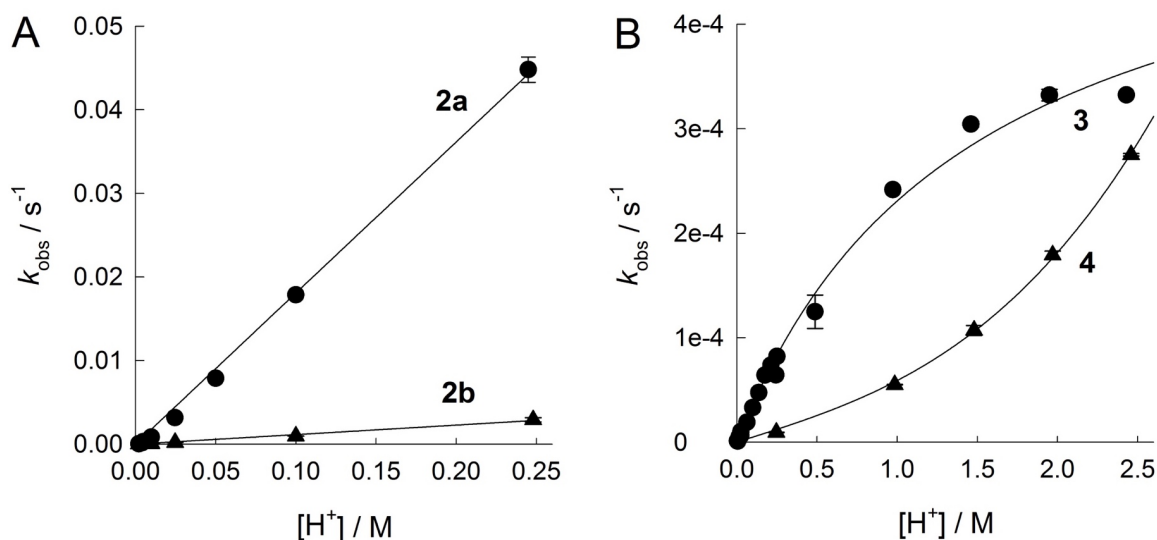


Figure 5.6 Dependence of  $k_{\text{obs}}$  on  $[\text{HClO}_4]$  for acid induced demetalation of **2a** and **2b** (A) and **3** and **4** (B) at 25 °C.

### 5.2.3 Catalytic Activity in Bleaching of Orange II with $\text{H}_2\text{O}_2$

Initial rates of bleaching of the model substrate Orange II were used to compare the reactivity of various catalysts.<sup>6,12</sup> Measurements focus on neutral pH to emphasize the superiority of NewTAMLs for use in water treatment applications. Kinetic investigations of NewTAML/ $\text{H}_2\text{O}_2$  catalyzed degradation of Orange II were consistent with the mechanism of catalysis in Figure 5.2, which is described by Equation 5.5.

$$-\frac{d[\text{S}]}{dt} = \frac{k_1 k_{\text{II}} [\text{ROOH}] [\text{S}] [\text{Fe}^{\text{III}}]}{k_{-1} + k_1 [\text{ROOH}] + k_{\text{II}} [\text{S}]}$$

Equation 5.5

The rate of bleaching is linearly dependent on catalyst concentration over the range of  $3 \times 10^{-8}$  to  $3 \times 10^{-6}$  M (data not shown) and hyperbolically dependent on both  $[\text{Orange II}]$  and  $[\text{H}_2\text{O}_2]$ . Figure 5.7 shows the dependence of the rate on  $[\text{Orange II}]$  for **2c**. At  $[\text{Orange II}] > 2.5 \times 10^{-5}$  M, the rate is nearly independent of dye concentration

such that Equation 5.5 collapses into  $-d[S]/dt = k_I[H_2O_2][Fe^{III}]$ . Under these conditions, the rate is directly proportional to  $[H_2O_2]$  up to  $1.5 \times 10^{-3}$  M for **2c**, as shown in the inset to Figure 5.7. The value of  $k_I$  determined from the linear portion of this plot is  $270 \pm 10$   $M^{-1} s^{-1}$ . Values of the rate constants  $k_I$  and  $k_{II}$  ( $k_{-I}$  is assumed to be negligible<sup>12</sup>) were estimated by fitting both plots in Figure 5.7 to Equation 5.5. The most accurate values for each rate constant in Table 5.1 were determined from linear double inverse plots of  $rate^{-1}$  vs.  $[Orange\ II]^{-1}$  and  $rate^{-1}$  vs.  $[H_2O_2]^{-1}$  and agree with estimates from the substrate-independent equation  $-d[S]/dt = k_I[H_2O_2][Fe^{III}]$  above. At neutral pH, all NewTAMLs are superior in terms of  $k_I$  and  $k_{II}$  compared to their structural OldTAML analogs (Table 5.1). Under the conditions used in these studies where  $k_I[H_2O_2] \ll k_{II}[Orange\ II]$ , the process described by  $k_I$  is the rate limiting step and therefore the best means for comparison. Values of  $k_I$  indicate that complex **2a** is tenfold more reactive than **1a** and **2b** is fourfold more reactive than **1b**. As expected, **2a** and **2c** perform similarly, as do **2b** and **2d**. The additional methyl group is only slightly deactivating because it is distant from the iron center.

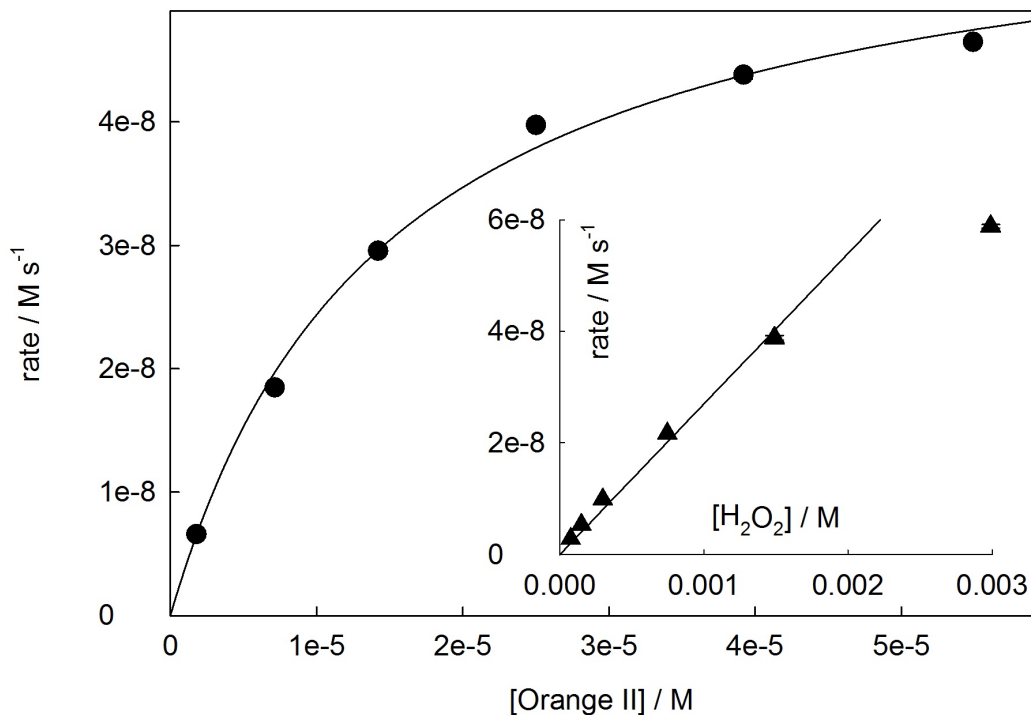


Figure 5.7 The initial rates of Orange II bleaching with **2c** ( $1 \times 10^{-7}$  M) and  $\text{H}_2\text{O}_2$  ( $1.5 \times 10^{-3}$  M) as a function of Orange II concentration with 0.01 M pH 7 phosphate at 25 °C. Inset: Rate as a function of  $[\text{H}_2\text{O}_2]$  with **2c** ( $1 \times 10^{-7}$  M), Orange II ( $2.5 \times 10^{-5}$  M), and 0.01 M pH 7 phosphate at 25 °C.

Values of the rate constant  $k_1$  for Orange II bleaching were determined for **2a** and **2b** in the range of pH 6.0–12.0. The bell shaped curves for **2a** and **2b** (Figure 5.8) are typical of TAML activators.<sup>6,13–15</sup> The process of  $\text{H}_2\text{O}_2$  activation by TAML described by  $k_1$  is dependent on the  $\text{p}K_a$  of deprotonation of the first axial water ligand of the catalyst ( $K_{a1}$ ), as discussed above, and deprotonation of the peroxide ( $K_{a2}$ ). The protonated and deprotonated species interact to yield the active catalyst according to Figure 5.9, described by Equation 5.6.

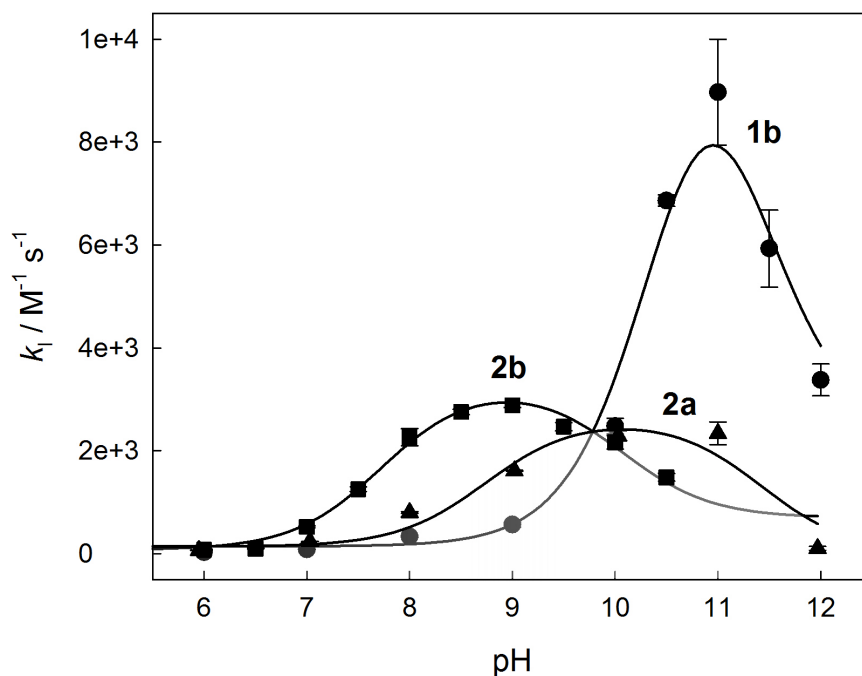


Figure 5.8 Rate constant  $k_1$  measured for **1b**, **2a**, and **2b** in the catalyzed bleaching of Orange II by  $\text{H}_2\text{O}_2$  at 25 °C in 0.01 M phosphate. The solid lines were calculated using Equation 5.6 and the parameters in Table 5.2.

Table 5.1 Parameters for TAMLs at 25°C. Values of  $k_1$  and  $k_{\text{II}}$  are for Orange II bleaching in 0.01 M phosphate at pH 7.

TAML	X/R <sub>1</sub> /R <sub>2</sub>	pK <sub>a</sub>	$k_1^* / \text{M}^{-1} \text{s}^{-1}$	$k_1 / \text{M}^{-1} \text{s}^{-1}$	$10^{-4} \times k_{\text{II}} / \text{M}^{-1} \text{s}^{-1}$
<b>1a</b>	H/Me/Me	$10.3 \pm 0.1$ <sup>6</sup>	$1.6 \pm 0.3$ <sup>10</sup>	$31.4 \pm 0.1$ <sup>2</sup>	$0.495 \pm 0.002$ <sup>2</sup>
<b>1b</b>	NO <sub>2</sub> /Me/Me	$10.00 \pm 0.05$ <sup>6</sup>		$152 \pm 5$ <sup>2</sup>	$2.7 \pm 0.2$ <sup>2</sup>
<b>2a</b>	H/H/H	$9.1 \pm 0.1$	$(1.8 \pm 0.1) \times 10^{-1}$	$330 \pm 20$	$9 \pm 2$
<b>2b</b>	NO <sub>2</sub> /H/H	$8.8 \pm 0.3$	$(1.1 \pm 0.1) \times 10^{-2}$	$630 \pm 50$	$10 \pm 2$
<b>2c</b>	H/H/Me	$9.4 \pm 0.1$		$389 \pm 4$	$4.2 \pm 0.1$
<b>2d</b>	NO <sub>2</sub> /H/Me	$8.8 \pm 0.1$		$690 \pm 20$	$8.9 \pm 0.2$
<b>3</b>	–/Me/Me	$11.38 \pm 0.01$ <sup>7</sup>	$(5.6 \pm 0.3) \times 10^{-4}$ <sup>a 10</sup>	$0.63 \pm 0.02$ <sup>2</sup>	$(1.19 \pm 0.03) \times 10^{-4}$ <sup>2</sup>
<b>4</b>	–/H/H	$10.18 \pm 0.04$	$(4.8 \pm 0.1) \times 10^{-5}$	$0.77 \pm 0.10$	$(1.8 \pm 0.1) \times 10^{-4}$

<sup>a</sup>  $k_1/K$ , see Equation 5.4

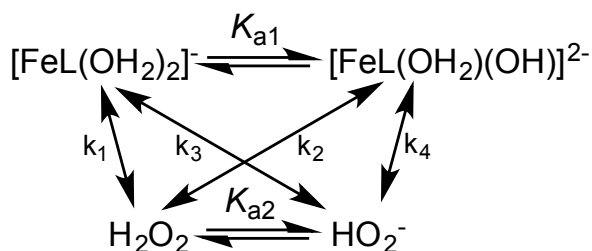


Figure 5.9 Mechanism of reaction of TAMLs with H<sub>2</sub>O<sub>2</sub> described by  $k_1$ .

$$k_1 = \frac{k_1[\text{H}^+]^2 + (k_2K_{a1} + k_3K_{a2})[\text{H}^+] + k_4K_{a1}K_{a2}}{[\text{H}^+]^2 + (K_{a1} + K_{a2})[\text{H}^+] + K_{a1}K_{a2}}$$

Equation 5.6

The curves in Figure 5.8 for **1b**, **2a**, and **2b** were fit to Equation 5.6. Catalyst  $\text{p}K_a$  measured above and literature  $\text{p}K_a$  of 11.2–11.6 for H<sub>2</sub>O<sub>2</sub><sup>16</sup> provided initial estimates for  $K_{a1}$  and  $K_{a2}$ , respectively. Pathways  $k_2$  and  $k_3$  are kinetically indistinguishable; the upper limit of  $k_2$  was determined by ignoring  $k_3$  and vice versa for  $k_3$ . Estimates for the rate constants  $k_1$ – $k_4$  for **1a**, **1b**, **2a**, and **2b** are given in Table 5.2. The relative magnitude of the rate constants is dependent on chemical factors involved in the interaction of each pair of species in solution, including differences in reduction potential and coulombic attraction. Deprotonated species  $[\text{FeL}(\text{OH}_2)(\text{OH})]^{2-}$  and  $\text{HO}_2^-$  are more electron rich and therefore react faster with protonated species H<sub>2</sub>O<sub>2</sub> and  $[\text{FeL}(\text{OH}_2)_2]^-$ , respectively, and less quickly with each other. Typically,  $k_2$  and  $k_3$  are larger than  $k_1$  and  $k_4$ , giving rise to the characteristic bell shaped curve (Figure 5.8).<sup>8</sup> Additionally, sulfonamide groups are highly electron withdrawing as evidenced by large positive Hammett constants of  $\sigma_m = 0.60$  and  $\sigma_p = 0.72$  for –SO<sub>2</sub>Me (**2a** and **2b**) compared to  $\sigma_m = 0.27$  and  $\sigma_p = 0.32$  for –CO<sub>2</sub>Me (**1a** and **1b**).<sup>17</sup> In NewTAMLs, this results in decreased reactivity of the

electron rich  $[\text{FeL}(\text{OH}_2)(\text{OH})]^{2-}$  species and therefore even larger  $k_3$  and smaller  $k_2$  values compared to OldTAMLs.

Table 5.2 Rate constants (in  $\text{M}^{-1} \text{s}^{-1}$ ) for the interaction of TAML with  $\text{H}_2\text{O}_2$  at pH 7 with 0.01 M phosphate at 25°C.

TAML	$10^{-2} \times k_1$	$10^{-4} \times k_2$	$10^{-4} \times k_3$	$10^{-3} \times k_4$	$\text{p}K_{\text{a}1}$	$\text{p}K_{\text{a}2}$
<b>1a</b> <sup>a</sup>	$1.3 \pm 1.0$	$1.2 \pm 5$	$40 \pm 20$	<sup>b</sup>	$10 \pm 1$	$11 \pm 2$
<b>1b</b>	$1.4 \pm 0.8$	$1.3 \pm 0.1$	$5.4 \pm 0.1$	$2.2 \pm 0.2$	$11 \pm 1$	$11 \pm 3$
<b>2a</b>	$1.4 \pm 1.5$	$0.26 \pm 0.02$	$130 \pm 10$	<sup>b</sup>	$9 \pm 4$	$11 \pm 5$
<b>2b</b>	$2.7 \pm 1.7$	$0.33 \pm 0.02$	$83 \pm 6$	<sup>b</sup>	$8 \pm 1$	$10 \pm 1$

<sup>a</sup>Data from ref 14 <sup>b</sup> Could not be reliably estimated.

The bell-shaped curves for NewTAMLs are shifted towards neutral pH due to decreased  $\text{p}K_{\text{a}1}$  values and broadened to span a wider pH range due to the increased separation between  $K_{\text{a}1}$  and  $K_{\text{a}2}$ . The resulting pH of maximum activity for **2a** and **2b**, at pH 9 and 10, respectively, are significantly lower than that of **1a** and **1b** at pH 11.<sup>14</sup>

#### 5.2.4 Comparison of Old- and NewTAMLs via Linear Free Energy Relationships

Linear free energy relationships relating various technical performance parameters of TAMLs such as  $\text{p}K_{\text{a}}$  and rate constants have proven useful in understanding TAML behavior.<sup>2</sup> The close adherence of NewTAMLs **2** and **4** to the previously described linear relationship between  $k_{\text{I}}$  and  $k_{\text{II}}$  (Figure 5.10) emphasizes the role of the metal center, unchanged between Old- and NewTAMLs, in the catalytic process in Figure 5.2.<sup>2</sup> As discussed above, catalyst activity also depends on  $\text{p}K_{\text{a}}$ . Figure 5.11 shows  $k_{\text{I}}$  and  $k_{\text{II}}$  for various catalysts at pH 7 as a function of  $\text{p}K_{\text{a}}$ . NewTAML activators follow the general trend of increasing activity with decreasing  $\text{p}K_{\text{a}}$  through the



expression  $\log k = \log k^0 + \alpha \times \text{p}K_{\text{a}}$ . Calculated values of  $k^0$  and  $\alpha$  for catalysts of only the **1–3** structural families (data from **4** were not included) of  $\log k^0 = 12 \pm 1$  and  $20 \pm 3$  and  $\alpha = -1.2 \pm 0.1$  and  $-1.6 \pm 0.3$  for  $k_{\text{I}}$  and  $k_{\text{II}}$ , respectively, agree with previously reported linearizations including all TAMLs (Figure 5.11).<sup>7</sup> Complex **4** deviates from the trend, evidenced by the low performance at pH 7 compared to **3** given the large difference in  $\text{p}K_{\text{a}}$  between the two catalysts. The low reactivity of **3** has been attributed to steric effects from the tetramethyl “head” in place of the phenylene group, but the electronic effects of the head group on stability have proven quite complex.<sup>10</sup> Theoretical modeling studies of the electronic environment of **4** during catalysis will be necessary to understand the low reactivity.

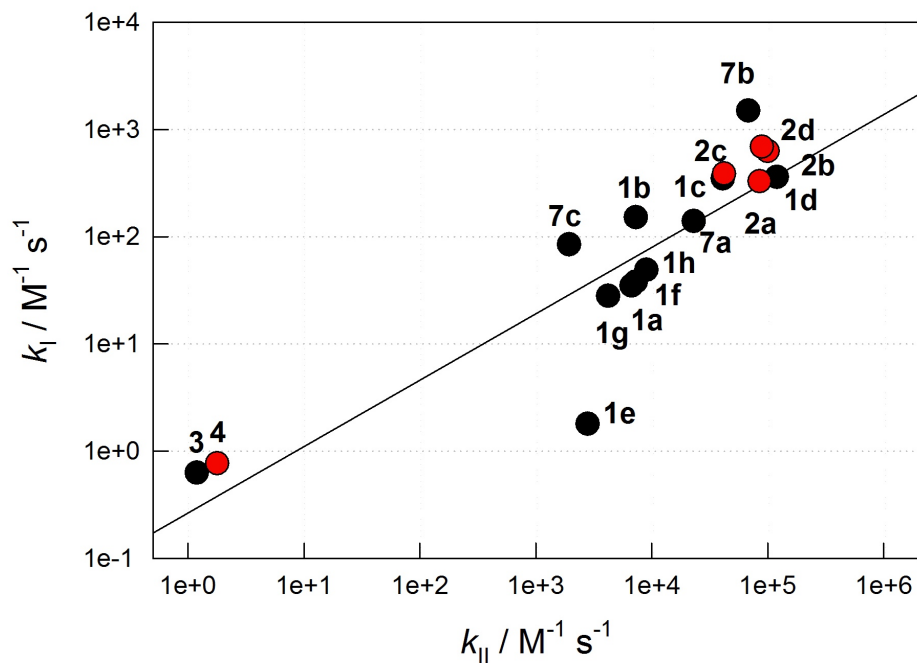


Figure 5.10 Linear free energy relationship between  $k_I$  and  $k_{II}$  for TAMs of the 1–4 structural families measured at pH 7 and 25 °C.

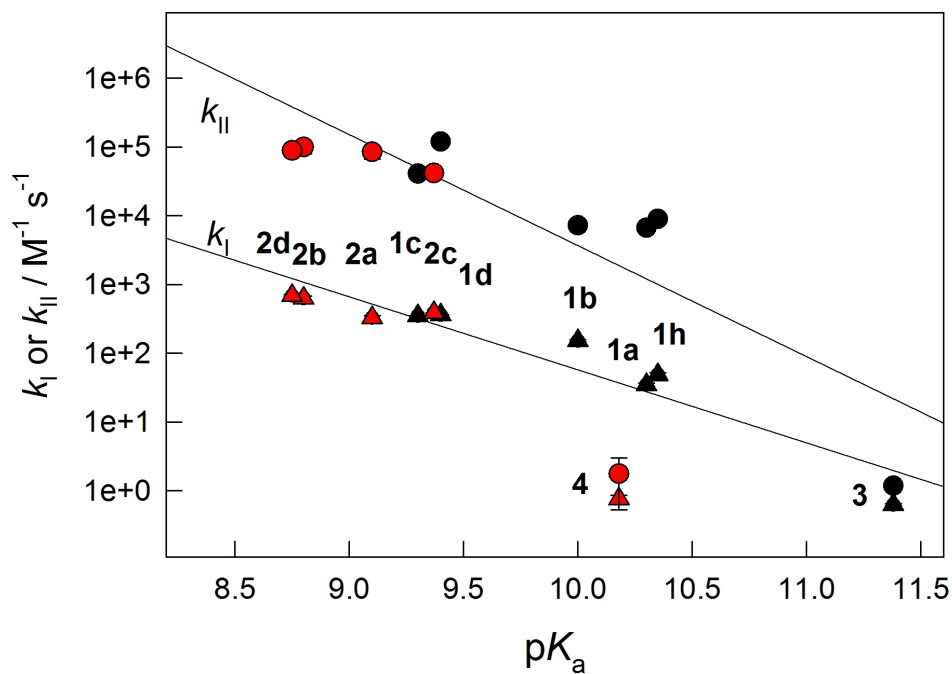


Figure 5.11 Linear free energy relationships between  $k_I$  or  $k_{II}$  and  $pK_a$  for TAMs of the 1–4 structural families measured at pH 7 and 25 °C. Lines do not include 4.

### 5.3 Conclusions

The NewTAML activators presented in this study follow the same mechanism of catalysis as previous TAML activators, but are significantly more reactive at neutral pH. For all NewTAMLs, electron-withdrawing sulfonamide groups in the ligand increase the Lewis acidity of the metal center resulting in lower  $pK_a$ 's of axial water deprotonation and high activity closer to pH 7. At neutral pH, **2b** and **2d** are the most active catalysts of the disulfonamide-tailed NewTAML family. The advances in catalysis presented here have important implication for treatment of micropollutants in municipal and industrial wastewater. Ease of preparation of disulfonyl dichloride derivatives compared to malonyl chloride derivatives and improved yield in cyclization of the ligand are estimated to decrease catalyst cost per kilogram by up to 50%. Furthermore, increased activity at neutral pH will reduce the amounts of both catalyst and peroxide required per treatment. The insight into the strengths of disulfonamide NewTAMLs provided by this investigation will help to shape future TAML catalyst development.

## 5.4 Experimental

### 5.4.1 Materials and Methods

Fe<sup>III</sup>-TAMLs **1a**, **1b**, and **3** were prepared according to published methods<sup>13,18</sup> or obtained from GreenOx Catalysts, Inc. Methods for the preparation of NewTAMLs **2** are giving in Chapter 4 and methods for the preparation of **4** are given below. Methane disulfonyl dichloride was purchased from TCI or prepared as described elsewhere.<sup>19</sup> Orange II was recrystallized from aqueous ethanol. H<sub>2</sub>O<sub>2</sub> (30% w/w) was purchased from Fischer and the concentration of dilutions was verified using  $\epsilon = 72.8 \text{ M}^{-1} \text{ cm}^{-1}$  at 230 nm via UV-Vis spectroscopy.<sup>20</sup> All other reagents and solvents (at least ACS reagent grade) were obtained from commercial sources and purified according to standard procedures when necessary.<sup>21</sup> Catalytic activity in bleaching of Orange II with H<sub>2</sub>O<sub>2</sub>, incomplete bleaching experiments, and measurement of pK<sub>a</sub> were determined as described in detail previously.<sup>2,6</sup>

### 5.4.2 Synthesis of **4**

The method for preparation of **4** is shown in Figure 5.12. *N,N'*-(2,3-dimethylbutane-2,3-diyl)bis(2-amino-2-methylpropanamide) (**A**) was prepared as previously described.<sup>2</sup> *Preparation of B*: A solution of **A** (0.21 g, 0.70 mmol) in dry CH<sub>2</sub>Cl<sub>2</sub> (20 mL) and triethylamine (0.6 mL) and a second solution of methane disulfonyl dichloride (0.09 mL, 0.70 mmol) in dry CH<sub>2</sub>Cl<sub>2</sub> (20 mL) were added dropwise with a syringe pump to a flask containing CH<sub>2</sub>Cl<sub>2</sub> (125 mL) at 0 °C. The solution was allowed to warm to room temperature and stir overnight. The solution was concentrated under reduced pressure until 20 mL remained, extracted with 2 × 20 mL 0.01 M HCl and 1 × 20 mL brine, and dried with MgSO<sub>4</sub>. Remaining solvent was removed under reduced

pressure to yield **B** (108 mg, 35%). ESI-MS: 425 m/z (100%),  $[M-H]^+$  *Preparation of 4*: A solution of *n*BuLi (0.90 mL, 1.41 mmol of 1.6 M in hexane, 4.4 eq) was added at -78 °C to a solution of **B** (0.135 g, 0.32 mmol) in 20 mL dry THF under Ar. The mixture was allowed to warm to 0 °C before addition of solid anhydrous FeCl<sub>3</sub> (0.057 g, 0.35 mmol). The mixture was stirred at room temperature for one hour and the solvent removed under reduced pressure. The product was purified by flash chromatography on basic alumina with 9:1 (v/v) CH<sub>2</sub>Cl<sub>2</sub>/methanol as the eluent. The lithium cation was replaced by tetramethylammonium using cationic exchange column (Amberlite IR-120) presaturated with  $[NMe_4]^+$ . The orange product was eluted in methanol. Compound **4** is hygroscopic and was produced in 9% yield (13 mg). UV-Vis in H<sub>2</sub>O:  $\lambda_{max} = 400$  nm ( $\epsilon = 2420$  M<sup>-1</sup> cm<sup>-1</sup>); ESI-MS (neg mode): m/z calcd: 478.06; found: 478.2 (M<sup>-</sup>, 100%).

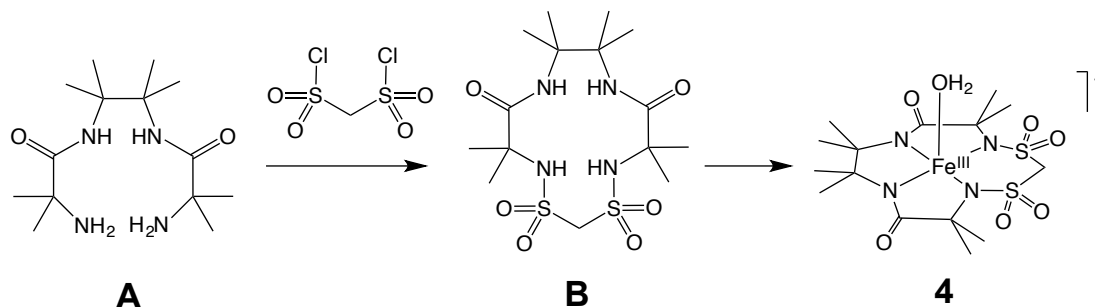


Figure 5.12 Preparation of **4**

#### 5.4.3 Acid Induced Demetalation

Stock solutions of catalysts and perchloric acid were prepared using HPLC grade water. Appropriate volumes of perchloric acid were added to quartz cuvettes, and the reactions were initiated by the addition of an aliquot of catalyst. Reactions were conducted at 25°C. Reaction progress was followed by measuring the decrease in absorbance at  $\lambda_{max}$ . The pseudo-first-order rate constant  $k_{obs}$  was calculated from

exponential decay plots of absorbance versus time by fitting the data to the equation  $A = A_{\infty} - (A_{\infty} - A_0) e^{(-k_{\text{obs}}t)}$  when the demetalation was at least 90%. Each reported value of  $k_{\text{obs}}$  is the mean of three determinations.

#### 5.4.4 EPR Studies of **2a**

X-band EPR spectra were recorded on a Bruker spectrometer equipped with an Oxford ESR-910 liquid helium cryostat operating at a field modulation of 100 kHz and microwave radiation power of 0.2 mW. The solid Fe(III) complex was taken in a quartz tube with 0.01 M phosphate and 15% glycerol and the spectrum was recorded at 13 K. The signal was quantified relative to a CuEDTA spin standard. The microwave frequency was calibrated with a frequency counter and the magnetic field with an NMR gaussmeter. The EPR simulation software (Spin Count) was written by one of the authors.<sup>22</sup>

## 5.5 References

1. Popescu, D. L.; Chanda, A.; Stadler, M. J.; Mondai, S.; Tehranchi, J.; Ryabov, A. D.; Collins, T. J. *J. Am. Chem. Soc.* **2008**, *130* (37), 12260–12261.
2. DeNardo, M. A.; Mills, M. R.; Ryabov, A. D.; Collins, T. J. *J. Am. Chem. Soc.* **2016**, *138* (9), 2933–2936.
3. DeNardo, M. A.; Tang, L. L.; Ryabov, A. D.; Collins, T. J. **2017**, in preparation.
4. Ghosh, A.; Ryabov, A. D.; Mayer, S. M.; Horner, D. C.; Prasuhn, D. E.; Sen Gupta, S.; Vuocolo, L.; Culver, C.; Hendrich, M. P.; Rickard, C. E. F.; Norman, R. E.; Horwitz, C. P.; Collins, T. J. *J. Am. Chem. Soc.* **2003**, *125* (41), 12378–12379.
5. Panda, C.; Ghosh, M.; Panda, T.; Banerjee, R.; Sen Gupta, S. *Chem. Commun.* **2011**, *47*, 8016–8018.
6. Warner, G. R.; Mills, M. R.; Enslin, C.; Pattanayak, S.; Panda, C.; Panda, T. K.; Gupta, S. Sen; Ryabov, A. D.; Collins, T. J. *Chem. - A Eur. J.* **2015**, *21* (16), 6226–6233.
7. Mills, M. R.; Weitz, A. C.; Zhang, D. Z.; Hendrich, M. P.; Ryabov, A. D.; Collins, T. J. *Inorg. Chem.* **2016**, acs.inorgchem.6b01988.
8. Ryabov, A.; Collins, T. *Adv. Inorg. Chem.* **2009**, *61*, 471–521.
9. Collins, T. *Science*. **2001**, *291*, 48–49.
10. Mills, M. R.; Shen, L. Q.; Zhang, D. Z.; Ryabov, A. D.; Collins, T. J. **2017**, in preparation.
11. Mills, M. R.; Weitz, A. C.; Hendrich, M. P.; Ryabov, A. D.; Collins, T. J. *J. Am. Chem. Soc.* **2016**, *138* (42), 13866–13869.
12. Chahbane, N.; Popescu, D.-L.; Mitchell, D. A.; Chanda, A.; Lenoir, D.; Ryabov, A. D.; Schramm, K.-W.; Collins, T. J. *Green Chem.* **2007**, *9* (1), 49–57.
13. Ellis, W. C.; Tran, C. T.; Denardo, M. A.; Fischer, A.; Ryabov, A. D.; Collins, T. J. *J. Am. Chem. Soc.* **2009**, *131* (50), 18052–18053.
14. Ghosh, A.; Mitchell, D. A.; Chanda, A.; Ryabov, A. D.; Popescu, D. L.; Upham, E. C.; Collins, G. J.; Collins, T. J. *J. Am. Chem. Soc.* **2008**, *130* (45), 15116–15126.
15. Popescu, D.-L.; Vrabel, M.; Brausam, A.; Madsen, P.; Lente, G.; Fabian, I.; Ryabov, A. D.; van Eldik, R.; Collins, T. J. *Inorg. Chem.* **2010**, *49* (24), 11439–11448.
16. Jones, C. W. *Applications of Hydrogen Peroxide and Derivatives*; Royal Society of Chemistry: Cambridge, 1999.
17. Hansch, C.; Leo, A.; Taft, R. W. *Chem. Rev.* **1991**, *91* (2), 165–195.
18. Collins Group Patents  
[http://igs.chem.cmu.edu/index.php?option=com\\_content&view=article&id=347&Itemid=505](http://igs.chem.cmu.edu/index.php?option=com_content&view=article&id=347&Itemid=505).
19. Fild, V. M.; Rieck, H.-P. *Chemiker-Zeitung* **1976**, *100* (9), 391–392.
20. George, P. *Biochem. J.* **1953**, *54*, 267–276.
21. Chai, C.; Armarego, W. L. F. *Purification of Laboratory Chemicals*, Fifth Ed.; Butterworth-Heinemann, 2003.
22. Petasis, D. T.; Hendrich, M. P. *Methods Enzym.* **2015**, *563*, 171–208.

## **CHAPTER 6**

### **Reactivity and Stability of a Second Generation Diphenyl**

#### **NewTAML**



## 6.1 Introduction

Iterative design<sup>1,2</sup> has consistently improved the reactivity, stability, and lifetimes of TAML activators to yield successful mimics of peroxidase enzymes for ultra-dilute aqueous degradation of micropollutants and deactivation of bacterial spores.<sup>3–10</sup> A new family of TAMLs called “NewTAMLs” are described in Chapters 4 and 5 (Figure 6.1). First generation sulfonamide-containing NewTAML activators **2** are superior in catalytic performance to OldTAML activators **1** and do not contain undesirable halogen substituents.<sup>11</sup> The introduction of electron-withdrawing sulfonamide groups into the tail has resulted in NewTAML activators **2** that show superior reactivity against the model substrate Orange II and more oxidation resistant pollutants at neutral pH. NewTAMLs **2** are also more resistant to specific acid demetalation compared to structurally analogous OldTAML activators **1**.

Previously, reactivity and stability of OldTAML activators of family **1** have been augmented through rearrangement of the ligand structure to include two phenyl groups bridged by an oxamide motif (OldTAMLs **5**, Figure 6.1).<sup>12,13</sup> The use of  $sp^2$  carbons  $\beta$  to the head amide nitrogens in place of  $\alpha$   $sp^3$  carbons increases the electron withdrawing properties of the ligand.<sup>12</sup> Strongly electron withdrawing ligand substituents increase the Lewis acidity at the  $Fe^{III}$  center, resulting in more active catalysts at neutral pH.<sup>14</sup> However, complex **5a** is highly unstable in aqueous solution, with a half-life of minutes at pH 7. The lifetime was increased in **5b** via inclusion of two electron-withdrawing  $NO_2$  groups on the phenyl rings.<sup>15</sup> As could be expected, complex **5b** is highly reactive, significantly outperforming fluorinated **1c** in the breakdown of the model substrate Orange II, without the use of halogen atoms.

We hypothesized that the lifetime and reactivity increases afforded by the NO<sub>2</sub> groups could be mimicked with sulfonamide groups in an easy-to-prepare NewTAML analog of **5a**. We hoped the electron-withdrawing properties of sulfonamides would be sufficient to stabilize the complex and increase reactivity to rival the best NewTAMLs of family **2**.

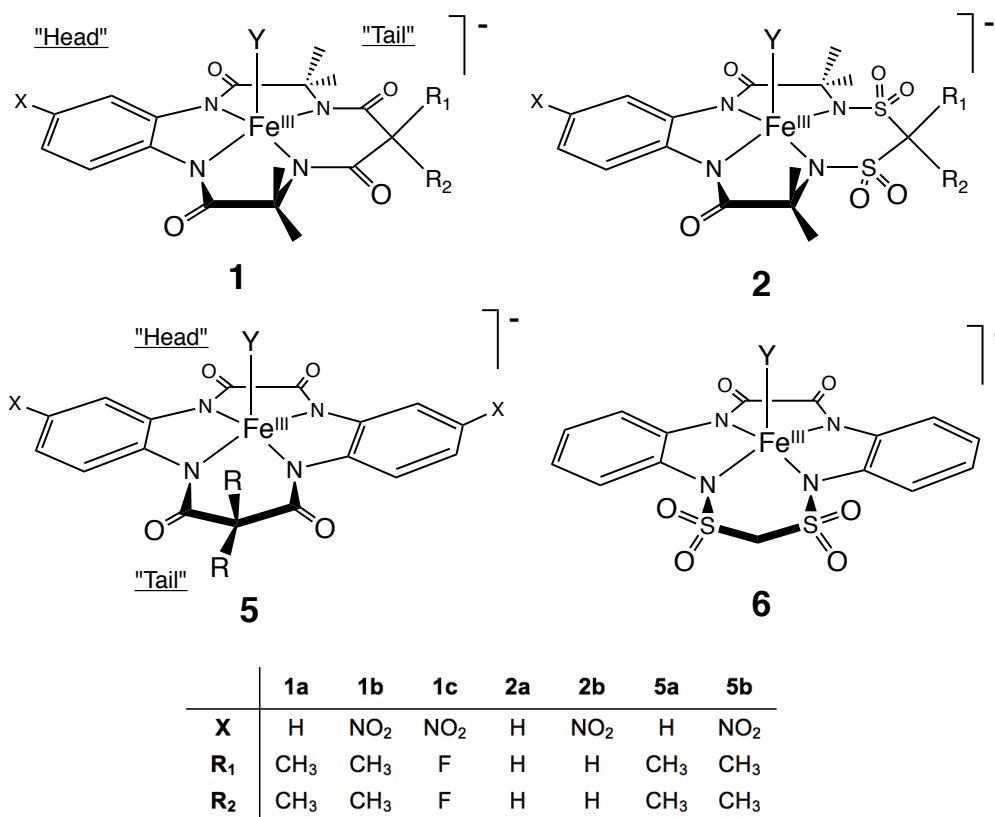


Figure 6.1 Old- and NewTAML activators discussed in this chapter; Y is typically water.

## 6.2 Results and Discussion

### 6.2.1 Preparation and Properties of **6**

NewTAML **6** was prepared following the method used to produce **5a** with the substitution of methanedisulfonyl dichloride for dimethylmalonyl dichloride in the preparation of intermediate **B** (Figure 6.2).<sup>16</sup> Complex **6** was prepared as a tetramethylammonium salt with an axial water molecule in the solid state and characterized by ESI-MS and elemental analysis.

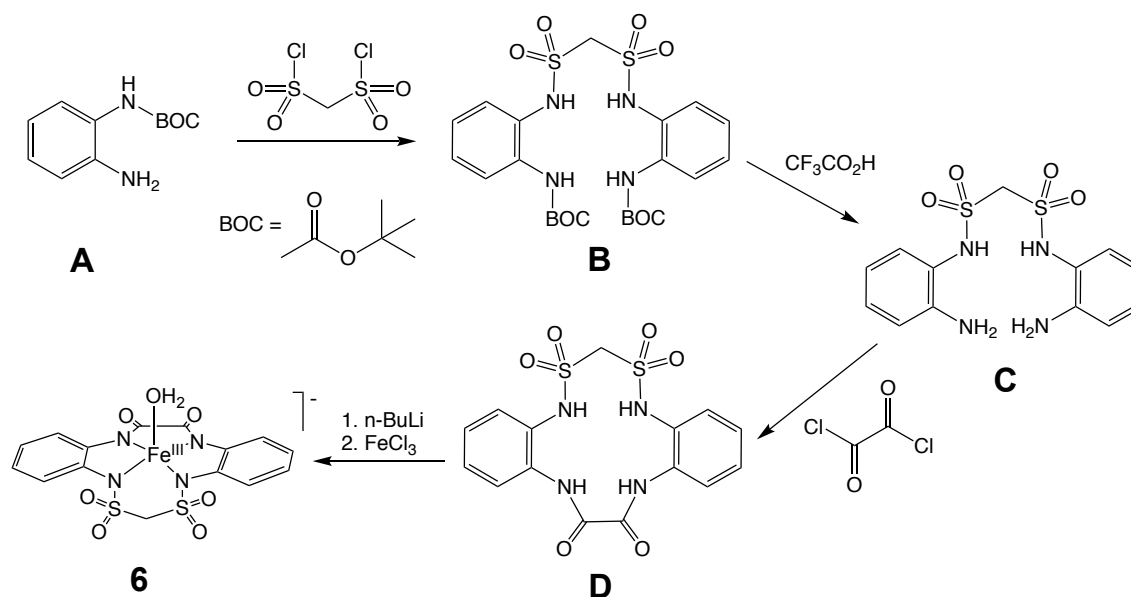
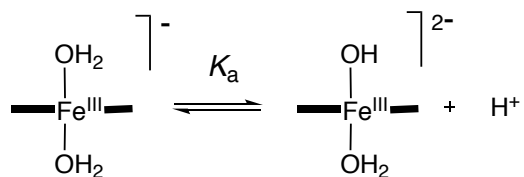


Figure 6.2 Method of synthesis of **6**.

In aqueous solution, TAMLs are typically 5- or 6-coordinate with one or two axial water molecules.<sup>15,17</sup> The unchanging UV/Vis spectra of **6** in the presence of 0.005–0.25 M KCl at pH 7 supports speciation in aqueous solution with one or two axial water ligands (Equation 2.1). There is no evidence of aggregation in buffered or unbuffered aqueous solution, with Beer's law holding across  $(0.02\text{--}2.3) \times 10^{-3}$  M for **6** ( $\epsilon_{330} = 8340$

cm<sup>-1</sup> M<sup>-1</sup>). Notably, **6** is much more stable in aqueous buffered solution than **5a**, suggesting that the sulfonamides block degradation occurring at the tail amides. Overall, the sulfonamides appear to provide the same stabilizing effect as the para-substituted NO<sub>2</sub> groups in **5b**.

The p*K*<sub>a</sub> of deprotonation of the first axial water molecule (Equation 6.1) is a key parameter for predicting the relative reactivity of any given TAML activator.<sup>18</sup> Catalysts with lower values of p*K*<sub>a</sub> (closest to neutral) have superior reactivity at neutral pH, which is desirable for water treatment applications. TAMLs of family **5** have p*K*<sub>a</sub> values closest to neutral pH of all OldTAML activators, suggesting promising reactivity for a NewTAML analog.



Equation 6.1

The p*K*<sub>a</sub> of **6** was determined following the previously described method (see Chapters 2 and 5) of monitoring the absorbance changes due to the deprotonation of the axial ligand. Similar to other TAMLs, the spectrum of **6** is strongly affected by pH (Figure 6.3). At λ<sub>max</sub> of 330 nm, increasing absorbance was linearized following Equation 6.2, where *A*<sub>H</sub>, *A*<sub>OH</sub>, and *A* are absorbances at the most acidic, most basic, and intermediate pHs, respectively. This is shown in Figure 6.3b as a straight line with a slope of one and a y-intercept equal to -p*K*<sub>a</sub> according to Equation 6.2. Values of p*K*<sub>a</sub> for Old- and NewTAMLs are given in Table 6.1.

$$\log \frac{A_H - A}{A - A_{OH}} = \text{pH} - \text{p}K_a$$

Equation 6.2

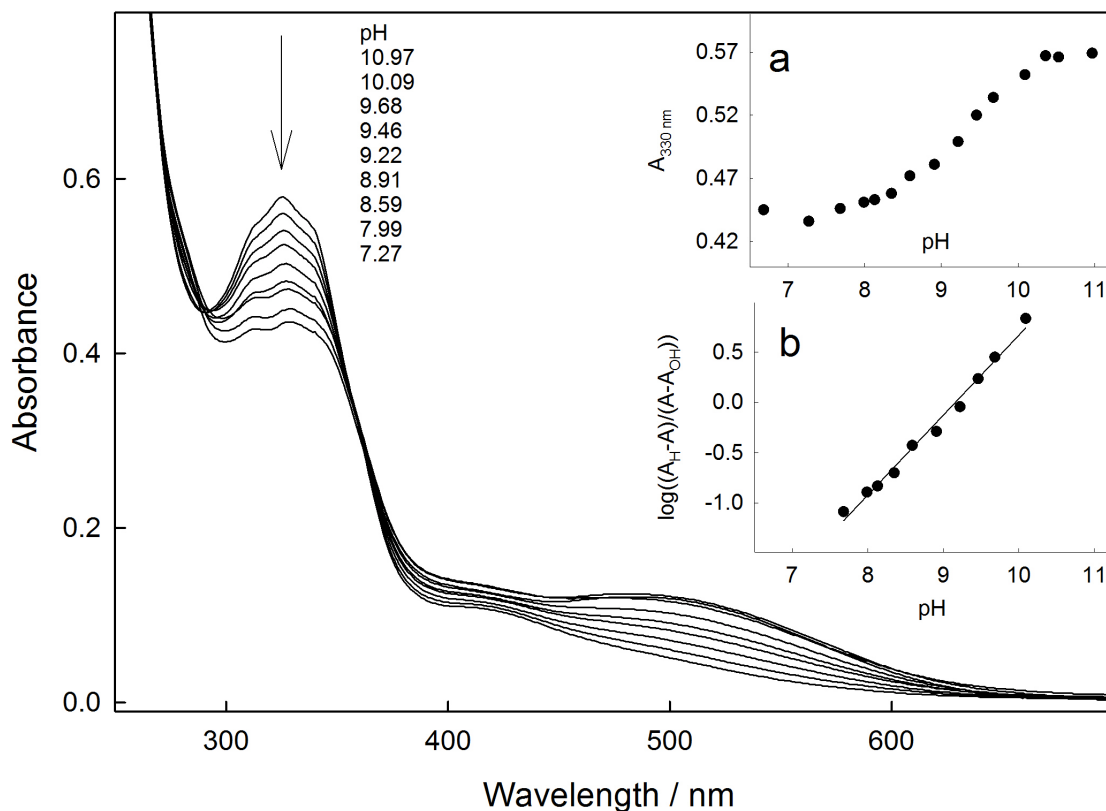


Figure 6.3 pH titration of **6** at 25°C with 0.01 M phosphate. Inset (a) shows absorbance at 330 nm versus pH. Inset (b) is a linearization of the data in inset (a) in terms of Equation 6.2.

Two  $\text{p}K_a$  values for deprotonation of each axial water molecule have been measured for the more stable **5b**,<sup>13</sup> but only one deprotonation event was evident for **6** in the range of 6–13. The  $\text{p}K_a$  of **5a** could not be measured due to its aqueous instability. However,  $\text{NO}_2$  groups typically decrease  $\text{p}K_a$  by 0.3 pH units in otherwise identical TAML activators.<sup>19</sup> Complex **5a** contains two fewer  $\text{NO}_2$  groups than **5b**, which has a  $\text{p}K_a$  of  $8.4 \pm 0.1$ .<sup>13</sup> Extrapolating the  $\text{NO}_2$  group effect to **5a**, assuming that  $\text{NO}_2$  group

effects are additive, predicts a  $pK_a$  of approximately 9. The  $pK_a$  of **6** at  $9.1 \pm 0.1$  is comparable to **5a**. In contrast, the difference in  $pK_a$  between the **1a/2a** and **1b/2b** structural analogs pairs is 1.2 units (Table 6.1). The absence of a decrease in  $pK_a$  of similar magnitude between **5** and **6** suggests that common structural features between **5** and **6** such as the larger region of conjugation created by the oxamide more heavily influence the  $pK_a$  of this catalyst family.

### 6.2.2 Catalytic Activity in the Bleaching of Orange II with $H_2O_2$

The reactivity of **6** in the  $H_2O_2$ -catalyzed bleaching of Orange II was studied in detail to enable comparison with other TAML activators.<sup>19–21</sup> Figure 6.4 shows the 3D dependence of the rate of Orange II bleaching on  $[H_2O_2]$  and  $[Orange\ II]$  for **6** at pH 7 and 25 °C. For all TAMLs, this catalytic processes follows the general mechanism of catalysis in Figure 6.5 and is described by Equation 6.3 under steady state conditions.

Values of the rate constants  $k_I$  and  $k_{II}$  for **6** at pH 7 were determined by fitting the data in Figure 6.4 to Equation 6.3, assuming  $k_{-I}$  is negligible.<sup>22</sup> For complex **6**,  $k_I$  is  $450 \pm 40\ M^{-1}\ s^{-1}$  and  $k_{II}$  is  $1300 \pm 100\ M^{-1}\ s^{-1}$ . The difference between  $k_I$  and  $k_{II}$  of only threefold is unusual and is reflected in the shape of Figure 6.4, in which the rate is nearly independent of  $[H_2O_2]$  and first order in  $[Orange\ II]$ . For **2**, the  $[H_2O_2]$  and  $[Orange\ II]$  relationships are reversed (Figure 4.3), and the differences between  $k_I$  and  $k_{II}$  for **2** are approximately 200-fold (Table 6.1). Values of  $k_I$  for **2** and **6** are similar, while  $k_{II}$  for **6** is significantly depressed. However, compared to **5a**, the structural analog of **6**, values of  $k_I$  and  $k_{II}$  for **6** are both increased twofold.

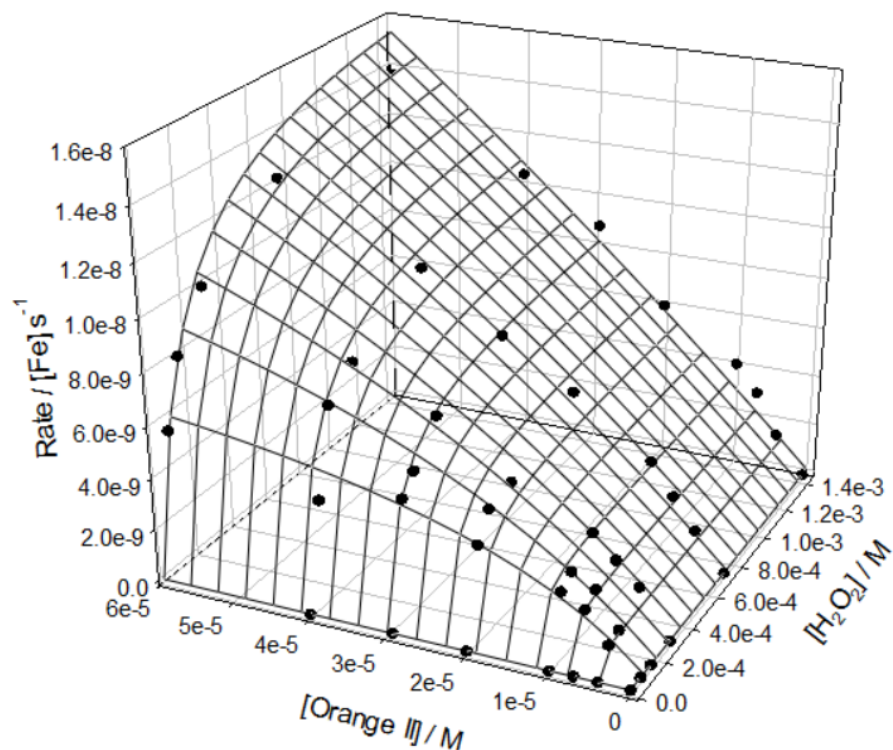


Figure 6.4 Initial rates of **6**-catalyzed bleaching of Orange II with  $\text{H}_2\text{O}_2$  as a function of  $[\text{H}_2\text{O}_2]$  and  $[\text{Orange II}]$  with **6** ( $2.2 \times 10^{-7} \text{ M}$ ) at pH 7 and  $25^\circ \text{C}$  with 0.01 M phosphate. The mesh was calculated by fitting the data to Equation 6.3.

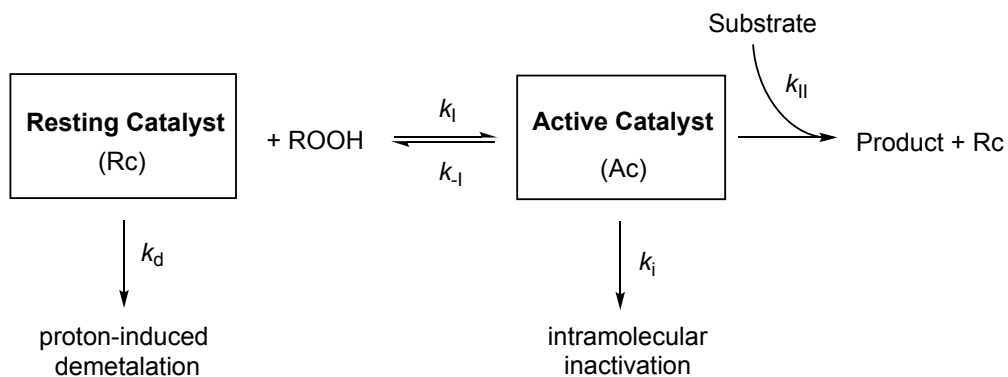


Figure 6.5 Mechanism of catalysis of TAMLs.

$$-\frac{d[\text{S}]}{dt} = \frac{k_i k_{ii} [\text{ROOH}] [\text{S}] [\text{Fe}^{\text{III}}]}{k_{-i} + k_i [\text{ROOH}] + k_{ii} [\text{S}]}$$

Equation 6.3

Interestingly, **6** is significantly less reactive than **5b**.<sup>23</sup> Nitro substitution in **5b** increases  $k_1$  and  $k_{II}$  substantially compared to all other TAMLs, with the value of  $k_{II}$  “recovering” in comparison to  $k_1$  to be ca. 200 times larger. The similarity of the **6** rate constants to those of **5a** and dissimilarity compared to those of **5b** demonstrate that although sulfonamides increase stability of the resting state catalyst complex, sulfonamide substitution is not able to replicate the beneficial effects of NO<sub>2</sub> group substitution on reactivity for the diphenyl TAML family.

The oxamide group (–NCOCON–) is a possible source of the discrepancy in  $k_{II}$  between NewTAMLs **2** and **6**.<sup>14</sup> Unlike the  $sp^3$  carbon-containing “arms” of **2**, the oxamide creates an extended region of conjugation connecting the two phenyl groups that may destabilize the active catalyst intermediate, resulting in low  $k_{II}$  values without impacting  $k_1$ . The “recovered” value of  $k_{II}$  for **5b** suggests that the NO<sub>2</sub> groups effectively quench this destabilization.

Table 6.1 Parameters for TAMLs at 25°C. Values of  $k_1$  and  $k_{II}$  are for Orange II bleaching with H<sub>2</sub>O<sub>2</sub> in 0.01 M phosphate at pH 7.

TAML	X/R <sub>1</sub> /R <sub>2</sub>	pK <sub>a</sub>	$k_1 / \text{M}^{-1} \text{s}^{-1}$	$10^{-4} \times k_{II} / \text{M}^{-1} \text{s}^{-1}$	Ref
<b>1a</b>	H/Me/Me	10.3 ± 0.1	31.4 ± 0.1	0.495 ± 0.002	19,23
<b>1b</b>	NO <sub>2</sub> /Me/Me	10.00 ± 0.05	152 ± 5	2.7 ± 0.2	19,23
<b>1c</b>	NO <sub>2</sub> /F/F		350 ± 2	4.1 ± 0.1	23
<b>2a</b>	H/H/H	9.1 ± 0.1	330 ± 20	8.5 ± 1.8	Ch. 4, 5
<b>2b</b>	NO <sub>2</sub> /H/H	8.8 ± 0.3	630 ± 50	10 ± 2	Ch. 4, 5
<b>5a</b>	H/Me/Me	9 <sup>a</sup>	250 ± 60	0.084 ± 0.003	this work
<b>5b</b>	NO <sub>2</sub> /Me/Me	8.4 ± 0.1	1900 ± 100	52 ± 7	13,23
<b>6</b>	H/H/H	9.1 ± 0.1	450 ± 40	0.13 ± 0.01	this work

<sup>a</sup> estimated value; see text for details.



Values of  $k_1$  for Orange II bleaching were also determined for **6** in the range of pH 6.0–11.0 to identify the pH of maximum activity. The expected bell-shaped curve typical of TAML activators (Figure 2.6, Figure 4.5, Figure 5.8) and consistent with the mechanism activation with  $\text{H}_2\text{O}_2$  in Figure 6.6 was not observed for **6**. Figure 6.7 shows a precipitous decline in reactivity between pH 9 and 10 due to the inactivation pathway unique to NewTAMLs introduced in Chapter 4. The effect of the inactivation pathway is much more pronounced for **6** than for **2** (Figure 5.8). As a result, the data in Figure 6.7 could not be fit satisfactorily to Equation 6.4 corresponding to Figure 6.6. Instead, only data up to pH 9 were included in the fit to estimate values for rate constants  $k_1$ ,  $k_2$ , and  $k_3$  before inactivation significantly compromises catalysts activity;  $k_4$  was set to 0. As the  $k_2$  and  $k_3$  pathways are kinetically indistinguishable, values for each rate constant were calculated by assuming the other pathway negligible. The values of  $300 \pm 200$ ,  $(1.00 \pm 0.05) \times 10^4$ , and  $(2.5 \pm 0.1) \times 10^6 \text{ M}^{-1} \text{ s}^{-1}$  were calculated for  $k_1$ – $k_3$ , respectively, with  $\text{p}K_{\text{a}1}$  and  $\text{p}K_{\text{a}2}$  values of  $8.6 \pm 0.2$  and  $11.0 \pm 0.1$ , respectively. These values are comparable to those of **2a** and **2b** (Table 5.2).

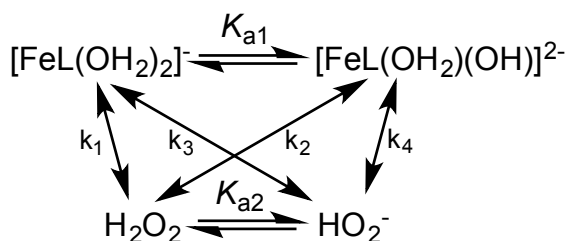


Figure 6.6 Mechanism of reaction of TAML with  $\text{H}_2\text{O}_2$  described by  $k_1$ .

$$k_1 = \frac{k_1[\text{H}^+]^2 + (k_2K_{\text{a}1} + k_3K_{\text{a}2})[\text{H}^+] + k_4K_{\text{a}1}K_{\text{a}2}}{[\text{H}^+]^2 + (K_{\text{a}1} + K_{\text{a}2})[\text{H}^+] + K_{\text{a}1}K_{\text{a}2}}$$

Equation 6.4

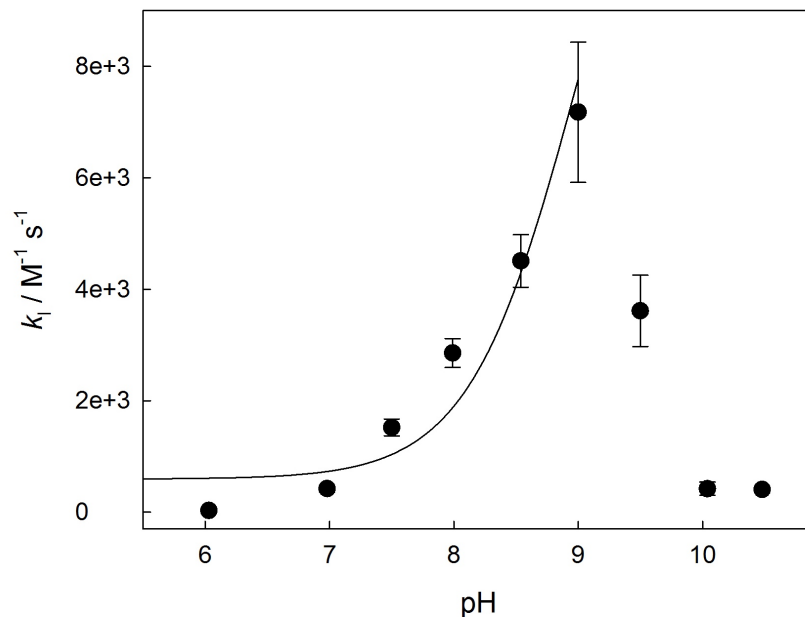


Figure 6.7 Rate constant  $k_1$  measured for **6** in the catalyzed bleaching of Orange II by  $\text{H}_2\text{O}_2$  at 25 °C in 0.01 M phosphate. Only pH 6–9 were included for the fit to Equation 6.4 with  $k_4 = 0$ .

### 6.2.3 Hydrolytic Stability of **6** in Acidic Solution

NewTAMLs **2** display superior stability under acidic conditions (Chapter 5). To assess the hydrolytic stability of **6**, the pseudo-first-order rate constants  $k_{\text{obs}}$  were measured in the presence of 0.0005–0.10 M  $\text{HClO}_4$  (Figure 6.8). The acceleration of  $k_{\text{obs}}$  with increasing  $[\text{H}^+]$  for **6** is typical of specific acid demetalation of TAML activators following Equation 6.5.

$$k_{\text{obs}} = k_1 * [\text{H}^+] + k_3 * [\text{H}^+]^3 \quad \text{Equation 6.5}$$

The first order term describes  $\text{Fe}^{\text{III}}$  ejection from the ligand in mildly acidic conditions due to a single protonation event. The third order term describes ejection that dominates under highly acidic conditions requiring three protons, including a peripheral

pre-equilibrium protonation of the macrocycle.<sup>24</sup> NewTAMLs **2** display only the first order term as the sulfonamide tails blocks the third order pathways in the presence of 0.002–0.25 M HClO<sub>4</sub>, resulting in a linear dependence. For **6**, the presence of a curved plot in Figure 6.8 indicates that the third order pathway is accessible, most likely through the oxamide.

Values of  $k_1^*$  and  $k_3^*$  for **6** of  $(2.8 \pm 0.1) \times 10^{-3} \text{ M}^{-1} \text{ s}^{-1}$  and  $0.16 \pm 0.01 \text{ M}^{-3} \text{ s}^{-1}$ , respectively, were determined by fitting the data in Figure 6.8 to Equation 6.5. Complex **6** is 100-fold more stable in  $k_1^*$  than **2a** ( $k_1^* = (1.8 \pm 0.1) \times 10^{-1} \text{ M}^{-1} \text{ s}^{-1}$ ) and 10-fold more stable than **2b** ( $k_1^* = (1.1 \pm 0.1) \times 10^{-2} \text{ M}^{-1} \text{ s}^{-1}$ ). In Old TAMLs, the values of  $k_1^*$  decrease by 5 orders of magnitude and  $k_3^*$  by 11 orders upon fluorine substitution. Compared to fluorinated OldTAMLs **1**, **6** is only 1 order of magnitude less stable in  $k_1^*$  and 3 orders less stable in  $k_3^*$ .

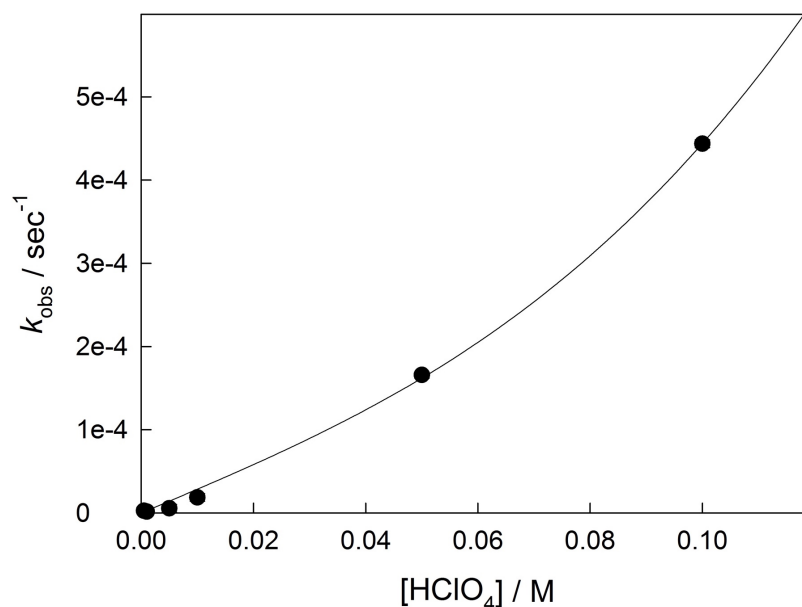


Figure 6.8 Dependence of  $k_{\text{obs}}$  on [HClO<sub>4</sub>] for acid induced demetalation of **6** at 25 °C.

### 6.3 Conclusions

Complex **6** is the first member of a promising new generation of NewTAML activators. It is as reactive towards Orange II as the first generation of NewTAMLs **2** and displays greater stability against specific acid demetalation. Although **6** does not contain any pendant NO<sub>2</sub> groups, the sulfonamides provide stability against demetalation in aqueous solution. However, the reactivity of **6** is significantly lower than NO<sub>2</sub>-containing **5b**. Future members of the **6** family of NewTAMLs should incorporate NO<sub>2</sub> groups into the ligand to try to replicate or surpass the useful properties and high reactivity of **5b**.

## 6.4 Experimental

### 6.4.1 Materials and Methods.

Fe<sup>III</sup>-TAMLs **1** and **5** were prepared according to published methods<sup>12,25</sup> or obtained from GreenOx Catalysts, Inc. NewTAMLs **2** were prepared according to Chapter 4. Methods for the preparation of **6** are given below. Methane disulfonyl dichloride was purchased from TCI or prepared as described elsewhere.<sup>26</sup> Orange II was recrystallized from aqueous ethanol. H<sub>2</sub>O<sub>2</sub> (30% w/w) was purchased from Fischer and the concentration of dilutions was verified using  $\epsilon = 72.8 \text{ M}^{-1} \text{ cm}^{-1}$  at 230 nm via UV-Vis spectroscopy.<sup>27</sup> All other reagents and solvents (at least ACS reagent grade) were obtained from commercial sources and purified according to standard procedures when necessary.<sup>28</sup> Catalytic activity in bleaching of Orange II with H<sub>2</sub>O<sub>2</sub> and measurement of  $pK_a$  were determined as described in detail previously.<sup>23,19</sup>

### 6.4.2 Synthesis of **6**.

*Tert*-butyl (2-aminophenyl)carbamate **A** (Figure 6.2) was prepared according to the literature.<sup>16</sup>

**Preparation of B:** A solution of methanedisulfonyl dichloride (0.28 mL, 2.5 mmol) in dry THF (30 mL) was added dropwise under Ar at 0°C to a solution of **A** (1.04 g, 5 mmol), triethylamine (0.7 mL, 5 mmol), and dry THF (30 mL). The mixture was allowed to warm to room temperature and stir overnight. The precipitate was filtered off and the solvent removed under reduced pressure. The resulting oil was sonicated in diethyl ether to yield **B**, a flaky solid that was used without further purification. <sup>1</sup>H NMR (300 MHz,

DMSO- $d_6$ ): 9.68 (s, 2H, NH), 8.29 (s, 2H, NH), 7.69 (dd, 2H, Ar), 7.27 (m, 4H, Ar), 7.05 (m, 2H, Ar), 4.86 (s, 2H, CH<sub>2</sub>), 1.46 (s, 18H, t-Bu). ESI-MS: 555.1 m/z (100%), [M-H<sup>+</sup>]<sup>-</sup>

**Preparation of C:** A mixture of trifluoroacetic acid (10 mL) in dry CH<sub>2</sub>Cl<sub>2</sub> (10 mL) was added dropwise under Ar at 0°C to a solution of **B** (1.77 g, 3.18 mmol) in CH<sub>2</sub>Cl<sub>2</sub> (20 mL). The solution was allowed to warm to room temperature. After stirring for two hours, the solvent was removed under reduced pressure. The resulting light brown oil was diluted with 75 mL of water and the pH was adjusted to 10 with 1 M sodium hydroxide. The solution was extracted with CH<sub>2</sub>Cl<sub>2</sub> (3 x 20 mL) and the organic layer was dried with magnesium sulfate, filtered, and evaporated to yield white solid **C**. <sup>1</sup>H NMR (300 MHz, DMSO- $d_6$ ): 7.00 (m, 4H, Ar), 6.75 (m, 4H, Ar), 6.55 (m, 2H, NH), 4.70 (s, 2H, CH<sub>2</sub>). ESI-MS: 355.1 m/z (100%), [M-H<sup>+</sup>]<sup>-</sup>.

**Preparation of D:** A solution of **C** (300 mg) and dry pyridine (0.27 mL) in dry THF (40 mL) and a second solution of oxalyl chloride (2 M in CH<sub>2</sub>Cl<sub>2</sub>, 0.42 mL) in dry THF (40 mL) were added dropwise with a syringe pump to a flask containing THF (250 mL) at 0 °C. The solution was allowed to warm to room temperature and stirred overnight. The solvent was removed and the residue purified by column chromatography (silica gel, eluent 2:1 ethyl acetate/heptane) to give **D** in 65% yield. <sup>1</sup>H NMR (300 MHz, DMSO- $d_6$ )  $\delta$  9.91 (s, 2H, NH), 9.76 (s, 2H, NH), 8.00 – 7.88 (m, 2H, Ar), 7.43 (ddt, 2H, Ar), 7.30 (dd, 4H, Ar), 5.19 (s, 2H, CH<sub>2</sub>). ESI-MS (neg mode): m/z 409 (M-H<sup>+</sup>, 100%).

**Preparation of 6:** A solution of *n*BuLi (0.36 mL, 0.567 mmol of 1.6 M in hexane, 4.1 eq) was added at 0 °C to a solution of **D** (0.057 g, 0.138 mmol) in dry THF (10 mL) under Ar. The mixture was stirred for 30 min before addition of solid anhydrous FeCl<sub>3</sub> (0.027 g, 0.166 mmol). The mixture was stirred at room temperature overnight. The solvent was removed and the solids were suspended in a minimum amount of 1:1 (v/v) water/methanol and filtered through a fine glass frit. The filtrate was partially reduced in vacuo and purified by flash chromatography on C-18 silica gel with 9:1 (v/v) water/methanol as the eluent. The lithium cation was replaced by tetramethylammonium using cationic exchange column (Amberlite IR-120) presaturated with [NMe<sub>4</sub>]<sup>+</sup>. The red product was eluted in methanol and further purified by flash chromatography (C-18 silica gel, CH<sub>3</sub>OH/H<sub>2</sub>O, gradient elution). UV-Vis in H<sub>2</sub>O:  $\lambda_{\text{max}} = 330 \text{ nm}$  ( $\epsilon = 8340 \text{ M}^{-1} \text{ cm}^{-1}$ ); ESI-MS (neg mode): *m/z* calcd: 461.9; found: 462.1 (*M*<sup>-</sup>, 100%).

#### 6.4.3 Acid Induced Demetalation

Stock solutions of catalysts and perchloric acid were prepared using HPLC grade water. Appropriate volumes of perchloric acid were added to quartz cuvettes, and the reactions were initiated by the addition of an aliquot of catalyst. Reactions were conducted at 25 °C. Reaction progress was followed by measuring the decrease in absorbance at  $\lambda_{\text{max}}$ . The pseudo-first-order rate constants  $k_{\text{obs}}$  were calculated from exponential decay plots of absorbance versus time by fitting the data to the equation  $A = A_{\infty} - (A_{\infty} - A_0) e^{-k_{\text{obs}}t}$  when the demetalation was at least 90%. Each reported value of  $k_{\text{obs}}$  is the mean of three determinations.

## 6.5 References

1. Collins, T. *Acc. Chem. Res.* **1994**, 27 (12), 279–285.
2. Collins, T. J. *Acc. Chem. Res.* **2002**, 35 (9), 782–790.
3. Gupta, S. Sen; Stadler, M.; Noser, C.; Ghosh, A.; Steinhoff, B.; Lenoir, D.; Horwitz, C. P.; Schramm, K.-W.; Collins, T. J. *Science* **2002**, 296 (5566), 326–328.
4. Banerjee, D.; Markley, A. L.; Yano, T.; Ghosh, A.; Berget, P. B.; Minkley, E. G.; Khetan, S. K.; Collins, T. J. *Angew. Chemie Int. Ed.* **2006**, 45 (24), 3974–3977.
5. Chanda, A.; Khetan, S. K.; Banerjee, D.; Ghosh, A.; Collins, T. J. *J. Am. Chem. Soc.* **2006**, 128 (37), 12058–12059.
6. Shen, L. Q.; Beach, E. S.; Xiang, Y.; Tshudy, D. J.; Khanina, N.; Horwitz, C. P.; Bier, M. E.; Collins, T. J. *Environ. Sci. Technol.* **2011**, 45 (18), 7882–7887.
7. Kundu, S.; Chanda, A.; Espinosa-Marvan, L.; Khetan, S. K.; Collins, T. J. *Catal. Sci. Technol.* **2012**, 2 (6), 1165–1172.
8. Kundu, S.; Chanda, A.; Khetan, S. K.; Ryabov, A. D.; Collins, T. J. *Environ. Sci. Technol.* **2013**, 47 (10), 5319–5326.
9. Mills, M. R.; Arias-Salazar, K.; Baynes, A.; Shen, L. Q.; Churchley, J.; Beresford, N.; Gayathri, C.; Gil, R. R.; Kanda, R.; Jobling, S.; Collins, T. J. *Sci. Rep.* **2015**, 5, 10511.
10. Tang, L. L.; DeNardo, M. A.; Gayathri, C.; Gil, R. R.; Kanda, R.; Collins, T. J. *Environ. Sci. Technol.* **2016**, 50, 5261–5268.
11. Collins, T. *Science* **2001**, 291, 48–49.
12. Ellis, W. C.; Tran, C. T.; Denardo, M. A.; Fischer, A.; Ryabov, A. D.; Collins, T. J. *J. Am. Chem. Soc.* **2009**, 131 (50), 18052–18053.
13. Ellis, W. C.; Tran, C. T.; Roy, R.; Rusten, M.; Fischer, A.; Ryabov, A. D.; Blumberg, B.; Collins, T. J. *J. Am. Chem. Soc.* **2010**, 132 (28), 9774–9781.
14. DeNardo, M. A.; Tang, L. L.; Ryabov, A. D.; Collins, T. J. **2017**, in preparation.
15. Ghosh, A.; Ryabov, A. D.; Mayer, S. M.; Horner, D. C.; Prasuhn, D. E.; Sen Gupta, S.; Vuocolo, L.; Culver, C.; Hendrich, M. P.; Rickard, C. E. F.; Norman, R. E.; Horwitz, C. P.; Collins, T. J. *J. Am. Chem. Soc.* **2003**, 125 (41), 12378–12379.
16. Sullivan, S. Z.; Ghosh, A.; Biris, A. S.; Pulla, S.; Brezden, A. M.; Collom, S. L.; Woods, R. M.; Munshi, P.; Schnackenberg, L.; Pierce, B. S.; Kannarpady, G. K. *Chem. Phys. Lett.* **2010**, 498 (4–6), 359–365.
17. Mills, M. R.; Shen, L. Q.; Zhang, D. Z.; Ryabov, A. D.; Collins, T. J. **2017**, in preparation.
18. Mills, M. R.; Weitz, A. C.; Zhang, D. Z.; Hendrich, M. P.; Ryabov, A. D.; Collins, T. J. *Inorg. Chem.* **2016**, acs.inorgchem.6b01988.
19. Warner, G. R.; Mills, M. R.; Enslin, C.; Pattanayak, S.; Panda, C.; Panda, T. K.; Gupta, S. Sen; Ryabov, A. D.; Collins, T. J. *Chem. - A Eur. J.* **2015**, 21 (16), 6226–6233.
20. Popescu, D. L.; Chanda, A.; Stadler, M. J.; Mondai, S.; Tehranchi, J.; Ryabov, A. D.; Collins, T. J. *J. Am. Chem. Soc.* **2008**, 130 (37), 12260–12261.
21. Chahbane, N.; Popescu, D.-L.; Mitchell, D. A.; Chanda, A.; Lenoir, D.; Ryabov, A. D.; Schramm, K.-W.; Collins, T. J. *Green Chem.* **2007**, 9 (1), 49–57.
22. Ghosh, A.; Mitchell, D. A.; Chanda, A.; Ryabov, A. D.; Popescu, D. L.; Upham,



- E. C.; Collins, G. J.; Collins, T. J. *J. Am. Chem. Soc.* **2008**, *130* (45), 15116–15126.
23. DeNardo, M. A.; Mills, M. R.; Ryabov, A. D.; Collins, T. J. *J. Am. Chem. Soc.* **2016**, *138* (9), 2933–2936.
24. Ryabov, A.; Collins, T. *Adv. Inorg. Chem.* **2009**, *61*, 471–521.
25. Collins Group Patents  
[http://igs.chem.cmu.edu/index.php?option=com\\_content&view=article&id=347&Itemid=505](http://igs.chem.cmu.edu/index.php?option=com_content&view=article&id=347&Itemid=505).
26. Fild, V. M.; Rieck, H.-P. *Chemiker-Zeitung* **1976**, *100* (9), 391–392.
27. George, P. *Biochem. J.* **1953**, *54*, 267–276.
28. Chai, C.; Armarego, W. L. F. *Purification of Laboratory Chemicals*, Fifth Ed.; Butterworth-Heinemann, 2003.

## **CHAPTER 7**

### **Lifetime Studies of NewTAML Activators**

## 7.1 Introduction

Understanding catalyst inactivation processes is important for improving productivity in homogeneous catalysis.<sup>1</sup> Even small changes in lifetime can yield substantial gains in turnover number and profitability. In the iterative design of TAML activators (Figure 7.1), the first fully functional mimics of peroxidase enzymes,<sup>2-4</sup> we have long emphasized the importance of understanding inactivation mechanisms and incorporating blocking functionalities into the ligand design.<sup>5-8</sup> The theory that advanced our polyanionic chelating ligand design program and led to TAMLs was that intramolecular oxidation of the high-valent reactive intermediate (Ac, Figure 7.2) was the lifetime-determining inactivation process. However, a recent study indicated that this intramolecular oxidative inactivation is just one of multiple inactivation pathways that active TAML catalysts undergo.<sup>6</sup>

All ultra-dilute<sup>9</sup> aqueous TAML catalysis of oxidations by peroxide follows a common stoichiometric mechanism (Figure 7.2). First, peroxide oxidizes the resting state catalyst (Rc) to give the active catalyst (Ac) in a process described by the rate constant  $k_i$ . The Ac then either oxidizes a substrate giving a product and Rc in a process described by  $k_{II}$ , or undergoes inactivation that is unimolecular in catalyst, described by  $k_i$ . The development of a new tool for obtaining  $k_i$  at near neutral pH enabled in depth studies<sup>6,10</sup> of the inactivation processes under ambient conditions.<sup>11</sup> The first of these showed that for TAML activators **1**, **3**, and **5**, ligand modifications that increase  $k_{II}$  also proportionally increase  $k_i$ .<sup>6</sup> The second demonstrated that this trend derives from the nucleophilic attack at the amido carbonyl carbons in the inactivation of TAML catalysts functioning in ultra-dilute aqueous conditions at near-neutral pH.<sup>10</sup>

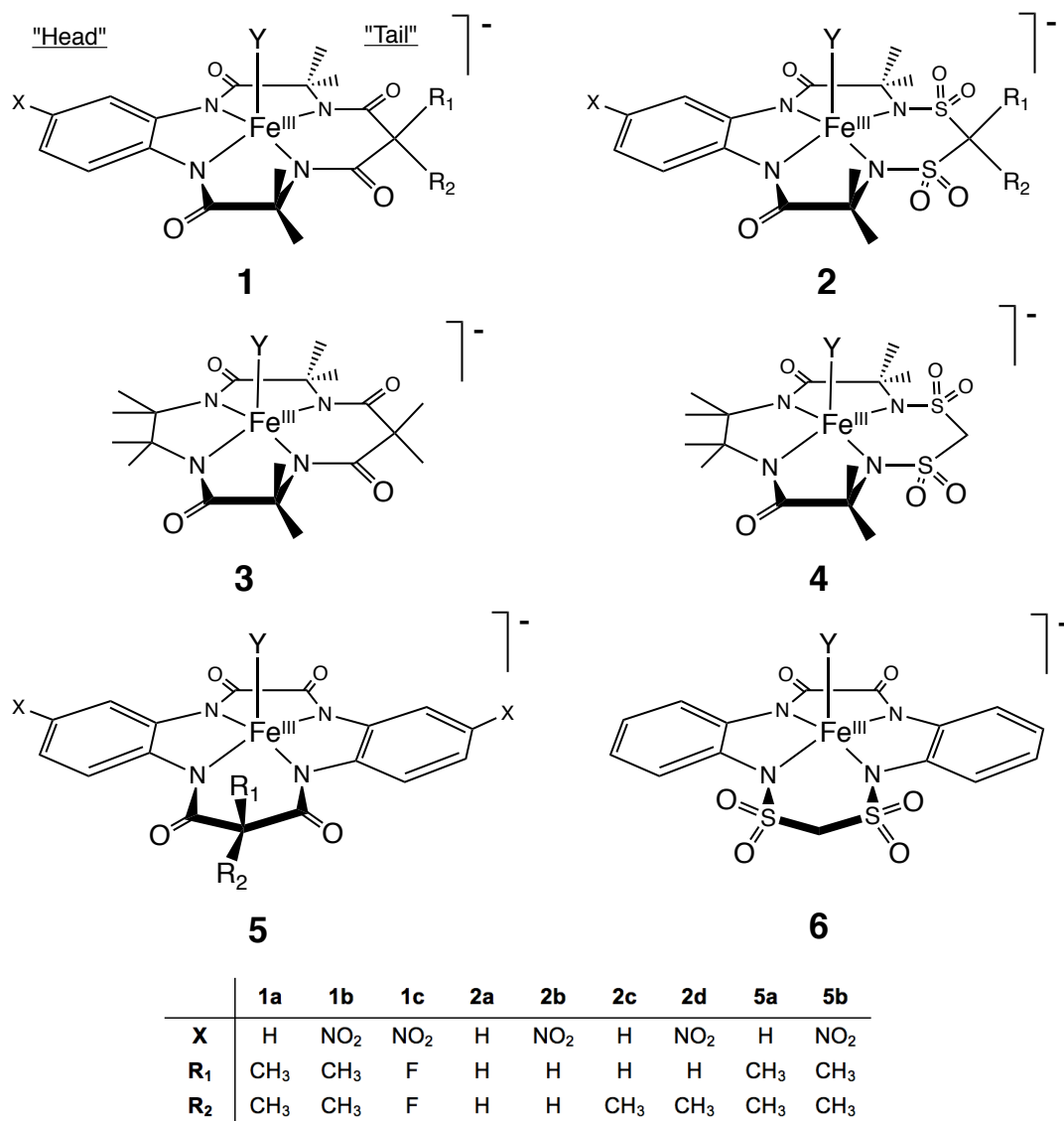


Figure 7.1 OldTAML activators (left) and NewTAML activators (right) discussed in this chapter; Y is typically H<sub>2</sub>O.

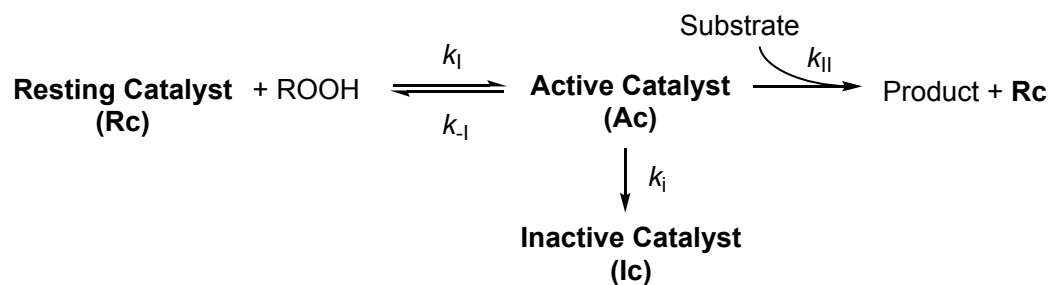


Figure 7.2 Mechanism of catalysis of TAMLs discussed in this chapter.

Consequently, we have begun to explore the impacts of substitution of the organic amides of **1**, **3**, and **5** with sulfonamides. This substitution gives a new class of TAML catalysts called NewTAMLs (Figure 7.1, **2**, **4**, **6**). Chapters 4–6 described studies of the NewTAML properties and kinetics of the catalyzed Orange II and propranolol oxidation by H<sub>2</sub>O<sub>2</sub>. The Orange II study demonstrates that the electron withdrawing properties of the sulfonamides provide significant increases in  $k_1$  and  $k_{II}$ . This is reflected in the enhanced degradation of the persistent pharmaceutical propranolol at neutral pH. In **2b** catalysis, the concentration of propranolol falls below the limit of detection in under five minutes. For comparison, the structurally similar **1b** removes 35% before inactivation after 75 minutes (Figure 4.7).

These  $k_1$  and  $k_{II}$  increases at neutral pH are exceptionally valuable. However, at elevated pH, **2b**  $k_1$  is disproportionately high, compromising the gains in  $k_1$  and  $k_{II}$ . The pH dependence of  $k_1$  led us to question whether the instability derives from an additional inactivation process associated with deprotonation of the methylene unit of the sulfonamide tail. The anion produced would then be vulnerable to intramolecular oxidation leading to instability of the complex. The additional inactivation pathway arising from deprotonation would then become lifetime-determining. We speculated that substitution of at least one of the methylene hydrogen atoms with an alkyl group such as that of **2d** would sufficiently disfavor the deprotonation to give an activator having increased stability at elevated pH. This was observed in the oxidation of both Orange II and propranolol by **2d**/H<sub>2</sub>O<sub>2</sub> (Chapter 4). Surprisingly, the performance gains were also observed at neutral pH in the oxidation of propranolol in Allegheny river water with **2b**

removing 77% before catalyst inactivation. Analogous treatment with **2d** gave 100% removal in less than 25 minutes (Figure 4.7).

In this chapter, the pH dependent lifetime of NewTAML activators is investigated and the rate constants for each inactivation pathway are quantified. The potential catalyst lifetime effects of blocking nucleophilic attack by substituting sulfonamides for carbonamides in the TAML framework are also explored and discussed.

## 7.2 Results and Discussion

### 7.2.1 Identification of the NewTAML Oxidative Inactivation Pathway

Overall TAML inactivation described by the first order rate constant  $k_i$  (Figure 7.2) is quantified through experiments in which the catalyst deactivates before all substrate has been converted to product in the presence of excess peroxide.<sup>11</sup> This incomplete bleaching paradigm allows values for  $k_i$  to be determined using Equation 7.1, where  $S_0$  and  $S_\infty$  are substrate concentrations at  $t_0$  and  $t_\infty$ , respectively. Values of  $k_{II}$  and  $k_i$  for TAMLs given in Table 7.1 were measured using the model substrate Orange II with  $H_2O_2$  and calculated using Equation 7.1.

$$\ln \left( \frac{S_0}{S_\infty} \right) = \left( \frac{k_{II}}{k_i} \right) [Fe^{III}]$$

Equation 7.1

Table 7.1 Rate constant  $k_{II}$  and  $k_i$  for TAMLs at pH 7 and 25 °C for the catalyzed bleaching of Orange II with  $H_2O_2$ .

TAML	X/R <sub>1</sub> /R <sub>2</sub>	$10^{-4} \times k_{II} / M^{-1}s^{-1}$	$10^3 \times k_i / s^{-1}$
<b>1a</b> <sup>a</sup>	H/Me/Me	$0.495 \pm 0.002$	$0.30 \pm 0.01$
<b>1b</b> <sup>a</sup>	NO <sub>2</sub> /Me/Me	$2.7 \pm 0.2$	$0.34 \pm 0.02$
<b>1c</b> <sup>a</sup>	NO <sub>2</sub> /F/F	$4.1 \pm 0.1$	$1.1 \pm 0.3$
<b>2a</b>	H/H/H	$9 \pm 2$ <sup>b</sup>	$4.3 \pm 0.7$
<b>2b</b>	NO <sub>2</sub> /H/H	$10 \pm 2$ <sup>b</sup>	$3.6 \pm 0.7$
<b>2c</b>	H/Me/H	$4.2 \pm 0.1$ <sup>b</sup>	$2.0 \pm 0.5$
<b>2d</b>	NO <sub>2</sub> /Me/H	$8.9 \pm 0.2$ <sup>b</sup>	$1.1 \pm 0.1$
<b>3</b> <sup>a</sup>	– /Me/Me	$(1.19 \pm 0.03) \times 10^{-4}$	$(4.1 \pm 0.1) \times 10^{-4}$
<b>4</b>	– /H/H	$(1.8 \pm 0.1) \times 10^{-4}$ <sup>b</sup>	$0.6 \pm 0.3$
<b>5a</b>	H/Me/Me	$0.085 \pm 0.005$	$\sim 6$
<b>5b</b> <sup>a</sup>	NO <sub>2</sub> /Me/Me	$52 \pm 7$	$85 \pm 6$
<b>6</b>	NO <sub>2</sub> /H/H	$0.13 \pm 0.01$ <sup>b</sup>	$0.49 \pm 0.05$

<sup>a</sup> reference 6 <sup>b</sup> Chapters 4–6

At pH 7, values of  $k_i$  for Old- and NewTAMLs increase roughly proportionally with increasing  $k_{II}$  with the exception of **4**, discussed below. For all amide-containing TAMLs,  $k_{II}$  and  $k_i$  correlate due to the importance of Lewis acidity in both processes such that catalysts with higher  $k_{II}$  values also have higher  $k_i$  values.

However, studies of the reactivity of NewTAMLs over a wide pH range clearly indicate the additional inactivation pathway not evident for OldTAMLs. Figure 7.3 compares  $k_{II}$  and  $k_i$  for OldTAML **1c**, a fluorinated<sup>12</sup> catalyst with similar activity to **2**, and NewTAML **2b** over the pH range of 6–11. For **1c**,  $k_{II}$  increases with pH while  $k_i$  is nearly pH independent (Figure 7.3A), typical of OldTAML activators.<sup>8</sup> However, for **2b**  $k_{II}$  peaks at pH 9 while  $k_i$  increases sharply with pH (Figure 7.3B). The different trends in  $k_i$  for **2b** and **1c** reveal the importance of the pH-dependent inactivation pathway that results in severely limited activity for **2b** at pH 9 and above.

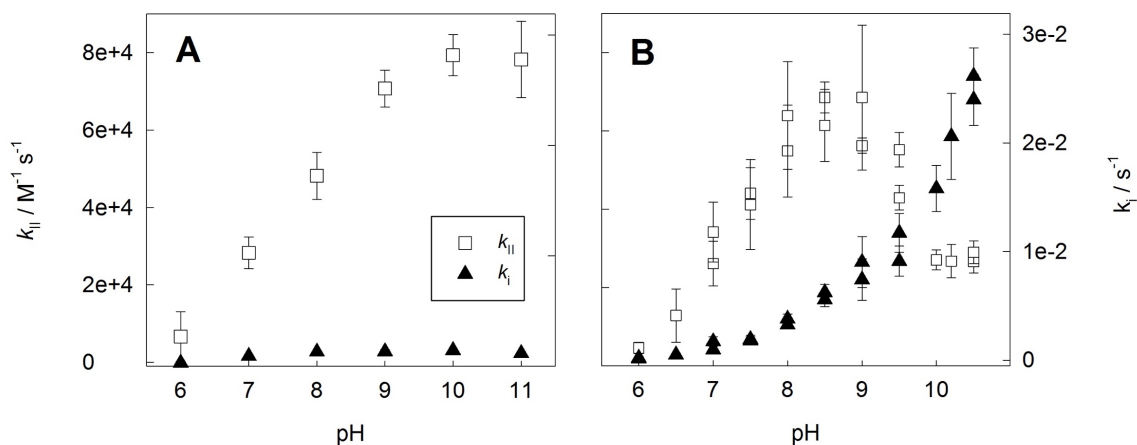


Figure 7.3 Comparison of  $k_{II}$  and  $k_i$  for **1c** (A) and **2b** (B) in the bleaching of Orange II with  $H_2O_2$  with 0.01 M phosphate at 25 °C. Adapted from Chapter 4.



The abovementioned fact is further illustrated in the linear free energy relationship in Figure 7.4. Figure 7.4 shows a  $\log k_{II}$  vs.  $\log k_I$  plot for **1c** and **2b** at various pHs using the data from Figure 7.3. Below pH 8, the two activators **1c** and **2b** show similar linear trends of increasing  $k_I$  with increasing  $k_{II}$  with slopes of  $0.77 \pm 0.03$  and  $0.98 \pm 0.05$ , respectively. Activity at pH 7 is nearly identical, but above pH 8,  $k_I$  for **1c** levels off (an interesting phenomenon requiring further investigation), while  $k_I$  for **2b** takes a distinctive turn as the NewTAML inactivation becomes unexpectedly significant.

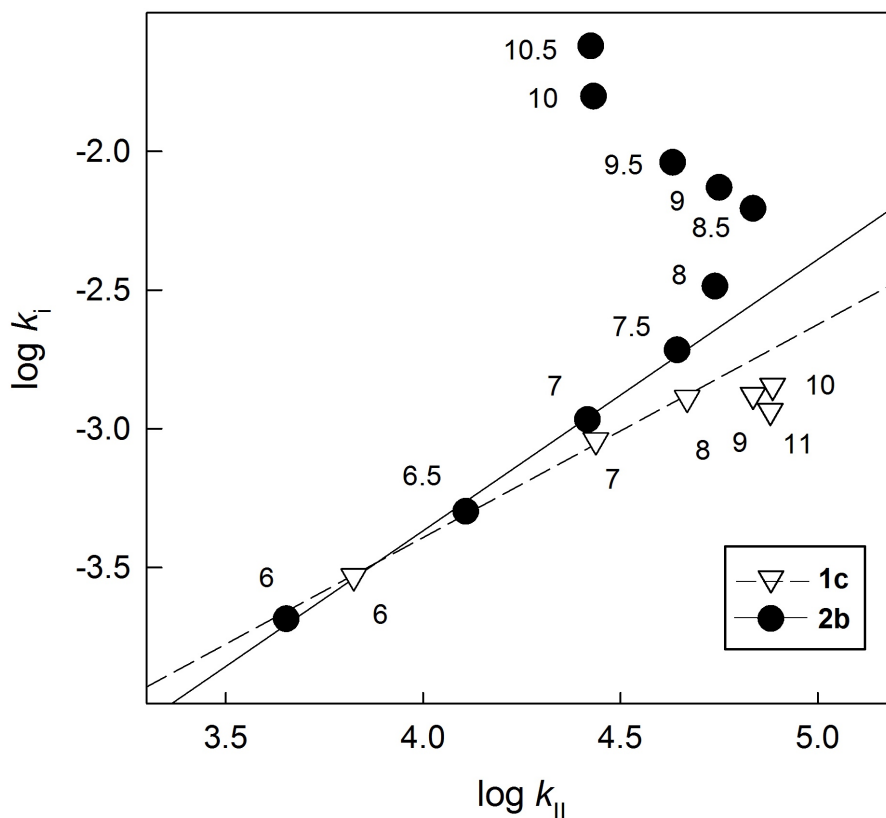


Figure 7.4 Linear free energy diagram of  $\log k_{II}$  vs  $\log k_I$  for **1c** and **2b** at various pH indicate the activation of the NewTAML inactivation pathway in **2b** above pH 8.

We have identified the methylene protons ( $R = H$ ) at the tail of NewTAMLs as a likely source of the oxidative inactivation pathway (Chapter 4). No OldTAMLs contain methylene protons at the tail because attempted preparation of **1** ligands with malonamide tails have failed (see Chapter 3), but **2** ligands with methylene disulfonamide tails are easier to prepare than ligands with  $R = \text{alkyl}$  tail groups. To confirm that the methylene tail protons could be responsible for the oxidative inactivation pathway, complex **2d** was prepared with one methyl group in the disulfonamide tail such that  $R_1 = H$  and  $R_2 = \text{Me}$ . Compared to **2b** ( $R_1 = R_2 = H$ ), complex **2d** shows a smaller rise in  $k_i$  above pH 8 (Figure 4.6) and a slightly lower  $k_i$  at pH 7 (Table 7.1). Complex **2d** demonstrates that changing one tail  $R$  group from  $H$  to methyl partially blocks the sharp increase in  $k_i$  above pH 8 in NewTAMLs. Furthermore, this ligand modification shows that the rate of inactivation for NewTAMLs can be altered during ligand design.

Further evidence for the enhanced acidity of the  $R = H$  groups is the labile nature of the methylene protons, observable via  $^1H$  NMR for the free ligand and ESI-MS for the  $Fe^{III}$ -complex **2b**. In the presence of  $D_2O$ , the acidic amide and sulfonamide N-H protons as well as the methylene protons at 5.15 ppm of ligand **A** exchange with deuterium (Figure 7.5). The H/D exchange is also observable in ESI-MS in negative mode for **2a** and **2b** as an increase in  $m/z$  by two units in  $D_2O$  compared  $H_2O$ . For **2a**  $m/z = 470.2$  in  $H_2O$  and 472.2 in  $D_2O$ . For **2b**  $m/z = 515.1$  in  $H_2O$  and 517.2 in  $D_2O$ . This increase was not observed in **1b** with  $m/z = 479.3$  in  $H_2O$  and 479.2 in  $D_2O$ .

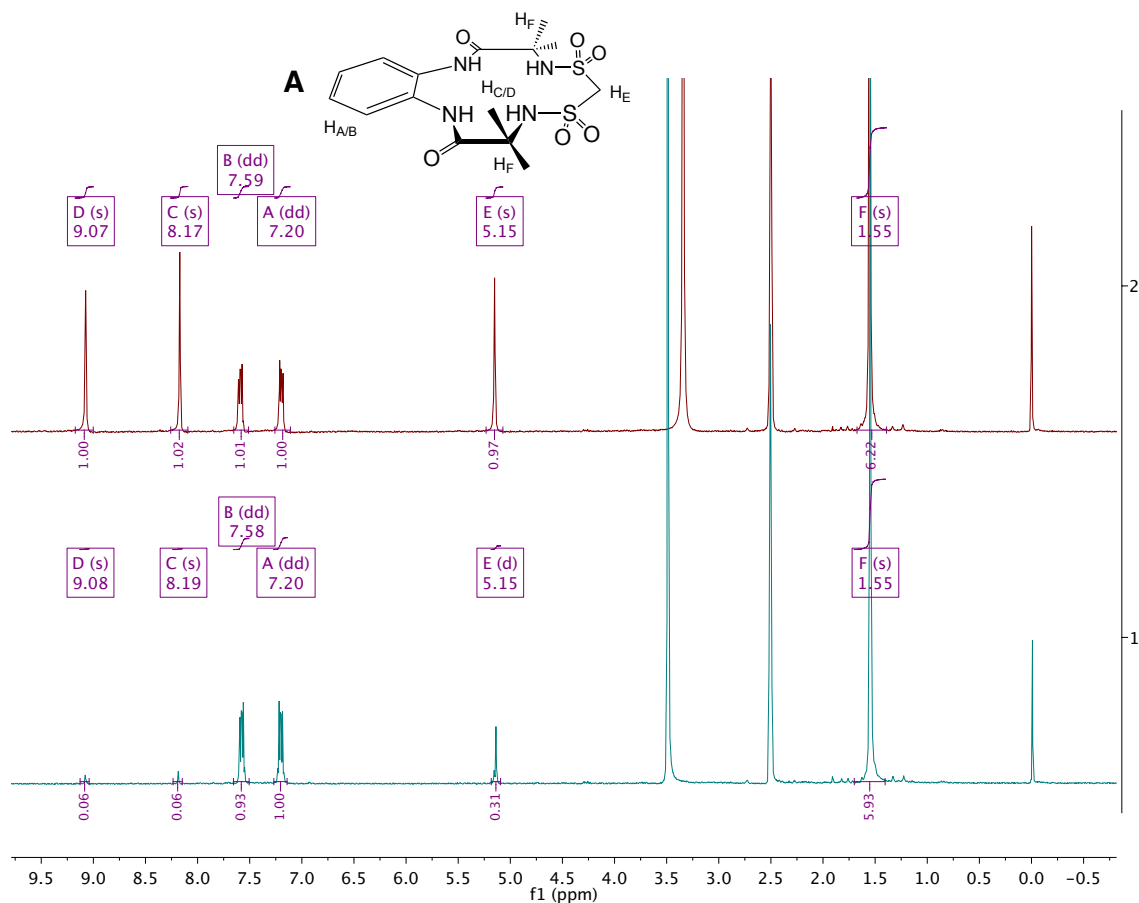


Figure 7.5 H/D exchange of methylene protons in D<sub>2</sub>O for ligand **A**. Top: <sup>1</sup>H NMR spectrum of ligand in DMSO-*d*<sub>6</sub>. Bottom: <sup>1</sup>H NMR spectrum of **A** in DMSO-*d*<sub>6</sub> after 19 h at 25 °C with one drop of D<sub>2</sub>O added. Amide protons at 9.07 and 8.17 ppm and methylene protons at 5.15 ppm exchange.

### 7.2.2 Nucleophilic Attack Inactivation Pathway in NewTAMLs

The dominant lifetime limiting inactivation pathway for amide-containing TAMLs was recently identified as nucleophilic attack of hydroxide and peroxide at the carbonyl carbons.<sup>10</sup> Because NewTAMLs **2**, **4**, and **6** still contain amides, they are subject to the same inactivation pathways. Decreasing the electron donating character of the TAML ligand with pendant NO<sub>2</sub> groups results in increased Lewis acidity at the iron center and therefore increases  $k_{II}$ . However, these seemingly desirable structural

modifications also increase Lewis acidity at the carbonyl carbons, causing the signature proportional increase in  $k_i$  that initially alerted us to this design problem (Figure 3.1).<sup>6</sup>

Including the NewTAML pH 7 rate constants in Table 7.1 in the LFER introduced in Chapter 3 (Figure 3.2), shown as Figure 7.6, confirms that  $k_{II}$  and  $k_i$  values for **2** and **6** are similar to OldTAMLs. However,  $k_i$  for **4** deviates significantly from the trend. For OldTAML **3**, the structural analog of **4**,  $k_{II}$  and therefore also  $k_i$  are reduced compared to other OldTAMLs by the elimination of the phenyl ring. The increased  $k_i$  for **4** may be indicative of the NewTAML inactivation pathway. Viewed as a set, values of  $k_i$  for NewTAMLs appear to be less dependent on  $k_{II}$ . The equation for the dashed line of best fit of is  $\log k_i = (0.14 \pm 0.08) \log k_{II} - (3.4 \pm 0.3)$ .

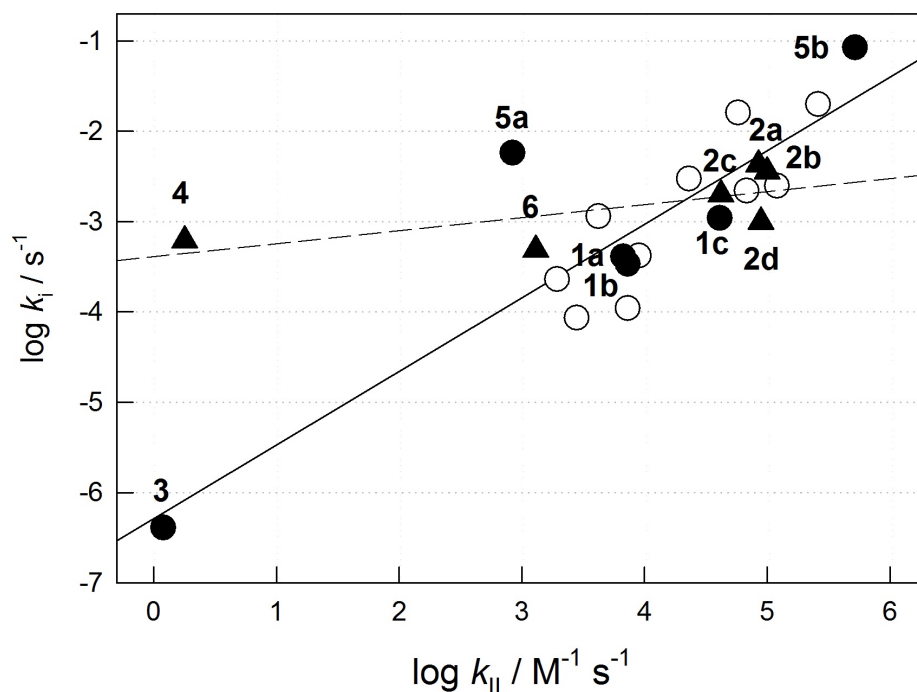


Figure 7.6 Linear free energy plot of  $k_{II}$  vs.  $k_i$  for OldTAMLs discussed here (black circles), all other OldTAMLs (white circles), and NewTAMLs (black triangles) at pH 7 and 25°C;  $k_{II}$  values are for the degradation of Orange II with  $H_2O_2$ .

For activators **2a** and **2b** at neutral pH, it is unclear which inactivation mechanism is dominant since  $k_{II}$  and  $k_i$  are similar to OldTAMLs (Figure 7.6). However, **2d** (with the substituted tail) falls almost one order of magnitude in  $k_i$  below the trend line with a similar  $k_i$  to less reactive **4** and **6**. The difference in  $k_i$  for **2b** and **2d** suggests that the difference is due to the NewTAML inactivation process. The location of **2d** below the OldTAML trend line is extremely promising because it shows that sulfonamide substitution at the tail can block nucleophilic attack. As only two carbonamides have been replaced, this shows that the tail carbonyls are more sensitive to nucleophilic attack than the head carbonyls. The ability of sulfonamides to block nucleophilic attack in the TAML ligand and decrease  $k_i$  without sacrificing  $k_{II}$  proves the value of sulfonamide

substitution in NewTAMLs. As we have recently demonstrated with the recalcitrant substrate metaldehyde, even small gains in catalyst lifetime can translate to massive gains in productivity for real world catalyst applications.<sup>9</sup>

### 7.2.3 Kinetic Analysis of Catalyst Inactivation

To separately quantify the inactivation mechanisms that contribute to  $k_i$ , the dependence of  $k_i$  on  $[\text{H}_2\text{O}_2]$  was measured for **2b**, **2d**, and **6** (Figure 7.7). The general trends of a hyperbolic decrease of  $k_i$  for **2** and a nearly linear increase for **6** with increasing  $[\text{H}_2\text{O}_2]$  is consistent with previous data for OldTAMLs **1** and **5**, respectively.<sup>10</sup>

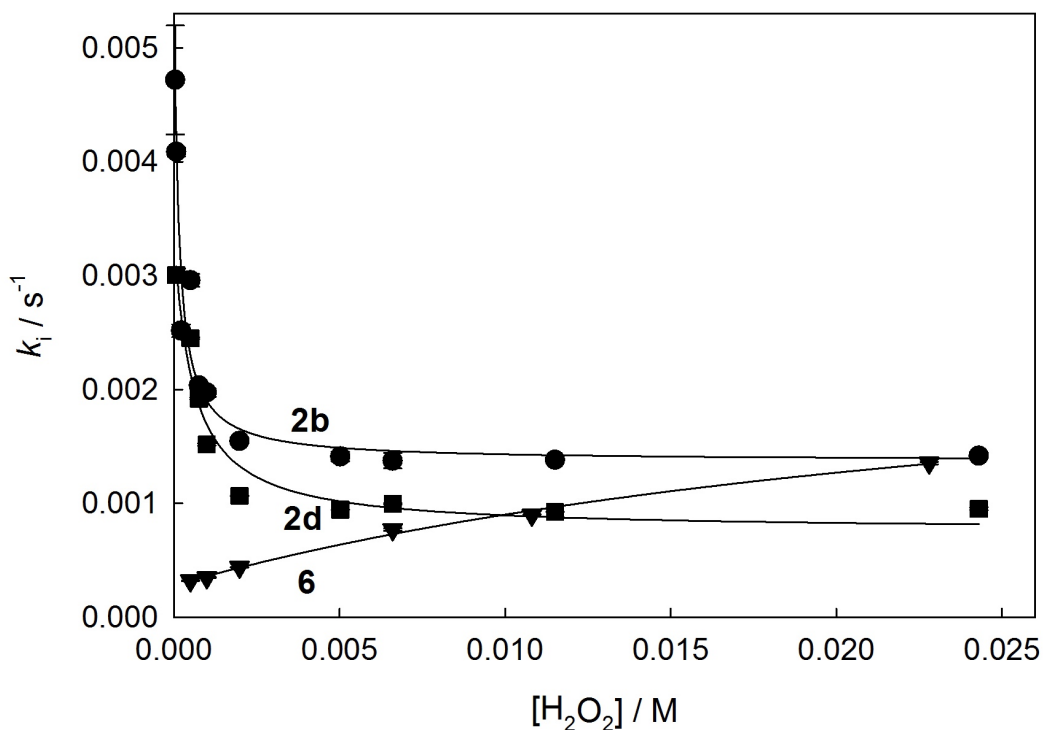


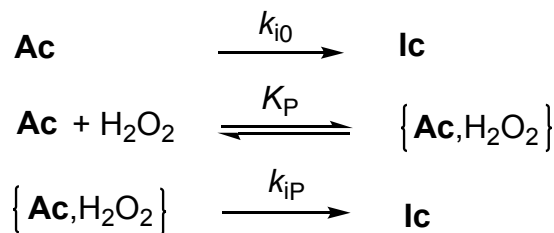
Figure 7.7 Dependence of  $k_i$  on  $[\text{H}_2\text{O}_2]$  in the incomplete bleaching of Orange II ( $5.0 \times 10^{-5} \text{ M}$ ) with **2b** ( $5 \times 10^{-8} \text{ M}$ ), **2d** ( $5 \times 10^{-8} \text{ M}$ ), and **6** ( $5 \times 10^{-9} \text{ M}$ ) at pH 7 and 25 °C with 0.01 M phosphate. Lines are fit to Equation 7.2.

The data presented in Figure 7.7 for **2b** and **2d** indicate that (i) hydrogen peroxide protects the active forms of the catalyst from deactivation, (ii) the dependence of  $k_i$  as a function of hydrogen peroxide concentration is described by Equation 7.2, and (iii) the deactivation occurs via two parallel pathways, viz. independent of  $\text{H}_2\text{O}_2$  ( $k_{i0}$ ) and induced by  $\text{H}_2\text{O}_2$  ( $k_{iP}$ ) via the formation of the adduct between Ac and  $\text{H}_2\text{O}_2$  with the equilibrium constant  $K_P$ .

$$k_i = \frac{k_{i0} + k_{iP}K_P[\text{H}_2\text{O}_2]}{1 + K_P[\text{H}_2\text{O}_2]}$$

Equation 7.2

The mechanism suggested by Equation 7.2 and derivation of the expression are shown in Figure 7.8.



equilibrium expression:  $K_P = \frac{[\{\mathbf{Ac}, \text{H}_2\text{O}_2\}]}{[\mathbf{Ac}][\text{H}_2\text{O}_2]}$

mass balance:  $\text{Ac}_t = [\mathbf{Ac}] + [\{\mathbf{Ac}, \text{H}_2\text{O}_2\}]$

substitution into mass balance:  $[\mathbf{Ac}] = \frac{\text{Ac}_t}{1 + K_P[\text{H}_2\text{O}_2]} \quad [\{\mathbf{Ac}, \text{H}_2\text{O}_2\}] = \frac{K_P \text{Ac}_t [\text{H}_2\text{O}_2]}{1 + K_P[\text{H}_2\text{O}_2]}$

rate expression:  $\frac{d[\mathbf{Ic}]}{dt} = k_{i0}[\mathbf{Ac}] + k_{iP}[\{\mathbf{Ac}, \text{H}_2\text{O}_2\}]$

substitution into rate expression:  $\frac{d[\mathbf{Ic}]}{dt} = \frac{k_{i0} \text{Ac}_t}{1 + K_P[\text{H}_2\text{O}_2]} + \frac{k_{iP} K_P \text{Ac}_t [\text{H}_2\text{O}_2]}{1 + K_P[\text{H}_2\text{O}_2]}$

$$= \frac{k_{i0} + k_{iP} K_P [\text{H}_2\text{O}_2]}{1 + K_P[\text{H}_2\text{O}_2]} (\text{Ac}_t)$$

$$\frac{d[\mathbf{Ic}]}{dt} = k_i \text{Ac}_t$$

$$k_i = \frac{k_{i0} + k_{iP} K_P [\text{H}_2\text{O}_2]}{1 + K_P[\text{H}_2\text{O}_2]}$$

Figure 7.8 Stoichiometric mechanism of the inactivation of the active catalyst **2b** and **2d** consistent with kinetic data presented in Figure 7.7 and subsequent derivation of Equation 7.2. Ac and Ic are active and inactive catalyst, respectively.

Values of  $k_{i0}$ ,  $K_P$ , and  $k_{iP}$  generated by fitting the data in Figure 7.7 (obtained at pH 7) for **2b**, **2d**, and **6** to Equation 7.2 are given in Table 7.2 along with previously determined values for **1**. It is important to note that the values of the rate constants  $k_{i0}$  and  $k_{iP}$  and the fact that  $k_{i0} > k_{iP}$  explains the observed stabilizing effect of **2** by hydrogen peroxide—at higher concentrations of  $\text{H}_2\text{O}_2$ , most all Ac is converted to the  $\{\mathbf{Ac}, \text{H}_2\text{O}_2\}$



adduct which is less vulnerable to deactivation than Ac itself. For **6**,  $k_{iP} > k_{i0}$  such that increasing  $[H_2O_2]$  further increases  $k_i$  with no protective effect. A leveling off of  $k_i$  with increasing  $[H_2O_2]$  begins to occur at the highest peroxide concentrations measured.

Table 7.2 Values of  $k_{i0}$ ,  $K_P$ , and  $k_{iP}$  for TAMLs at pH 7 and 25 °C generated from Equation 7.2.

TAML	X/R <sub>1</sub> /R <sub>2</sub>	$10^4 \times k_{i0} / s^{-1}$	$10^{-1} \times K_P / M^{-1}$	$10^4 \times k_{iP} / s^{-1}$
<b>1a</b> <sup>a</sup>	H/Me/Me	$4.00 \pm 0.05$	$3.5 \pm 0.7$	$7.1 \pm 0.2$
<b>1b</b> <sup>a</sup>	NO <sub>2</sub> /Me/Me	$3.9 \pm 0.8$	$31 \pm 7$	$18.5 \pm 0.5$
<b>1c</b> <sup>a</sup>	NO <sub>2</sub> /F/F	$36 \pm 8$	$40 \pm 30$	$14 \pm 1$
<b>2b</b>	NO <sub>2</sub> /H/H	$54 \pm 6$	$700 \pm 300$	$14 \pm 2$
<b>2d</b>	NO <sub>2</sub> /Me/H	$34 \pm 3$	$180 \pm 60$	$8 \pm 1$
<b>6</b>	NO <sub>2</sub> /H/H	$2.8 \pm 0.3$	$3 \pm 1$	$27 \pm 5$

<sup>a</sup> reference<sup>10</sup>

In order to reveal the nature of the NewTAML inactivation process, which manifests itself as spike-like increase in  $k_i$  for **2b** at higher pH (above 8.5) presented, for example, in Figure 7.3, the dependencies of  $k_{i0}$  and  $k_{iP}$  on the solution pH have been investigated. In particular, the data as in Figure 7.7 for **2b** and **2d** were also collected at six pH values in the range of 9.00–10.25. The corresponding data, which are presented in Figure 7.13 in the appendix, were fit to Equation 7.2 and the values of  $k_{i0}$ ,  $k_{iP}$ , and  $K_P$  obtained are summarized in Table 7.3 as functions of the concentration of OH<sup>-</sup> ions. This data allowed us to analyze how  $k_{i0}$  and  $k_{iP}$  depend on  $[OH^-]$  and resolve the NewTAML inactivation puzzle.

Table 7.3 Values of  $k_{i0}$ ,  $K_P$ , and  $k_{iP}$  for **2b** from pH 7.0–10.25 using Equation 7.2.

pH	$[\text{OH}^-] / \text{M}$	$10^3 \times k_{i0} / \text{s}^{-1}$	$10^{-2} \times K_P / \text{M}^{-1}$	$10^3 \times k_{iP} / \text{s}^{-1}$
7.0	$1.0 \times 10^{-7}$	$5.4 \pm 0.6$	$70 \pm 30$	$1.4 \pm 0.2$
9.0	$1.0 \times 10^{-5}$	$\sim 6.6$	$\sim 340$	$5.4 \pm 0.4$
9.25	$1.8 \times 10^{-5}$	<sup>a</sup>	$\sim 1600$	$10.2 \pm 0.7$
9.50	$3.2 \times 10^{-5}$	$9.1 \pm 0.6$	$6.9 \pm 0.2$	$8.1 \pm 0.9$
9.75	$5.6 \times 10^{-5}$	$30 \pm 10$	$40 \pm 120$	$18 \pm 2$
10.0	$1.0 \times 10^{-4}$	$43 \pm 6$	$8 \pm 10$	$10 \pm 13$
10.25	$1.8 \times 10^{-4}$	$35 \pm 3$	$7 \pm 9$	$14 \pm 8$

<sup>a</sup> could not be accurately determined

The dependence of  $k_{i0}$  ( $\text{H}_2\text{O}_2$  independent pathway) on  $[\text{OH}^-]$  presented in Figure 7.9 emphasizes a strong dependence of  $k_{i0}$  on the concentration of hydroxide ion. There is a significant positive intercept and the dependence can be cautiously approximated by a straight line, all consistent with kinetic Equation 7.3.

$$k_{i0} \approx k'_{i0} + k''_{i0} [\text{OH}^-]$$

Equation 7.3

Equation 7.3 reveals both the nucleophile and hydrogen peroxide independent pathway  $k'_{i0}$  and the *hydroxide-dependent* pathway  $k''_{i0}$ . The corresponding values of the rate constants equal  $(8 \pm 6) \times 10^{-3} \text{ s}^{-1}$  and  $200 \pm 70 \text{ M}^{-1} \text{ s}^{-1}$ , respectively. It is worth mentioning that the values of  $k'_{i0}$  for 15 different TAML activators have been actually used previously for LFER correlations of  $k_{II}$  and  $k_i$ .<sup>6</sup> In that work the  $k_i$  values were obtained at low  $[\text{OH}^-]$  (pH 7) and very low  $[\text{H}_2\text{O}_2]$ . The present results prove that under such conditions  $k_i \sim k'_{i0}$ .

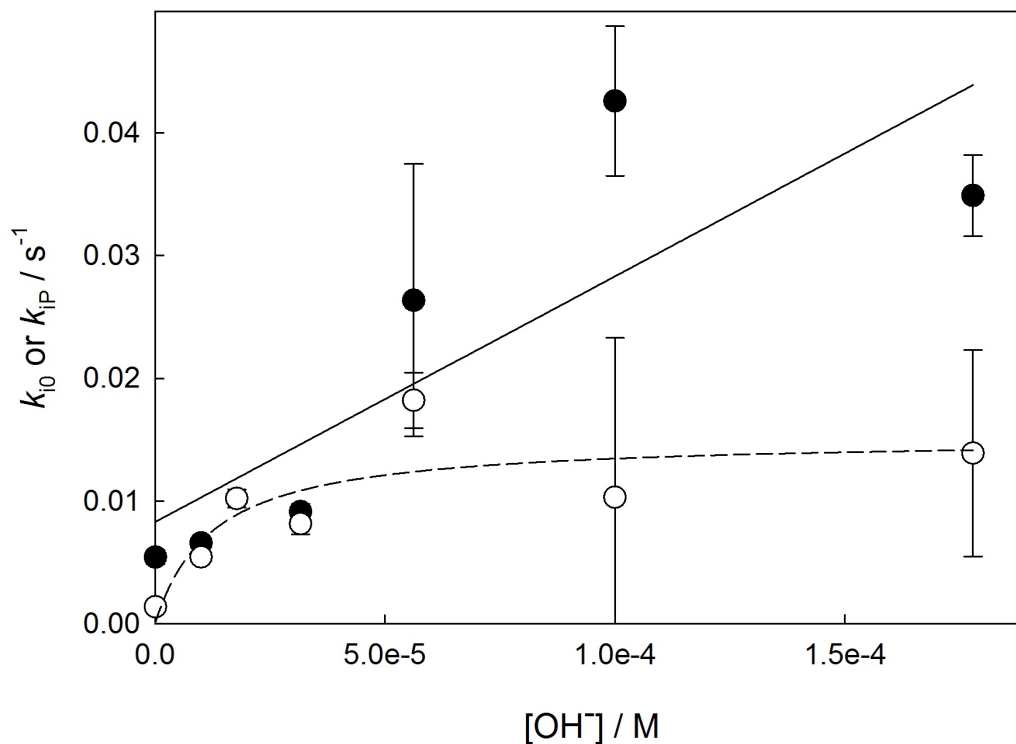


Figure 7.9 Dependence of the values of  $k_{i0}$  (black circles) and  $k_{ip}$  (white circles) from Table 7.3 on  $[\text{OH}^-]$  for **2b** fit to Equation 7.3 and Equation 7.4, respectively.

As opposed to  $k_{i0}$ , the rate constants  $k_{ip}$  are practically independent of the concentration of hydroxide ions (Figure 7.9). The dependence could be satisfactorily approximated by the Michaelis-type Equation 7.4 with the parameters  $k'_{ip}$  and  $K'_p$  of  $(1.5 \pm 0.3) \times 10^{-2} \text{ s}^{-1}$  and  $(1 \pm 1) \times 10^{-5} \text{ M}$ , respectively.

$$k_{ip} \approx \frac{k'_{ip}[\text{OH}^-]}{K'_p + [\text{OH}^-]}$$

Equation 7.4

It is worth substituting Equation 7.3 ( $k_{i0}$ ) and Equation 7.4 ( $k_{ip}$ ) into Equation 7.2. We could not detect a clear trend in variation of  $K_p$  with  $[\text{OH}^-]$  and therefore we assume it to be  $[\text{OH}^-]$  independent. The resulting Equation 7.5, which has been elaborated for

NewTAML activator **2b**, shows the primary importance of hydroxide ions in the deactivation scheme and explains the nature of the NewTAML pH-dependent inactivation process. The deactivation pathways associated with hydrogen peroxide have levelling off dependencies on both  $[H_2O_2]$  and  $[OH^-]$ , whereas  $H_2O_2$ -independent pathway  $k''_{i0}$  is a linear function of  $[OH^-]$  and therefore active forms of **2** die much more rapidly at higher pH.

$$k_i = \frac{k'_{i0} + k''_{i0} [OH^-] + \frac{k'_{iP}[OH^-]K_P[H_2O_2]}{K_P + [OH^-]}}{1 + K_P[H_2O_2]}$$

Equation 7.5

A 3D rendering of the dependence of  $k_i$  on  $[H_2O_2]$  and  $[OH^-]$  for **2b** using the data in Figure 7.13 (Appendix) was fit to Equation 7.5 (Figure 7.10). As expected,  $k_i$  increases sharply with  $[OH^-]$  while  $H_2O_2$  protects **2b** from  $OH^-$  induced inactivation. The values of  $k'_{i0}$ ,  $k''_{i0}$ ,  $k'_{iP}$ , and  $K_P$  estimated from the fit of  $7 \times 10^{-3} s^{-1}$ ,  $200 M^{-1} s^{-1}$ ,  $4 \times 10^{-4} s^{-1}$ , and  $200 M^{-1}$  agree reasonably with the calculated values given in the text above.

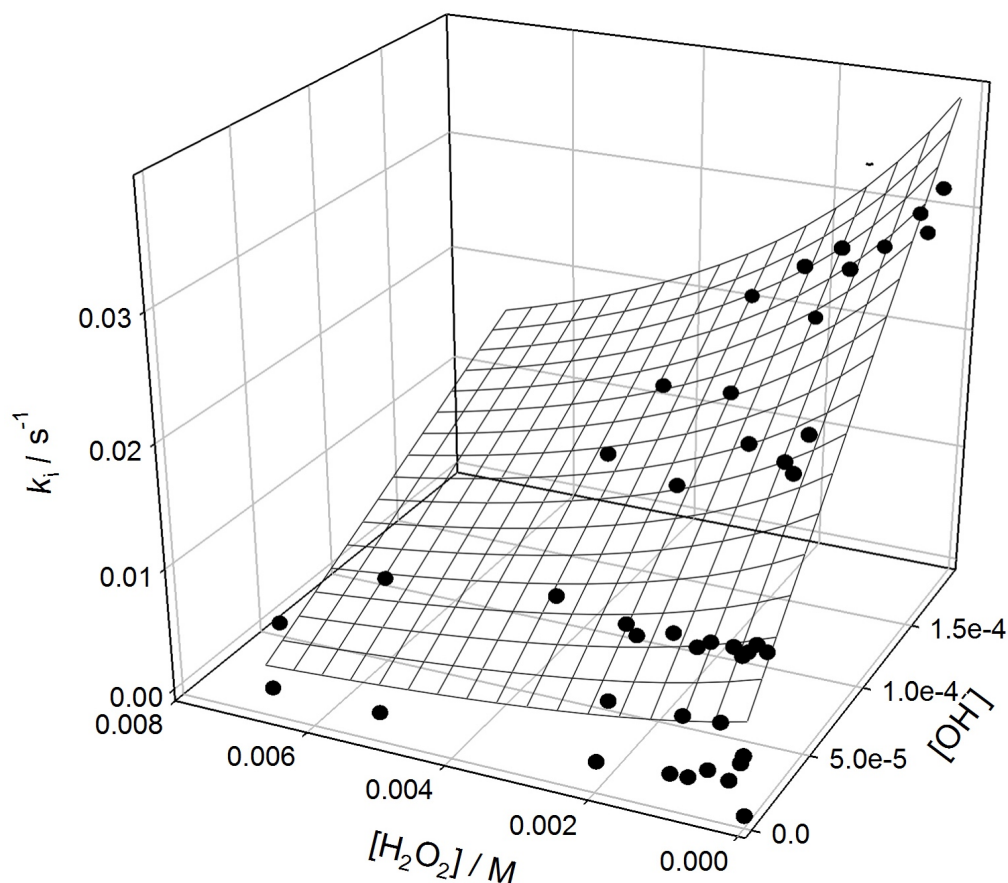


Figure 7.10 3D mesh of the dependence of  $k_i$  on  $[H_2O_2]$  and  $[OH^-]$  fit to Equation 7.5 for **2b** at pH 7.0–10.25 with 0.01 M phosphate or Carmody buffer at 25 °C.

#### 7.2.4 Effect of oxidative inactivation on a tetrasulfonamide NewTAML

The tetrasulfonamide NewTAML **8** (Chapter 3, Figure 7.11) is structurally similar to **5** and **6** with two phenyl rings, but contains two  $-SO_2CH_2SO_2-$  units bridging the phenyl to complete the macrocycle. As a result, the chelating ring for iron contains one additional bond. A previously prepared OldTAML with the same number of bonds in the ring formed a distorted, nonplanar complex that quickly demetalated in aqueous solution.<sup>13</sup> Complex **8** is more stable in water, forming a purple solution with unique

properties. In pH 9 buffered aqueous solution, **8** is stable as a purple solution. However, at neutral pH in buffered and unbuffered water, **8** quickly forms a black solution with decreasing absorbance that signifies demetalation. The  $pK_a$  of **8** is  $8.9 \pm 0.9$ , suggesting that the deprotonated form  $[\text{Fe}^{\text{III}}\text{L}(\text{OH})(\text{OH}_2)]^{2-}$  is the more stable purple species. The black solution may be a  $\mu$ -oxo dimer intermediate, a previously observed black species.<sup>14</sup> As a catalyst, **8** is ineffective both at pH 7 and 9 in the oxidation of Orange II with  $\text{H}_2\text{O}_2$ . We believe that the inactivity of **8** is due to the presence of two sites for the NewTAML inactivation process to occur. Future iterations of **8** with one or more substituted R group may yield a productive catalyst, at least at pH 9 where the complex is stable. The unique properties of **8** may also find it some use for future chemical study.

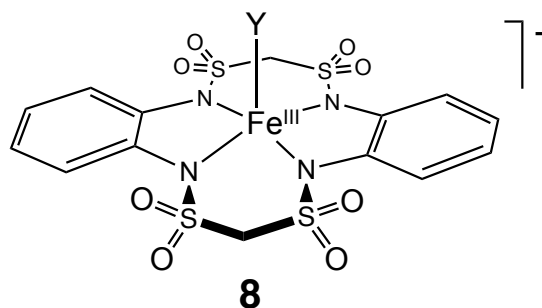


Figure 7.11 Tetrasulfonamide NewTAML **8**.

### 7.3 Conclusions

All sulfonamide NewTAML activators produced to date undergo an additional inactivation mechanism beyond those previously characterized for OldTAMLs. The H/D exchange observed in the ligand **A** and complex **2b** at the methylene tail provides evidence for an anionic intermediate following deprotonation by hydroxide. The new inactivation process is hydroxide dependent such that NewTAML lifetime is severely limited above pH 9. At all pHs, high hydrogen peroxide concentrations provide some protection against this process. Importantly, the rate of NewTAML inactivation can be tuned by changing the identity of the R groups at the tail during preparation of the ligand. As a result, it should be possible in future iterations of NewTAMLs to eliminate this inactivation mechanism altogether during catalyst design.

## 7.4 Experimental

### 7.4.1 Materials and Methods

Fe<sup>III</sup>-OldTAMLs **1a–c** and **3** were prepared according to published methods<sup>15,16</sup> or obtained from GreenOx Catalysts, Inc. Methods for the preparation of NewTAMLs **2**, **4**, and **6** are given in Chapters 4, 5, and 6 of this thesis. Orange II was recrystallized in aqueous ethanol. H<sub>2</sub>O<sub>2</sub> (30% w/w) was purchased from Fischer and the concentration of dilutions was verified using  $\varepsilon = 72.8 \text{ M}^{-1} \text{ cm}^{-1}$  at 230 nm via UV-Vis spectroscopy.<sup>17</sup> All other reagents and solvents (at least ACS reagent grade) were obtained from commercial sources and purified according to standard procedures when necessary.<sup>18</sup> Catalytic activity in bleaching of Orange II with H<sub>2</sub>O<sub>2</sub> and incomplete bleaching experiments were performed as described in detail previously.<sup>6,19</sup>

### 7.4.2 Preparation of **8**

Complex **8** was prepared according to the method of **6** (Chapter 6) with substitution of methanedisulfonyl dichloride for oxalyl chloride (Figure 7.12). The preparation of **A** is described in Chapter 6.

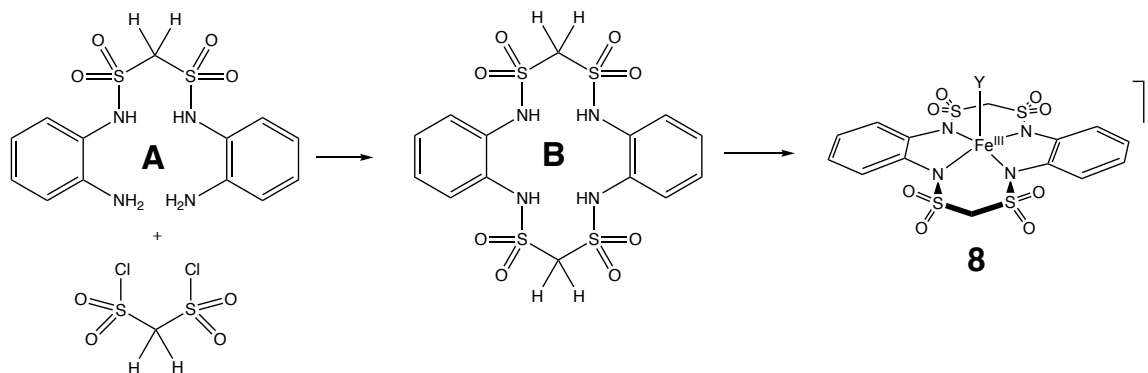


Figure 7.12 Preparation of **8**.



**Preparation of B:** To a small flask under Ar was added *N,N'*-bis(2-aminophenyl)methanedisulfonamide **A** (300 mg) in dry THF (40 mL) and pyridine (0.27 mL). To a second flask was added methanedisulfonyl dichloride (0.09 mL) in dry THF (40 mL). Both solutions were added dropwise with a syringe pump to a 3-neck flask containing THF (250 mL) at 0 °C. The flask was allowed to warm overnight, then filtered. The pink solid was rinsed with additional THF and taken up into a mixture of ethyl acetate and 0.1 M HCl. The layers were separated and the aqueous layer washed with a second aliquot of ethyl acetate. The organic fractions were combined, dried with sodium sulfate, filtered, and the solvent removed under reduced pressure to give light pink solid **B** in 33% yield. <sup>1</sup>H NMR (500 MHz, DMSO-*d*<sub>6</sub>) δ 9.23 (s, 4H), 7.53 (dd, 4H), 7.29 (dd, 4H), 5.48 (s, 4H). <sup>13</sup>C NMR (500 MHz, DMSO-*d*<sub>6</sub>) δ 129.50, 127.35, 126.63, 68.94. ESI-MS (neg mode): *m/z* 355 (M-H<sup>+</sup>, 100%).

**Preparation of 8:** To Ligand **B** (0.138 mmol) in 50 mL dry THF under Ar at 0 °C was added *n*BuLi (0.4 mL of 1.6 M in hexane, 0.567 mmol) and the mixture stirred for 30 min before addition of solid anhydrous FeCl<sub>3</sub> (0.166 mmol). The mixture was stirred at room temperature overnight. The solvent was removed and the solids were suspended in a minimum amount of 90% water/10% methanol and filtered through a glass frit. The filtrate was partially reduced in vacuo and purified by flash chromatography on C-18 silica gel with 9:1 (v/v) water/methanol as the eluent. The lithium cation was replaced by tetramethylammonium using cationic exchange column (Amberlite IR-120) presaturated with [NMe<sub>4</sub>]<sup>+</sup>. The purple product was eluted in methanol and further purified by flash chromatography (C-18 silica gel, CH<sub>3</sub>OH/H<sub>2</sub>O, gradient elution). X-ray quality crystals

were obtained by slow diffusion of ether into a solution of the complex in acetonitrile.

UV-Vis in pH 9 0.01 M phosphate:  $\lambda_{\text{max}} = 290 \text{ nm}$  ( $\epsilon = 7320 \text{ M}^{-1} \text{ cm}^{-1}$ ),  $\lambda_{\text{max}} = 516 \text{ nm}$  ( $\epsilon = 1640 \text{ M}^{-1} \text{ cm}^{-1}$ ); ESI-MS (neg mode):  $m/z$  calcd: 548.4; found: 547.9 ( $\text{M}^-$ , 100%); elemental analysis calcd (%) for  $\text{C}_{20}\text{H}_{27}\text{FeN}_6\text{O}_8\text{S}_4$ : C 36.20, H 4.10, N 12.67; found: C 37.56, H 5.09, N 12.42.

## 7.5 Appendix

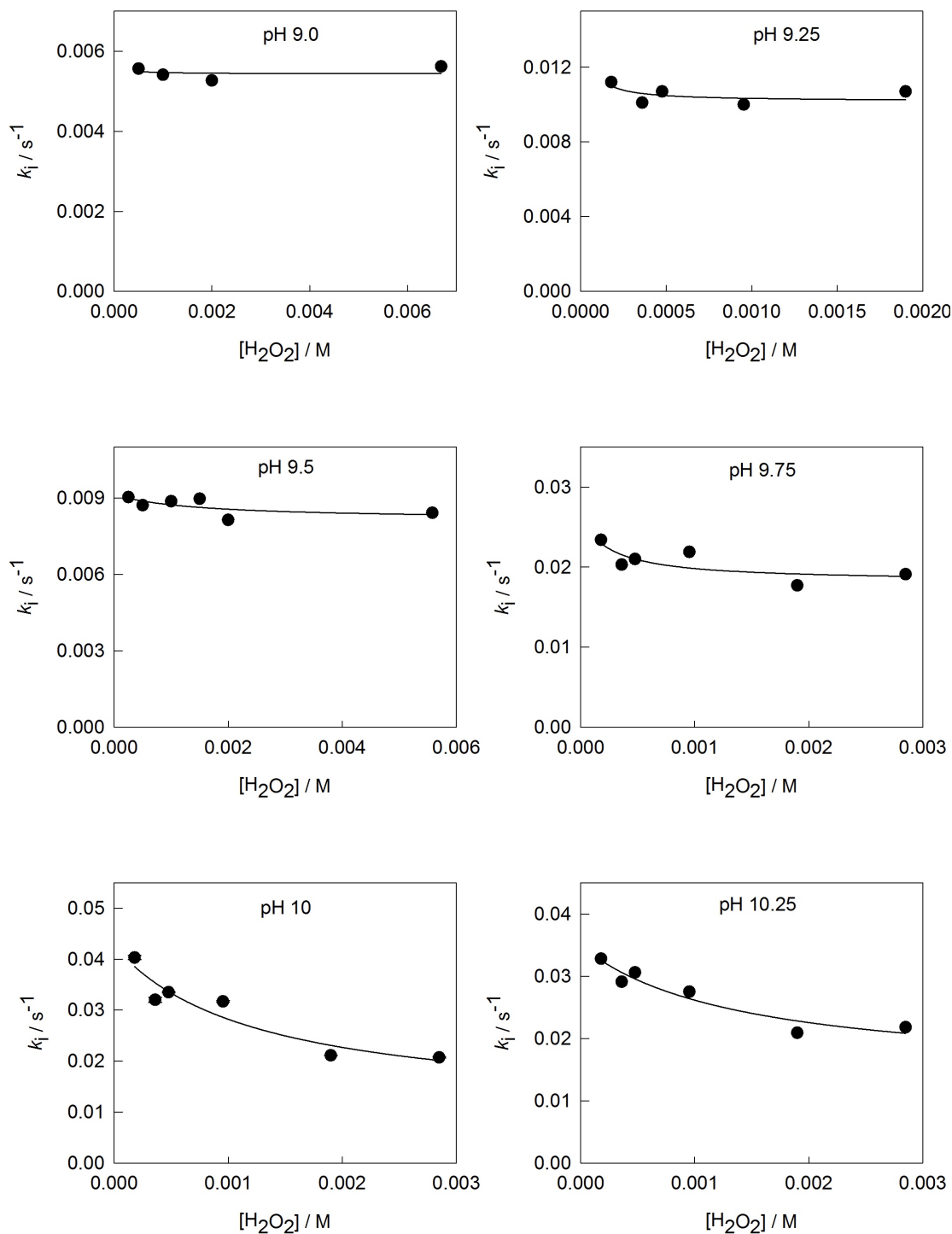


Figure 7.13 Dependence of  $k_i$  on  $[\text{H}_2\text{O}_2]$  in the incomplete bleaching of Orange II ( $5.0 \times 10^{-5}$  M) with **2b** ( $5 \times 10^{-8}$  M) at pH 7 and 25 °C with 0.01 M phosphate or Carmody buffer fit to Equation 7.2. Data are shown on a 3D plot in Figure 7.10.

## 7.6 References

1. Crabtree, R. H. *Chem. Rev.* **2015**, *115* (1), 127–150.
2. Collins, T. J. *Acc. Chem. Res.* **2002**, *35* (9), 782–790.
3. Ryabov, A.; Collins, T. *Adv. Inorg. Chem.* **2009**, *61*, 471–521.
4. Collins, T. *Acc. Chem. Res.* **1994**, *27* (12), 279–285.
5. Bartos, M.; Gordon-Wylie, S. *Coord. Chem. Rev.* **1998**, *174*, 361–390.
6. DeNardo, M. A.; Mills, M. R.; Ryabov, A. D.; Collins, T. J. *J. Am. Chem. Soc.* **2016**, *138* (9), 2933–2936.
7. Horwitz, C.; Fooksman, D. *J. Am. Chem. Soc.* **1998**, *1* (17), 4867–4868.
8. Chanda, A.; Ryabov, A. D.; Mondal, S.; Alexandrova, L.; Ghosh, A.; Hangun-Balkir, Y.; Horwitz, C. P.; Collins, T. J. *Chem. - A Eur. J.* **2006**, *12* (36), 9336–9345.
9. Tang, L. L.; DeNardo, M. A.; Schuler, C. J.; Mills, M. R.; Gayathri, C.; Gil, R. R.; Kanda, R.; Collins, T. J. *J. Am. Chem. Soc.* **2017**, *139* (2), 879–887.
10. DeNardo, M. A.; Tang, L. L.; Ryabov, A. D.; Collins, T. J. **2017**, in preparation.
11. Emelianenko, M.; Torrejon, D.; DeNardo, M. A.; Socolofsky, A. K.; Ryabov, A. D.; Collins, T. J. *J. Math. Chem.* **2014**, *52* (5), 1460–1476.
12. Collins, T. *Science*. **2001**, *291*, 48–49.
13. Ghosh, A.; Ryabov, A. D.; Mayer, S. M.; Horner, D. C.; Prasuhn, D. E.; Sen Gupta, S.; Vuocolo, L.; Culver, C.; Hendrich, M. P.; Rickard, C. E. F.; Norman, R. E.; Horwitz, C. P.; Collins, T. J. *J. Am. Chem. Soc.* **2003**, *125* (41), 12378–12379.
14. Ghosh, A.; de Oliveira, F. T. *J. Am. Chem. Soc.* **2005**, No. Iv, 2505–2513.
15. Ellis, W. C.; Tran, C. T.; Denardo, M. A.; Fischer, A.; Ryabov, A. D.; Collins, T. J. *J. Am. Chem. Soc.* **2009**, *131* (50), 18052–18053.
16. Collins Group Patents  
[http://igs.chem.cmu.edu/index.php?option=com\\_content&view=article&id=347&Itemid=505](http://igs.chem.cmu.edu/index.php?option=com_content&view=article&id=347&Itemid=505).
17. George, P. *Biochem. J.* **1953**, *54*, 267–276.
18. Chai, C.; Armarego, W. L. F. *Purification of Laboratory Chemicals*, Fifth Ed.; Butterworth-Heinemann, 2003.
19. Warner, G. R.; Mills, M. R.; Enslin, C.; Pattanayak, S.; Panda, C.; Panda, T. K.; Gupta, S. Sen; Ryabov, A. D.; Collins, T. J. *Chem. - A Eur. J.* **2015**, *21* (16), 6226–6233.